Light and Spectra in the Wild - Spectral Structures of Light Fields: Measurement, Simulation and Visualisation

Yu, C.

DOI
10.4233/uuid:3ec90e7c-c2e1-40f3-84b8-7b4a423a43b0

Publication date
2023

Document Version
Final published version

Citation (APA)
Yu, C. (2023). *Light and Spectra in the Wild - Spectral Structures of Light Fields: Measurement, Simulation and Visualisation*. [Dissertation (TU Delft), Delft University of Technology].
https://doi.org/10.4233/uuid:3ec90e7c-c2e1-40f3-84b8-7b4a423a43b0

Important note
To cite this publication, please use the final published version (if applicable).
Please check the document version above.

LIGHT AND SPECTRA IN THE WILD

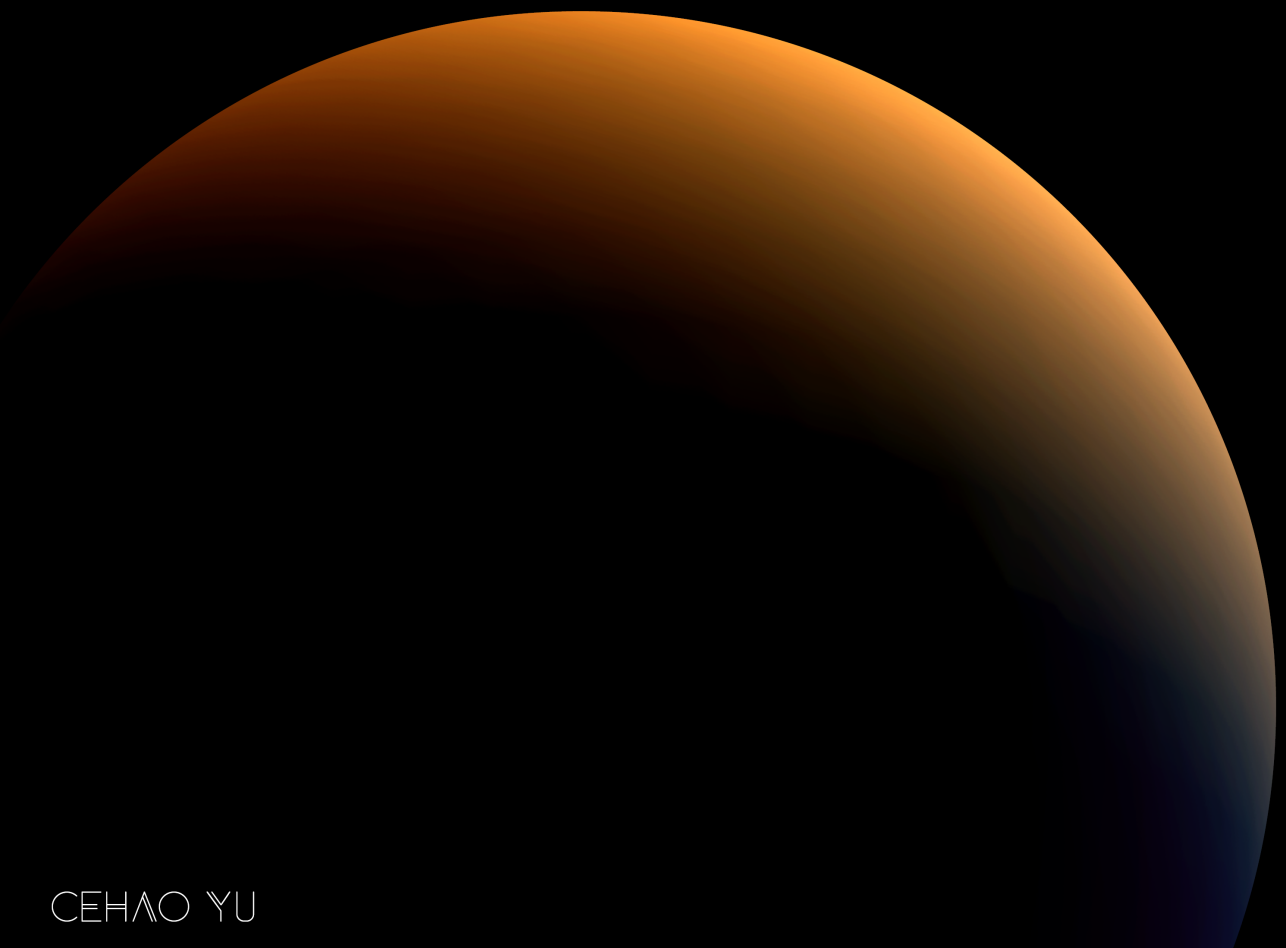

CEHAO YU

LIGHT AND SPECTRA IN THE WILD

SPECTRAL STRUCTURES OF LIGHT FIELDS: MEASUREMENT, SIMULATION AND VISUALISATION

LIGHT AND SPECTRA IN THE WILD

SPECTRAL STRUCTURES OF LIGHT FIELDS: MEASUREMENT, SIMULATION AND VISUALISATION

Dissertation

for the purpose of obtaining the degree of doctor
at Delft University of Technology
by the authority of the Rector Magnificus, prof. dr. ir. T.H.J.J. van der Hagen,
chair of the Board for Doctorates
to be defended publicly on
Tuesday 20 June 2023 at 12:30 o'clock

by

Cehao YU

Master of Science in Light and Lighting, University College London, United Kingdom
born in Chongqing, China

This dissertation has been approved by the promotors.

Composition of the doctoral committee:

Rector Magnificus,	chairperson
Prof. dr. S.C. Pont,	Delft University of Technology, *promotor*
Prof. dr. E. Eisemann,	Delft University of Technology, *promotor*
Dr. M.W.A. Wijntjes,	Delft University of Technology, *copromotor*
Independent members:	
Prof. P. Raynham,	University College London, United Kingdom
Prof. dr. S.F. te Pas,	Utrecht University
Prof. dr. ir. R.H.M. Goossens,	Delft University of Technology
Prof. dr. H. de Ridder,	Delft University of Technology


Keywords: Light field, colour science, lighting design, photometry, art perception

Printed by: Proefschrift All In One (AIO)

Cover by: C. Yu

ISBN 978-94-93315-75-4
This research was funded by the European Commission through the Marie Skłodowska-Curie Action – Innovative Training Network (MSCA-ITN-ETN) project DyViTo: 'Dynamics in Vision and Touch – the look and feel of stuff' (grant agreement ID 765121), under the European Union's Horizon 2020 research and innovation programme

An electronic copy of this dissertation is available at
https://repository.tudelft.nl/.

Colours are the deeds and suffering of light.

— Johann Wolfgang von Goethe

CONTENTS

SUMMARY

The study of the light field has become a valuable framework for capturing and analysing the complex distribution of light in natural environments. The directional, spatial, temporal and spectral structure of light, collectively influence the optical information available to an observer and thus impact our perception of the surrounding world. The extended definition of the light field, which is equivalent to the plenoptic function in perceptual studies, incorporates radiance as a function of spectral energy, position, direction, and time in space, quantifying all the optical information available to an observer. However, there is a considerable gap in measuring, describing, and visualizing the properties of the light field in the chromatic domain, which this thesis aimed to address.

The thesis focuses on the research question of how to effectively describe, measure, simulate, and visualize the spatiotemporal dynamics of the spectral structure of light fields. To address this research question, We outlined four main objectives in the thesis, which are addressed in separate chapters. The first objective is to investigate the interplay between the colours of surfaces and light sources in 3D indoor scenes, and its effects on the spatial and angular distribution of light. The second objective was to quantify the directional and spatial variations of chromatic light field effects on correlated colour temperature and colour rendering. The third objective was to explore the objective measurement, description, and visualization of the 7D light-field properties of outdoor illumination. Finally, the fourth objective was to examine the relationship between image statistics and perceived time of day in Western European paintings from the 17^{th} to 20^{th} centuries to determine if the representation of lighting in paintings serves as a contextual cue for the time of day.

In **Chapter 2** of the thesis, we systematically studied how the impact of indirect illumination, specifically reflections and inter-reflections, affects the colour appearance of materials and the diffuse and directed illumination in 3D spaces. The study employed theoretical modelling and simulation of basic colour effects, empirical testing, and visualization techniques. Our findings demonstrated the occurrence of systematic hue, saturation, and brightness effects in light fields, which are essential for understanding the 3D distribution of light in chromatic environments. This has important implications for various fields, such as perception research, architecture, and computer graphics, where knowledge of the chromatic properties of light can inform the design and creation of effective visual environments.

In **Chapter 3**, we explored how indirect illumination affects the effective colorimetric properties of actual light in uni-chromatic spaces. The research involved measuring the spectral irradiance of diffuse and directional light-field components in real and simulated uni-chromatic spaces illuminated with standard white light

sources. The results demonstrated significant differences between the lamp-specified correlated colour temperature and colour rendition and the actual light-based effective CCT and colour rendition. The results underscore the need for 3D colour checkers for lighting designers, architects, and computer graphics professionals, and we propose using simple Lambertian spheres as a solution.

In **Chapter 4**, we present a technique for capturing the 7-dimensional light field that a human observer experiences and translating it into perceptually meaningful information. The spectral cubic illumination method quantifies the objective aspects of diffuse and directed light components, including its fluctuations over time, space, wavelength, direction, after interaction with the environment, particularly the sky and sunlight. To validate this method, experiments were conducted in natural outdoor surroundings, and the data gathered shed light on how crucial aspects of light, such as direction, colour, and diffuseness, vary spatially and temporally in real-world conditions. This low-cost, high-benefit method is a valuable addition to capturing the subtler effects of lighting on scene and object appearance, such as natural chromatic gradients.

Finally, in **Chapter 5**, we explored the relationship between human subjective assessments of the time of day depicted in paintings and the paintings' image statistics, including luminance and chromaticity variations. Two online rating experiments were conducted, which showed that viewers could differentiate between morning and evening depictions based on image statistics such as brightness, contrast, saturation, and hue. A predictive model was created that explains 76% of the variance in time-of-day perception.

Through the studies presented in this thesis, we have addressed a critical gap in light field research by expanding its scope to include the chromatic domain. The studies presented provide a comprehensive understanding of how light changes spatially, directionally, temporally, and chromatically, as an integral component of our environment, and its influence on the colour of matte materials and light in space. These findings have important implications for architecture, computer graphics, and perception research. By integrating the chromatic properties into the light field framework, this research allows for a scientifically informed assessment of the actual light in space, considering the interactions between illuminants, material, shape, and space. This paves the way for more effective lighting design processes and narrows the gap between design expectations and outcomes, ultimately leading to better design outcomes.

SAMENVATTING

Onderzoek naar lichtvelden heeft geleid tot een waardevol framework om de verdeling van licht te begrijpen en te analyseren in natuurlijke omgevingen. De richtings-, spatiële-, temporele- en spectrale aspecten van licht beïnvloeden gezamenlijk de beschikbare optische informatie voor een waarnemer, en bepalen mede onze waarneming van de wereld om ons heen. De uitgebreide definitie van een lichtveld, in waarnemingsonderzoek ook wel bekend als de plenoptische functie, beschrijft radiantie als functie van spectrale energie, positie, richting, en tijd, en kwantificeert alle optische informatie in een ruimte voor een waarnemer. Deze omschrijving mist echter kleur bij het meten, beschrijven en visualiseren van lichtveldeigenschappen. Dit proefschrift richt zich op deze tekortkoming.

De onderzoeksvraag van dit proefschrift is hoe spatiotemporele dynamiek van de spectrale structuur van lichtvelden effectief beschreven, gemeten, gesimuleerd en gevisualiseerd kan worden. Om deze vraag te beantwoorden, hebben we ons op vier doelen gericht, ieder beschreven in een eigen hoofdstuk. Het eerste doel is om het samenspel tussen oppervlaktekleur en lichtbronnen in 3D binnenruimtes te onderzoeken, en het effect hiervan op de verdeling van het licht in positie en richting. Het tweede doel is om de richting- en spatiële variaties van chromatische lichtveldeffecten op kleurtemperatuur en kleurweergave te kwantificeren. Het derde doel is om de objectieve meting, beschrijving en visualisatie van de 7D lichtveldeigenschappen van natuurlijke buitenomgevingen te bestuderen. Het vierde en laatste doel is om de verhouding tussen beeldstatistieken en de waargenomen moment op de dag te onderzoeken in West-Europese schilderijen van de 17^e tot de 20^e eeuw, om te bepalen of de lichtweergave in schilderijen informatief is voor het herkennen van het moment.

In **Hoofdstuk 2** van dit proefschrift onderzoeken we de invloed van indirecte belichting – in het bijzonder reflecties en interreflecties – op de waargenomen kleur van materialen en op het diffuse en gerichte licht in 3D ruimtes. Hiervoor hebben we een theoretisch model ontwikkeld, simulaties gedaan van basaleleur-effecten, en verschillende experimenten en visualisaties uitgevoerd. De resultaten tonen aan dat er systematische tint-, verzadigings-, en helderheidseffecten kunnen optreden in lichtvelden, welkeessentieel zijn om de 3D-verdeling van licht in chromatische omgevingen te begrijpen. Dit is van belang voor meerdere onderzoeksgebieden, zoals waarnemingsonderzoek, architectuur en computergraphics, waar inzicht in de chromatische eigenschappen van licht bij kan dragen aan wetenschappelijk geinformeerd ontwerpen en de creatie van effectieve visuele omgevingen.

In **Hoofdstuk 3** onderzoeken we hoe indirecte belichting de effectieve colorimetrische eigenschappen van echt licht in unichromatische ruimtes beïnvloedt. Hiervoor onderzoeken we de spectrale irradiantie van diffuse en gerichte

lichtveldcomponenten in echte en gesimuleerde unichromatische ruimtes, beide verlicht met standaard witte lichtbronnen. De resultaten tonen aanzienlijke verschillen tussen de gecorreleerde kleurtemperatuur (CCT) en de kleurweergave van de lamp en van de effectieve CCT en kleurweergave op basis van het resulterende lichtveld. Dit bevestigt opnieuw de behoefte aan 3D-kleurcheckers voor verlichtingontwerpers, architecten en computergraphics-professionals. De door ons voorgestelde oplossing is het gebruik van eenvoudige Lambertiaanse bollen.

In **Hoofdstuk 4** presenteren we een methode om het zeven-dimensionale lichtveld te beschrijven en te vertalen naar perceptueel betekenisvolle informatie. De spectrale kubieke belichtingsmethode kwantificeert de objectieve aspecten van diffuse en gerichte lichtcomponenten, met inbegrip van de bijbehorende fluctuaties in tijd, ruimte, golflengte en richting, na interactie met de omgeving en in het bijzonder zoals beïnvloed door de kleur van de lucht en zonlicht. We hebben deze methode gevalideerd door middel van experimenten in een natuurlijke buitenomgeving. De resulterende data laat zien hoe cruciale aspecten van licht, zoals richting, kleur en mate van diffusie, in ruimte en tijd variëren in natuurlijke omstandigheden. Vanwege de lage kosten en hoge baten is deze methode een waardevolle toevoeging voor het vastleggen van de subtielere effecten van licht op een tafereel of een object, zoals het effect van natuurlijke chromatische gradiënten.

Ten slotte, in **Hoofdstuk 5**, bestuderen we de relatie tussen de menselijke subjectieve waarneming van het afgebeelde moment van de dag in schilderijen en de beeldstatistieken van het schilderij, met inbegrip van de variaties in belichting en chromaticiteit. We hebben twee online schalings-experimenten uitgevoerd, waarvan de resultaten aantonen dat deelnemers het verschil konden waarnemen tussen afbeeldingen van ochtend- en avondtaferelen door middel van beeldstatistieken zoals helderheid, contrast, verzadiging en tint. Op basis van dit experiment hebben we een voorspellend model gemaakt dat 76% van de variantie in het waargenomen moment van de dag verklaart.

De uitbreiding van lichtveldonderzoek naar het chromatische domein in dit proefschrift beantwoord het eerder genoteerde gebrek daarvan. De gepresenteerde resultaten bieden een veelomvattend inzicht in de verandering van licht in ruimte, richting, tijd en kleur, als een integraal onderdeel van de omgeving, en de invloed van die omgeving op de kleur van matte materialen en licht in een ruimte. Deze bevindingen zijn van grote betekenis voor architectuur, computergraphics en waarnemingsonderzoek. Door de chromatische eigenschappen te integreren in het lichtveldframework, maakt dit onderzoek het mogelijk om op een wetenschappelijk onderbouwde wijze het werkelijke licht in ruimtes te beschrijven, rekening houdend met de wisselwerking tussen lichtbronnen, materiaal, vorm en ruimte. Dit maakt de weg vrij voor effectievere processen voor verlichtingontwerp en verkleint de afstand tussen ontwerp en realisatie, wat uiteindelijk zal leiden tot betere ontwerpbeslissingen.

1

INTRODUCTION

1

1.1. BACKGROUND AND MOTIVATION

Understanding the complicated characteristics of environmental light

We live in a three-dimensional world that changes over time, and light is an integral component of our environment. In physics, "light" is defined as electromagnetic radiation in a range of wavelengths, that can be detected by the human eye. For humans, the exact boundaries of the visible spectrum are not rigidly defined, as they depend upon the amount of radiant flux reaching the retina and the individual observer's responsivity. However, the lower limit of this range is generally accepted to fall between 360 nm and 400 nm, and the upper limit between 760 nm and 830 nm. It's important to note that these limits can vary, which is reflective of the rich complexity of our visual perception.

Light is neither flat [1] nor static, but rather a dynamic and multifaceted phenomenon resulting from various optical processes. The properties of environmental light are influenced by various factors, including the reflective properties of surfaces, the geometrical shape of objects, and the presence of other light sources. The interactions between environment and lighting (illuminants), such as scattering, shading, reflecting, and refracting, can notably influence the optical properties of the light and therefore the perceived qualities of the resulting light, such as its colour [2–6], intensity [7–10], and direction [11–16]. Furthermore, the dynamic nature of our interaction with light through movement and changes in gaze creates continually changing visual elements that shape our perception and experience of space and time. To accurately capture these interactions, acquiring a spatially and directionally articulated measurement of the light is necessary.

The importance of understanding the principles behind the properties of environmental light cannot be overstated [17]. Such understanding is of course key in designing light itself. It profoundly impacts our visual perception [18], influencing factors such as colour perception [4, 19, 20], visual acuity [10], and how we perceive depth [21–23], shape [24], and materials [25] – which are determining requirements in perception-based lighting design. Furthermore, the characteristics of environmental light have implications for many fields, including architecture, solar technology and geo-engineering, agriculture, visual art and graphics. To design lighting environments that are both functional and visually pleasing, designers need to understand the principles behind the characteristics of environmental light in (architectural) lighting design. This knowledge about the properties and principles of environmental light can be incorporated into the design of spaces and environments, leading to lighting systems that support visual comfort, well-being, circadian rhythms and positive user experience.

Historically, there has long been a disjunction between light-based and lighting-based approaches to studying and assessing the quantity and quality of light in the built environment. A lighting-based approach acknowledges the impactful weights of primary illumination for environmental light and thus focuses on the properties of the light sources, such as the output and distribution of light from lamps and fixtures. While this approach is advantageous in evaluating the technical performance and efficiency of lighting systems, it falls short of fully capturing the complexity of interactions between light and environment and its impact on visual perception. In

contrast, a light-based approach recognises the interaction between the environment and light as a critical factor in determining actual context-dependent light properties. It focuses on the properties of light in three-dimensional space and its interactions with the environment and matter. Moreover, this approach accounts for the dynamics of human interactions with spaces and their impact on visual perception [8, 11, 26].

The design of lighting in the built environment is an imperative factor that shapes our perception and experience of the space we occupy. The visual impact of the environment is not limited to the light sources alone, but also encompasses the appearance of illuminated objects, materials, and surfaces. On the other hand, these objects, materials, and surfaces will again influence the light. Having a thorough understanding of the characteristics of environmental light is vital for enhancing the visual experience and atmosphere of a space through lighting design. A light-based approach, which takes into consideration the interactions between the environment and light, offers a comprehensive approach to environmental light and its effects on visual perception. This understanding is beneficial for designing lighting environments that meet both functional requirements and enhance the visual experience. To fully grasp the characteristics of environmental light and its impact on visual perception, it is urgent to develop methods for measuring it in a perceptually relevant way. Adopting a scientifically rigorous and interdisciplinary approach that encompasses optics, perception, and design science has been shown to provide insights into the complexity of environmental light and aid in creating functional and visually pleasing lighting environments suited to human needs [10, 18, 24, 27]. This change in perspective from evaluating primary illumination through a lighting-based approach to assessing the light that reaches the eye through a light-based approach, can be considered as a precursor for the advancement of the lighting profession.

The remainder of the introduction chapter is structured as follows: in **Section 1.2**, I will introduce a framework that draws on knowledge from optics, perception, and design to describe and measure the structure of light [18, 28]. While this framework has been developed in the photometric domain, it will be expanded to include wavelength information in the spectro-photometric domain. Spectro-photometric measurement and analysis involve characterising light in terms of both its spectral and photometric properties. Spectral properties describe the distribution of radiant energy across the electromagnetic spectrum's various wavelengths, while photometric properties describe the physical characteristics of light that are weighted according to the sensitivity of the human visual system, such as luminous flux, intensity, luminance, and illuminance. By combining information on the spectral and photometric properties of light, spectro-photometric measurements provide a comprehensive understanding of its luminous and chromatic characteristics and wavelength-dependent properties, offering a thorough understanding of the chromatic effects of light sources and materials on the structure of light and its implications in different fields of study.

Section 1.3 will focus on perceptually relevant metrics of environmental light resulting from the interactions between the environment and light. This section

will explore the distribution of light in terms of its direction, location in space, and chromaticity. By delving into these properties of environmental light, a deeper understanding of its characteristics and impact on human perception can be gained. This investigation led to the identification of scientific gaps and research questions, as outlined in **Section 1.4**. Finally, I will systematise the content of this thesis and explain the relationships between the chapters, providing an overview of the research and its significance.

Overall, the purpose of this introductory chapter is to set the foundation for the rest of the study. It focuses on highlighting the impact of chromatic effects and providing a comprehensive approach to capturing, analysing, describing, and visualising the chromatic structure of the environmental light. This will provide a framework for understanding and evaluating the perception-based lighting research presented in subsequent chapters [18, 24, 27, 29].

1.2. THE SPECTRAL STRUCTURE OF THE LIGHT FIELD

The understanding of the environmental light that fills a three-dimensional space is essential for lighting design. This is because the way light interacts with the surfaces and objects in a scene has a major impact on the optics and therefor on how we perceive the three-dimensional structure of that scene. Additionally, the appearance of a scene is largely dependent on the environmental light. The light-based approach captures the complexity of the light field by characterising the amount of spectral radiance (λ) that travels in every direction (θ, ϕ) through every point (x, y, z) in space at any given time (t). This method is well-established and has been used for measuring the variations of light properties across a scene and over time [14, 24, 30–34]. This function, termed the plenoptic function [33] in the field of perceptual science, expands on the original light field concept proposed by Gershun [30] by including the dimensions of wavelength and time. By capturing all the optical information present to an observer at a given point in space and time, the plenoptic function gives a complete description of the actual environmental light, making it an invaluable tool for quantifying and designing lighting environments.

The examination of the light field is a complex task, but it can be sampled as a spatially distributed collection of illumination maps that each can be represented as a High Dynamic Range (HDR) panoramic image (Figure 1.1). To account for the temporal component, a continuous capture of panoramic images is required. The light field is described in terms of radiometry, which takes into account the physical characteristics of light, such as its spectral power distribution and radiant intensity. However, since light and colour perception is ultimately based on the sensitivity of human observers, the raw radiometric measurements must be converted to photometric and colorimetric measurements to relate to how the light is perceived.

Light exhibits an additive nature, meaning the illumination from multiple sources can be calculated by summing the light emission of each source. This allows us to divide a single light source into multiple sources as long as their combined light emission is equal to that of the original source. To optimise the use of natural illumination maps, researchers in computer science [35, 36] have

employed a mathematical tool called spherical harmonics (SH) decomposition. SH decomposition is analogous to Fourier Analysis in that it can break down complex signals into simpler components, but it operates on the surface of a sphere.

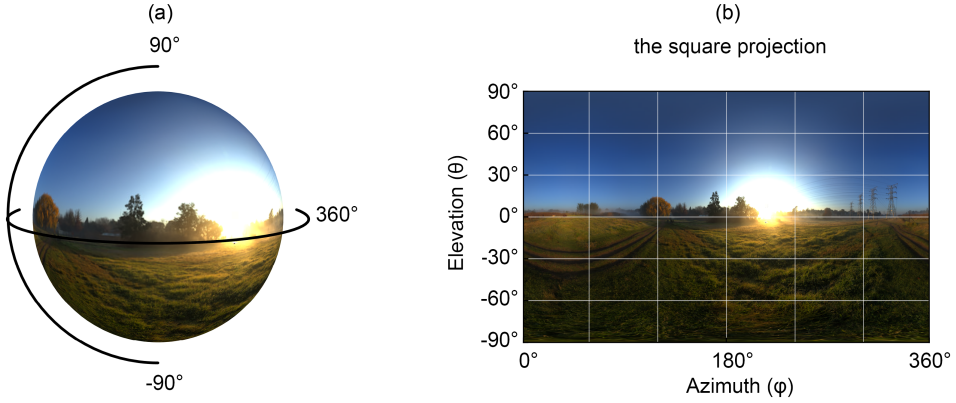

Figure 1.1: Illustration of a local light field. (A) An sRGB representation of the local light field captured as a high dynamic range panoramic image. (B) An 'unwrapped' version of the light field, where the azimuth angle (ϕ) is represented on the horizontal axis and the elevation angle (θ) is represented on the vertical axis. The environment map used in this illustration was downloaded from Blender under a Creative Commons Zero license, which allows for the free use, modification, and distribution of the work without any copyright or database restrictions.

This decomposition method represents an illumination map as a sum of mathematical components of different spherical frequencies or orders, facilitating the analysis and understanding of the light field (see Figure 1.2). Each order in the decomposition is controlled by two parameters: degree and order. The degree parameter determines the frequency of the basis functions, while the order parameter governs their alignment. This decomposition approach has been found to possess a direct physical meaning [37], and this representation is useful for quantifying the basic properties of lighting from spherical spectral measurements.

The fundamental spherical functions have increasing angular frequencies and can be expressed as a monopole, dipole, quadrupole, and so forth. The zeroth-order SH function is known as a monopole, a constant value representing the average spectral radiance in all directions. Its physical interpretation is the density of light, and it is commonly associated with fully diffuse illumination, also known as ambient light or Ganzfeld illumination [38]. An illustration of this is the light in a misty atmosphere over a snowy terrain during an overcast sky.

The first-order SH function, a dipole, features a positive and negative pole and can be portrayed as a vector that encompasses both direction and magnitude. The physical meaning of this function is the light vector or net spectral radiance transport [38]. It can be observed in light with a single dominant direction. Examples of this include spotlights and direct sunlight.

The second-order SH function, a quadrupole, is characterised by two negative or positive poles. The quadrupole contribution to the light field can be represented by a symmetric traceless tensor, commonly known as the squash tensor [37]. This tensor comprises two directions and magnitudes, and can be imagined as a light clamp or ring. For example, when light is emanating from opposite sides, it results in a light clamp with a dark ring in the centre, or in the opposite case a light ring will result accompanied by a dark clamp.

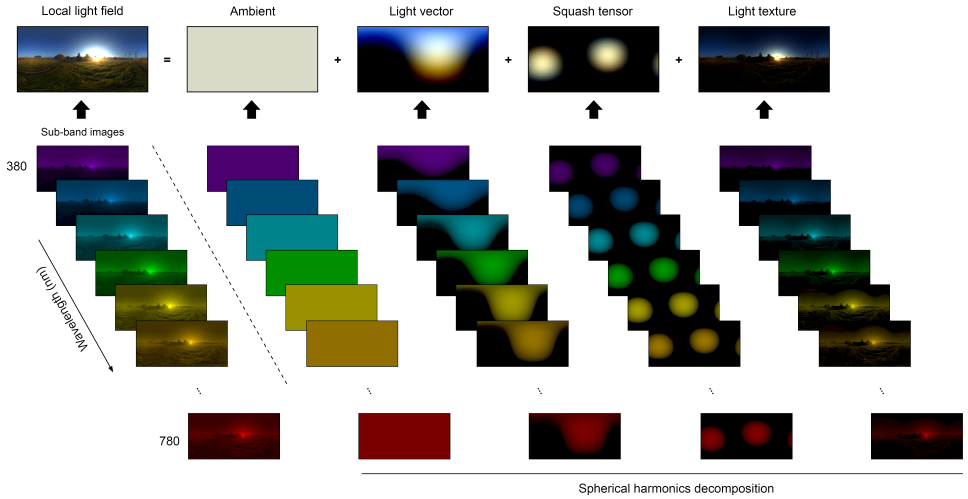

Figure 1.2: Application of spherical-harmonic decomposition to environmental illuminations. On the left, an illumination map is shown as a rectangular projection, which cannot preserve the correct area corresponding to the physical measurements on a sphere. The images on the right show the components of the SH decomposition, starting with the zeroth-order and proceeding through the first-, second-, and higher-order components. These components can be interpreted as the light density, the light vector, the squash tensor, and the fine-grained details of illumination (high-frequency angular variations in the light field). The spherical-harmonic decomposition was performed independently for each wavelength of the sub-band light-field image. The environmental illuminations were originally captured as 1024×512 RGB images, but were later approximated as hyperspectral data using Mallett *et al.*'s method [39].

The third-order and higher SH functions, which contain more complex arrangements of positive and negative poles, are less predictable in nature. However, they also display certain recurring patterns. In the domains of perception research and perception-based rendering, it is often sufficient to consider a statistical summary to grasp their characteristics [25]. This summary can be visualised as the pattern of light produced by these higher-order functions.

1.3. PERCEPTUALLY IMPORTANT PROPERTIES OF ILLUMINATION

It has been established that the three-dimensional distribution of light, which forms the foundation of a physics-based understanding of lighting, can be analysed quantitatively. By decomposing the light field into its physically meaningful components, it is possible to measure and describe its characteristics. However, understanding the physical meaning alone is insufficient for comprehending human perception of environmental light. Therefore, it is also necessary to identify the perceptually relevant properties of these light-field components and how they relate to perceptual attributes. In this regard, I reflect on recent studies on light-field properties that explore the distribution of light across directions, spatial positions, time and colour, with the goal of gaining a better understanding of the perceptual aspects of illumination. By understanding the impact of illumination on these perceptual attributes, lighting designers can strategically position and direct light sources to improve the appearance of objects, manipulate texture contrast [40, 41], accentuate certain features, and create a desired ambience, ultimately enhancing the overall visual experience in a space with a scientifically informed approach.

1.3.1. AMBIENT LIGHT

Ambient light is a type of global, uniform light source that illuminates all objects in a scene equally, providing a general level of illumination. In the perceptual domain, it reflects the overall brightness of a scene as perceived by an observer. It is used to provide a base level of illumination for all objects in the scene, and is an important property of lighting that contributes to the perception of lightness and darkness [9, 10, 42, 43]. It is often represented by the magnitude of the zeroth-order SH, and is used to estimate the brightness of environmental light [44, 45]. This illumination property is of great interest to lighting design professionals as it serves as a perceptually meaningful alternative to traditional 2D surface illumination metrics when assessing visual task performance [10]. By utilising this metric, lighting design professionals can consider whether a space appears to be bright or dim and make adjustments accordingly to create appropriate environmental lighting solutions [46].

1.3.2. FOCUS LIGHT

Focus light is a fundamental property of lighting that can be used to convey information about the position and location of objects within a scene [47]. It shapes the appearance of objects and scenes, producing shading or highlights. The direction of illumination, which corresponds to the direction of focus light, is defined as the direction of the first-order SH. The strength of focus light, as represented by the magnitude of the first-order SH, holds great importance in object shading, influencing the perception of shape, reflectance, and the ability to locate shaded targets [48]. Additionally, the direction and strength of focus light can impact the representation of corrugated surface structures, and influence the perception of surface roughness.

1

1.3.3. ILLUMINATION DIFFUSENESS

The degree to which light is dispersed across a range of 3D directions, known as illumination diffuseness, is an important property of lighting. While diffuse light, such as that found under an overcast sky, is dispersed in multiple directions, more directed light, such as that found on a sunny day, is concentrated in one direction. In an SH decomposition, diffuseness is represented by the magnitude of the zeroth-order component in relation to the first-order components [49, 50]. The diffuseness of the light is an important derived metric for the modelling characteristics of light, including the appearance of relief and volume in objects. Research has revealed that human perception has a tendency towards levels of diffuseness that are commonly found in nature [51], and that diffuseness can interact with estimates of light direction [26, 52]. In real-world scenes, measurements of light diffuseness can vary widely and are influenced by both the materials and geometry of the scene [51, 53, 54]. Grasping the interactions between material, shape, and lighting in architectural spaces poses a major challenge for lighting designers. The degree of light diffuseness is directly related to object modelling [55]. Lighting designers can leverage this metric to make informed decisions while designing, as it provides insight into how light will interact with various surfaces. Therefore, accurately measuring the light diffuseness is essential for creating optimal lighting designs.

1.3.4. HIGHER-ORDER FEATURES OF ILLUMINATION

The complexities and variations of natural illumination display recognisable patterns, such as a rise in light intensity with elevation [17]. The distribution of light intensity also tends to be skewed, following a $1/f^2$ power distribution [56, 57]. In addition to these regular patterns, natural illumination also has higher-order features such as texture and overall "gist" that can provide important information about the layout of a scene, the presence of certain objects or features, and the overall mood or atmosphere conveyed by the scene. These higher-order features aid in the rapid recognition and understanding of a scene and facilitate perception in a limited time frame.

Examining the appearance of matte and glossy objects under different levels of illumination complexity can help explain why the visual system needs to consider higher-order features in the light field [58, 59]. Research has demonstrated that even in a world that appears uniformly lit, the presence of high-frequency variations in the illumination can impact the ability to distinguish cast shadow boundaries from other types of image edges. For instance, high-frequency variations in illumination may not affect the appearance of a matte, rounded object, but the cast shadows will appear clearer when high frequencies are taken into consideration [58]. The appearance of glossy objects can be altered by the introduction of higher-order components, which impact the pattern of specular highlights [58].

The brilliance metric is a tool used to measure the degree of spikiness in the angular distribution of radiance in a light field, often referred to as brilliance. It calculates the ratio of high-order SH coefficients (orders 3 and higher) to the total sum of SH coefficients [25]. This results in a value between 0, indicating no

brilliance, and 1, indicating maximum brilliance. In practical applications, finite sampling is frequently employed, and according to Zhang *et al.* [25], the brilliance metric offers consistent results even when measurements extend beyond the 10^{th} order.

1.3.5. ILLUMINATION DISTRIBUTION OVER SPACE

The spatial distribution of light, commonly referred to as the global light field, profoundly affects the looks of objects and scenes. However, integrating the entire light-field framework and methods, including the global structure, into design can be challenging. Mury *et al.* [13] found that lower-order illumination components, which typically contain more energy, vary smoothly across spatial locations and relate to scene geometry. However, in specific situations, such as when light is filtered by trees in a forest, even lower-order components can experience sudden changes [38]. Despite the occurrence of instability, the first-order global structure of the light field, referred to as the flow of light [14, 55], can be visualised as 2D flux lines [14], which were later extended to 3D tubes by Mury *et al.* [13], and represented by arrows and ellipsoids (light "probes" or "gauge objects") in addition to tubes by Kartashova *et al.* [60].

The light flow describes the average illumination direction and its positional variability throughout the scene [61]. It can be obtained by interpolating the collection of light vectors present in the scene. The study of light flow is a topic of considerable interest due to its influential role in shaping the subjective impression of object modelling [14, 55]. The light flow is related to the perception of the (variation of) strength and direction of lighting in a space [14]. To examine how we estimate variations in illumination, researchers have used methods such as asking observers to adjust the illumination of a flat surface or spherical object, or to estimate the reflectance or shape of objects [3, 11, 59, 61, 62]. However, the local estimation does not cover the variation of light over space. Kartashova *et al.* [61] asked observers to adjust the illumination on a grid of spherical probes and reconstructed the perceived global structure of the light flow. They found that the visual light flow tubes were less curved than the ground truth optical light flow, suggesting that humans underestimate the influence of reflections on the light itself. These methods help researchers assess how accurately we can estimate the lighting in a scene and compare it to actual lighting conditions, gaining insights into the perceptual interactions between objects, material, and scenes with light.

The relationship between the perceived direction and diffuseness of light was found to be interconnected [7, 61, 63], suggesting a correlation between the perceived flow of light and its diffuseness. By estimating the distribution of light vectors across a scene, we can determine its first-order global structure. This information, combined with a measurement of light diffuseness, allows us to predict the overall appearance of the scene.

In summary, the study of the global structure of the light field, and how it is influenced by scene geometry and materials, is critical to achieving effective lighting design as it directly impacts the final appearance of scenes. Earlier efforts have laid the foundation for measuring and visualising the first-order global light field [64].

1

1.3.6. ILLUMINATION DISTRIBUTION OVER TIME

Outdoor environmental light is known to vary greatly depending on location [13, 14, 50, 65], time of day, season, and weather conditions [66–69]. Daylight, a mixture of sunlight and skylight, is spectrally dynamic, varying over short and long timescales. Downwelling irradiance spectral measurements (which are upward-facing 2D measurements taken on a horizontal plane) show that daylight typically has a correlated colour temperature (CCT) ranging from cool (~12,000 K) to warm (~2000 K), following the well-defined daylight locus [68, 70, 71]. The overall lux levels can vary over 10,000-fold, with a rapid rise and fall at dawn and dusk and a peak around midday.

Small variations in spectral properties of daylight, as measured through 2D hyperspectral imaging, over short intervals of time can have major effects on reflected light, impacting the appearance and perception of objects. Using information-theoretic methods, researchers have examined the maximum number of surfaces that can be identified as the same after an interval [69]. In the absence of illumination change, the average number of surfaces distinguishable by colour was around 10,000. However, in the presence of an illumination change, the average number of identifiable surfaces decreased rapidly with the duration of the change.

The implications of the findings discussed above extend to various aspects of colour perception, including colour appearance [72] , colour rendering [73], colour constancy [74], conspicuity of colour patterns [75], and scene articulation [76, 77]. However, relying solely on the measurement of downwelling irradiance spectra and 2D hyperspectral imaging for research into the temporal variation of daylight provides limited information on light, and not for instance its direction [78] and diffuseness. Moreover, human photoreceptor orientation is tilted toward the pupil and responds differently to light coming from various directions [79–81]. To fully capture the temporal distribution of illumination, it is essential to move beyond measuring only 2D irradiance spectra and include the capture of spherical light-field measurements.

1.3.7. ILLUMINATION COLOUR

So far, we have reviewed a series of important light-field properties that are perceptually meaningful and should be considered by designers when shaping environmental light. In lighting design, colour is an important aspect to consider. Nevertheless, most light field studies have focused on the achromatic domain and ignored the chromatic domain. Even if the sources radiate “white” light, once colours are present in a scene, the chromaticity of the light will be affected because the light reflected by one surface can fall on a second, becoming a component of the illumination incident on the second, and so on to a third, fourth, etcetera. The spectra of reflected and scattered light might be different from direct light sources, and a scene might contain several sources with different directional, spatial, and spectral characteristics, resulting in a chromatically structured light field. The influence of these differential spectral effects on the light-field structure had not been systematically studied.

1.4. RESEARCH GAP AND QUESTIONS

Advancing light field research in the chromatic domain

There exists a considerable deficit in measuring, describing and visualising the properties of the light field in the chromatic domain. Additionally, the properties of natural light, including its spectral, angular, spatial and temporal characteristics and how they interrelate and influence the scene properties, are not well understood. This thesis aims to fill these gaps in understanding and integrate the chromatic properties of the light field into lighting design processes. This will be accomplished by incorporating the chromatic domain into the light field framework, using advanced measurement techniques, computational simulations, and innovative design tools to gain insights into how light behaves in different environments and make more accurate predictions.

The research presented in this thesis is guided by four main objectives: 1) Investigating the interplay between multiple colour modes as surface and light sources in 3D indoor scenes to understand the interaction between illuminants and materials, and their effects on the spatio-spectral distribution of light and chromatic characteristics of the illumination, 2) Quantifying the directional and spatial variations of chromatic light field effects on CCT and colour rendering properties, and 3) Exploring the objective measurement, description, and visualisation of 7D light-field properties of outdoor illumination.

The initial three objectives of this study revolve around comprehending the spectral structures of light fields and their impact on colorimetric properties within the optical domain. After acquiring knowledge about the spectral characteristics of light fields and their spatial and temporal fluctuations, the subsequent step is to examine whether the human visual system is receptive to those fluctuations. Artists have a long history of exploring the qualities of light. Paintings can be seen as a human-made depictions of perceptions of a fraction of a panoramic image or a fraction of a local visual light field. Taken together, this led to objective 4) Examination of the relationship between image statistics and perceived time of day in Western European paintings from the 17^{th} to 20^{th} centuries, with the aim of determining if the representation of lighting in paintings serves as a contextual cue for the time of day.

1.5. STRUCTURE OF THE THESIS

The structure of this thesis is composed of six chapters in total, including an introduction and a conclusion. The core of the thesis is comprised of **Chapters 2-5**, which address specific research questions and present the corresponding findings and contributions. Each chapter is a standalone piece of work, presenting published (three) or submitted (one) papers.

Chapter 2: How do the chromatic effects of indirect illumination influence the different components of physical light fields in uni-chromatic spaces, and what systematic colour variations can be expected?

In this chapter, we delve into the systematic study of how indirect illumination, specifically reflections and inter-reflections, affects the different components of light

fields. Our research builds upon previous findings that the spectral power distribution of reflected light changes with the presence of inter-reflections [2]. To better understand the chromatic effects of indirect illumination, we conducted a systematic examination using a computational model that sampled representative RGB colours. Our findings indicate that these colour variations can result in changes in brightness, saturation, and even hue. We also tested the impact of coloured indirect illumination on light fields in three-dimensional spaces. By conducting cubic spectral irradiance measurements in a mock-up room setting, we quantified the chromatic variations of the first-order properties of light fields across various furnishing scenarios. Our results show that these chromatic variations are systematic and dependent on furnishing colour, lighting, and geometry. Additionally, we found that the diffuse component of light fields is more impacted than the focus component, as predicted by our computational model.

Chapter 3: How does indirect illumination affect the colorimetric properties of the effective light, specifically the correlated colour temperature and colour rendering, in uni-chromatic spaces?

In this chapter, we investigate the intricate world of colour in uni-chromatic spaces. These spaces, defined by their singular type of reflectance, offer a unique challenge as the light field is a mixture of emissive light sources and mutual surface reflections that results in a blend of diffuse and directional illumination. To better understand the impact of these factors, we measured the spectral irradiance of both the diffuse and directional light-field components in real and simulated uni-chromatic spaces, illuminating them with standard white light sources. Our findings reveal major disparities between the lamp-specified colour temperature and colour rendition and the actual light's effective correlated colour temperature and colour rendition. It becomes clear that indirect illumination holds sway over the colour temperature and rendition of the diffuse light component in comparison to the directional light component. This study underscores the need for a three-dimensional colour checker for lighting designers, architects, and computer graphics professionals, and proposes the use of simple Lambertian spheres as a solution.

Chapter 4: How can the 7-dimensional structure of the light field be effectively quantified and translated into perceptually-relevant information using the spectral cubic irradiance method, and how do variations in the light field impact the diffuse and directed components of the actual light over time, space, colour, and direction?

In this chapter, we unveil a technique for capturing the 7-dimensional essence of the light field that a human observer experiences, and translating it into perceptually meaningful information. Our spectral cubic irradiance method quantifies the objective aspects of both diffuse and directed light components, including its fluctuations over time, space, colour, direction, and its interaction with the environment, particularly sky and sunlight. Our experiments were carried out in natural surroundings and the data we gathered shed light on how vital aspects of light, such as direction, colour, and diffuseness, vary spatially and temporally in real-world conditions. This low-cost, high-impact method is a valuable addition for capturing the subtler effects of lighting on scene and object appearance, such as natural chromatic gradients, and its value is explored in detail.

Chapter 5: How do artists' depictions of natural illumination in paintings compare to the statistical regularities of actual light in terms of luminance and chromaticity, and how do these comparisons relate to human viewers' perceptions of depicted time of day in terms of image statistics, specifically luminance and chromatic variations?

In this chapter, we explore the relationships between human subjective assessments of the time of day depicted in paintings and the paintings' image statistics, including luminance and chromaticity variations. Through two online rating experiments, our findings indicated that viewers were able to differentiate between morning and evening depictions based on image statistics such as brightness, contrast, saturation, and hue. A predictive model was created that successfully explains 76% of the variance in time-of-day perception. These results show that humans are often capable of estimating the time of day in paintings by utilising cues that correspond to luminance and chromaticity variations of daylight.

In the end, **Chapter 6** brings the thesis to a close by summarising the key contributions and discoveries. Furthermore, limitations and potential avenues for future investigation are explored.

REFERENCES

[1] E. A. Abbott. *Flatland: A Romance of Many Dimensions (London: Seeley & Co.)* 1884.

[2] M. S. Langer. “A model of how interreflections can affect color appearance”. In: *Color Research & Application* 26.S1 (2001), S218–S221.

[3] K. Doerschner, H. Boyaci, and L. T. Maloney. “Human observers compensate for secondary illumination originating in nearby chromatic surfaces”. In: *Journal of vision* 4.2 (2004), pp. 92–105.

[4] M. G. Bloj, D. Kersten, and A. C. Hurlbert. “Perception of three-dimensional shape influences colour perception through mutual illumination”. In: *Nature* 402.6764 (1999), pp. 877–879.

[5] A. I. Ruppertsberg and M. Bloj. “Reflecting on a room of one reflectance”. In: *Journal of Vision* 7.13:12 (2007), pp. 1–13.

[6] J. Golz and D. I. A. MacLeod. “Influence of scene statistics on colour constancy”. In: *Nature* 415.6872 (2002), pp. 637–640.

[7] J. J. Koenderink, S. C. Pont, A. J. van Doorn, A. M. L. Kappers, and J. T. Todd. “The visual light field”. In: *Perception* 36.11 (2007), pp. 1595–1610.

[8] L. Xia, S. C. Pont, and I. Heynderickx. “The visual light field in real scenes”. In: *i-Perception* 5.7 (2014), pp. 613–629.

[9] A. Gilchrist and A. Jacobsen. “Perception of lightness and illumination in a world of one reflectance”. In: *Perception* 13.1 (1984), pp. 5–19.

[10] C. Cuttle. “Towards the third stage of the lighting profession”. In: *Lighting Research & Technology* 42.1 (2010), pp. 73–93.

[11] L. Xia, S. C. Pont, and I. Heynderickx. “Effects of scene content and layout on the perceived light direction in 3D spaces”. In: *Journal of Vision* 16.10 (2016), pp. 14–14.

[12] S. Pont and J. Koenderink. “Surface illuminance flow”. In: *Proceedings. 2nd International Symposium on 3D Data Processing*. Visualization and Transmission. IEEE. Thessaloniki, Greece, 2004, pp. 2–9.

[13] A. A. Mury, S. C. Pont, and J. J. Koenderink. “Representing the light field in finite three-dimensional spaces from sparse discrete samples”. In: *Applied optics* 48.3 (2009), pp. 450–457.

[14] J. A. Lynes, W. Burt, G. K. Jackson, and C. Cuttle. “The flow of light into buildings”. In: *Transactions of the Illuminating Engineering Society* 31.3_IEStrans (1966), pp. 65–91.

[15] J. J. Koenderink and S. C. Pont. “Irradiation direction from texture”. In: *Journal of the Optical Society of America A* 20.10 (2003), pp. 1875–1882.

[16] J. J. Koenderink, A. J. Van Doorn, and S. C. Pont. “Light direction from shad(ow)ed random Gaussian surfaces”. In: *Perception* 33.12 (2004), pp. 1405–1420.

[17] D.-E. Nilsson and J. Smolka. “Quantifying biologically essential aspects of environmental light”. In: *Journal of the Royal Society Interface* 18.177:20210184 (2021), pp. 1–12.

[18] S. C. Pont. “Light: toward a transdisciplinary science of appearance and atmosphere”. In: *Annual Review of Vision Science* 5 (2019), pp. 503–527.

[19] A. I. Ruppertsberg, M. Bloj, and A. Hurlbert. “Sensitivity to luminance and chromaticity gradients in a complex scene”. In: *Journal of Vision* 8.9:3 (2008), pp. 1–16.

[20] A. Hurlbert. “The Chromatic Mach Card”. In: *The Oxford Compendium of Visual Illusions*. Ed. by A. G. Shapiro and D. Todorovic. New York: Oxford Academic, 2017.

[21] A. J. van Doorn, J. J. Koenderink, J. T. Todd, and J. Wagemans. “Awareness of the light field: The case of deformation”. In: *i-Perception* 3.7 (2012), pp. 467–480.

[22] S. G. Narasimhan and S. K. Nayar. “Vision and the atmosphere”. In: *International journal of computer vision* 48.3 (2002), pp. 233–254.

[23] A. L. Gilchrist. “Perceived lightness depends on perceived spatial arrangement”. In: *Science* 195.4274 (1977), pp. 185–187.

[24] S. C. Pont. “Spatial and Form-Giving Qualities of Light”. In: *Handbook of experimental phenomenology: Visual perception of shape, space and appearance* (2013), pp. 205–222.

[25] F. Zhang, H. de Ridder, and S. C. Pont. “Asymmetric perceptual confounds between canonical lightings and materials”. In: *Journal of vision* 18.11:11 (2018), pp. 1–19.

[26] L. Xia, S. C. Pont, and I. Heynderick. “Separate and simultaneous adjustment of light qualities in a real scene”. In: *i-Perception* 8.1 (2017), pp. 1–24.

[27] L. Xia. “Perceptual metrics of light fields”. PhD thesis. Delft University of Technology, 2016.

[28] F. Zhang, H. de Ridder, P. Barla, and S. Pont. “A systematic approach to testing and predicting light-material interactions”. In: *Journal of Vision* 19.4:11 (2019), pp. 1–22.

[29] C. Cuttle. *Lighting design: a perception-based approach*. Routledge, 2015.

[30] A. Gershun. “The light field”. In: *Journal of Mathematics and Physics* 18.1-4 (1939), pp. 51–151.

[31] P. Moon and D. E. Spencer. “Modeling with light”. In: *Journal of the Franklin Institute* 251.4 (1951), pp. 453–466.

[32] P. Moon and D. E. Spencer. *The photic field*. MIT Press, 1981.

[33] E. H. Adelson, J. R. Bergen, *et al.* "The plenoptic function and the elements of early vision". In: *Computational models of visual processing* 1.2 (1991), pp. 3–20.

[34] I. Ashdown and P. Eng. "The virtual photometer: modeling the flow of light". In: *IESNA Annual Conference Technical Papers*. 1998, pp. 1–16.

[35] R. Ramamoorthi and P. Hanrahan. "An efficient representation for irradiance environment maps". In: *Proceedings of the 28th annual conference on Computer graphics and interactive techniques*. 2001, pp. 497–500.

[36] R. Basri and D. W. Jacobs. "Lambertian reflectance and linear subspaces". In: *IEEE transactions on pattern analysis and machine intelligence* 25.2 (2003), pp. 218–233.

[37] A. A. Mury, S. C. Pont, and J. J. Koenderink. "Structure of light fields in natural scenes". In: *Applied Optics* 48.28 (2009), pp. 5386–5395.

[38] A. A. Mury, S. C. Pont, and J. J. Koenderink. "Light field constancy within natural scenes". In: *Applied Optics* 46.29 (2007), pp. 7308–7316.

[39] I. Mallett and C. Yuksel. "Spectral Primary Decomposition for Rendering with sRGB Reflectance". In: *Eurographics Symposium on Rendering - DL-only and Industry Track*. Ed. by T. Boubekeur and P. Sen. The Eurographics Association, 2019.

[40] M. Mirmehdi, X. Xie, and J. Suri. *Handbook of texture analysis*. Imperial College Press, 2008.

[41] S. C. Pont and J. J. Koenderink. "Bidirectional texture contrast function". In: *International Journal of Computer Vision* 62 (2005), pp. 17–34.

[42] J. T. Todd. "On the ambient optic array: James Gibson's insights about the phenomenon of chiaroscuro". In: *i-Perception* 11.5 (2020), pp. 1–20.

[43] A. Gilchrist, C. Kossyfidis, F. Bonato, T. Agostini, J. Cataliotti, X. Li, B. Spehar, V. Annan, and E. Economou. "An anchoring theory of lightness perception." In: *Psychological review* 106.4 (1999), p. 795.

[44] L. Xia, N. Xiao, X. Liu, T. Zhang, R. Xu, and F. Li. "Determining scalar illuminance from cubic illuminance data. Part 1: Error tracing". In: *Lighting Research & Technology* 55.1 (2023), pp. 47–61.

[45] L. Xia, Y. Gu, X. Liu, T. Zhang, and R. Xu. "Determining scalar illuminance from cubic illuminance data. Part 2: Tests in real lighting environments and an approach to improve its accuracy". In: *Lighting Research & Technology* 55.1 (2023), pp. 62–78.

[46] P. Raynham, J. Unwin, and L. Guan. "A new metric to predict perceived adequacy of illumination". In: *Lighting Research & Technology* 51.4 (2019), pp. 642–648.

[47] S. C. Pont, A. J. van Doorn, and J. J. Koenderink. “Estimating the illumination direction from three-dimensional texture of Brownian surfaces”. In: *i-Perception* 8.2 (2017), pp. 1–12.

[48] W. J. Adams. “A common light-prior for visual search, shape, and reflectance judgments”. In: *Journal of Vision* 7.11:11 (2007), pp. 1–7.

[49] L. Xia, S. C. Pont, and I. Heynderickx. “Light diffuseness metric part 1: Theory”. In: *Lighting Research & Technology* 49.4 (2017), pp. 411–427.

[50] L. Xia, S. C. Pont, and I. Heynderickx. “Light diffuseness metric, Part 2: Describing, measuring and visualising the light flow and diffuseness in three-dimensional spaces”. In: *Lighting Research & Technology* 49.4 (2017), pp. 428–445.

[51] Y. Morgenstern, W. S. Geisler, and R. F. Murray. “Human vision is attuned to the diffuseness of natural light”. In: *Journal of Vision* 14.9:15 (2014), pp. 1–18.

[52] S. C. Pont and J. J. Koenderink. “Matching illumination of solid objects”. In: *Perception & psychophysics* 69.3 (2007), pp. 459–468.

[53] L. Xia, T. Zhang, X. Liu, and S. C. Pont. “Lighting effects, light distribution matters”. In: *SID Symposium Digest of Technical Papers*. Vol. 50. Wiley Online Library. 2019, pp. 956–958.

[54] S. Pont, L. Xia, and T. Kartashova. “The optics, perception and design of light diffuseness in real scenes”. In: *Journal of Vision* 17.10 (2017), pp. 131–131.

[55] C. Cuttle. “Lighting patterns and the flow of light”. In: *Lighting Research & Technology* 3.3 (1971), pp. 171–189.

[56] W. J. Adams, G. Kucukoglu, M. S. Landy, and R. K. Mantiuk. “Naturally glossy: Gloss perception, illumination statistics, and tone mapping”. In: *Journal of Vision* 18.13:4 (2018), pp. 1–16.

[57] R. O. Dror, A. S. Willsky, and E. H. Adelson. “Statistical characterization of real-world illumination”. In: *Journal of Vision* 4.9:11 (2004), pp. 821–837.

[58] R. F. Murray and W. J. Adams. “Visual perception and natural illumination”. In: *Current Opinion in Behavioral Sciences* 30 (2019), pp. 48–54.

[59] K. Doerschner, H. Boyaci, and L. T. Maloney. “Testing limits on matte surface color perception in three-dimensional scenes with complex light fields”. In: *Vision Research* 47.28 (2007), pp. 3409–3423.

[60] T. Kartashova, H. de Ridder, S. F. te Pas, and S. C. Pont. “A toolbox for volumetric visualization of light properties”. In: *Lighting Research & Technology* 51.6 (2019), pp. 838–857.

[61] T. Kartashova, D. Sekulovski, H. de Ridder, S. F. te Pas, and S. C. Pont. “The global structure of the visual light field and its relation to the physical light field”. In: *Journal of Vision* 16.10:9 (2016), pp. 1–16.

[62] M. Toscani, K. R. Gegenfurtner, and K. Doerschner. “Differences in illumination estimation in #thedress”. In: *Journal of Vision* 17.1:22 (2017), pp. 1–14.

[63] S. C. Pont and J. J. Koenderink. “Matching illumination of solid objects”. In: *Perception & psychophysics* 69.3 (2007), pp. 459–468.

[64] T. Kartashova, S. F. te Pas, H. de Ridder, and S. C. Pont. “Light shapes: Perception-based visualizations of the global light transport”. In: *ACM Transactions on Applied Perception (TAP)* 16.1 (2019), pp. 1–17.

[65] S. M. Nascimento, K. Amano, and D. H. Foster. “Spatial distributions of local illumination color in natural scenes”. In: *Vision research* 120 (2016), pp. 39–44.

[66] D. H. Foster, K. Amano, and S. M. Nascimento. “Time-lapse ratios of cone excitations in natural scenes”. In: *Vision research* 120 (2016), pp. 45–60.

[67] J. J. Granzier and M. Valsecchi. “Variations in daylight as a contextual cue for estimating season, time of day, and weather conditions”. In: *Journal of vision* 14.1:22 (2014), pp. 1–23.

[68] R. Pastilha and A. Hurlbert. “Seeing and sensing temporal variations in natural daylight.” In: *Progress in Brain Research* 273.1 (2022), pp. 275–301.

[69] D. H. Foster. “Fluctuating environmental light limits number of surfaces visually recognizable by colour”. In: *Scientific Reports* 11.1 (2021), p. 2102.

[70] J. Hernández-Andrés, J. Romero, J. L. Nieves, and R. L. Lee. “Color and spectral analysis of daylight in southern Europe”. In: *Journal of the Optical Society of America A* 18.6 (2001), pp. 1325–1335.

[71] G. Wyszecki and W. S. Stiles. *Color science: concepts and methods, quantitative data and formulae*. John Wiley & Sons, 2000.

[72] M. D. Fairchild and L. Reniff. “Time course of chromatic adaptation for color-appearance judgments”. In: *Journal of the Optical Society of America A* 12.5 (1995), pp. 824–833.

[73] M. J. Murdoch. “Dynamic color control in multiprimary tunable LED lighting systems”. In: *Journal of the Society for Information Display* 27.9 (2019), pp. 570–580.

[74] O. Rinner and K. R. Gegenfurtner. “Time course of chromatic adaptation for color appearance and discrimination”. In: *Vision research* 40.14 (2000), pp. 1813–1826.

[75] J. A. Endler. “The color of light in forests and its implications”. In: *Ecological monographs* 63.1 (1993), pp. 1–27.

[76] L. T. Maloney and J. A. Schirillo. “Color constancy, lightness constancy, and the articulation hypothesis”. In: *Perception* 31.2 (2002), pp. 135–139.

[77] K. J. Linnell and D. H. Foster. “Scene articulation: dependence of illuminant estimates on number of surfaces”. In: *Perception* 31.2 (2002), pp. 151–159.

[78] A. K. Diakite and M. Knoop. “Data-driven spectral sky models: A review”. In: *Journal of the International Colour Association* 23 (2019), pp. 55–61.

[79] A. M. Laties. “Histological techniques for study of photoreceptor orientation”. In: *Tissue and Cell* 1.1 (1969), pp. 63–81.

[80] A. M. Laties, P. A. Liebman, and C. E. Campbell. “Photoreceptor orientation in the primate eye”. In: *Nature* 218.5137 (1968), pp. 172–173.

[81] W. S. Stiles and B. H. Crawford. “The luminous efficiency of rays entering the eye pupil at different points”. In: *Proceedings of the Royal Society of London. Series B* 112.778 (1933), pp. 428–450.

2

EFFECTS OF INTER-REFLECTIONS ON THE CHROMATIC STRUCTURE OF THE LIGHT FIELD

Chromatic properties of the effective light in a space are hard to predict, measure, and visualise. This is due to complex interactions between materials and illuminants. Here we describe, measure and visualise the effects of inter-reflections on the structure of the physical light field for diffusely scattering scenes. The spectral properties of inter-reflections vary as a function of the number of bounces they went through. Via a computational model, these spectral variations were found to be systematic and correspond with brightness, saturation and hue shifts. We extended our light-field methods to measure and understand these spectral effects on the first-order properties of light fields, the light density and light vector. We tested the model via a set of computer renderings and cubic spectral illuminance measurements in mock-up rooms under different furnishing scenarios for two types of illuminants. The predicted spectral variations were confirmed and indeed varied systematically within the resulting light field, spatially and directionally. Inter-reflections predominantly affect the light density spectrum, and have less impact on the light vector spectrum. It is important to consider these differential effects for their consequences on the colour rendering of 3-dimensional objects and people.

Published as: C. Yu, E. Eisemann, and S. Pont. "Effects of inter-reflections on the chromatic structure of the light field". In: *Lighting Research & Technology*. 55.2 (2023), pp. 218–236. DOI: 10.1177/14771535211058202

2.1. INTRODUCTION

How can we completely describe the light in a space and understand its interactions with that space? The interaction between light and objects shapes the lighting distribution and determines scene appearance. Objects in common conditions are illuminated by both direct light sources and indirect light originating from secondary and higher-order sources, that is, light that is (inter-)reflected, scattered, refracted, *etc.* Hence, the effective light in a space is usually complex, varying directionally, spatially and spectrally. In former work, our lab addressed how the spatial and directional structure of the light field can be described, measured and visualised in perceptually-relevant ways [1–4]. In the current study, we extend these methods to the spectral domain, and we model the effects of inter-reflections in coloured spaces to understand its basic mechanisms impacting the spectral light-field structure.

The effective light can be described as a light field; the spectral power distribution (E) for a given wavelength λ, arriving from a direction (θ, ϕ) at a point (x, y, z) in the scene [5–9]. This real-valued spherical function describes the entire distribution of spectral power within the volume of the space. This function thus captures all optic information available in the space, including both the angular, spatial and spectral power variations.

The light field can be described in a tractable, physically and perceptually meaningful manner via a spherical harmonics approximation [2, 4, 10–12], a sort of Fourier decomposition for spherical functions. In this approach, the optical structure of the light field can be represented as a combination of components of different mathematical orders, which were found to represent physically and perceptually meaningful entities, *i.e.*, the light density, the light vector, the squash tensor, and statistical summary of the higher-order angular frequencies, plus their spatial variations. The light density, the zeroth-order light-field component, is a scalar property that can be measured by integrating the spectral power over all directions. The first-order light-field component, the light vector, indicates the direction of net transport of radiant energy. The spatial variation of the light vectors is referred to as light flow. The ratio between the light vector and light density provides an estimate of diffuseness [1]. The light density, light flow and light diffuseness form an integrated complete description of the lowest-order properties of the light field distribution in a three-dimensional space [12], which are directly related to our perceptions of the average illuminance, light direction, diffuseness, flow, and zones [13–15] and indirectly to our perceptions of space, shape, materials, and textures etcetera [16–22]. The light squash and higher-order light-field statistics are directly related to scene cohesion and gist [23] and indirectly to, for instance, material perception [9, 24, 25].

In natural scenes, the diffuse scattering mode forms a significant contribution to the bidirectional reflectance distribution function (BRDF) of most materials [26, 27] (NB: in a first order approach a BRDF can be approached as a linear combination of scattering modes). For matte or Lambertian materials, scattering diffusely, the BRDF acts as a low-pass filter on directional variations in the light field. Consequentially, in scenes primarily containing matte (or "Lambertian") materials, and scenes

containing materials with a significant diffuse scattering mode (which applies to most natural scenes), the appearance is determined predominantly by the low-pass components (up to the second order: light density, light vector and squash tensor) of the incident light [28]. The second-order light field structure can be measured by a dodecahedron shaped "plenopter" [12]. However, the resulting light-squash data is currently still hard to interpret and use in practical lighting design. With a cubic illumination meter, we can measure up to the first-order light-field structure [1, 29], and human observers can perceive and adjust the light density and light vector, both separately and simultaneously [3, 13, 30]. Representation of the light field up to its first order (light density and vector) still explains 94% of the appearance variations for Lambertian surfaces [31, 32]. Therefore, we employed the first-order approach for its practicality and ease of implementation with the current state of the art.

Inter-reflection refers to reciprocally reflected light from non-luminous surfaces, creating secondary sources. It is a common optical phenomenon occurring in concavities in natural scenes, for instance, corners between walls, ceiling and floor, or between objects and the ground they are on. The spectral power distribution (SPD) of inter-reflected light is dependent on the SPD of the light source and the spectral reflectance function (SRF) of the reciprocally reflecting surfaces. Undergoing many light reflections between mutual surfaces, the SPD undergoes a non-uniform and non-linear transformation except for perfectly neutral reflecting surfaces. Figure 2.1 shows an example of an ocre coloured room - which has high reflectivity in the long-wavelength part of the spectrum and low in the short- and middle-wavelength range. E2 was measured in the corner and showed the influence of the (inter-)reflections, compared to E1, which was measured in the centre, under the white source. Spectral power attenuation is exponential and relatively strong for wavelengths, where the surface displays low spectral reflectivity (Figure 2.1, E2, the left part). High spectral reflectivity, in contradistinction, results in insignificant attenuation (Figure 2.1, E2, the right part). Due to this non-uniform and non-linear spectral power attenuation in the presence of inter-reflections, the light field in non-neutrally coloured spaces will show spatial and directional spectral variations [33–37].

Acting as the major secondary sources of illumination in Lambertian scenes or any scene with materials having major diffuse reflectance modes (thus, almost any scene), inter-reflections influence the light field in a manner that depends on the geometry of space and sources, the spectral reflectances and the light spectrum. It has been intensely analysed how inter-reflections can affect the luminous properties of low-order light field components in the achromatic domain [3, 38–42]. A few studies have also shown the significance of inter-reflections in determining colour appearance [43–45]. However, the impact of inter-reflections on the spectral properties of the light field has not yet been described in an integral manner with its spatial and directional properties.

The current study aims to understand the basic optical mechanisms behind chromatic effects of inter-reflections and their influence on the first-order physical structure of the light field, and to extend our light-field framework and methods to the spectral domain. To this aim, we present a theory for how the spectra of

indirect light vary as a function of the number of inter-reflections or bounces they went through. We demonstrate these phenomena empirically in the second part of the paper via physically-based computer simulations and optical measurements in mock-up spaces, including how the light density and light vector are affected spectrally and spatially by colours in the environment. We also show how the spectral light density and vector can be simultaneously measured using a cubic spectral illumination meter, quantifying spatial, angular and spectral variations of chromatic light fields.

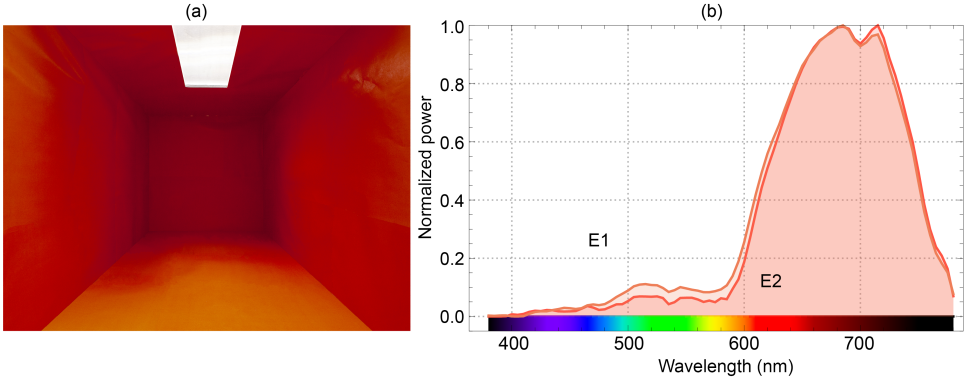

Figure 2.1: An example of chromatic inter-reflection effects. (a) Photograph of a box space with a uni-chromatic ocre finish illuminated by white light. (b) Two of the illuminance spectra measured in the box space. E1 indicates the spectrum measured in the centre facing the back wall. E2 indicates the spectrum measured at the same height and in the same attitude, in the back left corner.

2.2. THEORY

A coarse-grained spectral approach to understand basic mechanisms underlying chromatic inter-reflections

For hyperspectral representations, it is impossible to study all possible spectra and estimate their inter-reflection effects. In order to study the basic mechanisms of chromatic inter-reflection effects, we instead took a coarse-grained spectral approach. This was shown to work well to describe the human ecology [46, 47], because most object colours have rather smooth spectra [48]. Such smooth spectra can in a coarse-grained approach be described by the energy in three bins, say, BGR. Once the fundamental mechanisms are understood, it is relatively easy to extrapolate the methods to hyperspectral data.

Now consider Lambertian material or, more generic and omnipresent, the diffuse scattering mode of material, and neutral white (equal energy) direct lighting, that is, an $(E_B, E_G, E_R) = (1, 1, 1)$ spectrum. This lighting illuminates the material of a certain (S_B, S_G, S_R) spectral reflectance. The first bounce results in a "spectrum" of $(E_{1B}, E_{1G}, E_{1R}) = (S_B, S_G, S_R)$. The second bounce by the same material has a

"spectrum" of $(E_{2B}, E_{2G}, E_{2R}) = (S_B^2, S_G^2, S_R^2)$. The third bounce results in (S_B^3, S_G^3, S_R^3) and so forth. In summary, the spectrum of the n-th bounce is

$$(E_{nB}, E_{nG}, E_{nR}) = \left(S_B^n, S_G^n, S_R^n\right) \tag{2.1}$$

Since the spectral power in each band is attenuated exponentially, this can cause relative differences between them depending on the number of bounces. The respective ratios of spectral power between each band change with each reflection, and thus lead to a change of the spectrum's shape. In effect, this results in shifts towards colours corresponding with the peak(s) of the material reflectance spectrum. If applied in the coarse-grained BGR approach, we find that homogeneously sampled reflectance spectra result in higher-order reflections with spectra that are very non-homogeneously clustered in this space (Figure 2.2). In other words, inter-reflections can cause strong spectral changes.

The spectral changes and associated colour shifts can be of various types, depending on the ratios of the spectral reflectance (S_B, S_G, S_R). Spectra on straight lines between the vertex (0, 0, 0) and all other vertices show a power attenuation and associated brightness decrease with each inter-reflection until reaching (0, 0, 0) or "black" in the limit (see Figure 2.3 left), while the peak position / band remains constant. Note that for these spectra the ratios of the spectral reflectance are either 0, 1 or infinite. The ratios remain despite the exponential attenuation of the individual bands. Thus, the associated hues stay the same, while the power will decrease for individual orders of inter-reflections.

Spectra on straight lines between white (1, 1, 1) and the single-peaked or the double-peaked reflectance spectra become more peaked for higher orders. This can be associated with materials having pastel colours, which will show saturation increases in regions with many inter-reflections (see Figure 2.3 middle). For both types, for higher-order reflections, the power attenuations of the troughed band(s) are relatively stronger than the remaining band(s). The single-peaked type can be associated with a saturation increase towards the monochromatic colour corresponding with the peak, whereas the double-peaked type can be associated with a saturation increase towards mixing colour corresponding with the two peaks. Spectra on straight lines between the single-peaked spectra and their adjacent double-peaked spectra show different levels of power attenuations and associated hue shifts, *i.e.* in our coarse-grained model the reddish magentas and yellows shift to red, greenish cyans and yellows shift to green, and blueish cyans and magentas shift to blue. Those spectra have one band at peak value 1, another at 0, and the remaining band has a value between 0 and 1. The power attenuation of that remaining band leads to dominance of the spectral peak and an associated hue shift towards the monochromatic colour represented by that peak (see Figure 2.3 right).

Our simplified computational model using coarse-grained BGR spectra has outlined different categories of power attenuations and their associated colour effects that can happen as a consequence of inter-reflections. The associated brightness changes, saturation effects and hue shifts can happen simultaneously for other spectra which are not on the vertices, edges and diagonals. The model can easily be extended

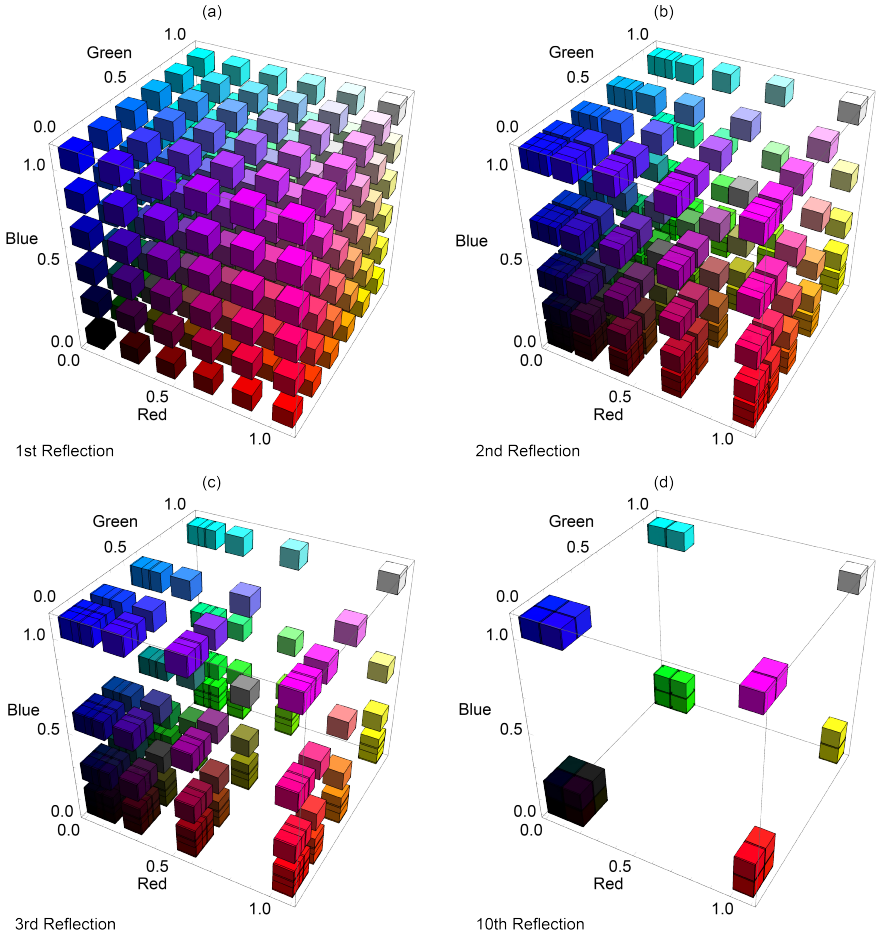

Figure 2.2: (a) First, (b) second, (c) third, and (d) tenth (inter-)reflections of colours plotted in the BGR coordinates under equal energy white lighting.

to hyperspectral cases with arbitrary illuminant spectra. If a material with spectral reflectance S_λ is illuminated by a light source with the SPD to be E_λ, the n-th bounce of the (inter-)reflections leads to

$$E_{n\lambda} = E_\lambda \cdot S_\lambda^n \tag{2.2}$$

Thus, for white(-ish) light with a continuous spectrum, the phenomena will be perceptually similar to the coarse-grained simplifications: the troughs of the reflectance spectrum are attenuated much more than the peaks, so that brightness, saturation and hue shifts can occur. As those spectral effects are also subject to the SPD of the direct lighting, these associated chromatic effects can be boosted

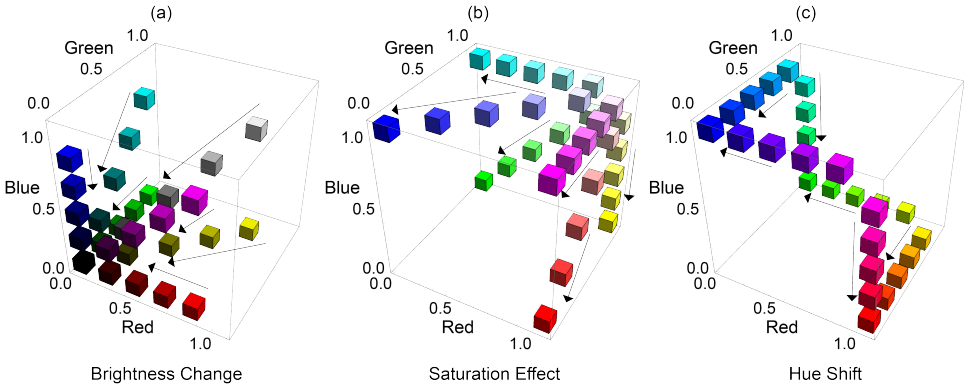

Figure 2.3: A schematic representation of the spectral effects of the (inter-)reflections in our coarse-grained model. It shows the categorised spectral effects in BGR space. The changes (in the directions of the arrows) can be associated with (a) brightness changes, (b) saturation effects, and (c) hue shifts.

or counteracted by spectral tuning of the source. However, since natural SPDs are usually quite smooth, and since the power distributions of white light sources are tuned to the sensitivity of the human visual system, it is expected that the phenomena can still be predicted and explained on the basis of this fundamental mechanism. Please also note that here we modelled the spectrum of each individual order of inter-reflection, while in natural scenes, the final effect will be a sum of (infinitely) many of them weighted by geometry-dependent factors [38, 43, 45]. In the following sections we will first test the effect of that summation in computer simulations, and next test effects in real scenes with realistic hyperspectral conditions.

2.3. EMPIRICAL TESTING 1

Chromatic inter-reflection effects in computer simulations of a box space

This experiment aims to empirically verify whether the three types of spectral effects indeed occur in simple scenes as predicted and test how accumulated orders of inter-reflections combined with direct lighting impact the final reflected spectra. We simulated a wide range of material spectral reflectance with homogeneous sampling over BGR space for a simple geometrical case and analyse the results in image space (Section 2.3.2). Next, we also analyse the effects on the first-order structure of the resulting light fields for two cases: a white room and an ocre room, for which we first explain how we extend our light field framework to the spectral domain (Section 2.3.3).

2.3.1. METHODS

A digital model of a simple box space was set up with the length, width and height to be 6000 mm × 3300 mm × 3300 mm. The space was illuminated by an 1884 mm × 773 mm uniform diffuse light panel recessed in the centre of the ceiling. Its luminous flux is 3500 lm with an equal energy flat spectrum. For the reflectance spectra we evenly sampled the BGR space with values of 0.1, 0.5 and 0.9, leading to 3 × 3 × 3 = 27 BGR spectra. We intentionally avoided sampling spectra on the vertices and edges (having a reflectance of 100% or 0% in at least one band) for physical realism. All surfaces within the box space were Lambertian and one of the twenty-seven herefore selected reflectance spectra. The space was rendered for only direct illumination and total (direct + indirect) illumination separately. Since the direct lighting from the diffuse light panel has an equal-energy-white spectrum, the spectrum of each individual reflection are exactly in line with the described inter-reflection theory. The simulations then show how these add up to a final appearance, depending on the walls' reflectance spectrum (and of course the scene geometry and the photometrical properties of the light source).

Based on the theory, we predicted what chromatic effects of inter-reflections would show in the total illumination images - especially for the corners, ceiling and deeper parts of the spaces, where inter-reflections have the biggest impact. Three types of chromatic effects of inter-reflections were expected to occur simultaneously, and the predominant types of spectral effects were predicted to be different depending on the walls' reflectance spectra. We divided the spectra into four groups named according to those predominant types. The first "control group" contains reflectance spectra that are adjacent to the vertices in the coarse-grained BGR space. The "brightness-change group" consists of spectra that have one or more bands with 0.5 spectral reflectance and the rest of the bands, if any, of 0.1. The "saturation-effect group" consists of spectra between neutral ("white") and the single-peaked or the double-peaked BGR spectra (associated with pastel colours). Those spectra have one or two bands with a reflectance of 0.9 and the rest of 0.5. The power attenuation of the band(s) that have 0.9 reflectance is comparatively smaller than that of the band(s) with 0.5 reflectance, resulting in saturation effects towards the peak reflectances. The spectra in the hue-shift group have one band with 0.9, one with 0.1 and the other one with 0.5 reflectance. These spectra are predicted to show hue shifts because higher-order reflections attenuate the bands with lower reflectance more. Consequently, shifts occur towards the peak reflectance.

We used the Autodesk Raytracer (ART) render engine (a physics-based renderer). The HDR output of the engine might include values beyond the display capability of a typical monitor. We used the tone-mapped LDR (Low Dynamic Range) images for display purposes. The tone mapping operator (TMO) first linearises the pixel values without any clamping and then applies a standard 2.2 gamma correction. This TMO aims to map brightness differences in a perceptually uniform manner but exaggerates the colour effects of inter-reflections (which also follow a power law) (see [49] for details). For physical accuracy, raw HDR (High Dynamic Range) outputs were used for the numerical analysis.

2.3.2. RESULTS IN IMAGE SPACE

The collection of tone mapped images is shown in Figure 2.4(a), in which the predicted inter-reflection effects can be seen. To analyse the spectral effects of the accumulated orders of inter-reflections, we measured the "dominant reflected BGR spectra" of the HDR direct illumination images and the HDR total illumination images, by applying a k-means clustering [50]. The dominant BGR spectra of the direct illumination images correspond to the first-bounce reflected spectra, whereas those of the total illumination images indicate the reflected spectra of accumulated bounces. The resulting spectra were plotted in the BGR space according to our grouping (Figure 2.4(b)). The perimeter of the hexagon indicates the coarse-grained spectral locus [46, 51]. The centre is the white point. The arrows indicate the shifts from the dominant spectra of the direct illumination images to those of the total illumination images, showing the chromatic effects of inter-reflections. Shifts between white point and spectral locus indicate saturation increases, whereas those in the directions along the spectral locus consider hue shifts.

2.3.3. RESULTS IN 3D SPACE: MEASURING AND VISUALISING THE CHROMATIC LIGHT FIELD

The former analysis tested how the effects of inter-reflections influence rendered appearance in image space. But how do these effects impact the light field in the box spaces? For this analysis, we use the Delft light field framework [4]. To this aim, the first-order structure of the light field at any given point was measured via the spectral illuminance on the six faces of a small cube, see Figure 2.5. The light density and light vector of the local light field were measured via the cubic spectral illuminance, with $E_{(x+)}$ and $E_{(x-)}$ the spectral illuminance measurements in the positive and negative directions along the X-axis, and analogous for the Y and Z directions. The light density was estimated via the mean SPD of the six cubic faces (2.3). The differences in three orthogonal directions together gave an estimate of the light vector, its direction ($E_{(x)}$, $E_{(y)}$, $E_{(z)}$), magnitude E_{Vector} (2.4)–(2.7), as a function of wavelength λ, which is not included in the formulas for simplicity.

$$E_{\text{Density}} = \frac{E_{x+} + E_{x-} + E_{y+} + E_{y-} + E_{z+} + E_{z-}}{6} \tag{2.3}$$

$$E_{(x)} = E_{x+} - E_{x-} \tag{2.4}$$

$$E_{(y)} = E_{y+} - E_{y-} \tag{2.5}$$

$$E_{(z)} = E_{z+} - E_{z-} \tag{2.6}$$

$$E_{\text{Vector}} = \sqrt{E_{(x)}^2 + E_{(y)}^2 + E_{(z)}^2} \tag{2.7}$$

For the analysis of the spectral effects on the light-field components, we first simplified the hyperspectral approach as described above to a coarse-grained approach. To this aim we integrated the spectral power for three bands representing the short-, middle- and long-wavelength parts, after this shortly called "BGR" bands. The zeroth- and the first-order coarse-grained "BGR" light densities and vectors were

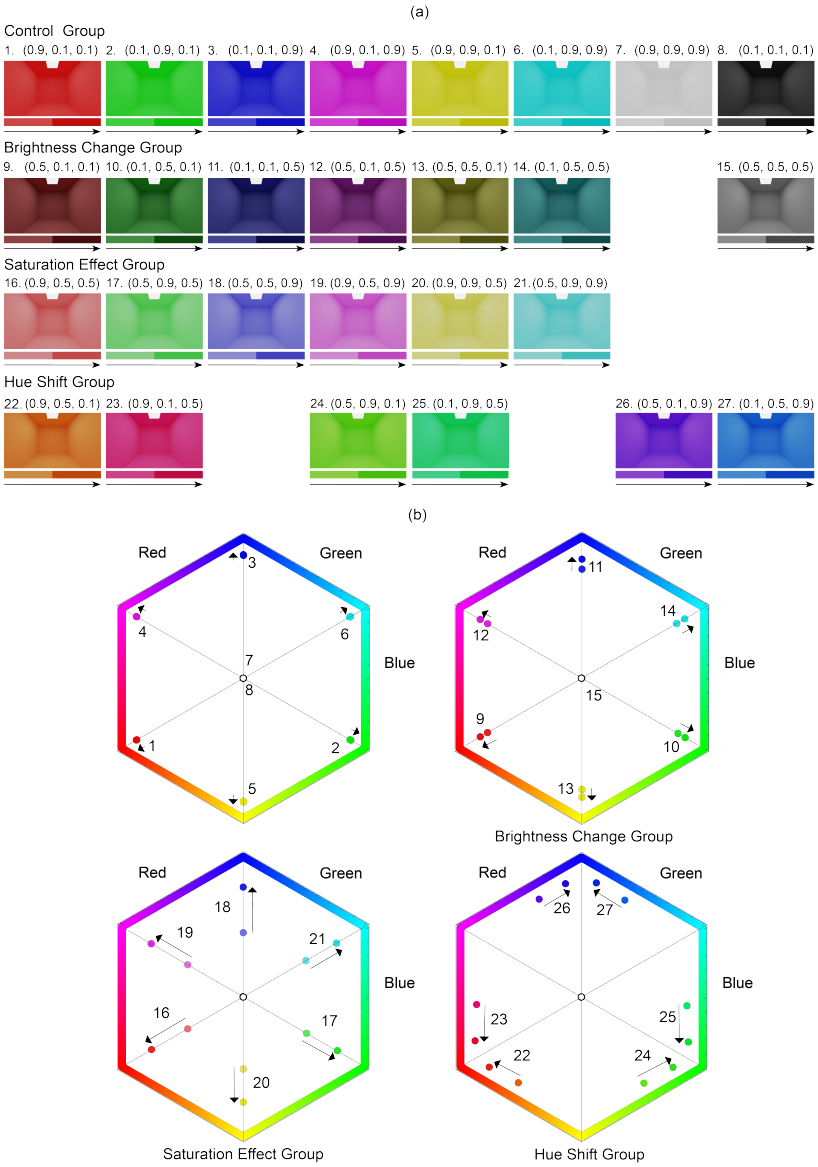

Figure 2.4: Box space renders and their associated spectral effects. (a) The collection of tone mapped total illumination images for the box spaces with different surface spectral reflectances. The selected spectra have been numbered for further reference. The renderings are divided into four groups based on the surface spectral reflectance and the corresponding predicted spectral effects of inter-reflections. (b) The power of the most dominant reflected BGR spectra within the direct and the total illumination renders plotted in the BGR space according to their grouping.

measured and visualised for a white (Figure 2.6(a)) and an ocre (Figure 2.6(b)) box space. These figures present cross sections of the room, with the light density in the upper rows and the vectors in the lower rows. The columns present the separate data for the three bands. The light density is mapped using a false colour scale (right of the plots) after scaling all data, and the light vectors are projected onto the 2D cross section. The distributions of the light densities and the light vectors for the three bands are identical in the white space, being strongest near the light source and diverging outwards, and aligned for the BGR light flows (that is, the flow structure or pattern formed by the vectors). The integrating effects of the white Lambertian surfaces cause a quite diffuse light throughout the room, which is clear from the vectors being small except near the source, and the density is quite high and uniform throughout the room. For the ocre space, the distributions of the light densities and the light vectors vary as a function of the spectral band. The higher the spectral reflectance in a particular band, the larger the magnitudes of the light densities and the smaller the magnitudes of the light vectors, due to the integrating effects. Since the spectral reflectance of the ocre finish increases from B to G to R, this effect is smallest in the B band, and largest in the R band. Thus, the BGR light flows no longer align. The light flow in the short wavelength B band diverges out from the source and ends (is absorbed) on the B light absorbing surfaces. The light flow of the long-wavelength R band is, by contrast, heavily curved. The light flow in the B band is thus much more directional than in the R band, and the G band in between.

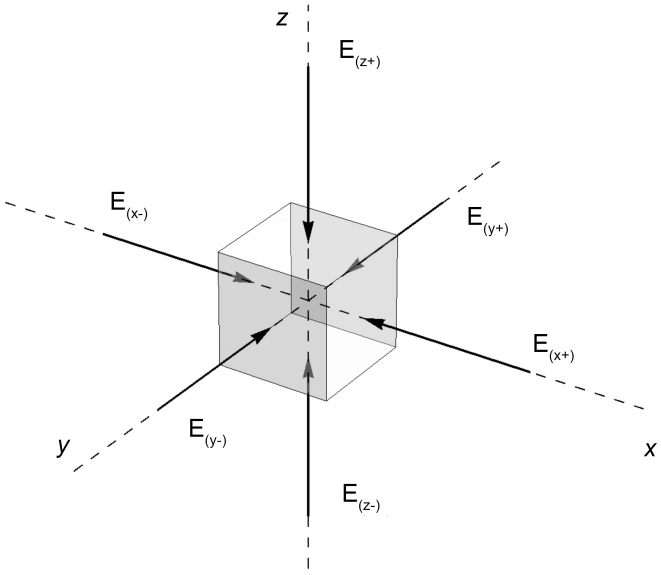

Figure 2.5: Schematic presentation of the cubic method via illuminance measurements on six faces of a small cube.

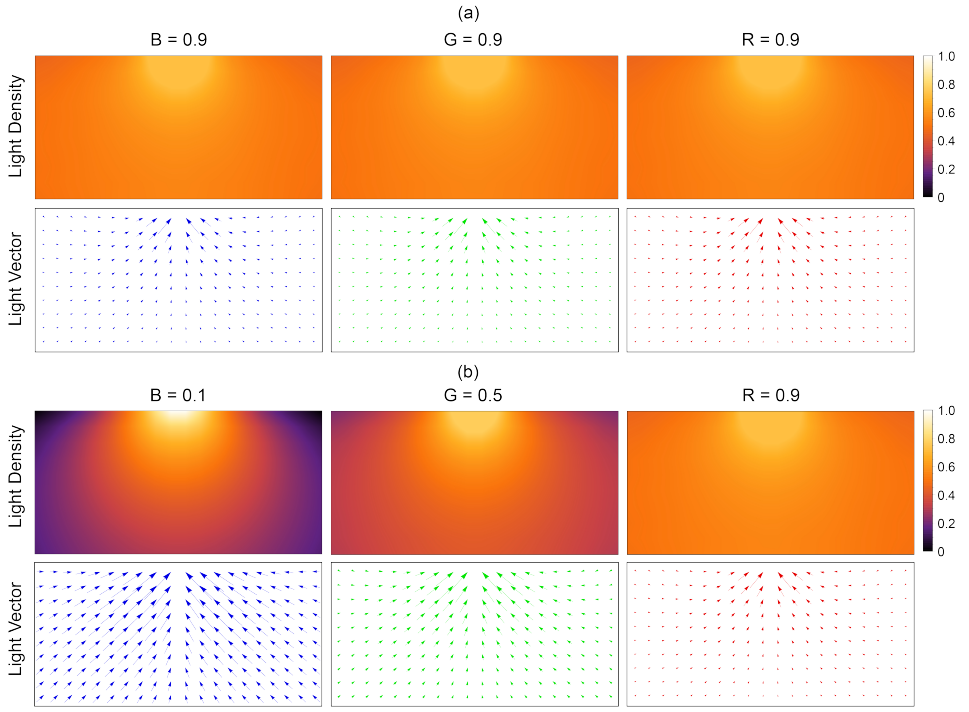

Figure 2.6: The zeroth- and first-order structure of the chromatic light fields in a white and an ocre room. Light density (top rows) and light vector (bottom rows) plots for a cross-section of the box spaces furnished in (a) white and (b) ocre. The pseudo colours of the light density plots indicate their normalised value. The vectors represent the local light vectors projected onto the cross section. The columns represent the short, middle and long wavelength bands or B, G, R bands.

2.4. EMPIRICAL TESTING 2
Chromatic inter-reflection effects in a physical box space

2.4.1. METHODS

Here, we further explore and quantify chromatic light-field effects in real room settings under natural lighting with fine spectral resolution (1 nm interval). Inter-reflections on diffusely scattering materials, because of their diffuse nature, boost the light densities and attenuate the light vectors – and, as we have seen herefore, in a manner that depends on the wavelength (band). The objective is to A) test whether the three categorised chromatic effects in the theory and computer simulations can be reproduced in a real setting with more articulated spectra and B) test the differential effects on the light-field components.

To these aims, a 1200 mm × 660 mm × 660 mm physical mock-up windowless box space (Figure 2.8 first row) was constructed. The space was illuminated by

a planar diffuse luminaire (377 mm × 155 mm). The SPD of the luminaire was tuned by modifying the lamps used. The SPDs of the two chosen illuminants are shown in Figure 2.7. Lighting scenario one was established by using a xenon lamp (CRI R_a 91.4, CCT 5461 K) only to backlight the planar diffuser, and scenario two by a fluorescent lamp (CRI R_a 84.2, CCT 4284 K). We combined these two sources with four furnishing materials to keep it tractable, representing neutral, brightness, saturation and hue shift cases (white, maroon, coral and ocre, respectively). The furnishing materials were created by white paint, or printing A3 sheets of paper with uniformly coloured BGR colours (0.1, 0.1, 0.5), (0.5, 0.5, 0.9) and (0.1, 0.5, 0.9). The SRFs of those materials were measured with a spectrophotometer. With the measurements of the SRFs of the four finishes (Figure 2.8 second row) and the SPDs of the two lamps taken, we can predict the spectral effects for separate bounces in both lighting scenes based on (2) (Figure 2.8). The spectral shape of the first, second, third and tenth bounces under both illuminants have been plotted by using the power functions presented in the theory section (third and fourth rows for the first and second lamps, respectively). Please note that the weight of each bounce in the final resulting light field is dependent on space geometry and lighting. To quantify and analyse these effects, we measured the cubic spectral illuminance in the left-back corner and the centre of the mock-up space in all four different furnishing conditions and for the two sources.

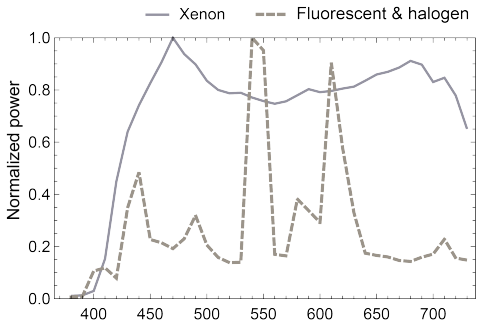

Figure 2.7: Normalised spectral power distributions of the two selected illuminants. Xenon lamp (solid line), a mixture of fluorescent and tungsten halogen (dashed line).

2.4.2. RESULTS

We first estimated and compared the light density and light vector for the centre measurements (Figure 2.9(a) first row) and corner measurements (Figure 2.9(a) second row) for all four selected finishes under the xenon lamp. The third row shows their hue (angle) and saturation (length vector with 0 representing white and 1 fully saturated). The chromatic coordinates of the spectra were calculated based on CIE 1964 10° colour-matching function.

In the white space, the SPDs of the light density and light vector were similar, as expected for the relatively flat SRF of the material, causing the light density and

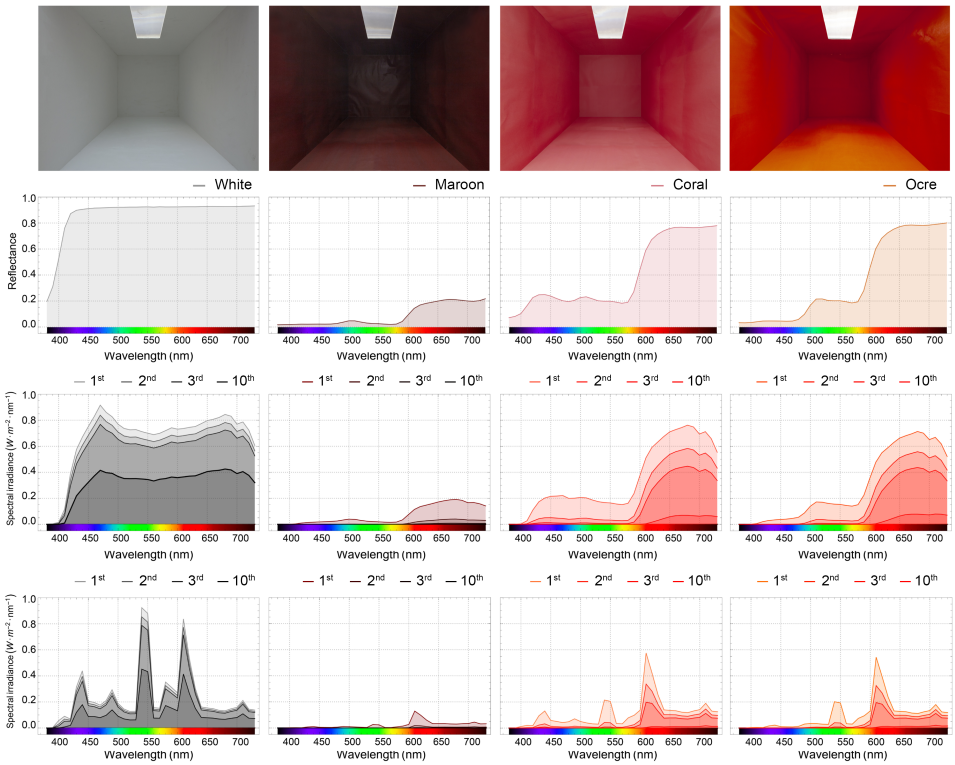

Figure 2.8: Physical mock-up windowless box spaces and predictions of the spectral effects for separate bounces in both lighting scenes. The first row shows the photographs of the box spaces. The second row shows the measured SRFs of the four selected finishes. The third row shows the associated calculated spectra for the first, second, third and tenth bounces under the xenon lamp, and the fourth row under a mixture of compact fluorescent and tungsten halogen.

light vector in the space to have a similar spectral shape as the illuminant (Figure 2.9(a) first column). The minor spectral variations might be due to the first author's skin reflections since he had to hold the meter into the box space during the measurements.

The light densities' SPDs in both the centre (D) and corner (D') of the maroon room showed minor but similar attenuations of the short- and middle-wavelength part of the spectrum relative to the long-wavelength part, while the light vectors' SPDs (V and V') were close to the illuminant spectrum (Figure 2.9(a) second column). However, the intensity for both light density and light vector decreased (not visible in the plots due to normalisations) in the corner showing the brightness effect. The hue and saturation plot showed that the light densities and vectors in both locations had similar hue and saturation.

In the coral space (Figure 2.9(a) third column), the light densities' SPDs in both

the centre (D) and corner (D') showed stronger attenuations of both the short- and middle-wavelength parts of the spectrum than the long-wavelength part, while the magnitude of attenuation was larger in the corner. The light vectors' SPDs (V and V') were closer to the illuminant spectrum in both locations, while that in the corner only showed minor attenuations of the short- and middle-wavelength part of the spectrum compared to that in the centre. The hue and saturation plot shows that the light densities were reddish and the light vectors were bluish in both locations. Meanwhile, the light density in the corner D' was more saturated than that (D) in the centre, but shared a similar reddish hue. The light vector in the corner V' was more reddish than that (V) in the centre.

The SPDs for the ocre room showed similar effects as for the coral room; that is the spectral attenuation mainly showed up for the light densities (D and D') relative to the light vectors (V and V') (Figure 2.9(a) fourth column). However, the short-wavelength part of the light density's SPD in the corner (D') attenuated more than that in the centre (D), resulting in a change of the relative difference between the short-, middle- and long-wavelength part of the spectrum. The hue and saturation plot shows that the light densities were reddish and the light vectors were bluish in both locations. Meanwhile, the light density in the corner D' was more reddish and saturated than that (D) in the centre. The light vector in the corner V' was more reddish than that in the centre (V).

In general, we see the hue variations between the light densities and the light vectors changing more and more towards red from V to D to V' to D'. The light density and light vector in the corner (D' and V') were also consistently more reddish than their corresponding light density (D) and light vector (V) in the centre. A closer look shows that the xenon source is quite blueish and so the hue plot shows that the effective spectra cover a wide range between blueish and reddish. The complex interactions between blueish direct light and reddish inter-reflections cause V' to be less saturated than V.

The second source was deliberately chosen with its highest peak at the middle-wavelength part of the spectrum (about 545 nm) and relatively poorer colour rendering to counteract the reddish material reflectance spectra somewhat. Here, the hue angle variations for the coloured rooms are relatively smaller than for the xenon lighting scenario (Figure 2.9(b)), showing the dependency on the illuminant. The V-D and V'-D' order however remained the same, as predicted before, going towards red and more saturated colours, corresponding with the expected order of impact of inter-reflections.

2.5. DISCUSSION

Light fields (the actual light in a space) are a function of position, direction and wavelength. In earlier work, the position and direction dependency was already described, measured and visualised [1–3]. Here we made the first steps to extend this concept to the spectral domain, explaining how to compute and understand the light density and light vector spectrally. We further presented several examples, including real measurements.

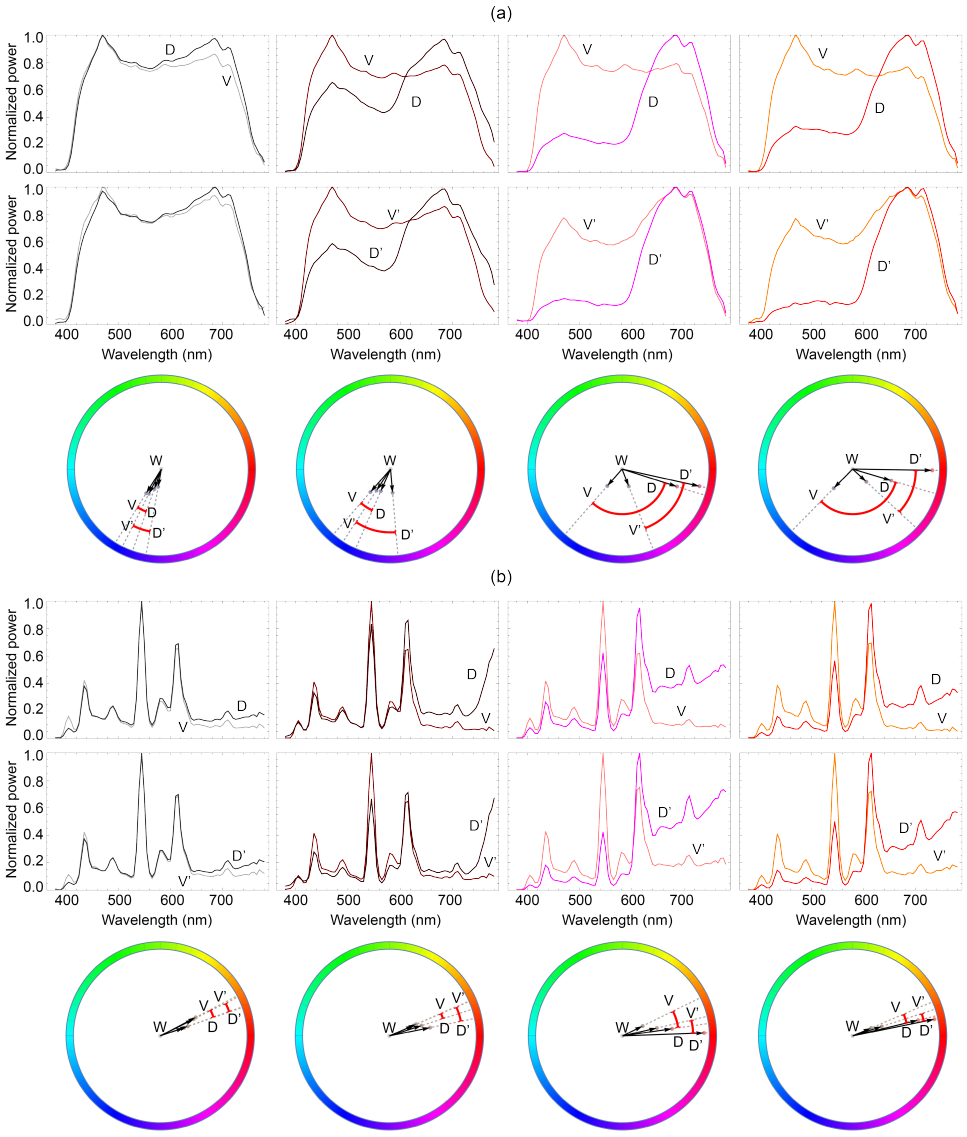

Figure 2.9: Spectral measurement results. (a) Normalised plots of the light density (D) and light vector (V) spectra of both the centre (first row) and corner (second row) measurements for four different finishes (in the rows) illuminated by a xenon lamp. The hue and saturation of the light density and light vector spectra were plotted in the hue and saturation wheel (third row). The arrows point from the reference white point W to the light density and light vector colours for the centre and corner measurements. An accent denotes the corner condition. (b) as (a) for a fluorescent lamp.

These chromatic effects of inter-reflections are dependent on the spatial arrangement, location and spectrum of the light source(s) and room furnishing spectra. In a coarse-grained approach, we derived and explained what optical mechanisms underlay the colour shifts we observed "in the wild", namely brightness, saturation and hue shifts. Under neutral white illumination with good colour rendering properties, a coarse-grained approach will suffice to describe and understand the inter-reflection phenomena of human optical ecology. Moreover, common "white" sources are tuned for optimised luminous efficiency and colour rendering and have spectra with their power distributed over the visible range. Such relative short, middle and long wavelength ratios remain rather robust, as the main effects that we demonstrated. However, if light spectra do not overlap with the material spectral peaks, the chromatic effects could be weakened or even violated. Such lighting conditions apply to metameric white illumination with poor colour rendering (*e.g.* high-pressure sodium lamp) and non-neutral illumination (*e.g.* blue skylight or a low-pressure sodium lamp). It should also be noted that most materials have rather smooth reflectance spectra and inter-reflections will therefore show the predicted shifts toward the peak of the reflectance spectra, as demonstrated in the empirical studies. Inter-reflections and chromatic light field effects are also subject to the spatial distribution of the light sources and their positions. A light source that is more directional (*e.g.* a narrow-beam spotlight) might cause weaker effects than a more diffuse light source such as a luminous planar panel.

In empirical testing 1, we simulated the colour effects of accumulated orders of inter-reflections in a uni-chromatic space under typical planar white lighting. The theoretically predicted and simulated spectral shifts could indeed be reproduced in computer-rendered spaces. Results for surfaces of which the spectral reflectance is less than 0.5 were also found to be consistent with a previous study in which it was found that for such surfaces the inter-reflections have almost no effect on the chromatic appearance [43]. Results for surfaces with higher spectral reflectances showed the predicted effects. Moreover, we extended our light-field methods to show how these spectral effects on the first-order properties of light fields, the light density and light vector, can be measured, visualised and understood.

In empirical testing 2, fine spectral measurements were taken in real room settings under white lighting. The shape of the light density spectrum was shown to be primarily affected by accumulated orders of (inter-)reflected light. The spectral shape of the light vector was found to be close to that of the illuminant with a minor impact of the (inter-)reflected light. These differential effects on the different components of the resulting light field were predicted and demonstrated using the extended light field methods. The differential effects were also shown to be dependent on the lighting spectrum. These effects can be spectrally tuned via the lighting. In general, the relative spectral differences between troughs and peaks of reflected light can be increased (or decreased) by tuning the troughs and peaks of the illuminant to be similar (or inverted) to those of the material. In natural scenes such differential effects will have an impact on the appearance of 3D objects: shadows will be filled in with mainly the light density and the lightest parts will be determined for a large part by the light vector. This will cause chromatic effects in addition

to the well-known modelling effects due to luminance gradients [52]. This raises questions such as whether these effects will be noticeable, under which conditions, and when they can safely be ignored. Colour adaptation and constancy mechanisms might discount such effects, certainly if the chromatic effects are within the ballpark of natural variations, such as happen with a blue sky and direct sunlight or under a canopy. However, in artificial conditions such as an art gallery with sculptures or in chromatic architectural spaces the effects described, measured and visualised in this paper will have significant effects on people and objects worth considering.

A tool can be used for coarse-grained predictions under typical white sources. Figure 2.10 shows variations of colours and their inter-reflection effects that one might judge to be more or less "harmonious" [53–56], and thus of importance for lighting professionals working on 3D designs. The interface above the boxes shows the BGR spectral values of the finish, which in practice can be estimated with a smartphone. In this manner, it is possible to get a quick idea of the appearance of a space for a specific finish and lighting. It should be noted however that the display medium and viewing conditions have a major impact on colour perception. Computer simulations currently are much used to communicate design concepts and evaluate colour schemes. Our tool provides a coarse visual guesstimation of the impact of chromatic inter-reflections on spatial and chromatic articulation.

This study was limited to spaces furnished with diffusely scattering materials and uniformly coloured rooms. In most natural scenes, diffuse scattering dominates the reflectance modes. Therefore, our results apply to most scenes. Moreover, in empirical testing 2 the boxes were furnished with paper that actually was quite glossy. Such materials still have a very significant diffuse scattering mode - in combination with a forward scattering mode. Many (or perhaps even most) materials in our natural ecology have a diffuse scattering mode. Our findings thus describe phenomena that occur widely "in the wild", not just in perfectly Lambertian scenes. They can be observed in many daily life scenes. More complex and exotic scenes composed of multiple coloured and non-diffusely scattering surfaces, such as mirror and transparent materials, might however show more complicated effects.

2.6. CONCLUSION

In conclusion, light in a space varies not just as a function of position in the space and the direction of observation, but also of spectral power. Reflectance spectra have a prominent effect on the chromatic properties of the light field due to inter-reflections, via the indirect contribution, and can influence the apparent brightness, saturation and even hue. Here we showed how these effects could be measured and visualised for the light density and light vector or flow in the room. The spectral properties of the light vector were indeed shown to be impacted only slightly, while the light density clearly showed the predicted effects, and both were impacted stronger in deep parts of the scene. Our findings show the importance to include 6D light field effects of light-material interactions in spatial designs.

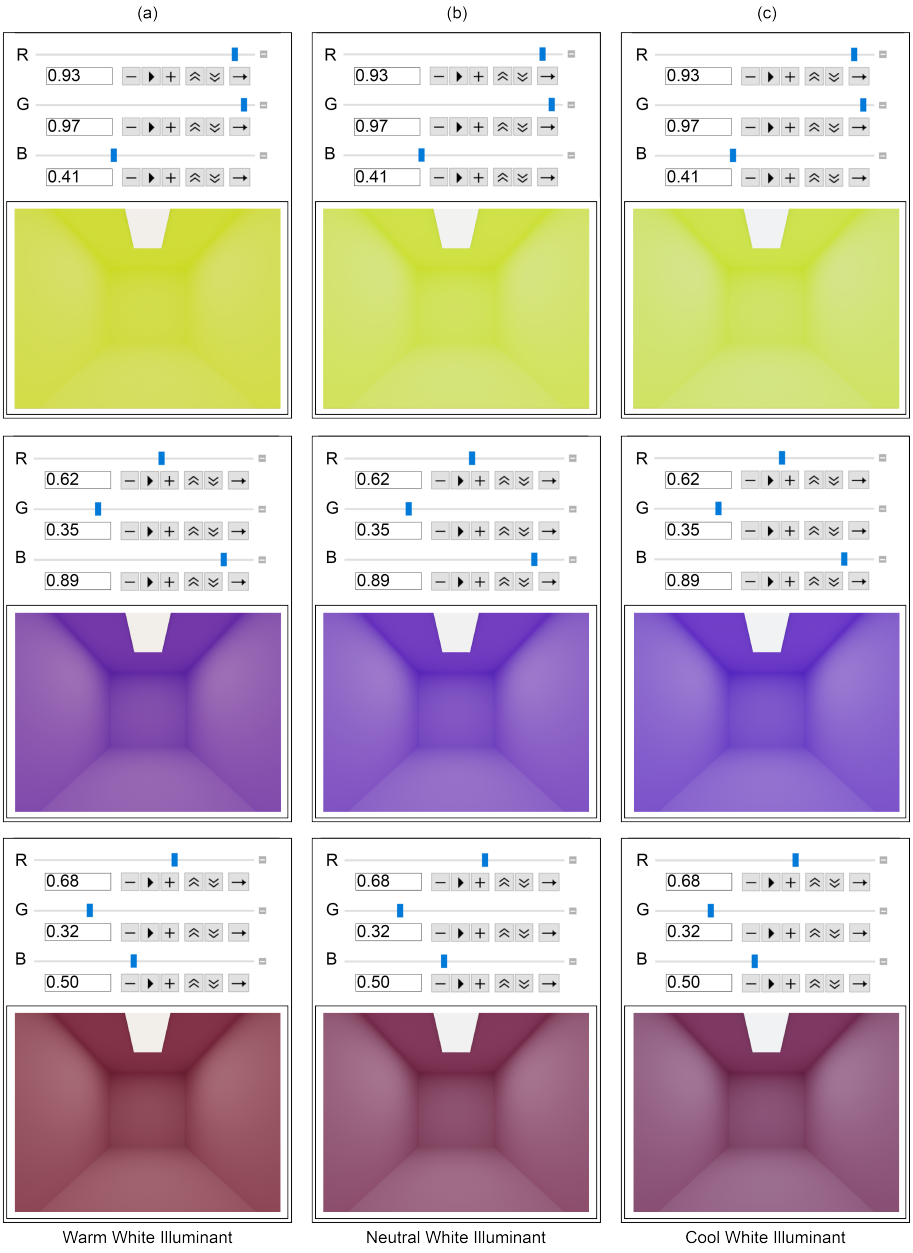

Figure 2.10: Coarse-grained predictions of spectral effects by our tool. The first column shows three box-space visualisations under a warm (a) white light source. The second and third columns show the same finished box spaces illuminated by neutral (b) and cool (c) white light sources. The computer-generated renders were made using standard 2.2 gamma correction after combining the BGR spectral bins and optical mixing.

REFERENCES

[1] L. Xia, S. C. Pont, and I. Heynderickx. “Light diffuseness metric, Part 2: Describing, measuring and visualising the light flow and diffuseness in three-dimensional spaces”. In: *Lighting Research & Technology* 49.4 (2017), pp. 428–445.

[2] A. A. Mury, S. C. Pont, and J. J. Koenderink. “Representing the light field in finite three-dimensional spaces from sparse discrete samples”. In: *Applied optics* 48.3 (2009), pp. 450–457.

[3] T. Kartashova, D. Sekulovski, H. de Ridder, S. F. te Pas, and S. C. Pont. “The global structure of the visual light field and its relation to the physical light field”. In: *Journal of Vision* 16.10:9 (2016), pp. 1–16.

[4] S. C. Pont. “Light: toward a transdisciplinary science of appearance and atmosphere”. In: *Annual review of vision science* 5 (2019), pp. 503–527.

[5] A. A. Mury, S. C. Pont, and J. J. Koenderink. “Representing the light field in finite three-dimensional spaces from sparse discrete samples”. In: *Applied optics* 48.3 (2009), pp. 450–457.

[6] P. Moon and D. E. Spencer. *The photic field*. MIT Press, 1981.

[7] A. A. Mury, S. C. Pont, and J. J. Koenderink. “Structure of light fields in natural scenes”. In: *Applied Optics* 48.28 (2009), pp. 5386–5395.

[8] K. Doerschner, H. Boyaci, and L. T. Maloney. “Testing limits on matte surface color perception in three-dimensional scenes with complex light fields”. In: *Vision Research* 47.28 (2007), pp. 3409–3423.

[9] F. Zhang, H. de Ridder, P. Barla, and S. Pont. “A systematic approach to testing and predicting light-material interactions”. In: *Journal of Vision* 19.4:11 (2019), pp. 1–22.

[10] R. Ramamoorthi. “Modeling illumination variation with spherical harmonics”. In: *Face processing: Advanced modeling methods* (2006), pp. 385–424.

[11] L. Xia, S. C. Pont, and I. Heynderickx. “Light diffuseness metric part 1: Theory”. In: *Lighting Research & Technology* 49.4 (2017), pp. 411–427.

[12] A. A. Mury, S. C. Pont, and J. J. Koenderink. “Light field constancy within natural scenes”. In: *Applied Optics* 46.29 (2007), pp. 7308–7316.

[13] L. Xia, S. C. Pont, and I. Heynderickx. “The visual light field in real scenes”. In: *i-Perception* 5.7 (2014), pp. 613–629.

[14] T. Kartashova, H. de Ridder, S. F. te Pas, and S. C. Pont. “Visual light zones”. In: *i-Perception* 9.3 (2018), pp. 1–20.

[15] L. Xia, S. C. Pont, and I. Heynderickx. “Effects of scene content and layout on the perceived light direction in 3D spaces”. In: *Journal of Vision* 16.10:14 (2016), pp. 1–13.

[16] F. Zhang, H. de Ridder, and S. C. Pont. “Asymmetric perceptual confounds between canonical lightings and materials”. In: *Journal of vision* 18.11:11 (2018), pp. 1–19.

[17] S. C. Pont. “Ecological optics of natural materials and light fields”. In: *Human vision and electronic imaging XIV*. Vol. 7240. SPIE. 2009, pp. 62–73.

[18] Y.-X. Ho, M. S. Landy, and L. T. Maloney. “How direction of illumination affects visually perceived surface roughness”. In: *Journal of vision* 6.5:8 (2006), pp. 634–648.

[19] S. C. Pont and J. J. Koenderink. “Bidirectional texture contrast function”. In: *International Journal of Computer Vision* 62 (2005), pp. 17–34.

[20] T. Kartashova, S. F. te Pas, H. de Ridder, and S. C. Pont. “Light shapes: Perception-based visualizations of the global light transport”. In: *ACM Transactions on Applied Perception (TAP)* 16.1 (2019), pp. 1–17.

[21] V. Zaikina, B. S. Matusiak, and C. A. Klöckner. “Luminance-based measures of shape and detail distinctness of 3D objects as important predictors of light modeling concept. Results of a full-scale study pairing proposed measures with subjective responses”. In: *LEUKOS* 11.4 (2015), pp. 193–207.

[22] Y. Morgenstern, W. S. Geisler, and R. F. Murray. “Human vision is attuned to the diffuseness of natural light”. In: *Journal of Vision* 14.9:15 (2014), pp. 1–18.

[23] J. Kahrs, S. Calahan, D. Carson, and S. Poster. “Pixel cinematography: a lighting approach for computer graphics”. In: *Proceedings of Siggraph*. 1996.

[24] W. J. Adams, G. Kucukoglu, M. S. Landy, and R. K. Mantiuk. “Naturally glossy: Gloss perception, illumination statistics, and tone mapping”. In: *Journal of Vision* 18.13:4 (2018), pp. 1–16.

[25] I. Motoyoshi and H. Matoba. “Variability in constancy of the perceived surface reflectance across different illumination statistics”. In: *Vision Research* 53.1 (2012), pp. 30–39.

[26] J. Filip and R. Vávra. “Template-based sampling of anisotropic BRDFs”. In: *Computer Graphics Forum*. Vol. 33. 7. Wiley Online Library. 2014, pp. 91–99.

[27] K. J. Dana, B. Van Ginneken, S. K. Nayar, and J. J. Koenderink. “Reflectance and texture of real-world surfaces”. In: *ACM Transactions On Graphics (TOG)* 18.1 (1999), pp. 1–34.

[28] R. Basri and D. W. Jacobs. “Lambertian reflectance and linear subspaces”. In: *IEEE transactions on pattern analysis and machine intelligence* 25.2 (2003), pp. 218–233.

[29] C. Cuttle. “Cubic illumination”. In: *Lighting Research & Technology* 29.1 (1997), pp. 1–14.

[30] T. Kartashova, H. de Ridder, S. F. te Pas, M. Schoemaker, and S. C. Pont. “The visual light field in paintings of Museum Prinsenhof: Comparing settings in empty space and on objects”. In: *Human vision and electronic imaging XX*. Vol. 9394. SPIE. 2015, pp. 554–563.

[31] R. Basri and D. W. Jacobs. “Lambertian reflectance and linear subspaces”. In: *IEEE transactions on pattern analysis and machine intelligence* 25.2 (2003), pp. 218–233.

[32] A. L. Yuille, D. Snow, R. Epstein, and P. N. Belhumeur. “Determining generative models of objects under varying illumination: Shape and albedo from multiple images using SVD and integrability”. In: *International Journal of Computer Vision* 35 (1999), pp. 203–222.

[33] C. Yu, E. Eisemann, and S. Pont. “Colour variations within light fields: Interreflections and colour effects”. In: *Perception* 48 (2019), pp. 59–59.

[34] C. Yu and S. Pont. “The influence of material colors on the effective color rendering and temperature through mutual illumination”. In: *Color and Imaging Conference*. Vol. 2020. 28. Society for Imaging Science and Technology. 2020, pp. 293–298.

[35] C. Yu and S. Pont. “Spatial and Angular Variations of Colour Rendition due to Interreflections”. In: *Proceedings of London Imaging Meeting*. Online, 2020, p. xv.

[36] C. Yu and Y. Zhu. “Surface-reflectance discrimination is optimized in the presence of inter-reflections”. In: *European Conference on Visual Perception*. Online, 2021.

[37] C. Yu, M. Wijntjes, E. Eisemann, and S. Pont. “Disentangling object color from illuminant color: The role of color shifts”. In: *Journal of vision* 22.3 (2022), pp. 37–37.

[38] J. J. Koenderink and A. J. van Doorn. “Geometrical modes as a general method to treat diffuse interreflections in radiometry”. In: *Journal of the Optical Society of America A* 73.6 (1983), pp. 843–850.

[39] D. Forsyth and A. Zisserman. “Shape from shading in the light of mutual illumination”. In: *Image and vision computing* 8.1 (1990), pp. 42–49.

[40] C. Cuttle. “Lighting patterns and the flow of light”. In: *Lighting Research & Technology* 3.3 (1971), pp. 171–189.

[41] A. Gilchrist and A. Jacobsen. “Perception of lightness and illumination in a world of one reflectance”. In: *Perception* 13.1 (1984), pp. 5–19.

[42] C. Cuttle. “Towards the third stage of the lighting profession”. In: *Lighting Research & Technology* 42.1 (2010), pp. 73–93.

[43] M. S. Langer. “A model of how interreflections can affect color appearance”. In: *Color Research & Application* 26.S1 (2001), S218–S221.

[44] B. V. Funt and M. S. Drew. “Color space analysis of mutual illumination”. In: *IEEE Transactions on Pattern Analysis and Machine Intelligence* 15.12 (1993), pp. 1319–1326.

[45] R. Deeb, D. Muselet, M. Hebert, and A. Tremeau. “Interreflections in computer vision: a survey and an introduction to spectral infinite-bounce model”. In: *Journal of Mathematical Imaging and Vision* 60 (2018), pp. 661–680.

[46] J. Koenderink, A. van Doorn, and K. Gegenfurtner. “Colors and things”. In: *i-Perception* 11.6 (2020), pp. 1–43.

[47] J. Koenderink, A. van Doorn, and K. Gegenfurtner. “RGB colors and ecological optics”. In: *Frontiers in Computer Science* 3 (2021), p. 630370.

[48] S. E. J. Arnold, S. Faruq, V. Savolainen, P. W. McOwan, and L. Chittka. “FReD: the floral reflectance database—a web portal for analyses of flower colour”. In: *PloS one* 5.12 (2010), e14287.

[49] E. Reinhard, W. Heidrich, P. Debevec, S. Pattanaik, G. Ward, and K. Myszkowski. *High dynamic range imaging: acquisition, display, and image-based lighting*. Morgan Kaufmann, 2010.

[50] M. Luo, Y.-F. Ma, and H.-J. Zhang. “A spatial constrained k-means approach to image segmentation”. In: *Fourth International Conference on Information, Communications and Signal Processing, 2003 and the Fourth Pacific Rim Conference on Multimedia. Proceedings of the 2003 Joint*. Vol. 2. IEEE. 2003, pp. 738–742.

[51] L. D. Griffin and D. Mylonas. “Categorical colour geometry”. In: *PloS one* 14.5 (2019), e0216296.

[52] C. Yu and S. Pont. “Quantifying Natural Light for Lighting and Display Design”. In: *SID Symposium Digest of Technical Papers*. Vol. 52. S2. Society for Information Display China. 2021, pp. 99–103.

[53] L.-C. Ou and M. R. Luo. “A colour harmony model for two-colour combinations”. In: *Color Research & Application* 31.3 (2006), pp. 191–204.

[54] L.-C. Ou, P. Chong, M. R. Luo, and C. Minchew. “Additivity of colour harmony”. In: *Color Research & Application* 36.5 (2011), pp. 355–372.

[55] C. Yu, E. Eisemann, M. W. A. Wijntjes, J. J. R. van Assen, and S. C. Pont. “Effects of inter-reflections in box spaces on perceived object color harmony and shape”. In: *Journal of Vision* 21.9 (2021), pp. 1992–1992.

[56] C. Yu, E. Eisemann, M. W. A. Wijntjes, J. J. R. van Assen, and S. C. Pont. “Chromatic light field effects on perceived modelling and colour harmony”. In: CIE Midterm Meeting. Online, 2021.

3

EFFECTS OF INTER-REFLECTIONS ON THE CORRELATED COLOUR TEMPERATURE AND COLOUR RENDITION OF THE LIGHT FIELD

In everyday scenes, the effective light can be defined as a complex light field, resulting from a mixture of emissive light sources and indirect mutual surface (inter-)reflections. Hence, the light field typically consists of diffuse and directional illumination and varies in spectral irradiance as a function of location and direction. The spatially varying differences between the diffuse and directional illumination spectra induce correlated colour temperature (CCT) and colour rendition variations over the light fields. Here, we aim to investigate the colorimetric properties of the actual light, termed the *effective* CCT and colour rendition, for spaces of one reflectance (uni-chromatic spaces). The spectra of the diffuse light-field component (light density) and the directional light-field component (light vector) were measured in both physical and simulated uni-chromatic spaces illuminated by ordinary white light sources. We empirically tested the *effective* CCT and colour rendition for the light density and the light vector, separately. There were significant differences between the lamp-specified CCT and colour rendition and the actual light-based *effective* CCT and *effective* colour rendition. Inter-reflections predominantly affected the CCT and colour rendition of the light density relative to the light vector. Treating the diffuse and directional light-field components in a linear model reveals the separate influences of the light source and scene. These effects show the importance of a 3D version of colour checkers for lighting designers, architects or in general computer-graphics applications, for which we propose simple Lambertian spheres.

Published as: C. Yu, M. Wijntjes, E. Eisemann, and S. Pont. "Effects of inter-reflections on the correlated colour temperature and colour rendition of the light field". In: *Lighting Research & Technology*. 0.0 (2022), pp. 1–22. DOI: 10.1177/14771535221126902

3.1. INTRODUCTION

IN natural scenes, light fields are often composed of directional illumination emanating from a radiating source and diffuse illumination from inter-reflections by objects (*e.g.* the floor, walls and ceiling of a room). The chromatic properties of inter-reflections are a product of the spectral power distribution (SPD) of the incident light and the spectral reflectance function (SRF) of a material. The dependency on the SRF varies exponentially as a function of the number of bounces the inter-reflections went through. Therefore, the SPDs of the illuminant and inter-reflections are different [1–5] except if the inter-reflections originate from spectrally neutral surfaces (ones which reflect light equally at all visible wavelengths). Here we will focus on the optical effects of material SRFs on the light field. Even if the light source SPD(s) and the material SRF(s) are invariant for most static natural scenes, the chromatic properties of the effective light are still subject to spatial and directional variations due to inter-reflections. Such material-space-light interactions impact how 3D objects and people will look in such spaces, in which the diffuse and directed components of the light will have differential effects on the shadowed and directly illuminated parts of the objects and people [6, 7]. Our aim is to capture and understand such spatially and directionally varying chromatic effects in a light-field framework.

Colour rendering [8] refers to the interaction between light SPD and surface SRF. This is one of the principal factors determining how objects appear, in addition to illuminance level and light diffuseness. Colour rendering metrics (CRMs) apply to lamps and characterise a specified source by its effects on the colour appearances of a representative set of surfaces, compared to a reference illumination. The reference illumination has a precisely defined broad-band spectrum. It is usually a Planckian radiator or a mathematical model of daylight illuminant that is close to or on the Planckian locus. The reference illumination is chosen as a common point of comparison [9] for normal colour vision.

There are multiple types of CRMs associated with lighting applications. These include colour fidelity, which refers to the degree to which colours appear under a test illumination as they are expected to appear on the basis of previous observations under a defined reference illumination [10]. Other attributes of colour rendering include memory [11], discrimination [12], preference [13], fluorescence [14] and many other effects, which tackle very specific visual tasks. For simplicity, we focus on the colour fidelity aspect in this study. SPDs that are reasonably smooth and evenly distributed tend to have higher fidelity.

With complete immersion in and adaptation to the chromaticity of the test illumination, CRMs assume that the reference illuminants have maximum colour fidelity [8]. Electric illumination spectra such as blue-pump LEDs often lack power in certain wavelength ranges compared to full-spectrum radiators, negatively impacting their colour fidelity. Illumination with high or low colour fidelity, in general, makes object colours appear as expected or unexpected under reference illumination.

There are multiple CRMs in use to quantify colour rendering performance, among which the CIE general colour rendering index (CRI) R_a is the most widely used measure. Despite its prominence, R_a has a variety of limitations [15–17], such as a

harsh cut-off at 5000 K for defining the reference illuminant. The scalar index also fails to indicate the types of colour effects, *i.e.* whether it concerns saturation and/or hue shifts.

Progress has been made in examining other CRMs as a replacement [11, 18–22] or an adjunct [23] to the CRI. The global consensus was reached on assessing colour rendering via TM-30 [10, 22, 24, 25]. TM-30 specifies both an improved fidelity index (R_f) and a gamut index (R_g), accompanied by a colour vector graphic. Its high number (99 in total) of colour evaluation samples (CESs) covers a wide range of reflectance spectra, corresponding to a range of consumer goods and natural materials. Instead of a sharp cut-off at 5000 K, TM-30 uses a proportional blend of Planckian radiation and a D Series illuminant between 4000 K and 5000 K. The additional (R_g), colour vector graphic and local measures provide detailed information on the hue and saturation shifts. In 2018, the TM-30 R_f was updated to match the new CIE R_f [26], as an agreed scientifically accurate measure of colour fidelity. However, in practice, a switch to TM-30 involves software upgrading and therefore time, so characterising colour rendition by the CRI is still in use. Therefore, the current study utilises both the conventional and the state-of-the-art colour fidelity measures to characterise the effects of inter-reflections on colour rendition, which we coin the effective colour rendering.

Lighting professionals generally rely on lamp-based colour rendering metrics, which apply well in common lighting applications. The impact of inter-reflections on the effective colour rendering throughout spaces is usually not considered. However, overlooking this can lead to unintentional colour distortion in lighting designs in which coloured materials are used [18, 27–30].

In order to quantify spatially varying lighting distributions, the current study uses the Delft light-field framework [31]. Light fields capture the effective light in a space, including inter-reflections, shadowing effects, etcetera, so it describes the complete lighting distribution that is potentially available to the human visual system (or plenoptic function [32]). The light field thus depends on the light source characteristics, the space's geometry and the materials. The physical light field (the spectral power as a function of location, direction and wavelength) can be decomposed as the sum of qualitatively different components via spherical harmonics (SH) [33–35]. Here we consider just the first two components since those are the main determinants of the modelling and (colour) contrast [36–39]. The 0th-order SH, the light density, is associated with the diffuse light-field component, namely the integration of the spectral power over the sphere. The 1st-order SH represents the light vector, indicating the net flux transport or directional light-field component. In past studies, up to 1st-order chromatic light fields were described, measured and visualised via cubic spectral irradiance measurements [3, 6, 40].

This study aims to predict and measure chromatic light fields and the impact of (inter-)reflections on the effective correlated colour temperature (CCT) and colour fidelity. Hypotheses are that A) the lamp-specified CCT and colour fidelity are noticeably different from the actual light-based effective CCT and effective colour fidelity in the presence of materials with non-neutral SRFs, and B) the major determinants of the CCT and colour fidelity for the light density are the scene

material SRFs, while that for the light-vector CCT and colour fidelity is the illuminant.

We first summarise our earlier work showing how different bounces of inter-reflections shape the chromaticity of the light field [3]. We then empirically demonstrate the disjunction between the lamp-specified and the light-based CCT and colour fidelity by measuring the spectra of the light density and the light vector in physical and simulated uni-chromatic spaces illuminated by ordinary white light sources. We also show how to understand the diffuse and directional light-field components' differential spectral properties and use their linear combination to capture the separate influences of the light source and scene material interactions.

3.2. CHROMATIC EFFECTS OF INTER-REFLECTIONS

The SPD of the lamp is denoted as $E_0(\lambda)$, and the surface SRF of the room as $\rho(\lambda)$. The spectrum of the i^{th} bounce of the inter-reflections is then:

$$E_i(\lambda) = \gamma_i E_0(\lambda)\rho(\lambda)^i \tag{3.1}$$

where γ_i is the geometrical factor, determined by the surfaces' geometry, the bidirectional reflectance distribution function (BRDF), and scene layout. The ith reflection results in a multiplier of $E_0(\lambda)$ with the i^{th} power of the material SRF or $\rho(\lambda)$. As a result, the SPDs of inter-reflections depend strongly on the SRF. If the room surfaces are achromatic, each reflection has the same SPD. But if the room surfaces are chromatic, the SPD will change with each reflection. Since the absolute spectral power attenuates exponentially, the relative differences between the peak(s) and trough(s) of the material SRF increase with each bounce. The ratios between the spectral power of short-, middle- and long-wavelength parts determine the chromatic effects of inter-reflections [3, 40], *i.e.* brightness, saturation, and hue shifts. For our earlier work on this topic and an extensive explanation of these fundamental mechanisms, see Yu *et al.* [3]

Figure 3.1 shows such effects for an achromatic material and three chromatic materials representing brightness, saturation, and hue effects under two typical white illuminations. The chromatic materials were selected based on their qualitatively different effects, namely on brightness, saturation, and hue, in a coarse-grained spectral approach that resembles the human ecological context [3, 41, 42]. The coarse-grained spectral bandwidths are similar to the spectral channels of human vision (50–120 nm half-widths) [43, 44], *i.e.* short-wavelength blue channel (400–500 nm), middle-wavelength green channel (500–600 nm) and long-wavelength red channel (600–700 nm) [45]. In ecological contexts, red, green and blue (RGB)–coordinates suffice to predict the chromatic effects of inter-reflections [41, 46, 47]. The maroon SRF peaks in the red channel, and the rest of the bands have minimal reflectivity. Thus, the exponential attenuation of high orders shows diminishing spectral energy in the red channel as a brightness effect. The coral SRF has its peak in the red channel with a relatively low but similar value in the green and blue channels, resulting in saturation effects towards the peak reflectance for high-order reflections. The orange has different reflectivity in the RGB channels, and

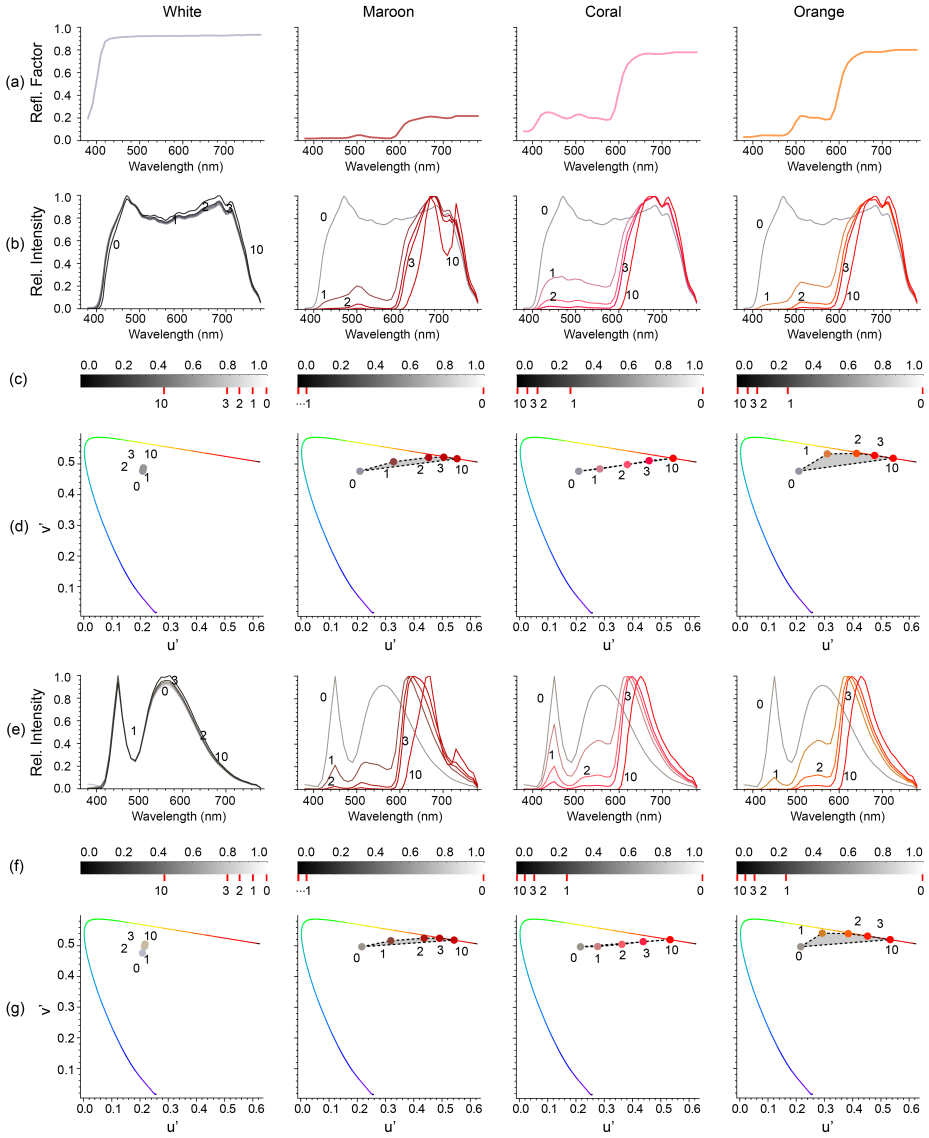

Figure 3.1: Chromatic effects of inter-reflections. (a) SRFs of white, maroon, coral and orange colours. For photographs, see Supplementary Materials Figure F2. (b-d) Inter-reflection effects under xenon lighting. (b) The normalised SPDs of the 0^{th}, 1^{st}, 2^{nd}, 3^{rd}, and 10^{th} reflections of selected materials. see Supplementary Materials Figure F1 for non-normalised SPDs. (c) The relative luminance of the associated reflections in ascending order marked by red dashes. (d) The chromaticity coordinates of the associated reflections in the CIE 1976 UCS diagram based on CIE 1964 10° colour-matching functions. (e-g) as (b-d) for blue-pump LED lighting.

the RGB ratios of reflected SPDs consecutively change, causing hue effects. Figure 3.1(a) shows the SRFs of the selected materials. Figure 3.1(b-g) shows the SPDs, luminous energy and chromaticity coordinates of the 0^{th}, 1^{st}, 2^{nd}, 3^{rd}, and 10^{th} reflections for broad-band xenon (R_f 94, CCT 5461 K) and blue-pump LED light (R_f 77, CCT 4745 K). The online supplementary files (see SupplementaryMaterial.docx [48] and SupplementaryMaterial_Spectra.xlsx [49]) include the SRFs of selected materials and the SPDs of the illuminants, so that the interested reader may reanalyse the data.

The chromaticity coordinates of high-order reflections hardly vary for the white room (see Figure 3.1, white-room chromaticity plots). However, the maroon material shows brightness effects; the relative luminance diminishes from the 1^{st} reflection on for its low albedo, regardless of the chromatic variations. The coral colour shows saturation effects at high-order inter-reflections, *i.e.* the chromaticity with each bounce shifts closer to the colour's dominant wavelength on the spectral locus. For the orange colour showing the hue shift effects, the chromaticity of individual bounces forms a curve in the chromaticity diagram, from orangish to reddish (see Figure 3.1(c-d) and (f-g), the right three columns). The line between the illuminant (point 0) and the material SRF's dominant wavelength on the spectral locus (approached by point 10) and the lines between points 0, 1, 2, ... span the area of the effective light chromaticities.

Rendering of object colours will be impacted by these chromatic effects of light-material-geometry interactions. This affects the CCT and CRM of the actual effective light in the space instead of the source-based CCT and CRM, in other words, light instead of lighting based. Moreover, these effects vary throughout space; spectrally, directionally, and spatially, thus forming important metrics to include in a light-field approach together with the already studied characteristics of light density, vector, diffuseness, squash, brilliance, flow, and zones. This paper tested these interaction effects in physical and simulated scenes for an extensive range of material and illuminant spectra.

3.3. EXPERIMENT 1

CCT and colour rendition variations in a physical box scene

Chromatic effects of inter-reflections have a major influence on the diffuse light-field component due to their omnidirectional nature and a minor influence on the directional light-field component [40]. The effective CCT and colour fidelity properties of the actual light in a space are therefore predicted to vary as a function of the contribution of the diffuse and directional light-field components: the more direct lighting (often consisting of a major directional and minor diffuse contribution), the more it will be consistent with the original CCT and colour fidelity of the lamp, and the more indirect lighting (often a major diffuse and minor directional contribution), the more the CCT and colour fidelity will deviate. Here we empirically test how chromatic effects of inter-reflections affect the CCT and colour fidelity for up to 1^{st}-order light-field components.

3.3.1. METHOD

PHYSICAL TEST SCENES

We constructed four physical windowless box spaces with a length, width, and height of 1200 mm × 660 mm × 660 mm. The spaces were uniformly covered in four different material colours. The surface materials were created by matte white paint, or A3 paper sheets printed with RGB colours including maroon (0.5, 0.1, 0.1), coral (0.9, 0.5, 0.5) and orange (0.9, 0.5, 0.1). The SRFs of those materials were measured with an X-Rite portable handheld spectrophotometer (Ci60 Series) (Figure 3.1(a)). As verified by full spectral modelling in Section 3.2, the selected chromatic material colours under typical white illumination show brightness, saturation and hue effects in the presence of inter-reflections, respectively [3].

The box spaces were illuminated by a ceiling-recessed planar luminaire (377 mm × 155 mm). The luminaire employed a micro prismatic diffuser that evenly dispersed the light in the space. We specifically selected two lamps with typical SPDs, *i.e.* xenon lights (R_f 94, CCT 5461 K) with a broad-band spectrum and fluorescent (R_f 83, CCT 4284 K) with a spiky spectrum. We combined these two illuminants with the four materials for a total of eight light scenes.

DATA COLLECTION

We measured the local light fields via the cubic illumination system [36, 50, 51] in the centre and left-back corner of the physical space for all eight scenes, capturing the spectral irradiance on the six faces of a small reference cube (Figure 3.2) centred at the measurement point. The cube was aligned with the principal surfaces of the surrounding environment. The spectral irradiance was acquired over a wavelength range from 380 to 780 nm in 11 nm increments and was internally interpolated to 1 nm increments. Each cubic measurement, including placement of the apparatus, lasted about 1 minute. The experimenter (the first author) was covered in black to minimise disturbing reflections. A total of 16 cubic measurements (96 irradiance spectra) were collected.

DATA PROCESSING AND ANALYSIS

For each cubic measurement, the six spectral irradiance values are designated $E_{(\lambda,x+)}$, $E_{(\lambda,x-)}$, $E_{(\lambda,y+)}$, $E_{(\lambda,y-)}$, $E_{(\lambda,z+)}$ and $E_{(\lambda,z-)}$, representing the measurements in the positive and negative directions along the coordinate axes. The subtractions of the opposed paired measurements correspond to the light vector components in the coordinate-axis directions, *i.e.* $E_{(\lambda,x)}$, $E_{(\lambda,y)}$ and $E_{(\lambda,z)}$ (Equations (3.2)–(3.4)) and define the direction of the light vector. The length of the vector corresponds with the magnitude of the light vector $E_{(\lambda,vector)}$ (Equation (3.5)). The light density $E_{(\lambda,scalar)}$ is obtained via the sum of the symmetric component $E_{(\lambda,symmetric)}$ and the weighted vector's contribution (Equation (3.10)). $E_{(\lambda,symmetric)}$ equals the average value of the symmetric components of all directions (Equation (3.9)). The light vector's contribution to the light density is $E_{(\lambda,vector)}/4$, which was derived analytically [36].

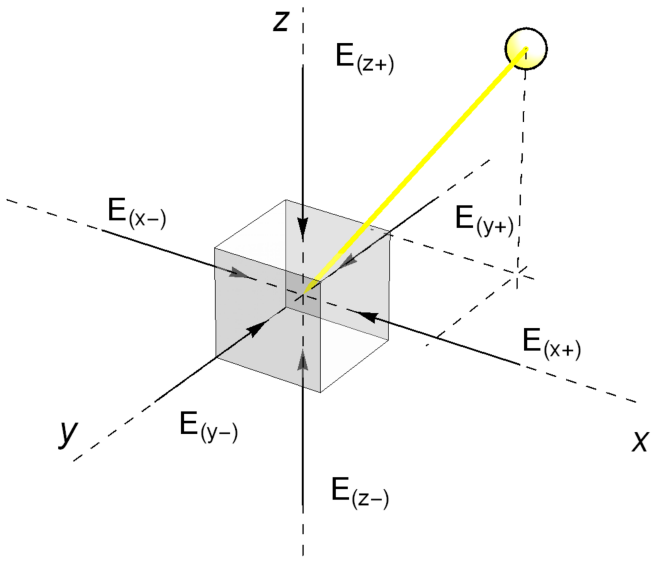

Figure 3.2: The frame of reference for the cubic illumination measurements.

$$E_{(\lambda,x)} = E_{(\lambda,x+)} - E_{(\lambda,x-)} \tag{3.2}$$

$$E_{(\lambda,y)} = E_{(\lambda,y+)} - E_{(\lambda,y-)} \tag{3.3}$$

$$E_{(\lambda,z)} = E_{(\lambda,z+)} - E_{(\lambda,z-)} \tag{3.4}$$

$$E_{(\lambda,\ \text{vector})} = \sqrt{E^2_{(\lambda,x)} + E^2_{(\lambda,y)} + E^2_{(\lambda,z)}} \tag{3.5}$$

$$\sim E_{(\lambda,x)} = \frac{E_{(\lambda,x+)} + E_{(\lambda,x-)} - \left|E_{(\lambda,x)}\right|}{2} \tag{3.6}$$

$$\sim E_{(\lambda,y)} = \frac{E_{(\lambda,y+)} + E_{(\lambda,y-)} - \left|E_{(\lambda,y)}\right|}{2} \tag{3.7}$$

$$\sim E_{(\lambda,z)} = \frac{E_{(\lambda,z+)} + E_{(\lambda,z-)} - \left|E_{(\lambda,z)}\right|}{2} \tag{3.8}$$

$$E_{(\lambda,\ \text{symmetric})} = \frac{\sim E_{(\lambda,x)} + \sim E_{(\lambda,y)} + \sim E_{(\lambda,z)}}{3} \tag{3.9}$$

$$E_{(\lambda,\ \text{scalar}\ )} = \frac{E_{(\lambda,\ \text{vector}\ )}}{4} + E_{(\lambda,\ \text{symmetric})} \tag{3.10}$$

We used both CRI R_a and TM-30 R_f to quantify the colour fidelity. The illumination's chromaticity is spatially and directionally varying within a scene, while chromatic adaptation is assumed to be based on the scene's white point (the anchor) [52, 53]. The reference illuminant of the whole scene is thus defined as the broad-band spectrum sharing the same CCT as the lamp, under the brightest-is-white

assumption [53–56]. The R_a was calculated in the conventional manner [57]. The R_f calculation was based on the TM-30-18 standard framework via Luxpy [58].

RESULTS

Figure 3.3 shows the SPDs of the light densities and vectors in the centre (a-b) and corner (c-d) of the box rooms under xenon illumination. We plotted the SPDs of the xenon lamp (black line) and CIE D Series reference illuminant having the same CCT (red line) as the baselines. The measured effective spectra were included in Supplementary Material Section S5.

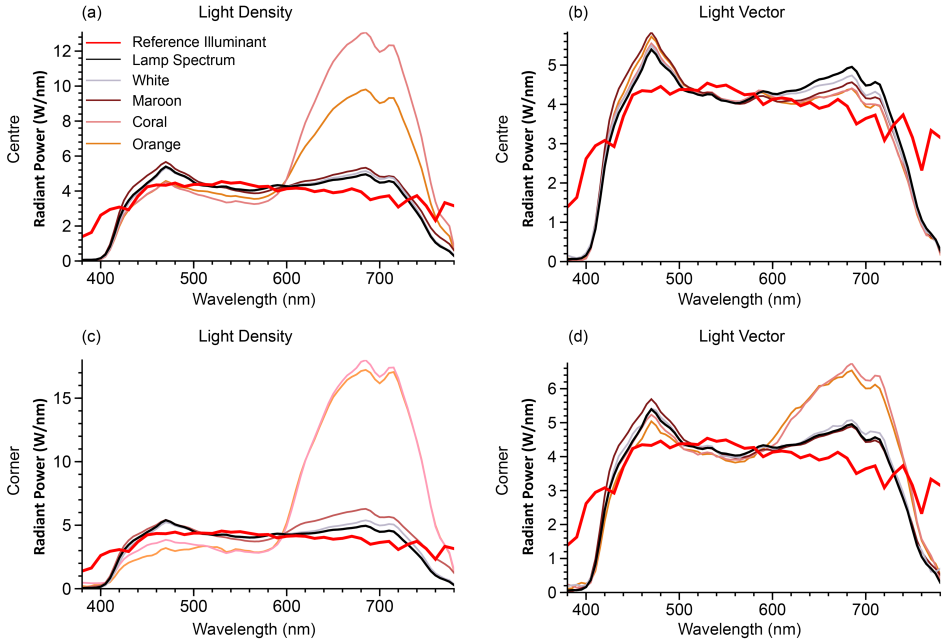

Figure 3.3: Spectral effects of light-material interactions. The SPDs of the light density ((a) and (c)) and light vector ((b) and (d)) in the centre (a-b) and corner (c-d) for the four finishes illuminated by a xenon lamp. The black line indicates the lamp spectrum. The red line is the reference spectrum (CIE D Series reference illuminant having the same CCT as the lamp). The other coloured lines are the effective light spectra corresponding to the room colours.

The light densities' and vectors' SPDs in the white room were consistently similar to the lamp spectrum. For the other three finishes, the SPDs of the light densities differed from the lamp spectrum, showing a peak in the long-wavelength part and attenuation in the short-wavelength part, corresponding to the materials' SRF shapes. The spectral differences in the corner were larger than those in the centre. The effects in the maroon room were smaller than in the coral and orange rooms. The light vectors' SPDs were quite similar to the lamp spectrum in the centre but also showed deviations in the corner of the coral and orange rooms.

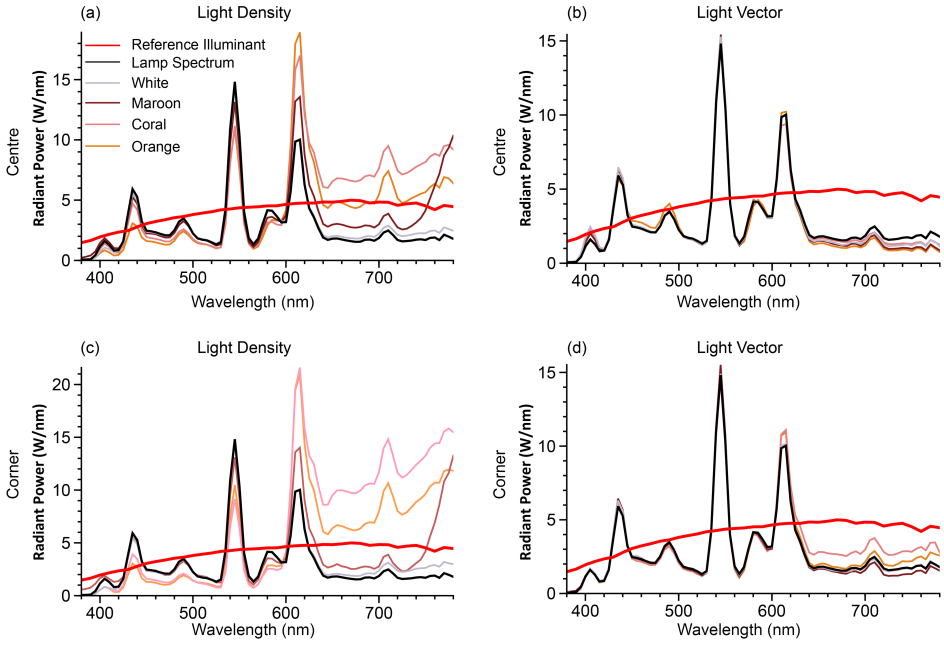

Figure 3.4: Spectral effects of light-material interactions. The SPDs of the light density ((a) and (c)) and light vector ((b) and (d)) in the centre (a-b) and corner (c-d) for the four finishes illuminated by a fluorescent lamp. The black line indicates the lamp spectrum. The red line is the reference spectrum (a mixture of Planckian radiation and the CIE D Series reference illuminant having the same CCT as the lamp). The other coloured lines are the effective light spectra corresponding to the room colours.

These results thus are in line with the hypothesis that the light vector (directional light-field component) corresponds better with the illuminant spectrum and the density (diffuse light-field component) with the paint reflection spectrum.

Figure 3.5 shows the relative differences of the effective CCT, D_{uv} (distance from the Planckian locus), R_a, and R_f of the light density (grey bars) and vectors (black bars) relative to those of the lamp for the centre (a) and the corner (b) of the box rooms under xenon illumination. R_a and R_f are designated to quantify the colour fidelity of white primary illumination. Multiple effective D_{uv} values are beyond R_a and R_f's stated limits, and thus, these metrics cannot be applied formally. However, this type of scene is intended to be illuminated by white light, and excessive D_{uv} is due to chromatic inter-reflections. These metrics are conventionally used in such a scene as a standard benchmark for the light qualities, and we thus still applied them to assess how inter-reflections can modify the effective light qualities. It is important to note that for the values beyond the D_{uv} limits, the effective light cannot even be classified as white anymore according to ANSI C78.377-2017 [59], but is actually chromatic. The associated absolute colour fidelity values are unlikely to correspond to perception, but the relative differences between light density and light vector in

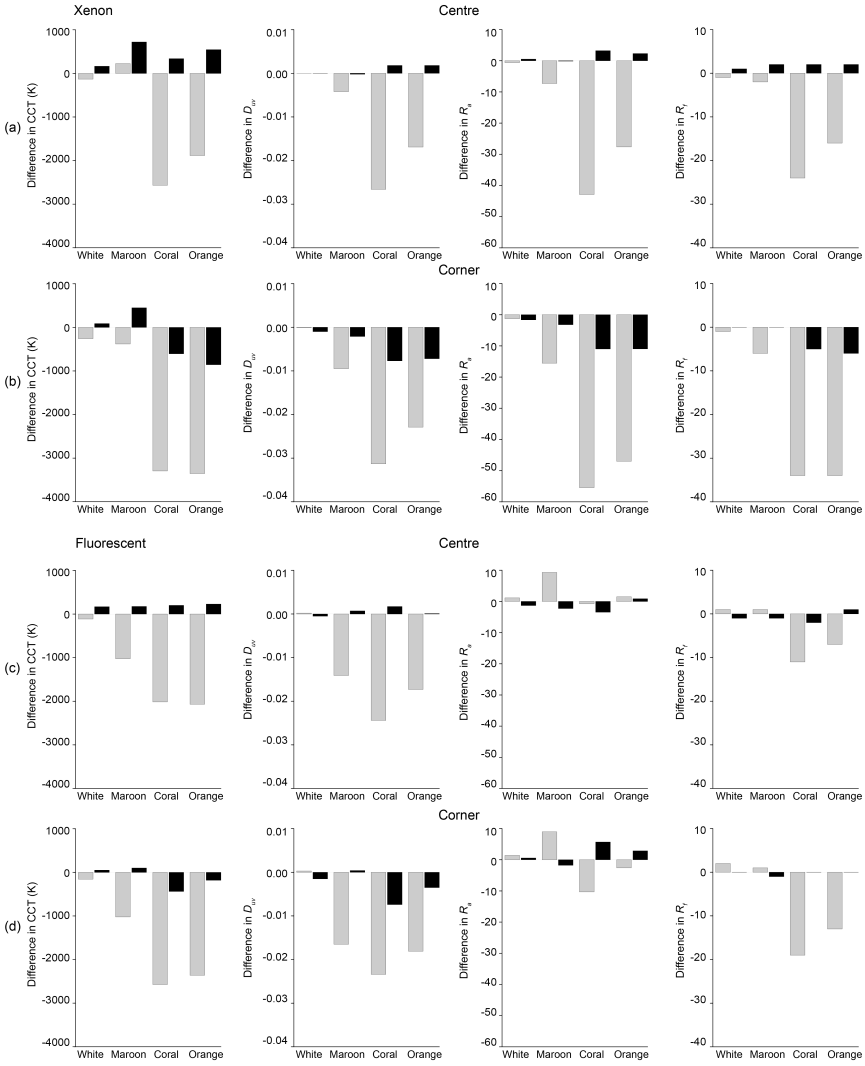

Figure 3.5: The relative differences between the Effective colour metrics and lamp-specified colour metrics. The CCTs, D_{uv}, R_a and R_f differences of the light densities (grey bars) and the light vectors (black bars) relative to those of the lamp in the centre (a) and corner (b) of the four selected finishes illuminated by a xenon lamp. (c) and (d) as (a) and (b) for a fluorescent lamp. The raw tabular colorimetric values are supplied in Supplementary Materials Section S7.

the centre and corner give an estimate of directional and spatial colour fidelity variations due to inter-reflections.

As shown in Figure 3.5, all colorimetric values for the white room are almost identical to the lamp's with minor variations. For the other three finishes, the

effective CCTs of the light densities (grey bars) are up to 2905 K lower than those of the light vectors (black bars) and up to 3353 K lower than the reference lamp CCT. The light vectors' CCTs were more consistent with the reference illuminant values and deviated maximally 857 K in the corner.

The D_{uv} of the light densities and vectors for all room cases were consistently negative, indicating that their chromaticity coordinates were below the Planckian locus. The D_{uv} for the light densities were lower than the lamp values.

The effective R_a and R_f results for xenon lighting were found to be similar in the sense that the colour fidelity measures for the light densities were consistently lower than for the vectors in the coloured rooms. However, light-density R_a values tended to be lower than R_f values for the chromatic rooms. The light densities' R_a and R_f decreased up to 63% and 36% compared to that of the lamp, respectively. The deviations in the corner were larger than in the centre. Also, material colours with a high albedo and brightness value (coral and orange) showed stronger effects than for a low albedo and brightness value (maroon).

Figure 3.4 and Figure 3.5(c-d) show the same information for fluorescent light. The reference illuminant was a mixture of Planckian radiation and the D Series illuminant. The lamp spectrum differs markedly from the reference illuminant. The measured effective spectra were included in Supplementary Material Section S6. The results in the white room were consistent with the lamp. The chromatic materials caused lower CCTs and larger D_{uv} magnitudes for the light density, similar to the xenon condition. The R_a of the light density in the maroon space increased. The decrease of R_a and R_f for the light densities in the coral and orange space was smaller than those under xenon illumination. We again found differential colorimetric properties between the light density and light vector and major differences between lamp-specified and light-based CCT and colour fidelity.

3.3.2. OVERVIEW OF FINDINGS

Chromatic materials of a space can alter the light density's colorimetric properties in that space due to inter-reflections. Their impact on the light vectors is relatively small, except for deep parts of the space where the chromatic diffuse inter-reflections dominate and directed white illumination attenuates, but on the light density can be large. The colour temperature of the lamp and effective light is in the coral and orange cases too large to be called the same "nominal" CCT [59]. Additionally, for those cases we find differences for the colour fidelity larger than five points, which tends to be noticeable [15]. This will cause chromatic gradients on 3D objects (and people) in the space, in which diffusely scattered light greatly affects the shadows and shaded parts and the direct light has major effects on highlights and directly lit parts. Effects were major in our uni-chromatic cases with high purity, namely the coral and orange rooms. For the maroon room the low reflectivity resulted in relatively minor effects on the effective metrics. Colour fidelity was impacted in most coloured rooms. The selected room colours also decreased the CCT, which can be explained by the profile of their SRFs, having peaks in the long-wavelength range. The colours used here were chosen for their qualitatively different effects (brightness, saturation, hue shifts) and all had long dominant wavelengths. This

raises the question how different types of SRFs will impact the effective light's chromatic properties.

3.4. EXPERIMENT 2

CCT and colour rendition variations in a simulated box space

This section aimed to quantify the spatial variations of the effective CCTs and colour fidelity measures for more extensive and representative material-light interactions in the box space. Using hyperspectral computer simulations, we systematically varied the room material SRFs and illuminant SPDs of the space to study their effects on the chromatic light-field properties and effective CCTs and colour fidelity measures.

3.4.1. METHODS

SIMULATED TEST SCENES

A digital model of a 6000 mm × 3300 mm × 3300 mm box scene was constructed. The space was uni-chromatic and illuminated by a planar luminaire (1884 mm × 773 mm) recessed in the centre of the ceiling. Its luminous flux was 3500 lm. The scene geometry was the same as the physical scene from experiment one but built at a scale of 5:1, representing a realistic single-floor space.

The illuminant spectra (see Supplementary Materials Figure F3) were selected from the sources enumerated in the CIE publication on colorimetry [60] and representative LEDs from the "example SPD library" of the ANSI/IES TM-30-18 Advanced Calculation Tool [61] (Table 3.1). We included representative sources that are extensively used in lighting research and applications. These spectral samples (380 nm to 780 nm with a 5 nm wavelength increment) comprise three broad-band spectra, three fluorescent sources and six LEDs. As the selected broad-band spectra have (nearly) perfect colour fidelity, the inclusion of these sources helps to understand how material colours influence effective CCTs and colour fidelity measures. Three fluorescents represent typical warm, neutral and cool white illuminants. The first three LEDs (NO. 7–9) are yellow phosphor-coated types with warm, neutral and cool white CCTs. Hybrid pump LED (NO. 10) utilises both phosphor coating and red LED to generate white illumination. The last two LEDs are three-primary and four-primary types with similar CCTs but with major colour fidelity differences.

The material colours were sampled based on the Munsell system due to its wide usage in colour testing and perceptual uniformity. We first selected five pure colours (high chroma and high value) from the Munsell principal hues, *i.e.* 5RV70C08, 5GV70C08, 5BV70C08, 5YV70C08 and 5PV70C08. Another fifteen colours were sampled systematically by reducing the chroma and values of the pure colours (see Supplementary Materials Figure F4). Altogether we sampled 20 colours with varying levels of colour purities. The SRFs of the sampled colours were from the "Munsell colours matt" dataset of the University of Kuopio [62] (see Supplementary Materials Figure F5), reported from 400 nm to 700 nm with a 5 nm increment. Thus, a total of 240 combinations of illuminant and reflectance spectral pairs were applied to the test scene.

Table 3.1: Specifications of lamps used.

No.	Type of Illuminant	CCT (K)	Ra	R_f
1	Equal Energy	5455	95	95
2	CIE st. illum. A	2855	100	100
3	CIE st. illum. D65	6500	100	100
4	CIE Fluor. Lamp FL 4	2940	51	57
5	CIE Fluor. Lamp FL 7	6490	90	92
6	CIE Fluor. Lamp FL 11	4000	83	80
7	LED (blue LED + phosphor)	2880	92	89
8	LED (blue LED + phosphor)	3551	91	89
9	LED (blue LED + phosphor)	4745	73	77
10	LED Hybrid Blue Pump	3417	91	95
11	RGB LED (450/525/625)	3000	53	65
12	RGBA LED (455/530/590/645)	3038	97	94

HYPERSPECTRAL SIMULATION AND ANALYSIS

We used the Autodesk® 3ds Max Mental Ray engine. This system's Lighting Analysis Assistant allows irradiance calculations via the virtual light sensor over a specific area without rendering the whole scene [63]. We placed two cubic light meters in each test scene, one in the centre and another in the left-back corner. The cubic light meter was configured by placing six sensors facing the negative and positive sides of the principal dimensional axes. The default lighting calculation in 3ds Max utilises RGB coarse-grained wavebands. The RGB radiant power weighted to approximate the CIE-Y tristimulus provides photometric outputs, such as illuminance and luminance. The simulated photometric outputs are reliable [64], but physically accurate colorimetric outputs demand finer spectral resolution [65].

Therefore, instead of default RGB bands, we implemented N-stepping [66, 67]. This approximates the radiant power per waveband in N steps, where N can be any positive integer. The spectrum is divided into N consecutive, equally spaced wavebands, with N defining the spectral resolution and the number of monochromatic channels during the calculations. The light sensor reading from each waveband indicates the irradiance value of the corresponding waveband. Since the spectral resolution of the sampled reflectance spectra was lower than the sampled light spectra, we subsampled the latter. So, we did hyperspectral cubic measurements based on 61 channels (from 400 nm to 700 nm with 5 nm steps) for all simulated box scenes. We then applied the same methods as in experiment one to estimate the light density and vector SPDs and their associated CCTs and colour fidelity measures.

3.4.2. RESULTS: COLORIMETRIC ANALYSIS

Figure 3.6 and Figure 3.7 show the CCT and R_f differences between the lamp and the two light-field components, ordered according to the numbers of the lamps in Table 3.1. Negative values indicate decreases of CCT or R_f relative to lamp

properties, while positive values show increases. The colours of the bars correspond to the room material colours grouped by their hues.

The effective CCTs (Figure 3.6) of the light density and vector were lower or higher depending on the room colours. The directions of CCT differences were consistent among the selected lamps except lamp NO. 8, while effect magnitudes varied. The SRFs with peaks in the long-wavelength part caused a decrease of the light densities' CCTs, whereas short-wavelength peaked SRFs induced increased CCTs for the light density. The variations in the corner were larger than those in the centre. The influences on light vectors' CCTs were minor (note that the plot scale differs from the light density plots), and the directions of the CCT changes in the centre and corner were opposite. The effects became smaller with reductions of material chroma or value.

The R_f (Figure 3.7) was found to be close to that of the lamp (note the plot scale differences) for the light vectors and to decrease up to 27% for the light density in the corner for the broad-band illuminants (No. 1–3). The effects in the corner were always larger than in the centre. Interestingly, in several cases (lamps 4, 6-9, 11, 12), the light densities' R_f under a lamp increases for some material colours while it decreases for other colours. In Supplementary Materials Figure F6 and Figure F7, we provided the measured spectra for reference.

3.4.3. RESULTS: VISUALISING THE LIGHT-FIELD COLORIMETRIC PROPERTIES

In the former sections we analysed how inter-reflection effects influenced light-field CCT and colour fidelity. Here we study visualisations of the consequences for object colour appearance. We spectrally simulated colour checkers in the white and orange rooms illuminated by a D65 lamp (see Figure 3.8). The standard colour checker was made of the 15 CIE test colour samples and 5 achromatic colour samples. The effects that we studied vary also as a function of angle, which is not visible on the 2D checkers. Varying the orientation of the 2D checkers would be one way to show those angular variations, but such variations demand either large numbers of images or videos. Therefore we propose using 3D checkers with hemispheres instead of flat colour patches, which allows visual inspection of a hemisphere of directions at once. Moreover, such 3D checkers also show the colour gradients that will result on 3D objects, in one glance. The checkers were placed in the centre and bottom left corner of the room. The colours of the checkers in the white room were primarily affected by the inter-reflections in terms of luminance but not their chromaticities, and thus provided the references to compare against the orange room. The apparent colour appearances of the colour checkers in the orange room were affected by inter-reflections showing an orange colour cast. The colour cast in the corner is visually stronger than in the centre for both 2D and 3D checkers. The 3D colour checker also showed differential apparent colour appearances for the shading and attached body shadow, creating colour gradients on 3D objects which designers might want to take into account in their decisions in practical applications.

Figure 3.9 shows an example of a technical visualisation of such effects throughout a space: the CCT and colour fidelity of the light density and vector for a cross-section

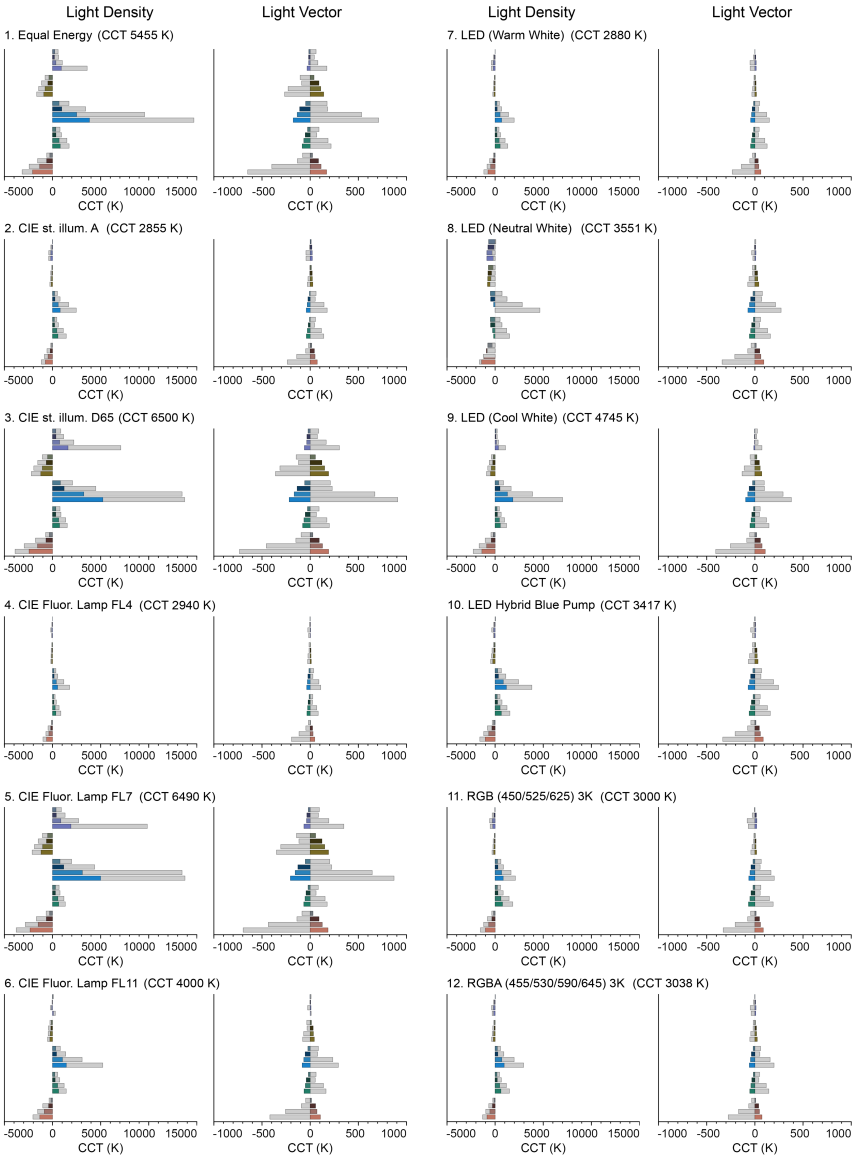

Figure 3.6: The relative differences between the light-field CCTs and lamp-specified CCTs. The plots were numbered as Table 3.1. The bars were grouped according to the hues of material colours in the order of R-G-B-Y-P. The colours within each hue group were arranged by decreasing colour purity from bottom to top. The coloured bars indicate the results of the centre location, while superimposed grey bars indicate those for the corner location. The associated tabular values are supplied in Supplementary Materials Section S13. The light-field D_{uv} values are included in Supplementary Materials Figure F8.

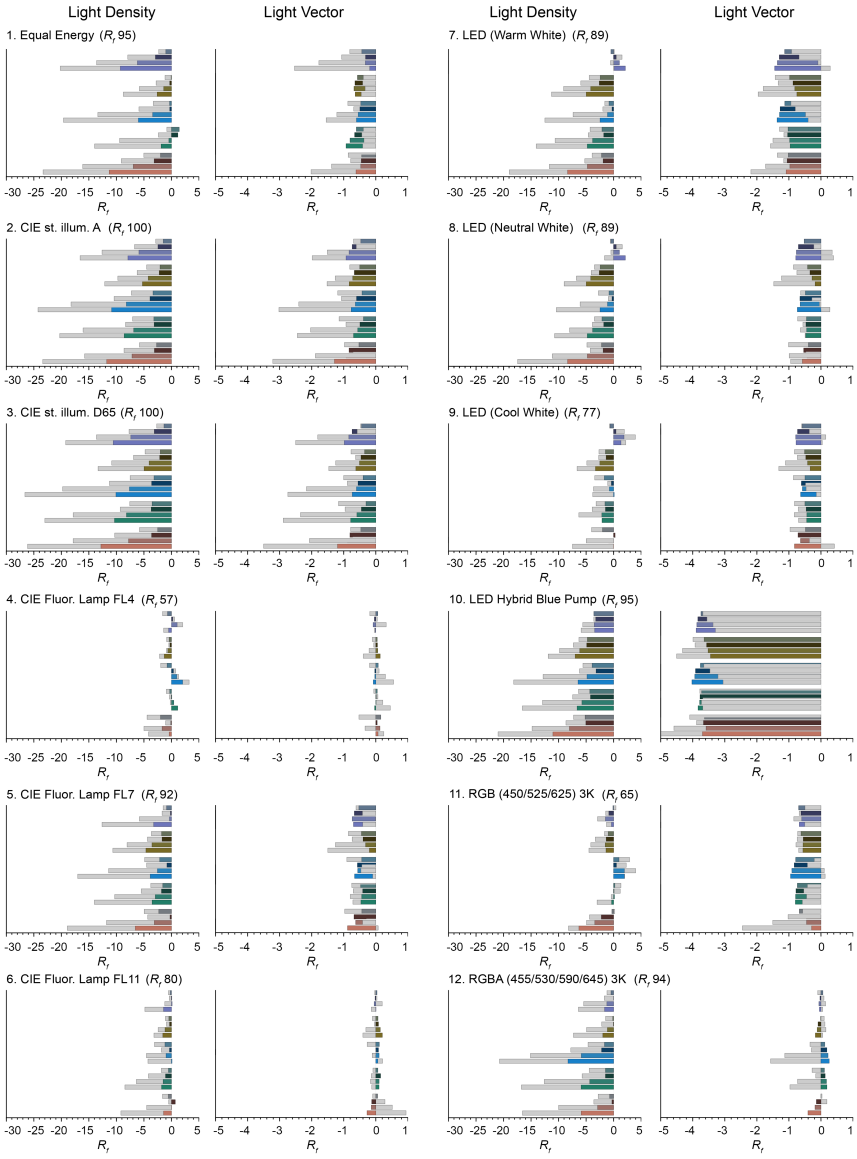

Figure 3.7: The relative differences between the light-field colour fidelity and lamp-specified colour fidelity. The plots were arranged in the same way as in Figure 3.6. The bars were grouped according to the hues of material colours in the order of R-G-B-Y-P. The colours within each hue group were arranged by decreasing colour purity from bottom to top. The coloured bars indicate the results of the centre location, while superimposed grey bars indicate those for the corner location. The associated tabular values are supplied in Supplementary Materials Section S13.

of an orange box room illuminated by the D65 spectrum. The spatial variations of the CCT and colour fidelity for the light density are large, while for the light vector they stay almost constant throughout the space. The connections between these technical visualisations and the foregoing visual impressions are providing insights into the complex interactions between scene and lighting.

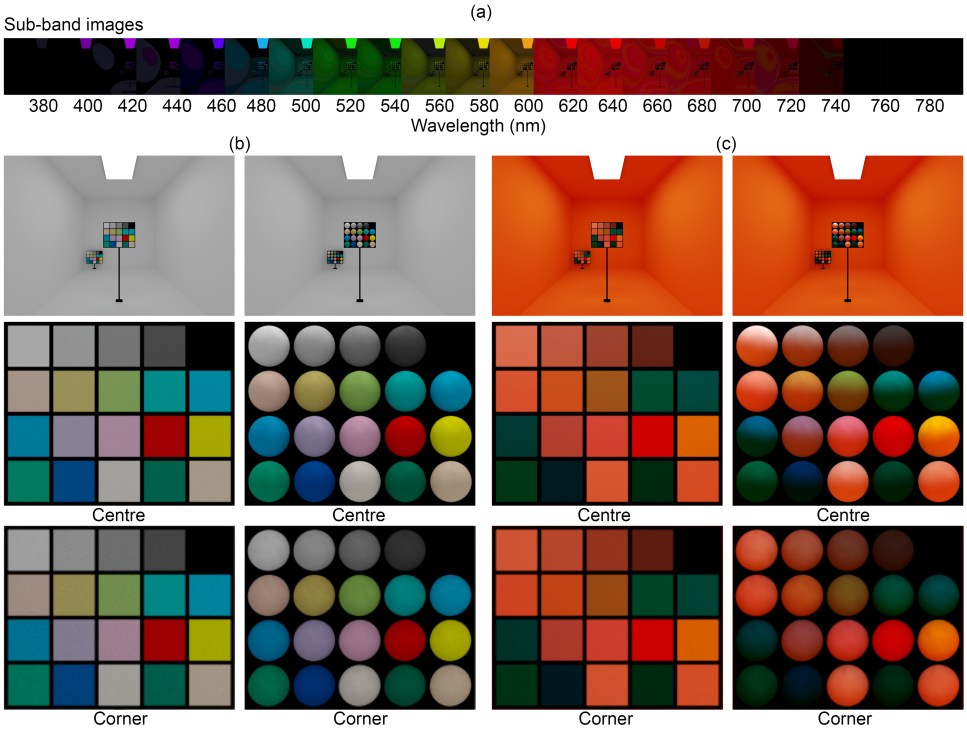

Figure 3.8: 2D versus 3D colour checkers. (a) Sample wavelength sub-band images for the orange room with 3D checkers made of Lambertian hemispheres. (b) The sRGB representations (gamma 2.2) of spectral renderings showing the white room with 2D (left) and 3D checkers (right) with their corresponding close-ups. (c) as (b) for the orange room. The mutual illumination between coloured spheres was omitted.

3.4.4. OVERVIEW OF FINDINGS

The results of experiment one were confirmed for simulated box spaces. In addition to that, we found systematic effects of material colour spectral properties. As expected, peaks in the long-wavelength and short-wavelength parts caused a decrease and increase of light densities' CCTs, respectively. In most cases, R_f decreased, but interestingly, R_f increased for some light sources and material colours. Effects showed the same dependencies as in experiment one, namely that the density was impacted more than the vector, and effects were stronger in the corner than in the centre. This has important implications for the appearance of 3D

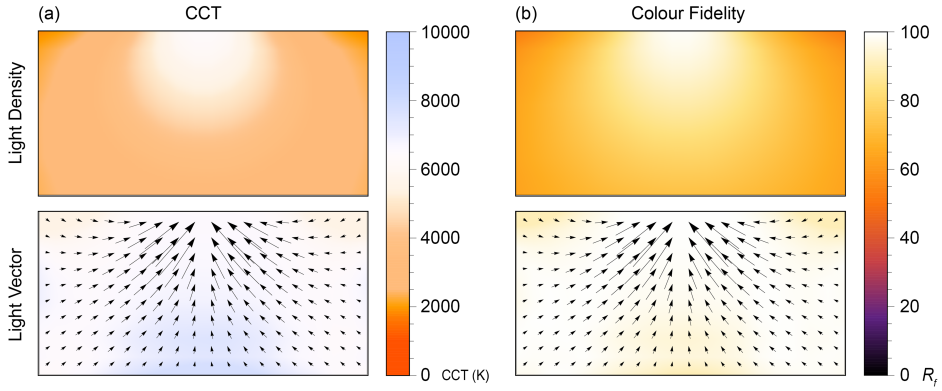

Figure 3.9: Chromatic light fields. The CCT (a) and colour fidelity (b) distributions of the light density (top row) and light vector (bottom row) light fields for a cross-section (a vertical plane right under the illuminant) of the box space furnished in orange illuminated by the D65 lamp in the centre. The ensemble formed by the superimposed light vectors represents the light flow.

objects and people in the space, dependent on where they are in the space. Our 3D colour checker allowed visual assessments of the diffuse and directed light's separate impacts on apparent object colour appearance.

3.5. DISCUSSION

In earlier work, we described spectral variations of natural light fields [6, 40, 68–70]. Here, we made initial steps to extend the light-field descriptions with colour metrics, presenting a method for measuring the effective CCT and colour fidelity for the light density and light vector and showing results for physical and rendered scenes to explore and understand the effects of material-light interactions. For non-neutral coloured scenes, the SPDs were found to vary spectrally, spatially, and directionally within the light field, and our approach revealed the complex effects of material-light interactions on colour rendition.

In experiment one, we measured spectral light fields in physical settings under white light. The light densities' chromatic properties were strongly affected by inter-reflections, while those of the light vectors were found to be closer to the lamp. It was demonstrated that in some cases the differences between the lamp-specified CCT and colour fidelity and the actual light-based effective CCT and effective colour fidelity were substantial and thus worth considering. Colour constancy mechanisms will certainly help to perceptually discount these optical effects in many cases. Nevertheless, discounting mechanisms of inter-reflections by human vision have neither been explored in depth for its differential effects of diffuse and directed lighting (impacting shadowed and highlighted parts differently and causing chromatic gradients) nor for the spatial and directional variations of these effects throughout spaces.

In experiment two, we simulated 20 coloured spaces under 12 typical white sources. The spatial and angular variations of CCT and colour fidelity due to (inter-)reflections were reproduced in hyperspectral renderings and confirmed the conclusions of experiment one. The CCT and colour fidelity differences between the lamp and the light field, and between the density and vector were again found to be substantial in many cases, and as expected were found to decrease with material colour value and chroma. Interestingly, combinations of material colours and lamp spectra were found to increase or decrease CCT and colour fidelity, offering possibilities for spectral tuning. These effects could be easily understood for the CCT; so-called warm or cold material colours increase or decrease the CCT, respectively. This is regularly implemented in practice and an example of it is covering lampshades inside with a golden layer. The effects on colour fidelity are much more complex and specific.

Since these context-dependent, spatially and directionally varying, space-material-light-interaction effects can be substantial, applications involving 3D objects (and people; and thus relevant for most applications) need to be tested. To that aim, we propose to test real samples in mock-ups or create physically accurate renders of spaces embedded with colour checkers in various locations. Traditional 2D checkers will not show these effects because they are flat and matt and thus will average out the differential effects of diffuse and directed light. The 3D version of the colour checkers in Figure 3.8 show those directional effects [38, 39, 71]. In this manner, it is possible to visually assess chromatic, spatial and directional effects of lighting-scene interactions on colour appearance.

We have identified the following limitations of our method, which will be addressed in future work. Both R_a and R_f are defined within certain D_{uv} limits and considered meaningful to quantify the colour fidelity of direct white illumination (lamp). Here we also considered spaces illuminated by direct white illumination, while the secondary illumination was chromatic due to inter-reflections originating from coloured materials. In some instances, the chromatic inter-reflections had major impacts. As a result, the light density due to diffuse scattering became highly chromatic, even beyond the D_{uv} limits of those metrics. Those spaces were intended to be illuminated by white light with suitable colour rendition rather than chromatic light. Additionally, those metrics assume complete chromatic adaption to the test illuminant while adaptation might be incomplete due to spatially and directionally varying chromaticities, and hence, the built-in CAT (chromatic adaptation transform) might overcompensate the colour constancy effect. Moreover, the differences between light density and light vector will have differential effects on shad(ow)ed and (high)lighted parts of 3D objects and people, rendering their appearance with chromatic gradients. Other cognitive and perceptual effects such as discounting inter-reflections might affect whether humans perceive such effects, but have only been investigated in limited settings [72, 73]. Nonetheless, these works showed that in many cases, discounting inter-reflections by human observers was far from complete, and the level of discounting depended on geometrical configurations and shape perceptions. In addition, Figure 3.8 shows how these mechanisms can have aesthetic effects that might be wanted or not, *e.g.* as can be seen when comparing

the colour appearance of the green spheres in the white and coloured rooms. Furthermore, we used simple box spaces furnished with materials mainly scattering diffusely and coloured evenly, while natural scenes have complex geometries and diverse materials with various BRDFs. Direct lighting can also exist in combinations of various spectral and spatial properties. Our spectral light-field framework is well-suited also for capturing angular, spatial and spectral power variations of light in such complex natural scenes.

3.6. CONCLUSION

This article aims to quantify the impact of (inter-)reflections on the effective CCT and colour fidelity within the light field. We measured light-density and light-vector spectra and calculated their associated colorimetric values in uni-chromatic box spaces illuminated by ordinary white light. The effective CCT and colour fidelity varied as a function of location and direction within the light field and depended on the illuminant SPDs, material SRFs and scene geometry. We found major differences between the lamp-specified CCT and colour fidelity and the actual light-based or effective CCT and colour fidelity. The SPD of the diffuse light-field component is predominantly defined by material SRFs, and the directional component by the illuminant. The existing lamp-based metrics work well in common lighting applications, however, we found that the effects of material-light interactions on the chromatic properties of effective light can be substantial and vary spectrally, spatially, and directionally. Therefore, applications that involve colour rendering in spaces composed of chromatic materials could potentially benefit from not only assessing the CCT and CRM of the light source but by also assessing the effective CCT and CRM in context. Further research that addresses the chromatic effects of inter-reflections on the overall perception of real scenes is necessary to confirm these findings. Capturing the light density and light vector and calculating their metrics separately allows us to understand the interactions between illuminant and scene and to systematically analyse the spatial and directional variations of spectral power throughout a scene; in other words, the chromatic light field. In addition, 3D versions of colour checkers, for which we proposed simple Lambertian spheres, allow lighting designers, architects, and computer graphics artists to visually assess the light density and vector effects [34, 63, 74–78]. In summary, we showed that our proposed methods of capturing the light density and vector, calculating their colour metrics separately and throughout spaces, and using 3D colour checkers for visual assessment provide insights to measure, visualise, and understand complex material-space-light interactions in a systematic approach.

SUPPLEMENTARY MATERIAL

See SupplementaryMaterial.docx [48] and SupplementaryMaterial_Spectra.xlsx [49] for supporting content.

REFERENCES

[1] M. S. Langer. “A model of how interreflections can affect color appearance”. In: *Color Research & Application* 26.S1 (2001), S218–S221.

[2] B. V. Funt and M. S. Drew. “Color space analysis of mutual illumination”. In: *IEEE Transactions on Pattern Analysis and Machine Intelligence* 15.12 (1993), pp. 1319–1326.

[3] C. Yu, E. Eisemann, and S. Pont. “Effects of inter-reflections on the chromatic structure of the light field”. In: *Lighting Research & Technology* 55.2 (2023), pp. 218–236.

[4] S. Bará and J. Escofet. “On lamps, walls, and eyes: The spectral radiance field and the evaluation of light pollution indoors”. In: *Journal of Quantitative Spectroscopy and Radiative Transfer* 205 (2018), pp. 267–277.

[5] C. Yu. “Effects of inter-reflections on the chromatic structure of the light field”. In: *British Congress of Optometry and Vision Science 2021 Abstracts*. Ed. by S. Strong. Vol. 42. 1. 2022, p. 253.

[6] C. Yu and S. Pont. “Quantifying Natural Light for Lighting and Display Design”. In: *SID Symposium Digest of Technical Papers*. Vol. 52. S2. Society for Information Display China. 2021, pp. 99–103.

[7] C. Yu, M. Wijntjes, E. Eisemann, and S. Pont. “Effects of inter-reflections on the correlated colour temperature and colour rendition of the light field”. In: *Lighting Research & Technology* 0.0 (2022), pp. 1–22.

[8] A. Hurlbert. “Challenges to color constancy in a contemporary light”. In: *Current Opinion in Behavioral Sciences* 30 (2019), pp. 186–193.

[9] M. P. Royer. “What is the reference? An examination of alternatives to the reference sources used in IES TM-30-15”. In: *LEUKOS* 13.2 (2017), pp. 71–89.

[10] A. David, K. A. G. Smet, and L. Whitehead. “Methods for assessing quantity and quality of illumination”. In: *Annual Review of Vision Science* 5 (2019), pp. 479–502.

[11] K. A. G. Smet, W. R. Ryckaert, M. R. Pointer, G. Deconinck, and P. Hanselaer. “Memory colours and colour quality evaluation of conventional and solid-state lamps”. In: *Optics Express* 18.25 (2010), pp. 26229–26244.

[12] M. P. Royer, K. W. Houser, and A. M. Wilkerson. “Color discrimination capability under highly structured spectra”. In: *Color Research & Application* 37.6 (2012), pp. 441–449.

[13] M. Wei, K. W. Houser, G. R. Allen, and W. W. Beers. “Color preference under LEDs with diminished yellow emission”. In: *LEUKOS* 10.3 (2014), pp. 119–131.

[14] K. W. Houser, M. Wei, A. David, and M. R. Krames. “Whiteness perception under LED illumination”. In: *LEUKOS* 10.3 (2014), pp. 165–180.

[15] K. Houser, M. Mossman, K. Smet, and L. Whitehead. “Tutorial: color rendering and its applications in lighting”. In: *LEUKOS* 12.1-2 (2016), pp. 7–26.

[16] X. Guo and K. W. Houser. “A review of colour rendering indices and their application to commercial light sources”. In: *Lighting Research & Technology* 36.3 (2004), pp. 183–197.

[17] J. A. Worthey. “Color rendering: asking the question”. In: *Color Research & Application* 28.6 (2003), pp. 403–412.

[18] D. Geisler-Moroder and A. Dür. “Color-rendering indices in global illumination methods”. In: *Journal of Electronic Imaging* 18.4 (2009), pp. 043015–043015.

[19] W. Davis and Y. Ohno. “Color quality scale”. In: *Optical Engineering* 49.3 (2010), p. 033602.

[20] C. Li, M. Ronnier Luo, C. Li, and G. Cui. “The CRI-CAM02UCS colour rendering index”. In: *Color Research & Application* 37.3 (2012), pp. 160–167.

[21] P. van der Burgt and J. van Kemenade. “About color rendition of light sources: The balance between simplicity and accuracy”. In: *Color research & application* 35.2 (2010), pp. 85–93.

[22] A. David, P. T. Fini, K. W. Houser, Y. Ohno, M. P. Royer, K. A. G. Smet, M. Wei, and L. Whitehead. “Development of the IES method for evaluating the color rendition of light sources”. In: *Optics Express* 23.12 (2015), pp. 15888–15906.

[23] M. S. Rea and J. Freyssinier. “Color rendering: Beyond pride and prejudice”. In: *Color Research & Application* 35.6 (2010), pp. 401–409.

[24] M. P. Royer. “IES TM-30-15 is approved—now what? Moving forward with new color rendition measures”. In: *LEUKOS* 12.1-2 (2016), pp. 3–5.

[25] M. P. Royer. “Tutorial: Background and guidance for using the ANSI/IES TM-30 method for evaluating light source color rendition”. In: *LEUKOS* 18.2 (2022), pp. 191–231.

[26] H. Yaguchi, A. David, T. Fuchida, K. Hashimoto, G. Heidel, W. Jordan, S. Jost-Boissard, S. Kobayashi, T. Kotani, R. Luo, *et al. CIE 2017 colour fidelity index for accurate scientific use*. CIE Central Bureau, 2017.

[27] L. Neumann and J. Schanda. “Effect of interreflections in a room on the colour rendering of light source”. In: *Conference on Colour in Graphics, Imaging, and Vision*. Society of Imaging Science and Technology. 2006, pp. 283–286.

[28] C. Yu and S. Pont. “The influence of material colors on the effective color rendering and temperature through mutual illumination”. In: *Color and Imaging Conference*. Vol. 2020. 28. Society for Imaging Science and Technology. 2020, pp. 293–298.

[29] C. Yu and S. Pont. “Spatial and Angular Variations of Colour Rendition due to Interreflections”. In: *Proceedings of London Imaging Meeting*. Online, 2020, p. xv.

[30] J.-J. Embrechts. “The effect of walls on colour rendering”. In: *Lighting Research & Technology* 17.3 (1985), pp. 122–128.

[31] S. C. Pont. “Light: toward a transdisciplinary science of appearance and atmosphere”. In: *Annual review of vision science* 5 (2019), pp. 503–527.

[32] E. H. Adelson, J. R. Bergen, *et al.* “The plenoptic function and the elements of early vision”. In: *Computational models of visual processing* 1.2 (1991), pp. 3–20.

[33] A. A. Mury, S. C. Pont, and J. J. Koenderink. “Structure of light fields in natural scenes”. In: *Applied Optics* 48.28 (2009), pp. 5386–5395.

[34] L. Xia, S. C. Pont, and I. Heynderick. “Separate and simultaneous adjustment of light qualities in a real scene”. In: *i-Perception* 8.1 (2017), pp. 1–24.

[35] L. Xia, R. Xu, T. Zhang, and X. Liu. “Theory and simulation of calculating local illuminance density based on high dynamic range panoramic maps”. In: *Lighting Research & Technology* 54.4 (2022), pp. 329–345.

[36] L. Xia, S. C. Pont, and I. Heynderickx. “Light diffuseness metric part 1: Theory”. In: *Lighting Research & Technology* 49.4 (2017), pp. 411–427.

[37] K. Doerschner, H. Boyaci, and L. T. Maloney. “Testing limits on matte surface color perception in three-dimensional scenes with complex light fields”. In: *Vision Research* 47.28 (2007), pp. 3409–3423.

[38] C. Yu, E. Eisemann, M. W. Wijntjes, J. J. R. van Assen, and S. C. Pont. “Effects of inter-reflections in box spaces on perceived object color harmony and shape”. In: *Journal of Vision* 21.9 (2021), pp. 1992–1992.

[39] C. Yu, E. Eisemann, M. W. A. Wijntjes, J. J. R. van Assen, and S. C. Pont. “Chromatic light field effects on perceived modelling and colour harmony”. In: CIE Midterm Meeting. Online, 2021.

[40] C. Yu, E. Eisemann, and S. Pont. “Colour variations within light fields: Interreflections and colour effects”. In: *Perception* 48 (2019), pp. 59–59.

[41] J. Koenderink, A. van Doorn, and K. Gegenfurtner. “RGB colors and ecological optics”. In: *Frontiers in Computer Science* 3 (2021), p. 630370.

[42] L. D. Griffin. “Reconciling the statistics of spectral reflectance and colour”. In: *Plos one* 14.11 (2019), e0223069.

[43] E. J. Warrant and S. Johnsen. “Vision and the light environment”. In: *Current Biology* 23.22 (2013), R990–R994.

[44] D.-E. Nilsson and J. Smolka. “Quantifying biologically essential aspects of environmental light”. In: *Journal of the Royal Society Interface* 18.177 (2021), p. 20210184.

[45] J. Koenderink, A. van Doorn, and K. Gegenfurtner. “Colors and things”. In: *i-Perception* 11.6 (2020), pp. 1–43.

[46] J. J. Koenderink. *Color for the Sciences*. MIT press, 2010.

[47] P. J. Marlow, K. R. Gegenfurtner, and B. L. Anderson. “The role of color in the perception of three-dimensional shape”. In: *Current Biology* 32.6 (2022), pp. 1387–1394.

[48] C. Yu, M. Wijntjes, E. Eisemann, and S. Pont. “sj-docx-2-lrt-10.1177_14771535221126902 – Supplemental material for: Effects of inter-reflections on the correlated colour temperature and colour rendition of the light field”. In: *Figshare* (2022).

[49] C. Yu, M. Wijntjes, E. Eisemann, and S. Pont. “sj-xlsx-1-lrt-10.1177_14771535221126902 – Supplemental material for: Effects of inter-reflections on the correlated colour temperature and colour rendition of the light field”. In: *Figshare* (2022).

[50] L. Xia, S. C. Pont, and I. Heynderickx. “Light diffuseness metric, Part 2: Describing, measuring and visualising the light flow and diffuseness in three-dimensional spaces”. In: *Lighting Research & Technology* 49.4 (2017), pp. 428–445.

[51] C. Cuttle. “Cubic illumination”. In: *Lighting Research & Technology* 29.1 (1997), pp. 1–14.

[52] S. Aston, K. Denisova, A. Hurlbert, M. Olkkonen, B. Pearce, M. Rudd, A. Werner, and B. Xiao. “Exploring the determinants of color perception using #thedress and its variants: The role of spatio-chromatic context, chromatic illumination, and material–light interaction”. In: *Perception* 49.11 (2020), pp. 1235–1251.

[53] A. Gilchrist, C. Kossyfidis, F. Bonato, T. Agostini, J. Cataliotti, X. Li, B. Spehar, V. Annan, and E. Economou. “An anchoring theory of lightness perception”. In: *Psychological review* 106.4 (1999), p. 795.

[54] V. Walsh and J. Kulikowski. *Perceptual constancy: Why things look as they do*. Cambridge University Press, 1998.

[55] M. E. Rudd and I. K. Zemach. “The highest luminance anchoring rule in achromatic color perception: Some counterexamples and an alternative theory”. In: *Journal of Vision* 5.11:5 (2005), pp. 983–1003.

[56] D. H. Foster. “Color constancy”. In: *Vision research* 51.7 (2011), pp. 674–700.

[57] T. Azuma, E. Barthés, H. Einhorn, M. Halstead, C. Jerome, J. de Kerf, J. Krtil, W. Münch, J. Ouweitjes, M. Richter, and G. Siljeholm. *Method of Measuring and Specifying Colour Rendering Properties of Light Sources*. CIE Central Bureau, 1995.

[58] K. A. Smet. “Tutorial: the LuxPy Python toolbox for lighting and color science”. In: *LEUKOS* 16.3 (2020), pp. 179–201.

[59] A. N. S. Institution. *ANSI C78.377-2017 - Electric Lamps - Specifications for the Chromaticity of Solid-State Lighting Products*. National Electrical Manufacturers Association, 2017.

[60] E. C. Carter, J. D. Schanda, R. Hirschler, S. Jost, M. R. Luo, M. Melgosa, Y. Ohno, M. R. Pointer, D. C. Rich, F. Viénot, L. Whitehead, and J. H. Wold. *Colorimetry, 4th Edition*. CIE Central Bureau, 2018.

[61] Illuminating Engineering Society. *IES Method for Evaluating Light Source Color Rendition*. New York, NY: Illuminating Engineering Society, 2018.

[62] J. P. S. Parkkinen, J. Hallikainen, and T. Jaaskelainen. "Characteristic spectra of Munsell colors". In: *Journal of the Optical Society of America A* 6.2 (1989), pp. 318–322.

[63] T. Kartashova, S. F. te Pas, H. de Ridder, and S. C. Pont. "Light shapes: Perception-based visualizations of the global light transport". In: *ACM Transactions on Applied Perception (TAP)* 16.1 (2019), pp. 1–17.

[64] C. Reinhart and P.-F. Breton. "Experimental validation of Autodesk® 3ds Max® Design 2009 and DAYSIM 3.0". In: *LEUKOS* 6.1 (2009), pp. 7–35.

[65] I. Ashdown. "The influence of color interreflections on lighting simulations". In: *LEUKOS* 7.3 (2011), pp. 159–166.

[66] A. I. Ruppertsberg and M. Bloj. "Creating physically accurate visual stimuli for free: Spectral rendering with RADIANCE". In: *Behavior Research Methods* 40.1 (2008), pp. 304–308.

[67] A. I. Ruppertsberg and M. Bloj. "Rendering complex scenes for psychophysics using RADIANCE: How accurate can you get?" In: *Journal of the Optical Society of America A* 23.4 (2006), pp. 759–768.

[68] C. Yu, M. Wijntjes, E. Eisemann, and S. Pont. "Spatial and temporal dynamics of effective daylight in natural scenes". In: *Journal of Vision* 22.14 (2022), pp. 3984–3984.

[69] C. Yu, M. Wijntjes, E. Eisemann, and S. Pont. "Disentangling object color from illuminant color: The role of color shifts". In: *Journal of vision* 22.3 (2022), pp. 37–37.

[70] C. Yu and Y. Zhu. "Surface-reflectance discrimination is optimized in the presence of inter-reflections". In: *European Conference on Visual Perception*. 2021.

[71] F. Szabo, P. Bodrogi, and J. Schanda. "Experimental modeling of colour harmony". In: *Color Research & Application* 35.1 (2010), pp. 34–49.

[72] M. G. Bloj, D. Kersten, and A. C. Hurlbert. "Perception of three-dimensional shape influences colour perception through mutual illumination". In: *Nature* 402.6764 (1999), pp. 877–879.

[73] K. Doerschner, H. Boyaci, and L. T. Maloney. "Human observers compensate for secondary illumination originating in nearby chromatic surfaces". In: *Journal of vision* 4.2:3 (2004), pp. 92–105.

[74] C. Cuttle. *Lighting by design*. Routledge, 2008.

[75] C. Cuttle. "Lighting patterns and the flow of light". In: *Lighting Research & Technology* 3.3 (1971), pp. 171–189.

[76] J. J. Koenderink, S. C. Pont, A. J. van Doorn, A. M. L. Kappers, and J. T. Todd. "The visual light field". In: *Perception* 36.11 (2007), pp. 1595–1610.

[77] M. Toscani, K. R. Gegenfurtner, and K. Doerschner. “Differences in illumination estimation in #thedress”. In: *Journal of Vision* 17.1:22 (2017), pp. 1–14.

[78] L. Xia, S. C. Pont, and I. Heynderickx. “The visual light field in real scenes”. In: *i-Perception* 5.7 (2014), pp. 613–629.

4

QUANTIFYING THE SPATIAL, TEMPORAL, ANGULAR AND SPECTRAL STRUCTURE OF EFFECTIVE DAYLIGHT IN PERCEPTUALLY MEANINGFUL WAYS

We present a method to capture the 7-dimensional light field structure, and translate it into perceptually-relevant information. Our spectral cubic illumination method quantifies objective correlates of perceptually relevant diffuse and directed light components, including their variations over time, space, in colour and direction, and the environment's response to sky and sunlight. We applied it "in the wild", capturing how light on a sunny day differs between light and shadow, and how light varies over sunny and cloudy days. We discuss the added value of our method for capturing nuanced lighting effects on scene and object appearance, such as chromatic gradients.

Published as: C. Yu, M. Wijntjes, E. Eisemann, and S. Pont. Quantifying the spatial, temporal, angular and spectral structure of effective daylight in perceptually meaningful ways. In: *Optics Express* 31.5 (2023), pp. 8953–8974. DOI: 10.1364/OE.479715

4.1. INTRODUCTION

MEASUREMENTS of the light environment play a crucial role in diverse fields such as architecture, lighting design, vision science and visual ergonomics. They need to characterize light in a human perception-based manner to provide meaningful information for human-centred fields and applications. In this context, photometry [1] instead of radiometry is required. Natural light varies as a function of space, direction, wavelength and time. In this paper, we focus on the question how to capture and describe perceptually meaningful light qualities relating to the complexity of all those variations in an effective manner.

Gershun first introduced the concept of the light field as a way to formally describe how light is structured in a three-dimensional scene [2]. He coined the light field as a function of radiance depending on location (x, y, z), direction (θ, ϕ), wavelength (λ) and time (t). This function is thus seven-dimensional, and in human vision it is known as the plenoptic function [3], which quantifies all optic information that is potentially available to an observer. In that sense it provides a starting point for studying objective aspects of the light environment. The visual light field describes the observers' subjective inferences of the physical light field, which generally differ from the objective physical ones [4–6]. Here we focus on the physical light field. However, in order to derive information from the light-field measurements that are meaningful for human-centred fields and applications, we take a perception-based approach in simplifying and quantifying the high-dimensional light-field data. So, in this study we capture the physical light field and analyze its structure in a perception-based manner.

Light fields in natural environments are dynamic and complicated, because natural scenes usually consist of complex spaces, shapes, materials, and lighting, that optically interact with each other. Luckily, any local light field can be decomposed as a weighted sum of basic spherical functions using spherical harmonics (SH) [7–11] and a scene's light field can thereby be sampled, described and visualized approximately via sparse measurements [10] in a simplified and intuitive manner [12]. Spherical harmonics are angular functions with increasing frequency that can be represented as monopoles, dipoles, quadrupoles, etc (see Figure 4.1 for an illustration). These functions form a complete basis for describing the variation of illumination on a sphere. This mathematical basis has an immediate optical meaning [9, 13–15], and its components have been shown to be directly related to perceptual judgments [4, 16, 17]. The zero-order SH component is a scalar known as light density, and the SH decomposition's first coefficient represents its strength. Its physical meaning is the spectral irradiance averaged over all directions. Perceptually, it is associated with the strength of the ambient light. The first-order SH component represents the light vector, whose strength and direction can be described with three coefficients. Its physical meaning is the net spectral irradiance transport [2, 9]. Perceptually, it is associated with the strength and direction of a directional source. Deducting the contribution of the vector component from the illumination solid gives an estimate of the symmetric component [8, 18]. The symmetric component has the property that, for any plane passing through the measurement point, it produces equal irradiance on opposite sides. The second-order SH component is the

squash tensor [9], requiring five coefficients. It can be considered as a light or dark clamp. The third- and higher-order SH components can be summarised statistically to represent the "brilliance" or "light texture" of the light environment [19].

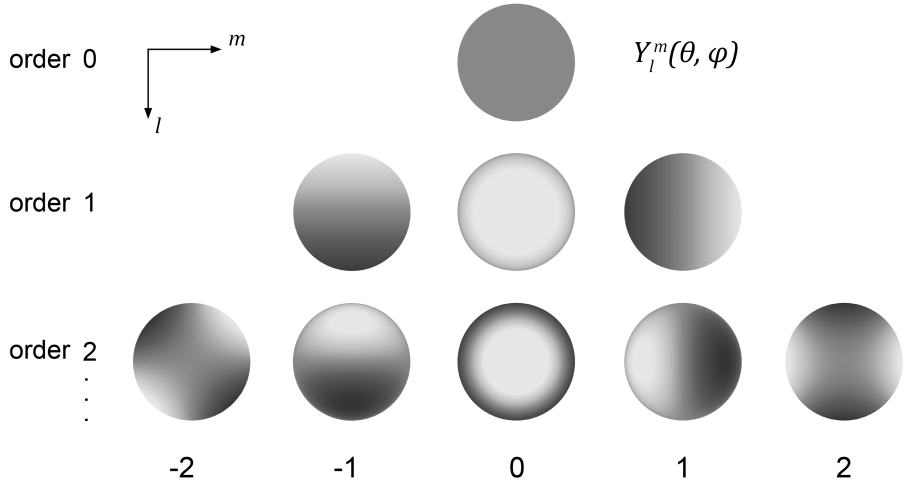

Figure 4.1: Real spherical harmonics of orders 0, 1, and 2, corresponding to first nine basis functions. The front of the sphere is shown, with white to light gray representing positive values and black to dark gray representing negative values. These images show the real form of the spherical harmonics. The connection between these functions and Gershun's theory is explained in detail in the work of Mury *et al.* [9–11].

Recently, progress has been made in measuring the optical light field. In several studies, the light field was captured using imaging or photosensor systems (Table 4.1). In the imaging approach, a digital camera is used to either photograph the environment directly [20] or indirectly via the reflection of the environment from a mirror sphere [11, 21, 22]. An advantage of these approaches is the high angular resolution. Direct photographing requires a digital camera equipped with a fisheye lens and rotation tripod. Such cameras typically possess only three spectral channels, *i.e.* red, green and blue (RGB) [20]. This coarse spectral resolution might not always be sufficient for accurate colorimetric description [14, 23, 24]. A (hyper)spectral camera provides a spectrally resolved solution [21]. However, taking a single hyperspectral image is time-consuming and thus this method cannot be used to capture fine temporal variations. Additionally, both imaging approaches have the disadvantage that the extremely high dynamic range (HDR) of natural exterior light environments often exceeds these devices' capturing ranges, and then need photos with multiple exposures to cover the environments' ranges. This is impossible in dynamic scenes because the light will change between different photos. Moreover, it results in relatively large measurement errors.

Omnidirectional photosensor systems combine many photosensors to capture the irradiance in all directions. Such a system provides a low-angular-resolution but high-dynamic-range, and real-time measurement of the local light field. Several

Table 4.1: Studies that employed light-field methods to characterize the light environment.

Studies	Light-field aspects taken into account							
	HDR*		Temporal resolution†		Spectral resolution‡		Directional resolution§	
Morimoto *et al.* [21]	-	2250:1 (11 stops)	-	40 minutes per spherical image	Hyperspectral	400–720 nm in 10 nm interval	✓	∞**
Li *et al.* [22]	-	400:1 with 2 integration times	-	up to 90 minutes per spherical image	Hyperspectral	400–1000 nm in 7 nm interval	✓	∞
Nilsson *et al.* [20]	-	2 orders with 3 integration times	-	up to 68.5 minutes per spherical image	Multispectral	RGB††	✓	∞
Adams *et al.* [25]	✓	63096:1 (26 stops)	-	up to 24 minutes per spherical image	Multispectral	RGB	✓	∞
Mury *et al.* [10]	✓	7 orders	✓	Real-time (1 second)‖	Multispectral	Luminance	✓	SH order 2
Morgenstern *et al.* [26]	✓	5 orders (ranging from low-lit indoor scenes to direct sunlight)	✓	Real-time (1 second)	Monospectral	Luminance	✓	SH order 2
Xia *et al.* [27]	✓	7 orders (0.01–299,900 lux)	✓	Real-time (1 second)	Monospectral	Luminance	✓	SH order 1

– denotes exclusion.
✓ denotes inclusion.
∗ Order of HDR means the order of magnitudes of the dynamic range.
† The temporal resolution is given for a measurement at a single location and the spatial resolution is ignored in this table.
‡ Mono-, multi- and hyperspectral refer to a single band, 3 to 10 wide bands and hundreds of narrow bands [28–30], respectively.
§ SH order means the order to which the spherical harmonics can be estimated.
∗∗ The notation ∞ at directional resolution should be interpreted as a very high angular resolution that is limited by the number of pixels in the panoramic image.
‖ Multidirectional photosensors arranged in a spherical configuration offer the ability to simultaneously measure the entire solid angle without the need for time-consuming reorientation.
†† RGB is here used as a coarse representation of the visible spectrum [24], divided into Red, Green and Blue bands, with Red typically around 568–700 nm, Green around 482–568 nm, and Blue around 400–482 nm, and dominant wavelengths of 457, 530, and 597 nm respectively.

researchers built such omnidirectional devices with varying numbers of sensors [8, 9, 31] but no spectral resolution. Connected to this approach is the question

of how many sensors are needed to measure the light field in a certain angular resolution, while keeping the information tractable. The SH description provides a fundamental basis for understanding what is needed depending on the objectives. The minimal number of sensors needed equals the total number of coefficients required for the order of the mathematical description of the local light field, e.g. one needs at least four sensors to estimate the first-order SH description and at least nine for the second-order approximation. Ramamoorthi *et al.* [32] proved formally that a second-order SH approximation of local illumination suffices to describe the appearance of convex matte objects, since the bidirectional reflectance distribution function (BRDF) of matte material acts as a low-pass filter on directional variations in the light field. In most natural scenes, diffuse scattering dominates in the material BRDFs. Much of the light field is then dominated by diffuse scattering [9], causing it to behave smoothly, and allowing capturing by sparse measurements [10]. It is thus sufficient to quantify the light environment of a diffuse scene or a scene dominated by diffuse scattering via a second-order light-field approach. A dodecahedron-shaped plenopter equipped with 12 evenly distributed sensors can measure a second-order approximation of the light field [9]. However, the resulting second-order squash tensor may be difficult for non-experts to interpret. Xia *et al.* [27] used a custom cubic apparatus with six sensors to robustly measure the first-order approximation of the light field. Their first-order SH decomposition [8] includes only the light density and light vector, and they found that Cuttle's approach [18, 31, 33], using a set of simple linear functions, can be used to estimate the same metrics. A first-order light field approach is able to explain 94% of matte object appearances [34] or diffuse scattering, making it a practical and effective choice for descriptive purposes. Moreover, this description captures the key elements of the subjective correlate of the light field, the visual light field [6, 13]. However, in environments with multiple highly directional light sources or strong reflections, higher-order components may be necessary to predict fine details of the appearance of the environment and especially objects with spiky reflectance functions such as shiny materials.

In this paper, we extended the cubic system to a spectral HDR cubic illumination system to capture up to the first-order spectral local light fields. The system is portable and suitable for field research. We also show how perception-based metrics can be derived from the cubic samples, to capture spectral, angular, temporal and spatial variations of effective daylight. We demonstrate the approach with measurements of data sets collected in natural exterior scenes. We found that the differential chromatic effects for the different light-field components in natural scenes were large. In our test cases, the spatial and temporal variations in illuminance and colour characteristics were the largest for the light vectors, medium for the light densities, and smallest for the symmetric component. Moreover, this approach allows capturing wavelength-dependent directional variations that we discuss to have important implications for predicting colour gradients in the appearances of objects and scenes. Our main contribution thus exists of the extension to the spectral domain under challenging HDR conditions, and showing how the complex 7-dimensional light field data can be captured and transformed into perceptually relevant information.

4.2. METHODS

Despite the fact that solar radiation is more or less static, effective daylight is dynamic. Earth's axial tilt along with rotation and revolution, complex atmospheric optical effects and the presence of occluders and mutual reflections cause variations in an observed effective daylight field [35–37]. We aimed to quantify temporal, spatial, angular and spectral variations of the effective light field in natural scenes by cubic measurements (spectrometers configured on the faces of a small cube). In order to quantify this complicated 7D function in a meaningful manner for humans, we convert the raw radiometric cubic data to perception-based light components and photometrical measures. In the subsections hereafter, we describe the cubic measurement systems, the data processing pipeline, and the two empirical studies.

4.2.1. SPECTRAL CUBIC ILLUMINATION MEASUREMENT

The spectral cubic irradiance was measured using two types of systems. The first system was relatively affordable and consisted of a portable handheld spectrophotometer (Sekonic C-7000, made in Japan in 2015) and a microscopic reference cube made of spectrally neutral white resin. Cubic measurements were done by placing the spectrophotometer consecutively on the cube's six faces and recording the spectral irradiances. The second system for measuring spectral cubic irradiance was a remotely addressable irradiance spectrophotometer (Konica Minolta CL-500A, made in Japan in 2011) mounted on a three-axis angle-adjustable tripod (shown in Figure 4.2(b)). The tripod occludes 2.97% of the entire solid angle. A laptop (Dell Latitude 7410) drove the irradiance spectrophotometer from a distance through an 8-meter-long USB cable via Data Management Software CL-S10w. The meter was oriented to all six cubic faces by adjusting the tripod. The operator then triggered and recorded the spectral irradiance measurement of each direction via the laptop.

The cube or tripod was aligned with the positive direction of the y-axis pointing North, and the positive direction of the z-axis facing upwards. Thus, the Cartesian coordinate system of the spectral cubic irradiance was oriented according to the principal directions in the geographic coordinate system. A compass was used to calibrate the orientations.

Dark calibrations were performed prior to the acquisitions. The spectral irradiance measurement was acquired over a wavelength range from 380 nm to 780 nm in 11 nm intervals for the Sekonic C-7000 and 360 nm to 780 nm in 10 nm intervals for the Konica Minolta CL-500A. The cubic measurements lasted one minute in daylight to five minutes at dawn and dusk. The Sekonic C-7000 can capture the irradiance over a dynamic range of five orders of magnitude (1 to 200,000 lux), and the Konica Minolta CL-500A of six orders (0.1 to 100,000 lux). The Sekonic C-7000 allows for fast reorientations, and thus it is suitable for spatial light-field measurements in an unstable light environment. The Konica Minolta CL-500A has the advantage of allowing measurements of dim light environments and remote control, minimizing the effects of (inter-)reflections from the operator. The operator was dressed in black to reduce the influence from (inter-)reflections as much as possible.

4.2.2. DATA PROCESSING AND ANALYSIS

THE BASIC COMPONENTS OF THE LIGHT FIELD

Estimates of the spectral light-field components were derived as follows. The systems give spectral cubic data, namely $\mathbf{E}_{(\lambda,x+)}$, $\mathbf{E}_{(\lambda,x-)}$, $\mathbf{E}_{(\lambda,y+)}$, $\mathbf{E}_{(\lambda,y-)}$, $\mathbf{E}_{(\lambda,z+)}$ and $\mathbf{E}_{(\lambda,z-)}$ [31, 38] (Figure 4.2(a)). The cubic measurements $\mathbf{E}_{(\lambda,x+)}$ and $\mathbf{E}_{(\lambda,x-)}$ represent the opposed pair of spectral irradiances along the x-axis (East and West), and analogous for the y (North and South) and z axes (up and down). The spectral irradiances of the light-vector components in the x, y and z directions were estimated by subtracting the associated opposed paired measurements, respectively. For example, on the x axis,

$$E_{(\lambda,x)} = E_{(\lambda,x+)} - E_{(\lambda,x-)} \tag{4.1}$$

The light vector is defined as

$$E_{(\lambda,\text{vector})} = \left[E_{(\lambda,x)}, E_{(\lambda,y)}, E_{(\lambda,z)}\right] \tag{4.2}$$

The magnitude of the light vector in spectral irradiance, then is

$$\left|\mathbf{E}_{(\lambda,\text{vector})}\right| = \sqrt{E^2_{(\lambda,x)} + E^2_{(\lambda,y)} + E^2_{(\lambda,z)}} \tag{4.3}$$

The magnitude of the symmetric sub-component $\sim E_{(\lambda,x)}$ equals the magnitude of the lesser of $E_{(\lambda,x+)}$ and $E_{(\lambda,x-)}$,

$$\sim E_{(\lambda,x)} = \frac{E_{(\lambda,x+)} + E_{(\lambda,x-)} - \left|E_{(\lambda,x)}\right|}{2} \tag{4.4}$$

The mean of the symmetric sub-components for the three axes gives a measure of the magnitude of the symmetric component.

$$E_{(\lambda,\text{symmetric})} = \frac{\sim E_{(\lambda,x)} + \sim E_{(\lambda,y)} + \sim E_{(\lambda,z)}}{3} \tag{4.5}$$

The light density is defined as the average spectral irradiance from every direction. It equals Cuttle's light scalar, the sum of the symmetric component and weighted light vector magnitude, up to a normalization constant [8].

$$E_{(\lambda,\text{scalar})} = E_{(\lambda,\text{symmetric})} + \frac{\left|\mathbf{E}_{(\lambda,\text{vector})}\right|}{4} \tag{4.6}$$

The linear combination of the symmetric and vector components forms a spherical harmonics (SH) approximation of the illumination map up to the first order, as

shown in Figure 4.2(c-d). It is important to note that the symmetric component is actually a spherical distribution which is generally not uniform, but in practice can be defined adequately by its magnitude [39]. Research by Xia *et al.* has shown that Cuttle's scalar-vector approach provides the same information as the SH density-vector approach, with some normalization constants applied. Each of these components can also be spectrally resolved, as demonstrated in Figure 4.2(g). It is worth mentioning that the illustration here uses 21 spectral bands with a 20 nm increment, but the number of bands can be as large as the equipment's resolution capabilities.

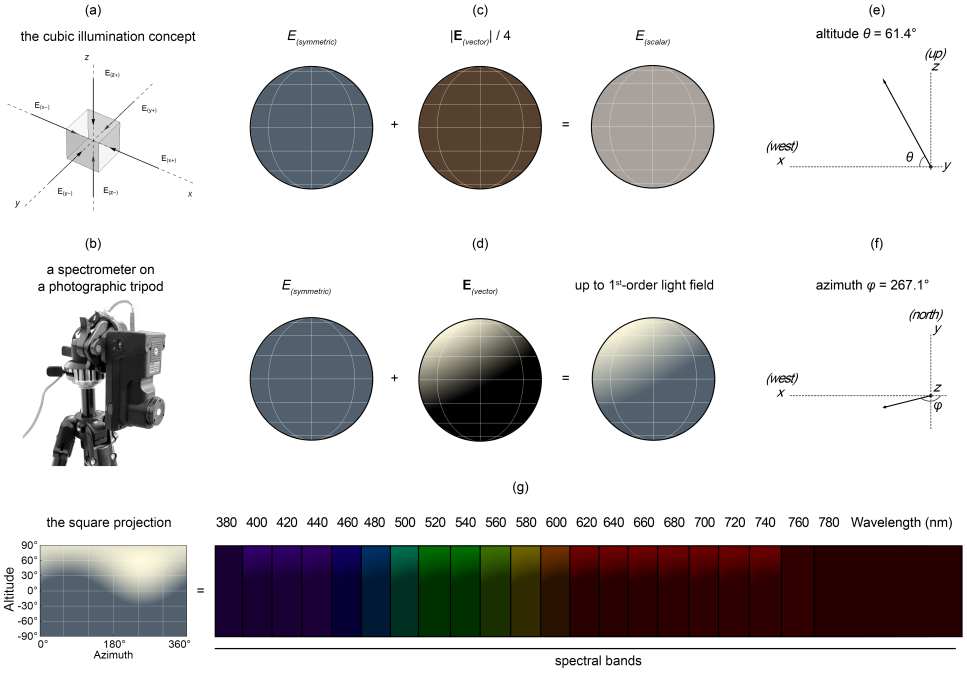

Figure 4.2: Quantification of up to the first-order light field with the spectral cubic illumination method measured outdoors in the afternoon. (a) Six spectral irradiances on the faces of a small reference cube define the spectral cubic illumination (local light field). (b) The spectrophotometer mounted on a tripod to capture spectral cubic illumination. (c) The symmetric and vector components' magnitudes add up to the light scalar. (d) The symmetric component's magnitude plus the light vector gives up to the first-order light field. (e) The altitude of the light vector. (f) The azimuth of the light vector. (g) Representation of the square-projected illumination map, computed independently for each wavelength. Here we show 21 spectral bands from 380 nm to 780 nm in an increment of 20 nm for simplification. See Figure S1 of Supplement 1 for a 360-degree panoramic view of the surrounding measurement environment.

The photometric values of the components were calculated in the following way. The inner product of the luminosity function $\bar{y}_{(\lambda)}$ with the spectral irradiance over the visible spectral range gave their illuminance, as below for the x-direction.

$$E_{(x)} = 683 \cdot \int_{\lambda=380}^{780} \bar{y}_{(\lambda)} E_{(\lambda,x)} d\lambda \tag{4.7}$$

For each of the metrics, the corresponding CIE tristimulus values, (x,y) chromaticity coordinates and CCT were calculated according to standard methods [40]. We used the CIE physiologically relevant 2-degree photopic luminosity function and the CIE standardized 2015 2-degree XYZ colour matching functions [40, 41] to perform these calculations.

The vector altitude (θ) and azimuth angles (ϕ) were derived from the direction of the light vector, which is entirely determined by $(E(x), E(y), E(z))$ in Cartesian coordinates (see Figure 4.2(e-f)). Thus,

$$\theta = \tan^{-1}\left(\frac{E_{(z)}}{\sqrt{E_{(x)}^2 + E_{(y)}^2}}\right) \tag{4.8}$$

$$\phi = \tan^{-1}\left(\frac{E_{(y)}}{E_{(x)}}\right) \tag{4.9}$$

The light diffuseness [8] was defined as one minus the ratio between the light-vector and light-scalar magnitudes divided by 4 and ranges from 0 for fully collimated light to 1 for spherically diffuse or Ganzfeld light.

$$D_{\text{normalized}} = 1 - \frac{|\mathbf{E}_{\text{vector}}|}{4E_{\text{scalar}}} \tag{4.10}$$

4.2.3. MEASUREMENTS OF NATURAL LIGHT FIELDS

Our proposed approach allows for measuring 7D light fields in any scene in real time. This however would need a matrix of cubic systems to be operated remotely. In practice, financial limitations made it necessary to split our measurements into two experiments, showing spectral and directional variations as a function of space in one experiment, and as a function of time in the other experiment.

In Experiment 1 (spatial experiment), we aimed to capture and compare spectral and directional variations of the daylight field over space. Therefore we chose to compare the light field in direct sunlight and in shadow parts of exterior scenes. We took cubic measurements of natural outdoor scenes during daytime in July 2020 and August 2021 at multiple locations around the Delft University of Technology campus (52.0116° N, 4.3571° E; elevation 0 m), located in the Northern hemisphere, on sunny days with a blue sky, around noon. A total of 24 natural scenes were selected. The scenes included a variety of coloured surfaces in both rural and urban settings. They were chosen to contain surfaces that were partly lit by sunlight and partly in the shade as to capture two light zones [42, 43] in the light field. In each of the 24 scenes, the local light fields of the sample points in the light and shade were acquired within 1 minute, yielding a total of 48 local light field measurements.

The acquisition was done via the Sekonic C-7000. For illustration purposes, we also photographed all scenes via a Canon EOS 5D Mark II camera as raw images with a constant 5500 K white balance, matching to average noon daylight.

In Experiment 2 (temporal experiment), we aimed to capture temporal variations over the day for a sunny and a cloudy day. We used the Konica Minolta CL-500A device to collect local light fields from a rural location (51.9795° N, 4.3850° E; elevation 0 m) in the Delft region of the Netherlands at a 5-minute interval from dawn to dusk on September 22 in autumn and on December 8, 2021 in winter. The location was an area where anthropogenic light sources were minimal for exclusive characterization of effective daylight. The sky on the first day was clear, while that on the second day was cloudy with strong wind. The full-day measurements took place within the just-before-dawn to just-after-dusk periods of 06:30–20:15 in September and 07:20–17:40 in December. In total, 165 cubic measurements were collected on the sunny day and 124 on the cloudy day (the daytime was shorter in winter). Meanwhile, we also used a spherical camera (Panono Camera) to capture HDR illumination maps at a 60-minute interval for visual illustration.

In our study, we used two systems for measuring spectral cubic irradiance: the Sekonic C-7000 and the Konica Minolta CL-500A. The Sekonic C-7000 was used in Experiment 1, where fast reorientation was needed in a complex dynamic environment. The Konica Minolta CL-500A was used in Experiment 2, where a high dynamic range was necessary for measuring dim light environments. These systems were chosen to effectively address the unique challenges presented in each scenario, and by using them together we were able to gather more accurate and reliable data to analyze the light environment.

Dataset 1 [44] contains raw spectral cubic illumination measurements of both experiments, which are made freely available.

4.3. RESULTS

4.3.1. EXPERIMENT 1: SPATIAL VARIATIONS OF CHROMATIC LIGHT FIELDS IN NATURAL SCENES

In Figure 4.3, we show the photographs of the measured scenes, showing that sunlit parts appeared brighter with more directed yellowish light and shadow parts appeared darker with more diffuse blueish light. We can also see clear effects on the appearance of the scenes. For example, in Scene 12, the colour appearance of the slender vervain flower was reddish magenta in the light but blueish purple in the shade. The step between the cast shadow and the illuminated area did not just form an illuminance edge but also a chromatic edge (see Figure S2 of Supplement 1 for detailed results).

In order to visualize the results, a light probe, a white Lambertian sphere [6], was superimposed on a photograph of the location where the cubic measurement was taken. The appearance of the probe was then rendered under each approximated illumination map derived from the cubic measurements. For ease of understanding, the spectral images of the rendered probes were then converted to RGB colour

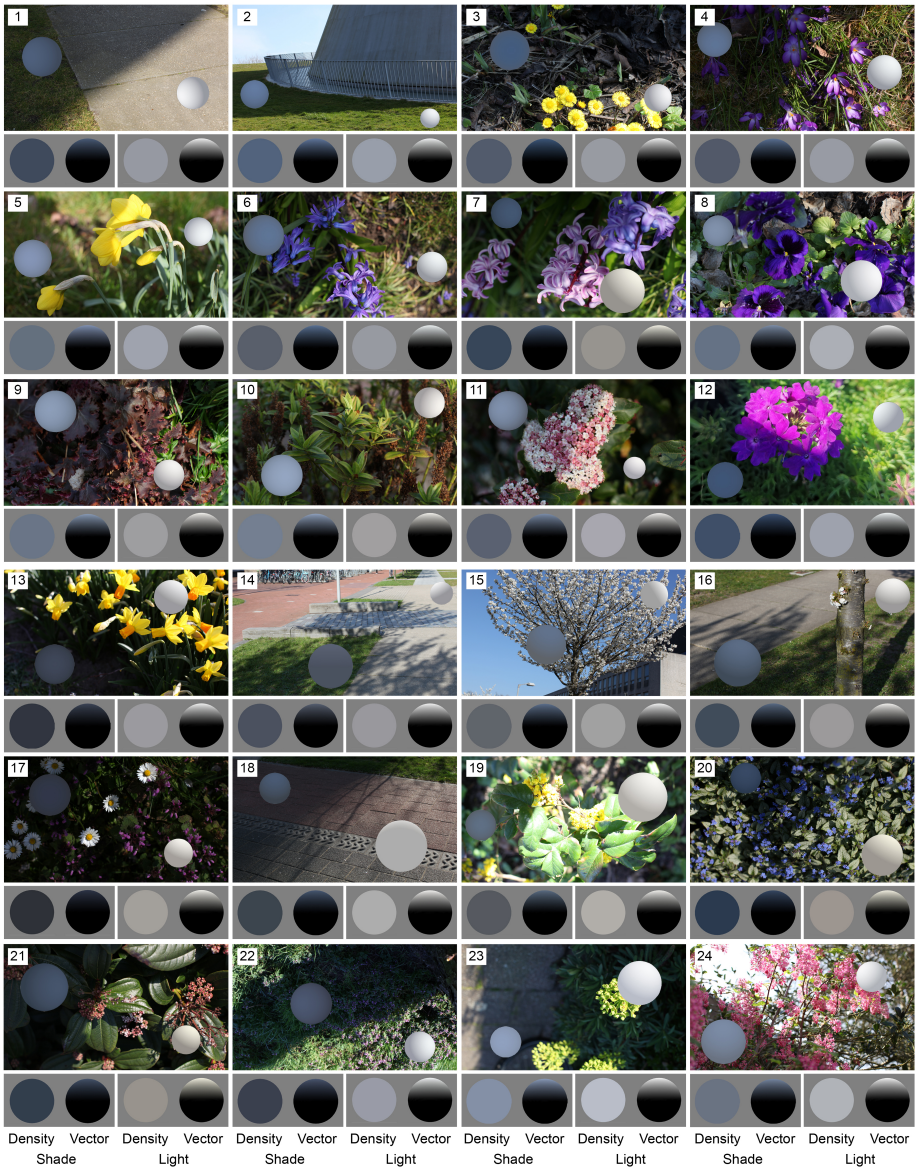

Figure 4.3: The collection of all the selected natural scenes' photographs. Light probes were rendered for 1st-order local light field approximations as if they were embedded in the scenes. Below each scene photograph, the decomposed local light fields are shown. The light-vector directions were normalized to point upward in the decomposed light-field probe renderings. The 24 scenes were arranged from left to right and top to bottom in numerical order from 1 to 24.

images. Additionally, a gamma value of 2.2 was applied to the linearized rendered spheres for display on a screen. Please note that only six spectra per image were considered, which corresponds to the six facets of the cube. The images of the spheres presented in Figure 4.3 should not be taken as actual spectral data, but rather as a reference for visualization purposes. The light probes in the cast shadow appeared bluer and darker than those in the sun. In addition, the light probes indicate a diffuseness difference between sunlit and shadowed, which causes a difference in texture contrast [45].

Figure 4.4(a) shows the CCT of the light-field components in the shade and light for all measured scenes. The light density CCTs in the shade (blue bars) were consistently higher than in the light (yellow bars), with an average difference of 1821 ± 1232 K (mean ± 1SD). The light vectors in shade and light had even larger CCT differences, 3542 ± 1680 K (mean ± 1SD). By contrast, the CCTs of the symmetric components in the shade were not consistently higher than in the light, and their differences were relatively small, 655 ± 1183 K (mean ± 1SD). The data presented in the form of inverse CCT can be found in Supplement 1, Figure S3.

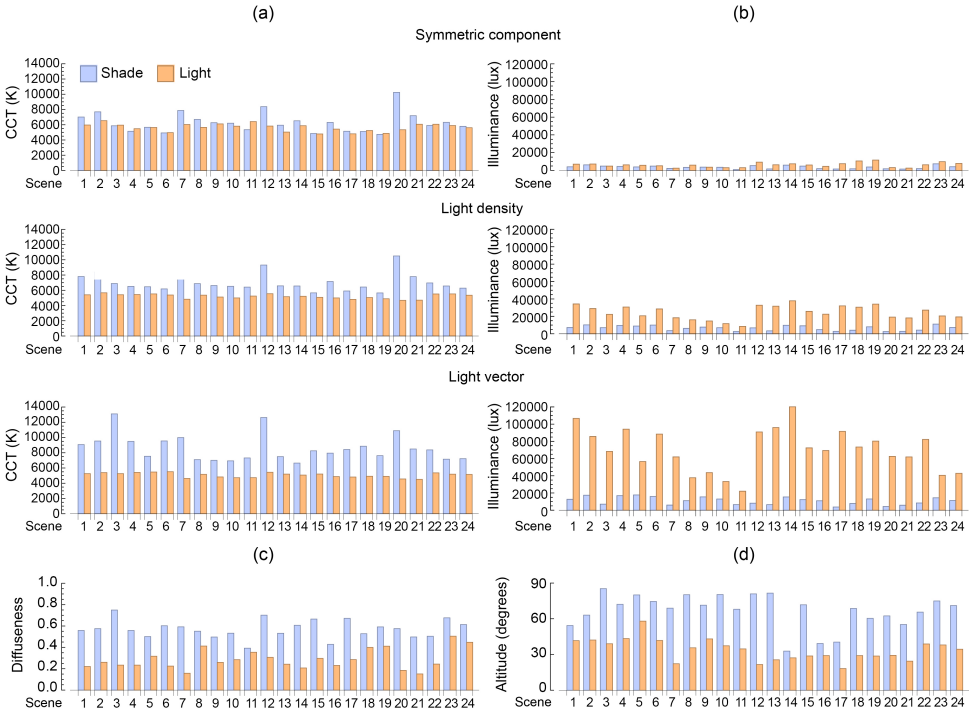

Figure 4.4: The scene metrics in the shade and light. The (a) CCTs and (b) illuminance of symmetric component (top), light density (middle) and light vector (bottom) for the shade (blue bars) and light (yellow bars) regions. The (c) diffuseness and (d) altitude of the light vector for the shade (blue bars) and light (yellow bars) regions. The number on the horizontal axis indicates the scene number.

Figure 4.4(b) shows the illuminance of the different light-field components in the same format. The illuminance of the light densities and vectors showed considerable differences in the shade and light regions as expected, while the light vectors' differences were larger (up to five orders of magnitude, 15,577–104,803 lux) than for the light densities (up to four orders of magnitude, 4716–29,259 lux). The illuminance differences between shadow and light for the symmetric component were smaller (up to four orders of magnitude, 12–10,077 lux).

Figure 4.4(c) shows the measured scenes' diffuseness in the shade and light. The illuminance of the light density in the shade was relatively high compared to the light vector, resulting in overall high diffuseness values (0.4–0.8). The light vector is much stronger than the density in the light region, resulting in high directionality or low diffuseness values (0.1–0.5). The altitudes of the light vector in the shade (33°–85°) were higher than in the light (18°–58°), revealing an average light-direction difference (Figure 4.4(d)).

Figure 4.5(a) shows the average spectra of the different light-field components in the shade and light. Before averaging, all spectra were converted to have equal luminous flux (CIE tristimulus value Y = 100). Overall, the spectra in the shade and light for the symmetric component showed a resemblance, with peaks in the long-wavelength part. The light-density spectra in the shade differed from those in the light, especially in the long-wavelength part. Those differences were larger for the light vector.

Figure 4.5(b) shows the associated chromaticities, which closely followed the daylight locus. The chromaticities of the symmetric components for shade and light regions overlapped, while that in the shade showed a larger spread along the daylight locus towards the blue region (Figure 4.5(b) left). The chromaticities of the light density of the shade and light regions separated in different clusters on the daylight locus at both sides of D55 (mid-morning or mid-afternoon daylight) (Figure 4.5(b) middle), and those of the light vector were even more apart (Figure 4.5(b) right).

In Figure 4.5(c), we present the colour differences between the shade and light conditions for the three light-field components. These colour differences were estimated using the CIE ΔE2000 metric in the CIELAB colour space, which is known to be perceptually uniform within a reasonable approximation [46]. To calculate the ΔE values, we first converted the tristimulus CIE XYZ values derived from the light-field component spectra into CIELAB using the D50 white point. A ΔE value of 1 represents the just noticeable difference, values between 1 and 5 are considered to be discriminable when viewed adjacent, values between 5 and 10 are considered perceptible, and values greater than 10 are considered different colour categories [47]. As shown in the figure, the colour differences of the symmetric components (1–23) were smaller than those of the light densities (14–43), which in turn were smaller than those for the light vectors (25–67). Additionally, the colour differences varied over the different scenes. The colour differences of the light densities had a strong positive correlation with those of the light vector (r = 0.91, $p < 0.001$), as well as with those of the symmetric component (r = 0.62, $p < 0.001$). However, the correlation between the colour differences of the light vector and symmetric component was weak and not statistically significant (r = 0.32, $p > 0.1$).

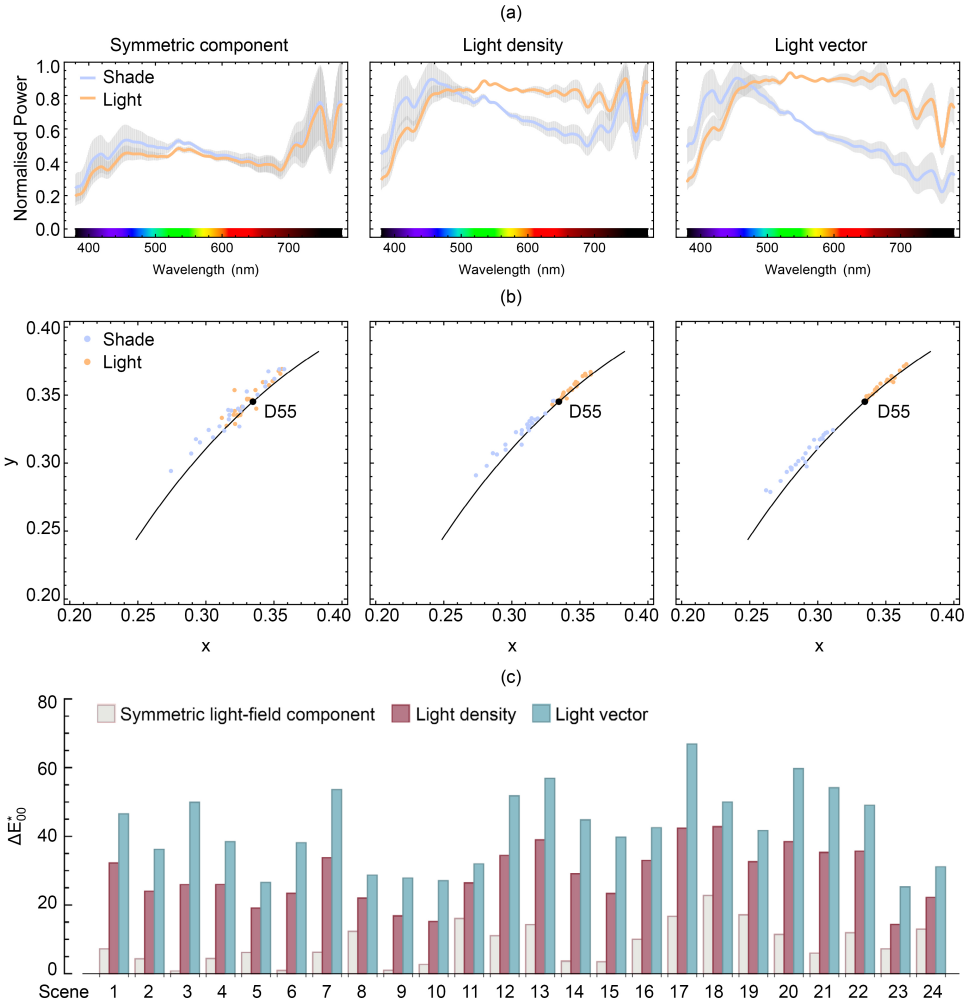

Figure 4.5: Spectra and chromatic properties for the scenes of Figure 4.2. (a) normalized mean spectra with the gray area depicting ± SD and (b) chromaticity coordinates of the 24 scenes for symmetric component, light density and light vector (left to right) in the shade (blue) and light (yellow) regions. The black dot represents D55 for reference. (c) colour differences (CIE ΔE2000) between the shade and light regions for the symmetric component (grey bar), light density (brown bar) and light vector (blue bar).

4.3.2. CONCLUSIONS EXPERIMENT 1

Natural daylight constitutes a varying mix of sunlight and skylight. As demonstrated by local light-field measurements, the light densities and vectors in the shade consistently showed higher CCT and lower illuminance than in the light, and those differences for the light vectors were even larger. This was expected since

the blue-rich and low luminous skylight is the prime light source in the shade, though the magnitude of the effects differs for different scenes. The CCT and illuminance of the symmetric components were found to be more or less similar in shade and light. The most credible reason is that the omnidirectional nature of (inter-)reflected light results in a relatively constant symmetric component over the scenes. Additionally, the light fields in the shade showed higher diffuseness relative to those in the light. These spatial variations in local light field illuminance, diffuseness, directions and spectral properties were found to be large. Moreover, our light-field data highlighted the differential luminous and chromatic properties for diffuse and directed components of natural light fields.

4.3.3. EXPERIMENT 2: TEMPORAL VARIATIONS OF CHROMATIC LIGHT FIELDS IN NATURAL SCENES

Figure 4.6 shows the panoramic images of the scene at different times of day in a light probe format for sunny (a) and cloudy (b) weather conditions. These low-dynamic-range images are only for illustrative purposes. We can see the atmospheric features, such as clouds, and how they varied on the sunny day (Figure 4.6(a)) and cloudy day (Figure 4.6(b)).

SUNNY DAY

Figure 4.7(a) shows the temporal changes in CCT on the sunny day. The CCTs of the light vector ranged from 2764–20118K, covering a larger span than the symmetric component (3796–11,364 K) (Figure 4.7(a) upper row). The CCT range of the light density (3819–14,544 K) was in between those ranges, as expected.

During effective daytime from 8:30 to 18:30 (when the sun appeared visible at the measurement location), the light vector CCTs expressed smooth changes from lower (3981 K) to higher (5740 K) and then back to lower (4063 K) values with an average speed (AVs) of 0.23 K/s. The light density behaved similarly, while the changes were less smooth but faster (0.25 K/s). However, the CCTs of the symmetric component fluctuated in a higher range (5005–7332 K) with an even faster average speed (0.51 K/s).

The effective twilight (when the sun was invisible to the measurement location) expressed extremely high CCTs, as high as 20,118 K for the light vector, 14,544 K for the light density and 11,364 K for the symmetric component. The fastest CCT changes occurred at effective sunrise (from high to low CCTs) and sunset (from low to high CCTs) rather than astronomical sunset and sunrise. During the effective twilight period, the speed of CCT changes for the light vector (3.9 K/s) was fastest relative to the light density (2.7 K/s) and symmetric component (2.1 K/s). Around effective sunrise, the transition from high to low CCTs for the symmetric component ended around 9:00, almost 0.5 hours later than for the light vector and light density. The transition from low to high CCTs during sunset for the symmetric component started 1.5 hours earlier, around 17:00, whilst the CCTs for the light vector and light density were still decreasing. Right after the effective sunrise and before the effective sunset, contrary to the warm light vector, the symmetric component at ground level

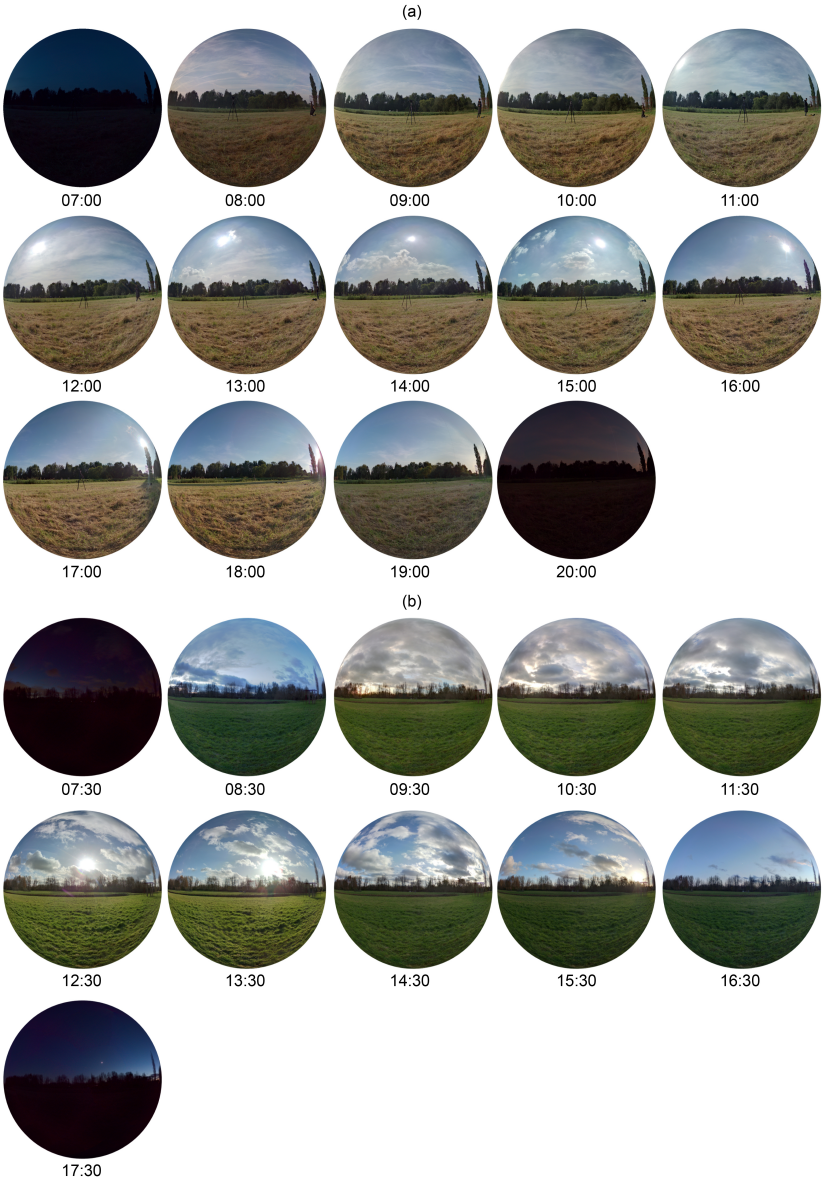

Figure 4.6: sRGB representations of illumination maps measured at a 60-minute interval via a Panono spherical camera.

was bluish and diffuse. Additional data presented in the form of inverse CCT can be located in Supplement 1, under Figure S4(a).

Figure 4.7(d) shows the hemispherical plots of the light vectors against the sun path of that day. The light-vector directions closely follow the sun path during the

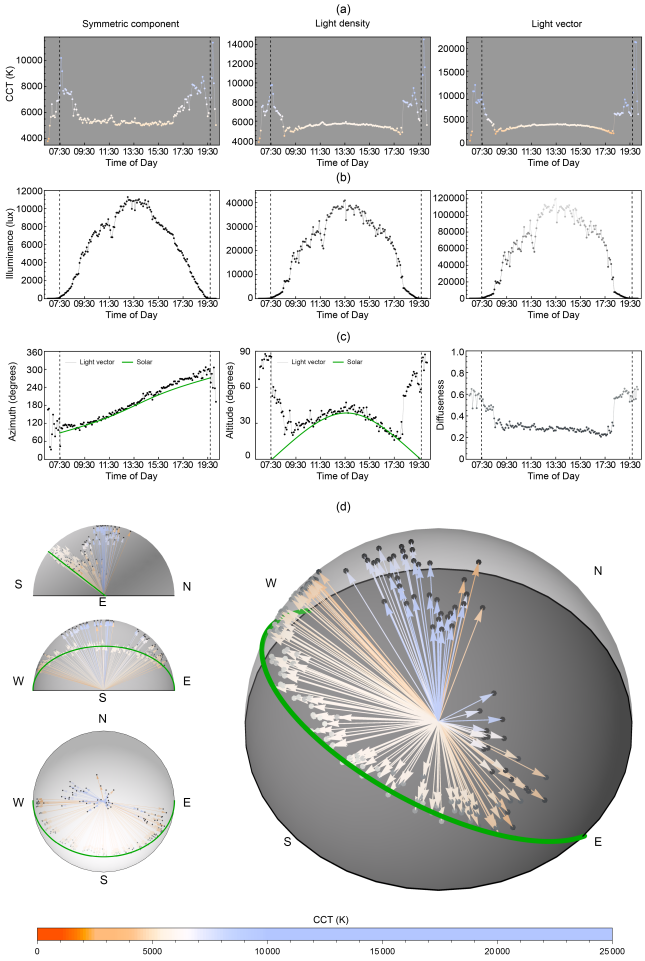

Figure 4.7: Presentation of temporally-resolved spectral cubic illumination data on the sunny day. Temporal CCT (a) and illuminance (b) variations for the symmetric component (left column), light density (middle column) and light vector (right column) within the natural light field. (c) Temporal light-vector azimuth (left column), light-vector altitude (middle column) and diffuseness (middle column) variations. The black dashed lines indicate astronomical sunrise and sunset time. (d) Temporal variations of sun positions and light-vector directions. Normalized light vectors plotted as east elevation (left column first row), south elevation (left column second row), top view (left column bottom row) and orthogonal view (right). The chromaticities of the light vectors are represented by the colours of the arrows, with the bar legend at the bottom of the figure providing a reference for the corresponding CCT values. The lightness of the points at the end of the arrowheads indicate the relative luminance of the light vectors. The green path indicates the sun's movement. The data was collected at a temporal resolution of every 5 minutes. Additional data presented in the form of inverse CCT can be found in Supplement 1, under Figure S4(a) for further analysis.

effective daytime, while those of effective twilight pointed upward (see also Figure 4.7(c) left two columns for the corresponding angles). The effective daytime light diffuseness was low with minor fluctuations and slightly dropped from 0.370 to 0.208 (Figure 4.7(c) right column). By contrast, the diffuseness of the effective twilight was up to 3 times higher, ranging from 0.444 to 0.669. The light-vector altitude and the diffuseness correlated (r = 0.873, $p < 0.001$) (Figure 4.9(a)). From Figure 4.7(b-c) right column, we can observe slight asymmetries of the vector's magnitude and the light diffuseness between morning and afternoon.

CLOUDY DAY

The day length shortened on the cloudy day, and the clouds periodically occluded the sun. Figure 4.8(a) shows temporal changes in CCT on the cloudy day. Throughout the whole day, the CCT ranges for the symmetric component (5122 K to 21,408 K), light density (4218 K to 20,625 K) and light vector (3853 K to 20,500 K) were large.

Over effective daytime between 9:30 to 16:00, the CCT of the light vector ranged from 3853 K to 10,170 K and fluctuated more than light density (4218 K to 10,210 K) and symmetric component (5122 K to 10,243 K) (Figure 4.8(a) upper row). The symmetric component expressed relatively higher CCT than the light vector around effective sunrise and sunset when the sun was present without cloud occlusions. The CCT difference between the symmetric and vector component was large at sunset (up to 5757 K at 15:40) and still considerable at sunrise (up to 1269 K at 09:30). The light vector showed larger and faster (2.7 K/s) CCT changes than the light density (2.4 K/s) and symmetric component (1.5 K/s) during effective daytime.

The effective twilight metrics were all rather bluish with a maximum CCT of 21,408 K. Approaching the effective sunrise (9:30) and sunset (16:00), there were the fastest CCT changes for the light vector (4.6 K/s), light density (4.2 K/s) and symmetric component (3.7 K/s). Further data presented in the form of inverse CCT can be found in Supplement 1, within Figure S4(b).

Figure 4.8(b) shows the temporal changes in illuminance on the cloudy day. The illuminance of the light vector was consistently higher (0.02–79,411 lux) than of the light density (0.006–25,125 lux) and symmetric component (0.0002–5273 lux). The values were lower than for the sunny day, and also fluctuated more, together, resulting in faster changes. The average speed for the light vector was the fastest (31.5 lux/s), followed by the light density (8.3 lux/s) and symmetric component (0.9 lux/s).

As Figure 4.8(b) the left column shows, the light-vector azimuth closely aligns with the sun position during the astronomical daytime. However, the light-vector altitude did not (Figure 4.8(b) middle). Effectively, the light-vector directions do not correspond to the sun positions (Figure 4.8(d)). Figure 4.8(b) right shows the diffuseness ranging from 0.135–0.620 with frequent fluctuations. Although these fluctuations look random, in Figure 4.8(b), we see that the light-vector altitude and diffuseness showed strong correlations (r = 0.821, $p < 0.001$).

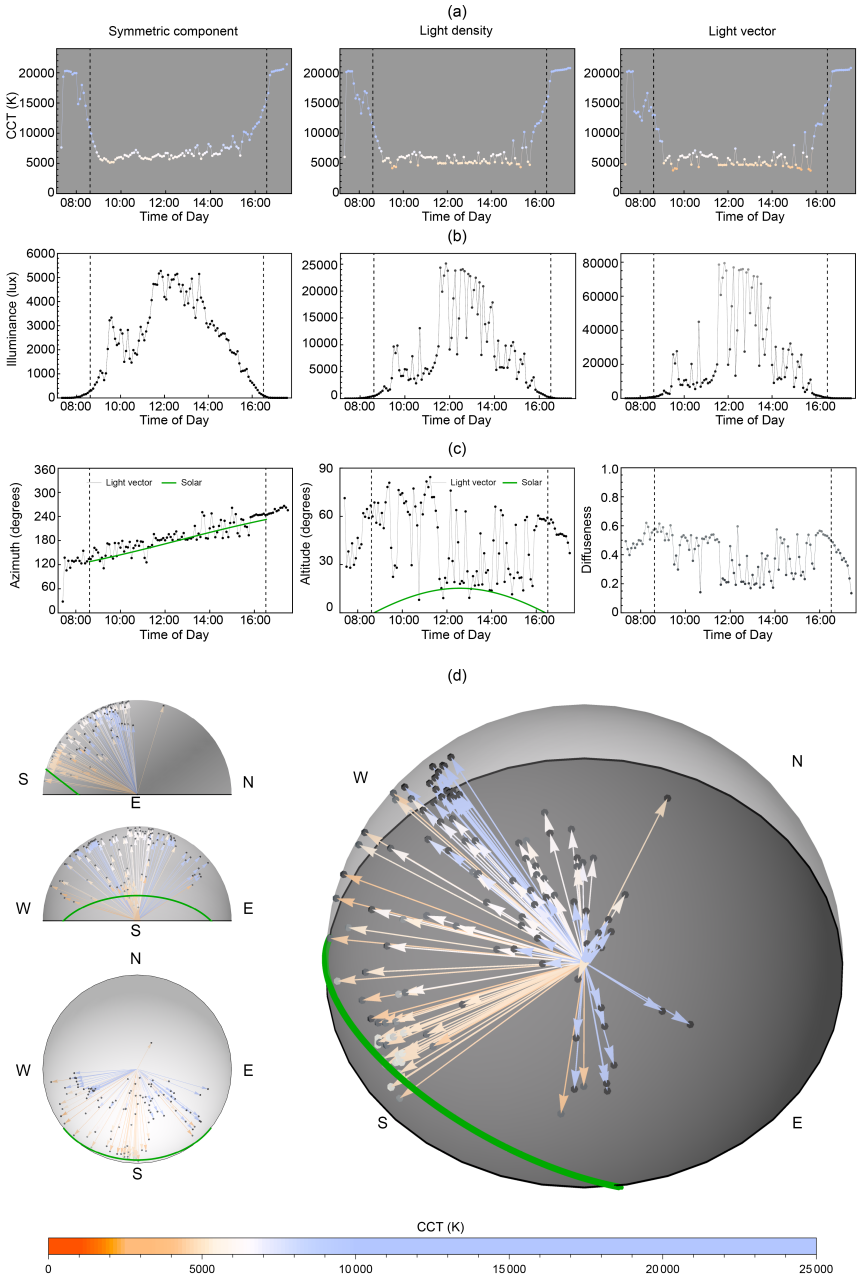

Figure 4.8: Presentation of temporally-resolved spectral cubic illumination data on the cloudy day. The figure configuration is the same as Figure 4.7. Additional data presented in the form of inverse CCT can be found in Supplement 1, under Figure S4(b) for further analysis.

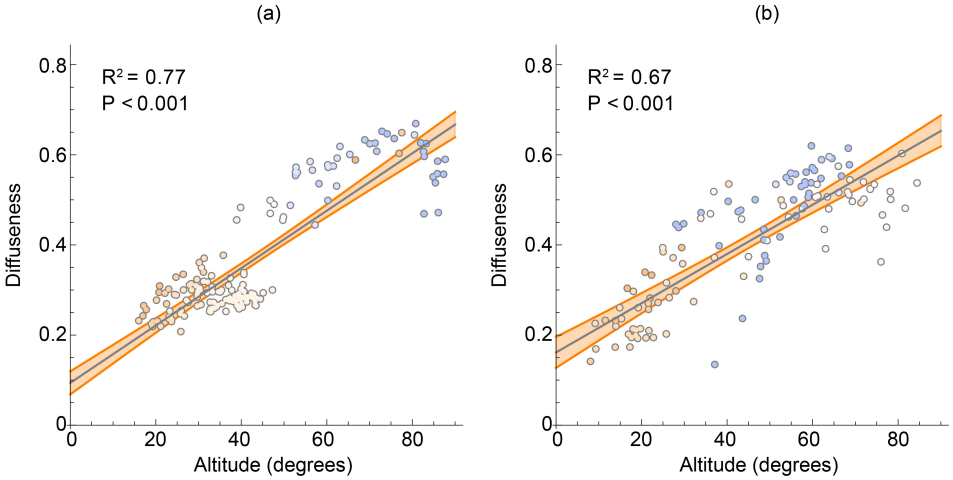

Figure 4.9: The scatterplots and correlations between light-vector altitude and diffuseness for the sunny day (a) and cloudy day (b). The area around the fitted lines represent the 95% CI. Disk colours approximately represent light-vector chromaticities.

4.3.4. CONCLUSIONS EXPERIMENT 2

Natural light (including both twilight and daylight) changes temporally in terms of CCT, illuminance, diffuseness and directions over the day. On both sunny and cloudy days, the CCT of all the light-field components expressed two blue spikes during dawn and dusk. For the effective daytime, the light-vector CCT changes on the sunny day showed a bell-shaped curve. On the cloudy day, this was disrupted with major fluctuations. The symmetric component showed relatively stable CCTs at a near-neutral white level (~D55) for both weather conditions, while the CCTs were overall higher and fluctuated more on the cloudy day than the sunny day. Again, a credible reason for its stability is that the omnidirectional nature of (inter-)reflected light results in a relatively constant symmetric component over the scenes. A plausible explanation for the higher CCT is that it also diffuses out the separate contributions from the yellowish sun and bluish sky. Additionally, overcasts are far from spectrally neutral transmitters [48] causing a bluer ambience than the sunny day. Light-density CCTs behaved more similarly to the light vectors than the symmetric component, which can be explained by the light-vector contribution to the density. The temporal profiles of the illuminance changes showed similar patterns (a bell-shaped curve) for the sunny and cloudy days. On the cloudy day, the illuminance fluctuated around the characteristic temporal profile. The temporal diffuseness changes correlated with light-vector altitude changes. This can probably be attributed to direct sunlight being present or absent. When the sun is behind the clouds or below the horizon, the diffuse skylight becomes the prime light source causing high diffuseness and light-vector altitude relative to sunlight-present conditions. The measurements revealed large variations in CCT and illuminance of

natural light over the days, and the temporal profiles for the different light-field components showed differential effects under both sunny and cloudy weather conditions.

4.4. DISCUSSION

In experiment one, we measured up to the first-order light fields in the shade and in the light for 24 sunlit rural and urban scenes across multiple days. Spectrally dependent Rayleigh scattering causes low-luminance highly diffuse bluish skylight and high-luminance highly directional yellowish sunlight during daytime, which was confirmed by the data. The spatially varying contributions from skylight and sunlight caused large CCT, illuminance, diffuseness, direction and colour differences between light and shade locations. In the shadowed parts of a scene, the diffuse light from the blue sky has the largest gain. The light field in the shade thus had much lower illuminance, higher CCTs and higher diffuseness relative to that in direct sunlight. These variations were found to be of the same prominence as the well-known temporal variations of daylight [49–51]. The spatial variations in terms of both illuminance and CCTs were larger for the light vectors than the light densities and symmetric components. We found experimentally that the symmetric component of the light field was rather constant over the scenes. This is consistent with Mury *et al.*'s study on light field constancy [11], which shows most materials diffusely scatter light causing relatively stable low-order components.

In experiment two, we measured spectral light fields throughout a sunny and cloudy day with 5-minute intervals. The different light-field components showed differential CCT and illuminance variations as a function of time. The light vector changed more in magnitudes of CCT and illuminance than the light density, and again than the symmetric component. The magnitude differences between different light-field components were smaller on the cloudy than sunny day, and this is presumably due to diffusion by the clouds. The light-field components expressed high CCT during the effective twilight period. This can be explained by Chappuis absorption [37, 52, 53] due to Ozone, inducing a progressive enrichment in the blue end of the spectrum ($< 500\,\text{nm}$) for the primary lighting. The slight asymmetries of the vector's magnitude and the light diffuseness between morning and afternoon on the sunny day might be attributed to Mie scattering by water droplets in the morning [54–58]. On the cloudy day the temporal variations were too large to signal such asymmetry.

The light-vector directions followed the sun's positions on the sunny day when the diffuseness was low. The misalignment of the light-vector directions and sun positions might be due to occlusion. High light-vector altitudes occur when the sun is absent from the measuring devices, including during twilight time and overcast conditions. The primary illumination then comes from the hemispherically diffuse skylight, resulting in high diffuseness and the observed positive correlations between light-vector altitude and diffuseness.

Those measurements however can be analyzed even further with regard to the spectral and directional properties. In Figure 4.10(a), we present a detailed

analysis of the light vectors measured at 18:10 on the sunny day (close to effective sunset when the sun appears at a low angle in the sky) in Experiment 2. The light vector direction is shown, which was computed based on the photometric values of the luminance channel, in line with the methodology used in the analysis of our experiments. In reality, the light-vector directions might also be wavelength-dependent, especially around sunset and sunrise. Figure 4.10(b-d) shows the light vectors sampled at different levels of spectral resolution, including multispectral (3 bands), hyperspectral (21 bands), and full spectral (401 bands) in the visible spectrum. The wavelength-dependent light vectors have similar azimuths, but the short-wavelength light vectors had higher altitudes than the long-wavelength ones. This can be explained by wavelength-dependent Rayleigh scattering resulting in the short wavelengths being scattered more than the long wavelengths. Figure 4.10(f) shows a white Lambertian sphere rendered under spectral light vectors ranging from 380 nm to 780 nm in 20 nm intervals. The shading induced by the spectral light vectors not only showed intensity differences but also varied in directions. The misalignment of these sub-band images can, after superposition, cause complex colour gradients for object shading (Figure 4.10(g) right), while such complex colour gradients get lost in renderings that only consider a single, average light-vector direction based on the luminance (Figure 4.10(g) left). Thus, the spectral rendering considering the wavelength dependency of light-vector directions provided more accurate colour gradient estimations than just relying on average light-vector directions. In the presence of multiple direct light sources with different chromaticities, quantifying both light-vector magnitudes and directions as a function of wavelength might be necessary to predict object appearance in such detail.

In addition, we represented the symmetric component as a constant, as indicated in Figure 4.2(d), instead of by its actual spherical distribution. Such simplification is adequate when the symmetric component is relatively uniform [8, 18]. In the case of non-uniform symmetric components, a physically correct rendering would need to take into account the symmetric component as distribution. Furthermore, a complete representation of the symmetric component should also include its wavelength dependency for precise object colour appearance estimation.

Our spectrometer system and the cubic illumination data-processing pipeline were shown to be well-suited for capturing spatial, temporal, angular and spectral variations of effective daylight. A limitation of the present study is related to the angular resolution that only suffices to quantify a light field SH description up to the first order. The second limitation is that the operator needs to manually adjust the 3D orientations of the spectrometer rather than take the multidirectional measurement simultaneously. Each spectral irradiance measurement can take approximately 0.5 seconds during daytime and 27 seconds during twilight time. A solution is to construct omnidirectional devices embedded with multiple spectrometers. The number of meters can be adjusted to the desired angular resolution or order of the SH approximation. Such a method can also further improve temporal resolutions. This will allow the measurement of additional spectral light-field datasets at different locations and times of day, seasons and weather conditions to further generalize the findings. Nevertheless, the present study provides a step toward quantifying the

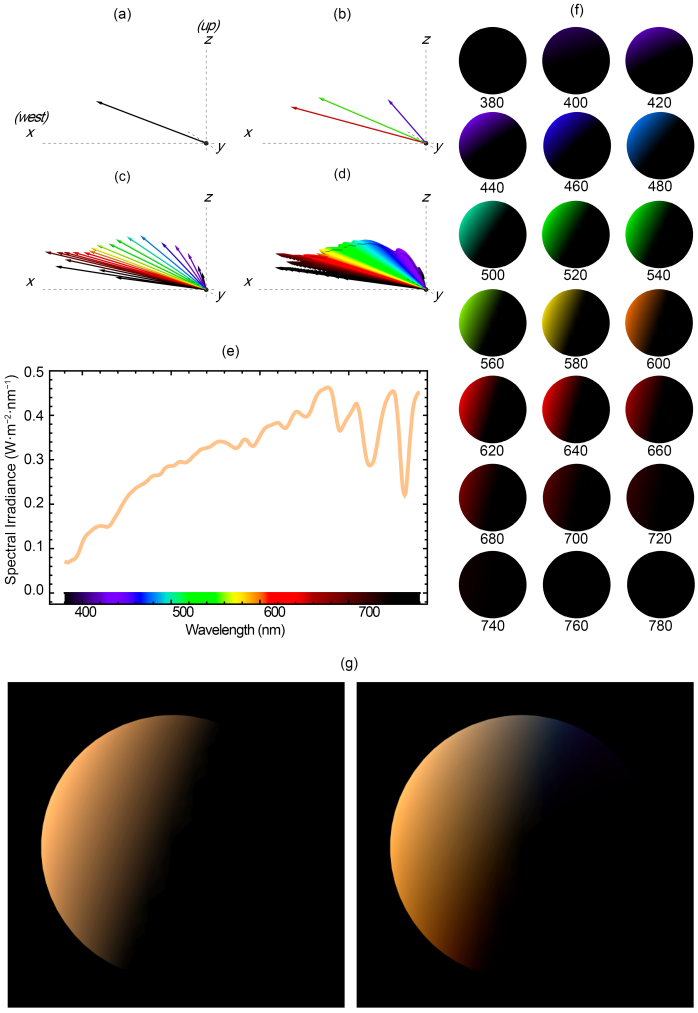

Figure 4.10: Spectral light-vector properties for a sample cubic measurement measured at 18:10 on the sunny day. The light-vector plots in Cartesian coordinates ordered from low spectral resolution to high spectral resolution, starting with the monospectral plot (a) which shows the luminance channel, followed by the multispectral plot (b) that samples the light vectors at 50 nm–120 nm intervals, the hyperspectral plot (c) that samples the light vectors at 20 nm intervals, and finally the full spectral plot (d) that samples the light vectors at 1 nm intervals, covering the wavelength range of 380 nm–780 nm. The lengths of the arrows indicate the relative radiant power. (e) The irradiance spectrum of the sample light vector (a), which is equivalent to light-vector magnitudes as a function of wavelength (d). (f) Wavelength sub-band images of a white Lambertian sphere rendered under hyperspectral light vector (c). (g) sRGB representations of spectral rendering by ignoring (left) or considering (right) wavelength-dependent light-vector directions.

temporal, spatial, angular and spectral variations of the light field.

4.5. CONCLUSION

In conclusion, the combination of the geometrical structure of scenes, the presence or absence of clouds, atmospheric scattering and varying sun angles leads to large illuminance, direction, colour and diffuseness differences from location to location and over time. The spectral cubic illumination method allows measuring these characteristics of effective light in the environment, providing temporally, spatially, spectrally and directionally resolved measurements. We also demonstrated how to separately analyze the differential contributions of the effective diffuse and directed day-light-field components and reveal their differential statistical properties. The spectral cubic illumination method offers a novel and convenient tool for assessing light environments, which will enable the characterization of visual signals crucial to various disciplines. Furthermore, we discussed how our method can be extended to full light field measurements of any order, and how the analysis can be extended to accurately predict natural chromatic gradients in scene appearance by incorporating the spectral dependency of light-vector directions. The dynamic nature of daylight can make it challenging to quantify fully, but our research has taken initial steps in capturing and decomposing the 7D light-field structure.

DATA AVAILABILITY

Data underlying the results presented in this paper are available in Dataset 1, Ref. [44].

SUPPLEMENTAL DOCUMENT

See Supplement 1 [59] for supporting content.

REFERENCES

[1] T. Kruisselbrink, R. Dangol, and A. Rosemann. “Photometric measurements of lighting quality: An overview”. In: *Building and Environment* 138 (2018), pp. 42–52.

[2] A. Gershun. “The light field”. In: *Journal of Mathematics and Physics* 18.1-4 (1939), pp. 51–151.

[3] E. H. Adelson, J. R. Bergen, *et al.* “The plenoptic function and the elements of early vision”. In: *Computational models of visual processing* 1.2 (1991), pp. 3–20.

[4] L. Xia, S. C. Pont, and I. Heynderickx. “The visual light field in real scenes”. In: *i-Perception* 5.7 (2014), pp. 613–629.

[5] T. Kartashova, H. de Ridder, S. F. te Pas, M. Schoemaker, and S. C. Pont. “The visual light field in paintings of Museum Prinsenhof: Comparing settings in empty space and on objects”. In: *Human vision and electronic imaging XX*. Vol. 9394. SPIE. 2015, pp. 554–563.

[6] J. J. Koenderink, S. C. Pont, A. J. van Doorn, A. M. L. Kappers, and J. T. Todd. “The visual light field”. In: *Perception* 36.11 (2007), pp. 1595–1610.

[7] R. Ramamoorthi. “Modeling illumination variation with spherical harmonics”. In: *Face Processing: Advanced Modeling Methods* (2006), pp. 385–424.

[8] L. Xia, S. C. Pont, and I. Heynderickx. “Light diffuseness metric part 1: Theory”. In: *Lighting Research & Technology* 49.4 (2017), pp. 411–427.

[9] A. A. Mury, S. C. Pont, and J. J. Koenderink. “Structure of light fields in natural scenes”. In: *Applied Optics* 48.28 (2009), pp. 5386–5395.

[10] A. A. Mury, S. C. Pont, and J. J. Koenderink. “Representing the light field in finite three-dimensional spaces from sparse discrete samples”. In: *Applied optics* 48.3 (2009), pp. 450–457.

[11] A. A. Mury, S. C. Pont, and J. J. Koenderink. “Light field constancy within natural scenes”. In: *Applied Optics* 46.29 (2007), pp. 7308–7316.

[12] T. Kartashova, D. Sekulovski, H. de Ridder, S. F. te Pas, and S. C. Pont. “The global structure of the visual light field and its relation to the physical light field”. In: *Journal of Vision* 16.10:9 (2016), pp. 1–16.

[13] S. C. Pont. “Light: toward a transdisciplinary science of appearance and atmosphere”. In: *Annual review of vision science* 5 (2019), pp. 503–527.

[14] C. Yu, M. Wijntjes, E. Eisemann, and S. Pont. “Effects of inter-reflections on the correlated colour temperature and colour rendition of the light field”. In: *Lighting Research & Technology* 0.0 (2022), pp. 1–22.

[15] S. C. Pont. “Ecological optics of natural materials and light fields”. In: *Human vision and electronic imaging XIV*. Vol. 7240. SPIE. 2009, pp. 62–73.

[16] L. Xia, S. C. Pont, and I. Heynderick. “Separate and simultaneous adjustment of light qualities in a real scene”. In: *i-Perception* 8.1 (2017), pp. 1–24.

[17] L. Xia, S. C. Pont, and I. Heynderickx. “Effects of scene content and layout on the perceived light direction in 3D spaces”. In: *Journal of Vision* 16.10:14 (2016), pp. 1–13.

[18] C. Cuttle. “Lighting patterns and the flow of light”. In: *Lighting Research & Technology* 3.3 (1971), pp. 171–189.

[19] F. Zhang, H. de Ridder, P. Barla, and S. Pont. “A systematic approach to testing and predicting light-material interactions”. In: *Journal of Vision* 19.4:11 (2019), pp. 1–22.

[20] D.-E. Nilsson and J. Smolka. “Quantifying biologically essential aspects of environmental light”. In: *Journal of the Royal Society Interface* 18.177 (2021), p. 20210184.

[21] T. Morimoto, S. Kishigami, J. M. Linhares, S. M. Nascimento, and H. E. Smithson. “Hyperspectral environmental illumination maps: characterizing directional spectral variation in natural environments”. In: *Optics Express* 27.22 (2019), pp. 32277–32293.

[22] L. Shiwen, L. Steel, C. A. Dahlsjö, S. N. Peirson, A. Shenkin, T. Morimoto, H. E. Smithson, and M. Spitschan. “Hyperspectral characterisation of natural illumination in woodland and forest environments”. In: *Novel Optical Systems, Methods, and Applications XXIV*. Vol. 11815. SPIE. 2021, pp. 32–41.

[23] A. I. Ruppertsberg and M. Bloj. “Creating physically accurate visual stimuli for free: Spectral rendering with RADIANCE”. In: *Behavior Research Methods* 40.1 (2008), pp. 304–308.

[24] J. Koenderink, A. van Doorn, and K. Gegenfurtner. “RGB colors and ecological optics”. In: *Frontiers in Computer Science* 3 (2021), p. 630370.

[25] W. J. Adams, J. H. Elder, E. W. Graf, J. Leyland, A. J. Lugtigheid, and A. Muryy. “The southampton-york natural scenes (syns) dataset: Statistics of surface attitude”. In: *Scientific reports* 6.1 (2016), p. 35805.

[26] Y. Morgenstern, W. S. Geisler, and R. F. Murray. “Human vision is attuned to the diffuseness of natural light”. In: *Journal of Vision* 14.9:15 (2014), pp. 1–18.

[27] L. Xia, S. C. Pont, and I. Heynderickx. “Light diffuseness metric, Part 2: Describing, measuring and visualising the light flow and diffuseness in three-dimensional spaces”. In: *Lighting Research & Technology* 49.4 (2017), pp. 428–445.

[28] T. J. Bihl, J. A. Martin, K. C. Gross, and K. W. Bauer. “Data and Feature Fusion Approaches for Anomaly Detection in Polarimetric Hyperspectral Imagery”. In: *NAECON 2021-IEEE National Aerospace and Electronics Conference*. IEEE. 2021, pp. 157–163.

[29] A. F. H. Goetz, G. Vane, J. E. Solomon, and B. N. Rock. “Imaging spectrometry for earth remote sensing”. In: *science* 228.4704 (1985), pp. 1147–1153.

[30] C. Fischer and I. Kakoulli. “Multispectral and hyperspectral imaging technologies in conservation: current research and potential applications”. In: *Studies in Conservation* 51.sup1 (2006), pp. 3–16.

[31] C. Cuttle. “Cubic illumination”. In: *Lighting Research & Technology* 29.1 (1997), pp. 1–14.

[32] R. Ramamoorthi and P. Hanrahan. “An efficient representation for irradiance environment maps”. In: *Proceedings of the 28th annual conference on Computer graphics and interactive techniques*. 2001, pp. 497–500.

[33] L. Xia, T. Tian, R. Xu, T. Zhang, and X. Liu. “Measuring low-order photometric parameters of light fields: Methods exploration and simulations”. In: *IEEE Access* 8 (2020), pp. 97408–97417.

[34] R. Basri and D. W. Jacobs. “Lambertian reflectance and linear subspaces”. In: *IEEE transactions on pattern analysis and machine intelligence* 25.2 (2003), pp. 218–233.

[35] J. Hernández-Andrés, J. Romero, J. L. Nieves, and R. L. Lee. “Color and spectral analysis of daylight in southern Europe”. In: *Journal of the Optical Society of America A* 18.6 (2001), pp. 1325–1335.

[36] D. B. Judd, D. L. MacAdam, G. Wyszecki, H. W. Budde, H. R. Condit, S. T. Henderson, and J. L. Simonds. “Spectral distribution of typical daylight as a function of correlated color temperature”. In: *Journal of the Optical Society of America A* 54.8 (1964), pp. 1031–1040.

[37] M. Spitschan, G. K. Aguirre, D. H. Brainard, and A. M. Sweeney. “Variation of outdoor illumination as a function of solar elevation and light pollution”. In: *Scientific reports* 6.1 (2016), pp. 1–14.

[38] C. Yu, E. Eisemann, and S. Pont. “Effects of inter-reflections on the chromatic structure of the light field”. In: *Lighting Research & Technology* 55.2 (2023), pp. 218–236.

[39] C. Cuttle. *Lighting by design*. Routledge, 2008.

[40] E. C. Carter, J. D. Schanda, R. Hirschler, S. Jost, M. R. Luo, M. Melgosa, Y. Ohno, M. R. Pointer, D. C. Rich, F. Viénot, L. Whitehead, and J. H. Wold. *Colorimetry, 4th Edition*. CIE Central Bureau, 2018.

[41] A. Stockman and L. T. Sharpe. “The spectral sensitivities of the middle-and long-wavelength-sensitive cones derived from measurements in observers of known genotype”. In: *Vision research* 40.13 (2000), pp. 1711–1737.

[42] T. Kartashova, H. de Ridder, S. F. te Pas, and S. C. Pont. “Visual light zones”. In: *i-Perception* 9.3 (2018), pp. 1–20.

[43] M. Madsen *et al.* “Light-zone(s): as Concept and Tool”. In: *Enquiry The ARCC Journal for Architectural Research* 4.1 (2007).

[44] C. Yu. *Spectral dataset of natural light fields measured in the Netherlands*. Zenodo, Nov. 2022.

[45] S. C. Pont and J. J. Koenderink. “Bidirectional texture contrast function”. In: *International Journal of Computer Vision* 62 (2005), pp. 17–34.

[46] M. R. Luo, G. Cui, and B. Rigg. “The development of the CIE 2000 colour-difference formula: CIEDE2000”. In: *Color Research & Application* 26.5 (2001), pp. 340–350.

[47] A. Akbarinia and K. R. Gegenfurtner. “Color metamerism and the structure of illuminant space”. In: *Journal of the Optical Society of America A* 35.4 (2018), B231–B238.

[48] R. L. Lee and J. Hernández-Andrés. “Colors of the daytime overcast sky”. In: *Applied optics* 44.27 (2005), pp. 5712–5722.

[49] S. M. Nascimento, K. Amano, and D. H. Foster. “Spatial distributions of local illumination color in natural scenes”. In: *Vision research* 120 (2016), pp. 39–44.

[50] C. Yu and S. Pont. “Quantifying Natural Light for Lighting and Display Design”. In: *SID Symposium Digest of Technical Papers*. Vol. 52. S2. Society for Information Display China. 2021, pp. 99–103.

[51] D. H. Foster, K. Amano, and S. M. Nascimento. “Time-lapse ratios of cone excitations in natural scenes”. In: *Vision research* 120 (2016), pp. 45–60.

[52] R. L. Lee Jr, W. Meyer, and G. Hoeppe. “Atmospheric ozone and colors of the Antarctic twilight sky”. In: *Applied Optics* 50.28 (2011), F162–F171.

[53] S. Hillaire. “A scalable and production ready sky and atmosphere rendering technique”. In: *Computer Graphics Forum*. Vol. 39. 4. Wiley Online Library. 2020, pp. 13–22.

[54] J. E. Hansen and L. D. Travis. “Light scattering in planetary atmospheres”. In: *Space science reviews* 16.4 (1974), pp. 527–610.

[55] P. Minnis, S. Mayor, W. L. Smith, and D. F. Young. “Asymmetry in the diurnal variation of surface albedo”. In: *IEEE Transactions on Geoscience and Remote Sensing* 35.4 (1997), pp. 879–890.

[56] O. Pechony, C. Price, and A. P. Nickolaenko. “Relative importance of the day-night asymmetry in Schumann resonance amplitude records”. In: *Radio Science* 42.02 (2007), pp. 1–12.

[57] S. Rickel and A. Genin. “Twilight transitions in coral reef fish: the input of light-induced changes in foraging behaviour”. In: *Animal behaviour* 70.1 (2005), pp. 133–144.

[58] D. H. Deutsch. “A mechanism for molecular asymmetry”. In: *Journal of molecular evolution* 33 (1991), pp. 295–296.

[59] C. Yu, M. Wijntjes, E. Eiseman, and S. Pont. “Supplementary Document for "Quantifying the Spatial, Temporal, Angular and Spectral Structure of Effective Daylight in Perceptually Meaningful Ways"”. In: *Figshare* (2023).

5

TIME OF DAY PERCEPTION IN PAINTINGS

The spectral shape, irradiance, direction and diffuseness of daylight vary regularly throughout the day. The variations in illumination and their effect on the light reflected from objects may in turn provide visual information as to time of day. We suggest that artists' colour choices for paintings of outdoor scenes might convey this information and that therefore time of day might be decoded from colours of paintings. Here we investigate whether human viewers' estimates of depicted time of day in paintings correlate with their image statistics, specifically chromatic and luminance variations. We tested time-of-day perception in 17^{th}-20^{th} century Western European paintings via two online rating experiments. In Experiment 1, viewers' ratings from 7 time choices varied significantly and largely consistently across paintings, but with some ambiguity between morning and evening depictions. Analysis of the relationship between image statistics and ratings revealed correlations with the perceived time of day: higher "morningness" ratings associated with higher brightness, contrast, saturation, and darker yellow/brighter blue hues; "eveningness" with lower brightness, contrast, saturation, and darker blue/brighter yellow hues. Multiple linear regressions of extracted principal components yielded a predictive model that explained 76% of the variance in time-of-day perception. In Experiment 2, viewers rated paintings as morning or evening only; rating distributions differed significantly across paintings; and image statistics predicted people's perceptions. These results suggest that artists used different colour palettes and patterns to depict different times of day, and the human visual system holds consistent assumptions about the variation of natural light depicted in paintings.

Manuscript in preparation for journal submission: C. Yu, M. J. P. van Zuijlen, C. Spoiala, S. Pont, M. W. A. Wijntjes, and A. Hurlbert. "Time of day perception in paintings".

5.1. INTRODUCTION

PAINTERS have long been attuned to real world properties that are relevant to the perceiver [1], and have developed effective techniques to represent everyday scenes in pictorial space [2]. While not aiming for physical accuracy, their depictions often contain invariants [3] or perceptual shortcuts [4] that support the viewer's understanding of the scene. As such, paintings provide a rich source of image features that vision scientists can use to better understand human visual perception.

Analysis of these features has largely focused on aesthetic preference [5, 6] or material properties, such as transparency [7], translucency [8], gloss [9] or velvetiness [10], Less well explored is how perceivers may also infer more abstract yet ecologically important dimensions from paintings, such as time of day or weather. For these, painters may use explicit cues such as human activities, shadow length or sun position. Yet other image features, independent of pictorial content, may powerfully convey the time of day. Here we examine the relationship between low-level image statistics, in particular the distribution of chromaticities and luminances, in paintings and the depicted time of day.

In representational paintings, painters deploy pigment on canvas to capture the effects of light interacting with surfaces in the scenes they depict. Variations in chromaticity and luminance across the image, induced by complex material-light interactions, may containessential information about three-dimensional structure [11, 12]; these painted patterns may in turn evoke perceptions of 3D shape and surface colour. Luminance shading defines fundamental elements of volume and space [13] and provides cues to the location and orientation of objects and the direction of the light [14, 15]. In paintings, cast shadows may indicate the light source position, even when simplified beyond physical plausibility [2, 16, 17]. Cast shadow lengths [18] might give an additional indication of time of day.

Chromatic content might also be used in paintings to depict time of day. J. M. W. Turner's pair of paintings, *The Morning after the Deluge and The Evening of the Deluge*, seem by their titles and content to demonstrate an association between colour and time of day, as well as weather. *The Morning after the Deluge* features a cyclone of brilliant colours, converging on yellow and white, evoking a sunny day. In contrast, *The Evening of the Deluge* features blackness encircling a grey-blue core, suggesting a stormy night. The paintings not only pay explicit homage to Goethe's colour theory [19], but also express an implicit rule about the depiction of time. In his series paintings of Rouen Cathedral, Claude Monet painted different still moments of the cathedral in markedly different colour palettes, titling them with different times of day. In *Rouen Cathedral, Facade (sunset)* (Figure 5.1, upper row second), the orangish glow of the solid stone partially covered by a crisp bluish shadow under a blue sky creates a visual impression distinct from *The Portal of Rouen Cathedral in Morning Light* (Figure 5.1, upper row first), in the more uniform and inarticulate façade is smoothly shadowed and dissolves into the background sky. The questions we pose are whether in deploying such chromatic cues painters are deliberately capturing natural variations in illumination over the course of the day and seasons, and whether people consistently read time of day from these cues.

Figure 5.1: Claude Monet's painting series of Rouen Cathedral. The paintings in the series each capture the façade of the Rouen Cathedral at different times of the day and year under various weather conditions, which exaggerates the changes in its colour appearance under different lighting conditions. Downloaded from Wikimedia Commons, a free online media repository that provides access to a wide range of images, videos, and other media.

5.1.1. CHARACTERISTICS OF TERRESTRIAL ILLUMINATION

The spectrum, direction, and diffuseness of natural illumination in the terrestrial world regularly change over a day. These variations in natural illumination, and their effect on the light reflected from objects, might be incorporated by painters' choices of colour palettes. It is argued that all visual sensory mechanisms have evolved to be attuned to the characteristics of the heterogeneous terrestrial illumination [20, 21], which comprises all the light originating from extraterrestrial sources such as sunlight and penetrating the Earth's atmosphere, as well as artificial light sources like lamps and fires. Terrestrial illumination exhibits heterogeneity due to interactions among sunlight, atmospheric conditions, environment and anthropogenic light. The daily and seasonal terrestrial illumination follows a tripartite pattern, classified as diurnal, crepuscular, and nocturnal. During the day, diurnal illumination, or daylight, is the total light originating from the sky and sun after sunrise and before sunset, while crepuscular illumination, or twilight, is the sum of the skylight and artificial anthropogenic light when the sun disk is below the horizon. Nocturnal illumination, on the other hand, is commonly provided by moonlight, starlight, and light pollution between astronomical dusk and astronomical dawn.

Solar elevation is a main determinant of the illuminance and chromaticity of natural illumination [22, 23]. The illumination is more spread out and less intense during early morning and late afternoon compared to midday [24, 25]. This is due to the longer path sunlight travels through the atmosphere and is being scattered, also resulting in a lower intensity. Additionally, low sun angles also result in lower illuminance, as the amount of light reaching a surface is proportional to the cosine of the angle of incidence. The chromaticity of illumination also changes throughout the day, with more reddish-yellow hues during sunrise and sunset and more bluish-white tones during midday. This is due to the wavelength-dependent scattering of light by atmospheric molecules, known as Rayleigh scattering. Short wavelength light is much more heavily scattered, resulting in the transmitted beam becoming skewed to the long wavelengths [26–30]. These variations have implications for visual perception and activities relying on visual cues.

5.1.2. SUNRISE–SUNSET ASYMMETRY

As we ponder upon the light of the morning and the evening skies, we may be led to assume their similarity due to the sun's proximity to the horizon. Gombrich acknowledged this ambiguity when he wrote of Corot's work [31], "Corot softens the shadow of the fallen tree and of the goose, thus convincingly suggesting the mellow light of morning or evening." Beurs, in his observations from the 17^{th} century, noted that although the techniques used to depict sunrise and sunset may be similar, there are distinct differences in the colour palette and temperature of the sky [32]. He observed that sunrise often features cooler colours and more mists, while sunset has warmer colours and reflects the warmth of the day. As the sun sinks below the horizon during sunset, the air cools, causing larger water molecules to gather in the atmosphere and scatter the long-wavelength component of the sunlight, resulting in a mesmerizing orangey-red hue [33]. Meanwhile, airlight, which specifically refers to the scattered light in a scene caused by atmospheric conditions such as haze or fog [34–36], exhibits different characteristics during the morning and evening hours. In the morning, the air is more saturated with denser water vapor, haze, and fog [37–40], causing airlight to appear milkier and more diffuse, and giving a hazy, dreamlike quality to the light. These differences in hue and character of airlight between morning and evening light arise from temperature and moisture distinctions and offer artists the chance to portray a unique facet of the world's natural beauty.

In the present study, we set out to investigate whether human observers can estimate depicted time of day in paintings, and if so, whether this can be related to image statistics. Although our visual perception mostly relies on the light that is reflected from objects, the fact that illumination changes with such a conspicuous daily cycle is likely to have played some part in indicating ecologically essential dimensions, such as the time of day. We hypothesize that the image statistics of paintings contain information about the characteristics of terrestrial illumination, and that human observers use this statistical regularity to judge the time of day depicted in a painting. To test this hypothesis, we conducted two rating experiments with 17^{th}-20^{th}-century paintings. Experiment 1 involved participants viewing digital reproductions of paintings and selecting the time of day depicted from seven options.

The observation that bimodal distributions resulted for certain paintings, with some participants rating them as morning and others as evening, motivated Experiment 2. Here, the aim is to examine whether observers were able to distinguish between morning and evening in paintings when given only those choices, using a stimulus set with metadata to provide "ground truth".

5.2. METHODS

To recruit participants, we utilized Amazon Mechanical Turk (AMT) to conduct two online experiments. In Experiment 1, participants were presented with digital reproductions of paintings and asked to choose the time of day depicted from seven options: sunrise, morning, noon, afternoon, evening, sunset, and night. In Experiment 2, participants were asked to select between morning or evening. We analyzed the perceptual data in relation to image statistics to better understand whether humans use image statistics to judge the time of day depicted in paintings.

5.2.1. IMAGE DATASET

The images of paintings were downloaded from online open-access datasets , including the Materials in Painting (MIP) dataset by van Zuijlen *et al.*, 2021 [4] (https://materialsinpaintings.tudelft.nl) and the National Gallery (NG) dataset (https://nationalgallery.org.uk/paintings). The paintings from both datasets depict various subject matters, including landscapes, seascapes, urban scenes, architecture, etc. These datasets were chosen because they display a wide diversity of natural outdoor scenes under a variety of illumination conditions.

5.2.2. STIMULI

In order to focus specifically on the role of image statistics related to light and colour and their relationships with people's perceptions of the time of day in paintings, we selected primarily outdoor scenes that would be influenced by natural light. We also chose paintings that lacked explicit social or contextual cues, such as human activities, which might easily indicate the depicted time of day.

In Experiment 1, we chose 104 high-resolution digital images of 17^{th}-20^{th}-century oil paintings (see Figure 5.A3). This collection comprised 50 from the MIP dataset and 54 from the NG dataset. For 8 paintings out of the total selection, the title contained information about the depicted time of day, *e.g.* Evening at Medfield, Massachusetts by George Inness. We also selected four paintings from the NG dataset as catch trials. These four catch trials clearly depicted nighttime scenes and were also identified as nighttime depictions according to their titles or metadata, *e.g.* A River near a Town, by Moonlight by Aert van der Neer. The metadata consists of information about a painting that is not necessarily provided by the painter, but rather by curators or other art experts. This data may be subjective, but is generally considered to be based on art historical knowledge and expertise.

In Experiment 2, we chose a new set of 90 digital images, distinct from those in Experiment 1, featuring 17^{th} to 20^{th}-century paintings from the MIP dataset (refer

to Figure 5.A3). The titles of these paintings provided cues to the time of day represented in each scene: sunrise (10 paintings), morning (17 paintings), sunset (36 paintings), and evening (27 paintings). To standardize the stimuli, we resized the images to 1000 pixels along the longer dimension, while preserving the original aspect ratio.

All paintings reproduced within this paper are available under open access at a Creative Commons Zero (CC0) or Creative Commons Attribution-NonCommercial (CC BY-NC) 4.0 license. The complete list of all paintings used within this study, including those reproduced in this paper, is available in Dataset 1 [41].

5.2.3. OBSERVERS

A total of 112 unique (Experiment 1, n=51; Experiment 2, n=61) participants were recruited via the AMT platform. Each agreed to the informed consent before data collection. Data collection was approved by the Human Research Ethics Committee (HREC) of the Delft University of Technology and adhered to the ethical guidelines of the Declaration of Helsinki. All observers were naive to the purpose of the experiments.

Previous experience with AMT recruitment has suggested that data might be noisy due to a small but considerable portion of participants that appear to perform poorly in experiments [10, 42]. We thus set an exclusion criterion in Experiment 1 to automatically remove participants who scored below an 80% correct rate for the catch trials (detailed below). In total, 25 participants were removed this way. The exclusion was performed prior to data analysis.

5.2.4. PROCEDURE AND TASK

We used a similar procedure for both Experiments 1 and 2. Experiment 1 consisted of seven alternative choices, and Experiment 2 comprised two alternative choices. Participants were informed that they would be presented with images of paintings and that they would indicate the time of day in each trial. After each labeling, participants had to press the continue button for the subsequent trial. Participants were also allowed to go back and redo the previous trials. The trials were randomized across participants. In Experiment 1, there were 109 trials per observer. Experiment 2 was composed of three blocks, and each contained 41 trials. Block 1 involved 21 observers, while blocks 2 and 3 had 20 observers each. Within each block, there was no repetition of stimuli. Among three blocks, there were 70 unique stimuli. Seven stimuli appeared in either of the two blocks, and 13 stimuli were used in all three blocks.

5.2.5. IMAGE ANALYSIS

Our hypothesis is that painters capture the variation in illumination and reflected light from scenes over the course of a day, and therefore the paintings will vary in their luminance and chromatic content according to the time of day they depict. We hypothesize that participants will be able to discern and interpret this content, and that its statistical characteristics will predict people's perception of the time of day.

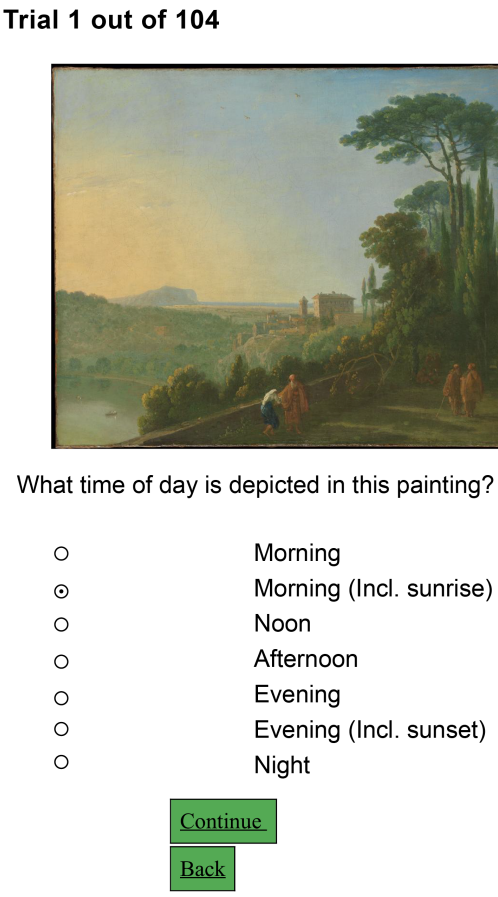

Figure 5.2: The interface of Experiment 1.

We therefore examined whether the image statistics of paintings predict participants' time-of-day ratings.

The images in this dataset were downloaded as photographic jpegs or pngs, and displayed directly without further transformation in the participants' internet browser windows. The images do not contain information about the photographic setups which would enable us to derive the colour appearance of the original painting under any specified illumination. We also do not have information about the colour calibration of the individual displays used by the participants in the online experiment. To model the colour appearance of the paintings as viewed by each participant, and from this calculate the image statistics of the paintings, we therefore make several assumptions: We assume that for each participant (1) the display calibration characteristics and (2) the external viewing conditions stayed constant throughout the experiment. For each session, the same colour transformation from

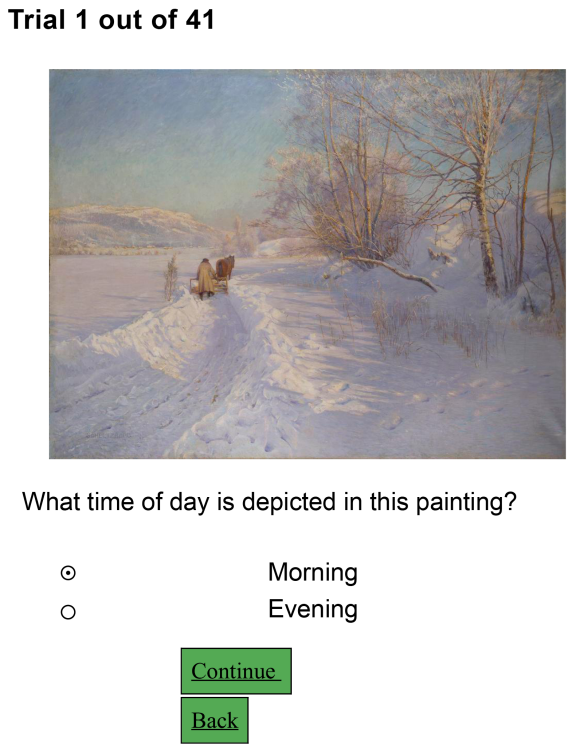

Figure 5.3: The interface of Experiment 2.

RGB pixel values to colour appearance will therefore apply across the entire image dataset. For the main analyses, we use the sRGB colour space model as the basis for that transformation. sRGB is the widely adopted standard colour model for image display on monitors and the web. It defines chromaticities for the RGB primaries, based on original CRT phosphors, and a nonlinear transfer function between input digital value (v) and output intensity (I), with $I = v^{\gamma}$ and $\gamma = 2.2$. Using the sRGB model, we calculated the colour appearance of the paintings displayed, by converting RGB pixel values into chromaticity and luminance coordinates in CIE standard colour spaces, and derived further image statistics from these. Although the sRGB model might not perfectly predict colour appearance for each participant's display, it is the optimal transformation for approximating the average appearance, and it also allows for consistent comparison and analysis of the image statistics across all images in the dataset. Although the participants probably did not have "average screens", we regard this as the best modeling approach not having chromatic gauging information. We also show in further analyses that the main results hold when using alternative white points in RGB colour transformations (Appendix Section 5.A5).

The colour appearance attributes and image statistics, as described in detail in Appendix Section 5.A1, were computed for our analysis. To the reader less well

versed in colorimetry: we are essentially converting colours from screen-dependent coordinates (*i.e.*, the RGB values of the digital images) to screen-independent, standardized colour coordinates. We then employed these standardized colour metrics as input for a Principal Component Analysis (PCA) to reduce the dimensionality of the data.

COLOUR SPECIFICATIONS AND APPEARANCE METRICS

Assuming the sRGB model and a default white point of D65, we calculated 1931 CIE XYZ values for each pixel, and from these, CIELAB and LCH, according to standard formulae, as detailed in Appendix Section 5.A1. Furthermore, we directly converted the sRGB pixel values to cone, rod, and melanopic photoreceptor activations. We used the cone fundamentals specified by Stockman *et al.* [43, 44], the melanopsin curve by Lucas *et al.* [45], and the scotopic curve by Crawford [46] to compute the scotopic irradiance. We combined pre-computed spectra for sRGB primaries, which have minimal round-trip errors (as established by Mallett & Yuksel [47]), to generate the corresponding spectrum for given sRGB pixel values.

For brightness and lightness measures, we used the CIE Y tristimulus value (termed luminance in the analyses below) and CIELAB L^* (termed lightness below).

For chromaticity measures, we used CIELAB a^* and b^*, hue (calculated from CIELAB a^* and b^*, as in Appendix Section 5.A1), saturation (calculated from CIELAB a^*, b^* and L^*, as in the Appendix Section 5.A1), and chroma (calculated from CIELAB a^* and b^*, as in Appendix Section 5.A1). Because the chromaticity of daylight may be summarized by its correlated colour temperature (CCT), which is the temperature of the black-body radiator with the nearest chromaticity on the Planckian locus in CIE 1960 (u, v) space, we therefore also convert CIE XYZ values for each pixel into CCT (in Kelvin).

STATISTICAL MEASURES

For each of the luminance, lightness, and chromaticity metrics above, we calculated descriptive statistics (max, min, mean, variance, and skewness) of their pixel value distributions for each image. For the luminance and the blue channel in sRGB, we also calculated RMS contrast. See Appendix Section 5.A1 for formal definitions.

In addition, we derived further image descriptors relating to interactions between chromaticity and luminance across each image:

Colour difference at maximum luminance difference: To summarise overall contrast including both luminance and chromatic contrast, we calculated the colour difference between the brightest and darkest pixels in each image, using the CIE ΔE 2000 colour-difference formula (ΔE_{00}). The CIE ΔE 2000 colour-difference formula [48], based on CIELAB coordinates, is the recommended standard for computing colour differences that are perceptually uniform across colour space.

Luminance-weighted CCT: The luminance-weighted CCT is calculated for each pixel as the product of the pixel's CCT and its corresponding luminance. Luminance thereby serves as a weighting factor, reducing the contribution of

darker pixels and increasing the contribution of brighter pixels. Effectively, this weighting recognizes the greater salience of brighter pixels in chromaticity perception.

Pixel-wise luminance-chromaticity correlations: We also calculated the correlation between pixel luminance and chromaticity measures (CIELAB b^*, saturation, and chroma) [5] within each image using Pearson's correlation coefficients.

IMAGE AIRLIGHT COLOUR

To provide further insight into the atmospheric conditions conveyed by the variation in chromaticity and luminance within each image, we computed an estimate of airlight appearance using the dark channel prior method [49]. This approach identifies and removes areas where at least one spectral band is darker than the others before averaging the remaining pixel values which correspond to clusters with the highest average luminance and lowest chromatic saturation. The resultant airlight colour has been shown to relate to the presence of scattered light in hazy images. For more information, please refer to Appendix Section 5.A1. By considering the atmospheric conditions in hazy images, we aimed to better understand whether they relate to the perceived time of day in the image.

5.2.6. STATISTICAL ANALYSIS

To quantify participants' responses, we used a scoring system based on chronology. In Experiment 1, we assigned scores of 1 to 7 to seven rating categories: sunrise, morning, noon, afternoon, sunset, evening, and night. To reduce potential confusion between certain terms, we merged morning and sunrise into a single category, noon and afternoon into another, and evening and sunset into a third. We kept night as its own category, resulting in four merged categories (morning, noon, evening, and night) assigned scores of 1, 3, 5, and 7, respectively. We used the merged-categories scoring for subsequent correlational analyses and linear model prediction. However, for the principal component analysis, we used the original 7-point scale to examine the distribution of the original categories and identify potential overlaps. In Experiment 2, we simplified the scoring system to two categories, scoring morning as 0 and evening as 1.

We used three types of scores for data analysis in our study. a) The mean score: This is the sum of all the scores divided by the number of scores, and it provides an overall measure of the perceived time of day for each painting. b) The proportional score per category: This is the ratio between the total count of scores for a particular category and the total number of scores, or the proportion of scores that fall into each category. c) Categorical score: This refers to the mode of the scores given by participants for a particular painting, indicating the most frequently perceived time of day for that painting.

Two types of analyses were conducted to investigate the relationship between participants' responses and image statistics. The first type consisted of independent correlation analyses on each of the image metrics for both experiments using mean

scores. In addition, PCA was performed to identify the image metric combinations that best differentiated between paintings depicting different times of day. The derived principal components were used as predictors in a multiple regression analysis to model the perceived time of day from Experiment 1, and the accuracy and quality of the model were evaluated using the Akaike information criterion (AIC). Results with a p-value less than 0.05 were considered statistically significant.

5.3. RESULTS

5.3.1. EXPERIMENT 1

There was no significant difference between results with and without the data that did not pass the catch-trial selection criterion (Mann-Whitney test, $p = 0.82$). Figure 5.4 displays sample paintings that received consistent ratings from participants. In the evaluation of observer ratings across the images, significant differences were observed (ANOVA; $\alpha = 0.05/5356$, $p = 2.63655 \times 10^{-196}$, $F(103, 2600) = 15.2289$). Notably, even after implementing Bonferroni correction, a substantial 24.9% of pairwise comparisons (equating to 1335 pairs) still presented significant differences.

Figure 5.4: Sample paintings with high-consistency ratings . (a) Sanford Robinson Gifford, A Gorge in the Mountains (Kauterskill Clove), 1862. (b) Willard Metcalf, The North Country, 1923. (c) Emanuel Murant, The Old Castle, 1642–1700. (d) Arnold Böcklin, Island of the Dead, 1880. Downloaded from the online repository of the Metropolitan Museum of Art, New York

To investigate the average chromatic characteristics of the paintings, we plotted their mean coordinates on the CIE chromaticity diagram. Figure 5.5 displays the mean chromaticities of the paintings in Experiment 1, with one disk representing each painting. The chromaticities tend to cluster along the daylight locus, varying from blueish to orangish. Almost all lie above the daylight locus, with a positive D_{uv} value indicating a green and yellow shift. This green shift is also evidenced by the negative a^* values, while the yellow shift is indicated by positive a^* values. This chromatic relationship holds across different white points (Appendix Section 5.A5). Figure 5.6 presents the mean luminance of the paintings, providing additional descriptive statistics for the image set. Together with Figure 5.5, it illustrates the distribution of mean chromaticities and luminances across the images.

As detailed in the Methods section, we calculated 30 image statistics which capture the chromaticity and luminance variations within and across the image set. To evaluate whether these statistics predict time-of-day ratings, we performed

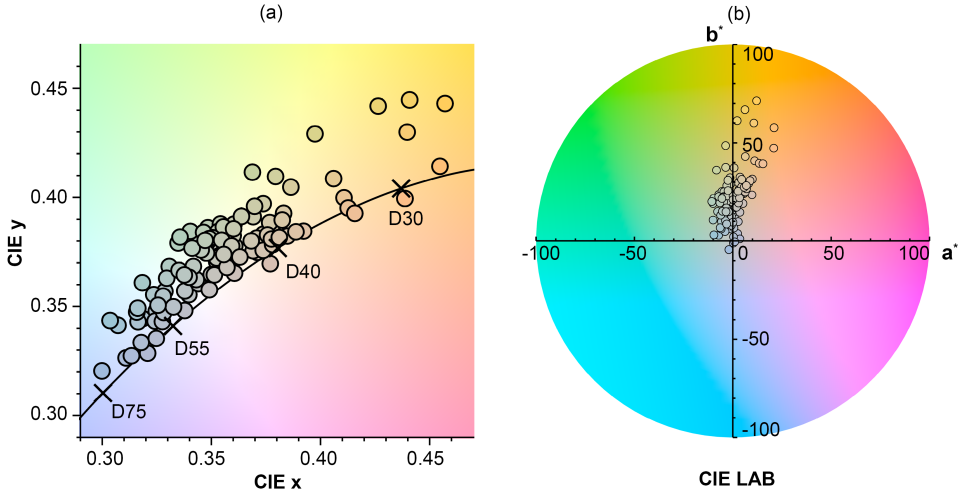

Figure 5.5: (a) Mean image chromaticities in CIE xy plane for paintings, one disk per image. Disk colours approximately represent image chromaticity. The black line indicates the daylight locus; the locations of D30, D40, D55 and D75 are marked. (b) The CIELAB plane at a lightness level (L^*) of 0.8, also showcasing the mean image chromaticities for each painting as distinct disks. Again, the disk colours provide an approximate representation of each image's chromaticity.

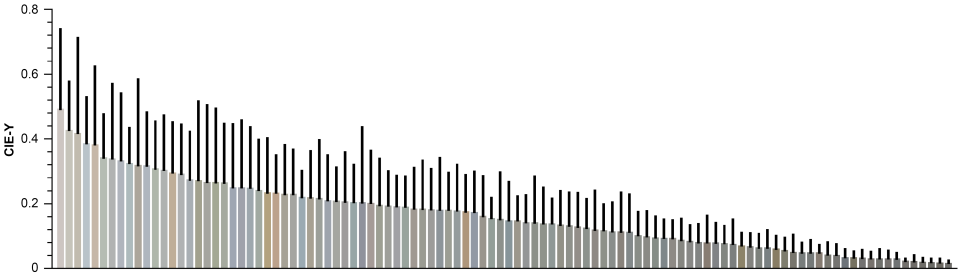

Figure 5.6: Illustration of mean image luminance for each painting, depicted by individual bars arranged in descending order from highest to lowest luminance. The colours of the bars represent mean image chromaticity, while the black line on top of the bars shows the standard deviation.

correlations (visualized in Appendix Section 5.A2 Figure 5.A1) and found that all 30 statistics were significantly correlated with average time-of-day ratings ($p < 0.0001$ for all). We report correlations where the absolute value of r is greater than 0.6, namely positive correlations for luminance skewness (r = 0.82) and saturation-luminance correlation (r = 0.62), as well as negative correlations for mean image luminance (r = -0.81), mean image luma (r = -0.81), mean melanopsin input (r = -0.78), mean L-cone input (r = -0.82), mean M-cone input (r = -0.81), mean S-cone input

(r = -0.73), mean rod input (r = -0.79), RMS luminance contrast (r = -0.81), RMS contrast (B channel) (r = -0.71), b^* standard deviation (r = -0.72), ΔE_{00} (r = -0.67), mean luminance-weighted CCT (r = -0.69), b^*-luminance image distance (r = -0.72), saturation-luminance image distance (r = -0.69), and chroma-luminance image distance (r = -0.73). These findings underscore the intricate interplay between diverse chromatic and luminance attributes in modulating our perception of time-of-day, as derived from visual stimuli.

We conducted a PCA to uncover the underlying dimensions of the space, because the image statistics are not independent of each other (refer to Appendix Section 5.A2 Figure 5.A1 and Section 5.A3 Table 5.A1). We extracted five principal components, as defined by eigenvalues greater than 1 (Appendix Section 5.A3 Table 5.A2). The first two components (Dim1 - PC1 on the horizontal axis and Dim2 - PC2 on the vertical axis) accounted for 71.1% of the variability in the image statistics data, as visualized in Figure 5.7. Adding a third, fourth, or fifth component captured 81.7%, 86.8%, and 90.4% of the variability, respectively. In the PCA space, there were three distinct clusters of factor loadings, indicated by the red arrows, which were distributed on the positive and negative sides of the horizontal axis and the negative side of the vertical axis (Figure 5.7(a)).

The distribution of covariance error ellipses across different time-of-day classifications was found to be systematic in the PCA space, see Figure 5.7(b). These ellipses were formulated based on the mean coordinates and covariance matrix of the data points for each category, using the mode or the highest proportion. By calculating the eigenvalues and eigenvectors of the covariance matrix, we determined the lengths and directions of the major and minor axes of the ellipses. In our analysis, we designed the ellipses to enclose 68% of the data points within each category, which corresponds to one standard deviation from the mean for normally distributed data.

Principal component 1 (PC1) is highly negatively loaded with measures such as luminance, cone, rod, and melanopic photoreceptor activations, contrast, luminance-weighted CCT, and chroma-luminance image distance. Meanwhile, on the other hand, luminance-channel skewness, which loads highly on PC1 with a positive magnitude, is significantly positively correlated with these measures. We observed that the substantial positive loading on luminance suggests PC1 is negatively associated with the overall luminance levels across the images. Photoreceptor activations are connected to radiance levels over the images, and contrast is also related to the distribution across images. Luminance-channel skewness, on the other hand, pertains to the luminance histogram or distribution within each image. We speculate that this observation may be associated with the upper correlations, as strong daylight typically results in increased brightness and heightened contrast via shad(ow)ing. Consequently, we deduce that PC1 is primarily luminance-related. The luminance-weighted CCT and chroma-luminance distance associations link to the distribution within the images. This finding indicates that PC1 not only encapsulates luminance-related aspects but also offers insights into the relationships within the images. The measures that had a high loading on the second principal component (PC2) include mean image saturation, mean image chroma, mean b^*,

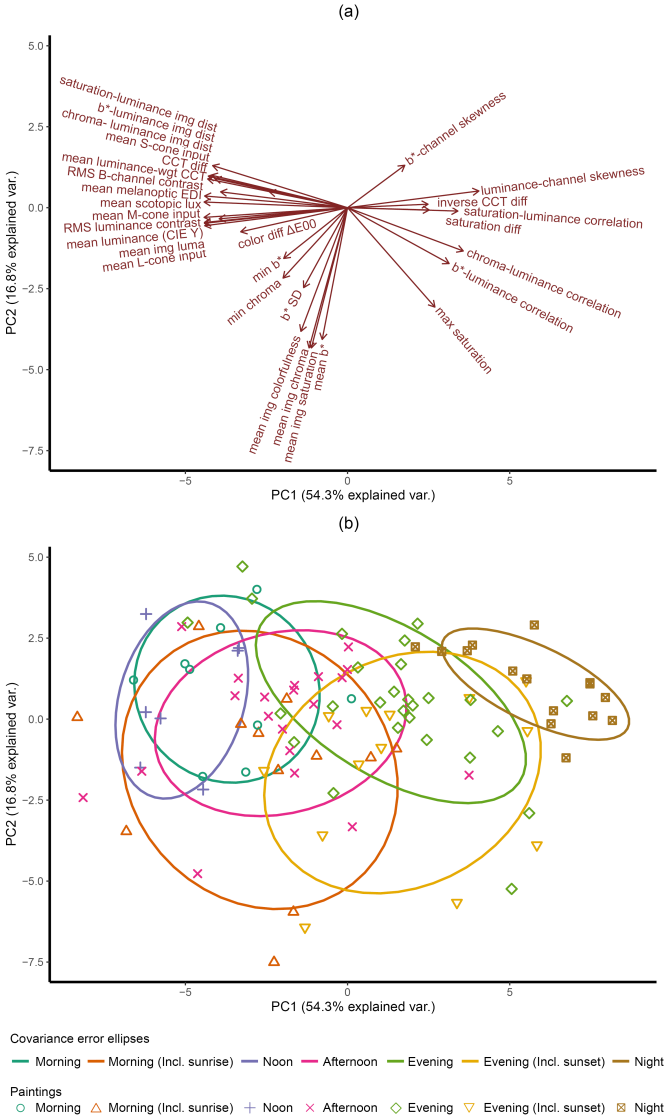

Figure 5.7: Visualization of the first two dimensions of PCA. (a) Factor loadings of 30 image statistics, with text labels, and the red vectors indicating the factor loadings of the original dimensions. (b) The covariance ellipses that were fitted for each time-of-day class, in which each point represents one of the 104 paintings and is colour-coded based on its perceived time-of-day classification.

and mean image colourfulness. Therefore, we infer that PC2 is negatively related to chromaticity. CCT, inverse CCT difference, and saturation differences loaded the third principal component (PC3). The highest loadings on the fourth and fifth

principal components (PC4, PC5) came from minimal image b^* and image b^* standard deviation, respectively.

To predict the mean time-of-day rating, which spans from morning to night across four combined categories, we applied a multiple linear regression analysis using the components extracted from our PCA. By applying the forward technique, we added one extra component as a predictor at a time. Accordingly, we computed five candidate models and compared them using Akaike Information Criterion (AIC) model selection. A lower Akaike weight can be interpreted as a higher probability that a certain model performs best. Table 5.1 shows the statistical summary for all the candidate models. We selected the model with the lowest Akaike weights, which included only PC1 and PC2. The equation for the best-fitting line is

$$mean\ time\ of\ day\ rating = 0.583 + 0.034 \times PC1 + 0.017 \times PC2 \tag{5.1}$$

This model explained (R2) 76% of the perceived time of day variance (see Figure 5.8 for scatterplot).

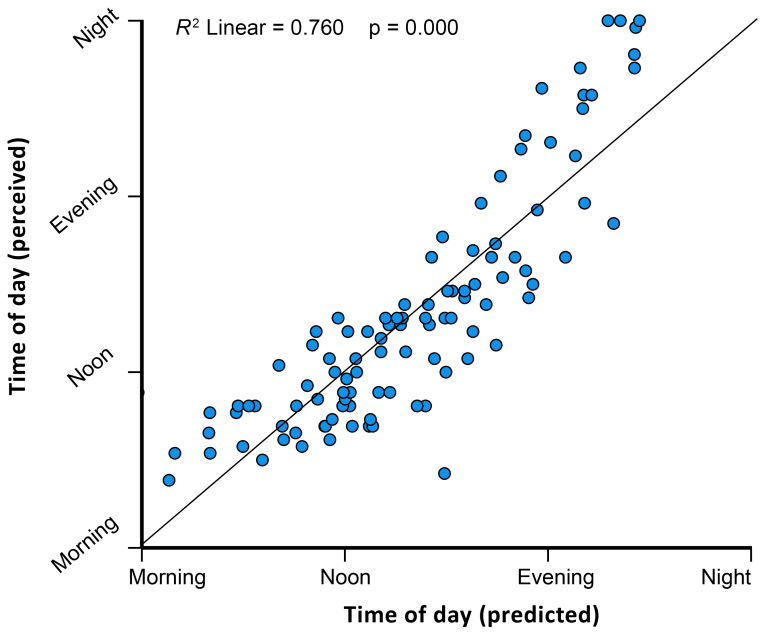

Figure 5.8: Scatterplot comparing the average perceived time-of-day scores (y-axis) to the predicted time-of-day scores (x-axis) based on the linear model established with the merged 4 time-of-day category scores. The ratings correspond to the 4-category scale, varying from 1, 3, 5, to 7, respectively.

Because the average time of day score potentially conflated morning and evening scores, we also analyzed the categorical data. Figure 5.9 shows the percentages of responses for the four merged categories of images from the MIP dataset. As the NG does not permit to reproduce their images, we only showed the MIP dataset. The

Model Summary[f]

R	R Square	Adjusted R Square	Std. Error of the Estimate	AIC	Change Statistics				
					R Square Change	F Change	df1	df2	Sig. F Change
0.840[a]	0.706	0.703	0.09046	-202.675	0.706	245.379	1	102	0.000
0.872[b]	0.760	0.755	0.08218	-221.675	0.054	22.599	1	101	0.000
0.872[c]	0.761	0.754	0.08245	-220.010	0.001	0.322	1	100	0.571
0.876[d]	0.767	0.758	0.08173	-220.878	0.007	2.769	1	99	0.099
0.876[e]	0.768	0.756	0.08205	-219.129	0.001	0.236	1	98	0.628

a. Predictors: (Constant), *PC1*
b. Predictors: (Constant), *PC1*, *PC2*
c. Predictors: (Constant), *PC1*, *PC2*, *PC3*
d. Predictors: (Constant), *PC1*, *PC2*, *PC3*, *PC4*
e. Predictors: (Constant), *PC1*, *PC2*, *PC3*, *PC4*, *PC5*
f. Dependent Variable: *mean time of day rating*

Table 5.1: Model Summary

5

response distributions reveal that, for some images, the answers were concentrated in a single category, with maximum categorical scores of 77% for morning, 81% for noon, 77% for evening, and 100% for nighttime. In contrast, other images exhibited a more evenly distributed mixture of answers, and we identified a considerable group of paintings with bipolar distributions of morning-evening ratings. Thus these images are evidently more ambiguous concerning the time of day. Additionally, bipolar distributions are distinct, but we often observed mixtures of three or four categories as well.

Figure 5.9: Results of Experiment 1. Percentages of population responses for the four merged categories for the MIP subset of the paintings.

5.3.2. INTERMEDIATE DISCUSSION

In Experiment 1, we found that the mean image chromaticities of the paintings were distributed over a large range, close to and slightly above the daylight locus. This implies that the mean image chromaticities of the stimuli ranged from so-called warm to cool daylight, with a slight green shift. The green shift might be due to a large portion of landscape features in the painting content. Perceived time of day correlated with various image statistics incorporating luminance and chromatic information. Multiple linear regressions of extracted principal components resulted in a two-dimensional predictive model that could explain 76% of the variance in time-of-day perception. People seem to use assumptions about the variation in brightness and colour of natural light depicted in paintings to infer the time of day, though there is a large amount of variance in these perceptions. It is worth noting that some paintings were perceived quite consistently as morning, noon, evening or night, while for many paintings we found mixtures of three or four answers. Some paintings were rated predominantly as either morning or evening. This raises questions about whether artists depicted morning and evening differently and whether human observers can distinguish between those times of day.

5.3.3. EXPERIMENT 2

In Experiment 2, we aimed to investigate further whether observers could discriminate specifically between morning and evening in paintings that explicitly portrayed these times of day. We ordered the metadata-indicated morning (upper panel) and evening paintings (lower panel) according to the average (or percentage) scores, and the results are presented in Figure 5.10. Average and percentage scores are equivalent here since the rating was binary. The order from left to right corresponds to morningness to eveningness. The morning paintings are clustered towards the left, and evening paintings lean towards the right. However, both morning and evening paintings cover a large timeline span. The top 33% of paintings rated morning and evening, indicated by a line above the paintings, were then selected to further analyze whether these more extreme cases reflect salient characteristics of morningness and eveningness.

The results of the experiment indicated that there was a significant difference in observer ratings across the images (ANOVA; $\alpha = 0.05/4005$, $p = 1.0537 \times 10^{-181}$, $F(89, 4235) = 14.5139$, with 27.9% of Bonferroni corrected pairwise comparisons showing significant differences). The distributions for morning and evening paintings spanned a wide range, with some morning paintings being rated as morning by 95% of the participants, while some evening paintings were rated as evening by 100% of participants. In Figure 5.11, we present several paintings that received consistent ratings from participants.

We computed the same image statistics as in Experiment 1. After that, we conducted single linear regressions between the 30 image statistics and the perceived time of day, which is visualized as a correlation matrix in Appendix Section 5.A2 Figure 5.A2. We found that several image statistics, including Min chroma, mean b^*, min b^*, b^* SD, mean image colourfulness, CCT difference, inverse CCT difference, and saturation difference, were no longer significantly correlated with the human

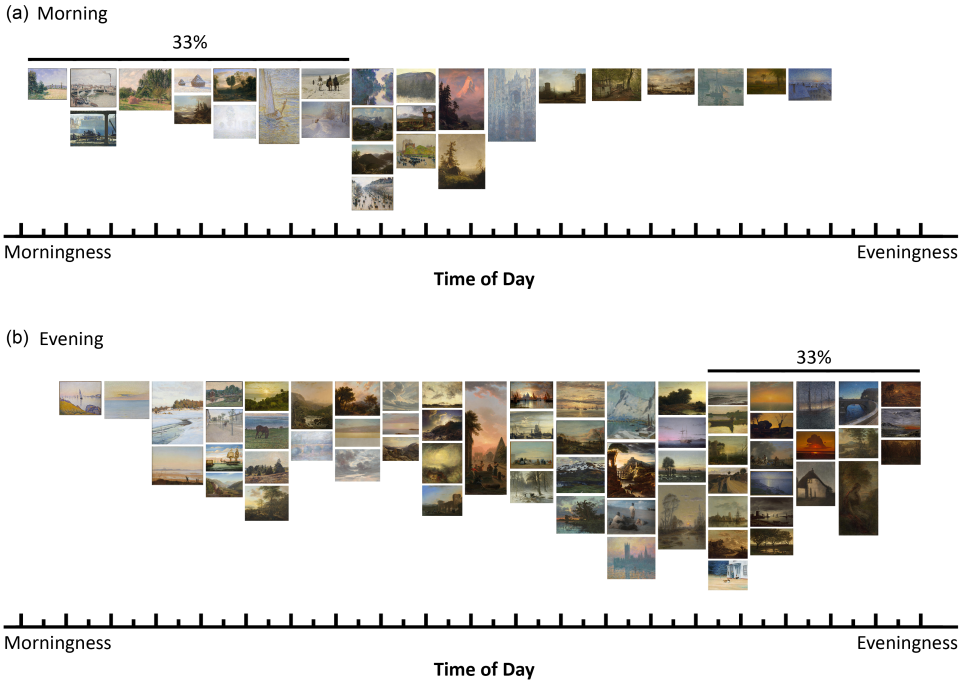

Figure 5.10: Morningness-eveningness perception in Experiment 2. Digital images of paintings from the MIP dataset were ordered according to the average time-of-day score. The order from left to right corresponds to a progression from morningness to eveningness. (a) Metadata-indicated morning scenes. (b) Metadata-indicated evening scenes. The top 33% rated morning and evening paintings are marked by the solid line.

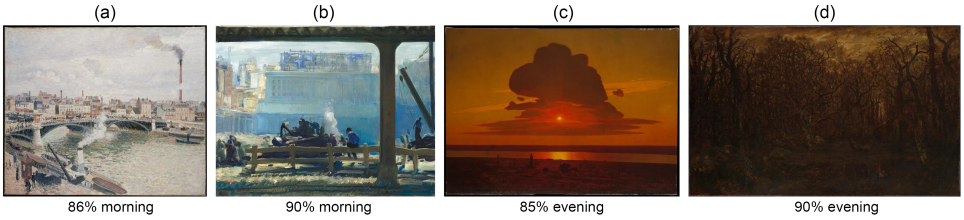

Figure 5.11: Sample paintings and their ratings. (a) Camille Pissarro, Morning, An Overcast Day, Rouen, 1896. (b) George Bellows, Blue Morning, 1909. (c) Arkhip Ivanovich Kuindzhi, Red Sunset on the Dnieper, 1905–1908. (d) Théodore Rousseau, The Forest in Winter at Sunset, c. 1846–c. 1867. Downloaded from the online repository of the Metropolitan Museum of Art, New York

ratings. Surprisingly, the correlations between the human ratings and mean image saturation and chroma even reversed in direction.

We did a PCA analysis on the 30 image statistics for the image stimuli, and the resulting PCA biplots are illustrated in Figure 5.12. Subpanel (a) displays the

factor loadings, while subpanels (b) and (c) display the positioning of the metadata-classified and observer-classified morning and evening paintings, respectively, in the multidimensional image feature space. The observer-classified categories are based on classifications selected by a majority of the participants. We used the same method as in Experiment 1 to fit ellipses designed to enclose 68% of the data points within each category.

Notably, the clusters for morning and evening paintings based on metadata classification showed significant overlap (Figure 5.12(b)), while the clusters based on observer classification demonstrated less overlap (Figure 5.12(c)). This difference in overlap is primarily attributable to the reduction in the size of the ellipses, rather than shifts in their positions. Despite these differences in overlap, the shapes of the covariance ellipses remained largely consistent across both classification methods.

The factor loadings for the PCs identified in this analysis were similar to those found in Experiment 1 on the negative side of the horizontal axis, but different for the remaining factor loadings (Figure 5.12(a)). This could be attributed to the selection of paintings, which only consisted of morning and evening paintings, compared to the broader time-of-day selection in Experiment 1.

Observers rated paintings classified as "morning" by metadata significantly different from those classified as "evening" by metadata (Mann-Whitney test, $p = 0.000$). Furthermore, the Chi-Square test provided a significant agreement between the metadata and the participants' labeling, with $\chi^2(1) = 10.145$ and a highly significant p-value ($p = 1.45 \times 10^{-3}$). This indicates that the observer ratings were, overall, in alignment with the metadata classifications. While PC1 exhibited significant differences between "morning" and "evening" paintings based on metadata (Mann-Whitney test, $p = 0.000$), PC2 did not show such a difference (Mann-Whitney test, $p = 0.294$). However, when considering observer classification, there were significant differences in both PC1 (Mann-Whitney test, $p = 0.000$) and PC2 (Mann-Whitney test, $p = 0.005$) between morning and evening paintings. The less overlapping covariance ellipses in the PCA plot in Figure 5.12(c) compared to the overlap in the metadata-based covariance ellipses in Figure 5.12(b) supports this finding. Thus, our results suggest that the differences between morning and evening paintings are more pronounced when considering observer ratings than metadata classification.

To better understand the factors that influence human perceptions of morning and evening in paintings, we analyzed the distributions of luminance-related and chromaticity-related image statistics based on both metadata classification and observer rating classification. In Figure 5.13 we show the CIE-Y and CCT distributions for all paintings, with the observer classifications shown in the right plots and metadata classifications in the left plots. Our analysis revealed that while there were no significant differences between mean image luminance for metadata-indicated morning and evening paintings (Figure 5.13(a)), there was a significant difference based on observer classifications (Figure 5.13(b)). The mean image chromaticity (CCT) differed significantly between morning and evening paintings based on both metadata classifications and observer rating classifications (Figure 5.13(c-d)). This observation suggests that chromaticity could play a role in artists' depictions of

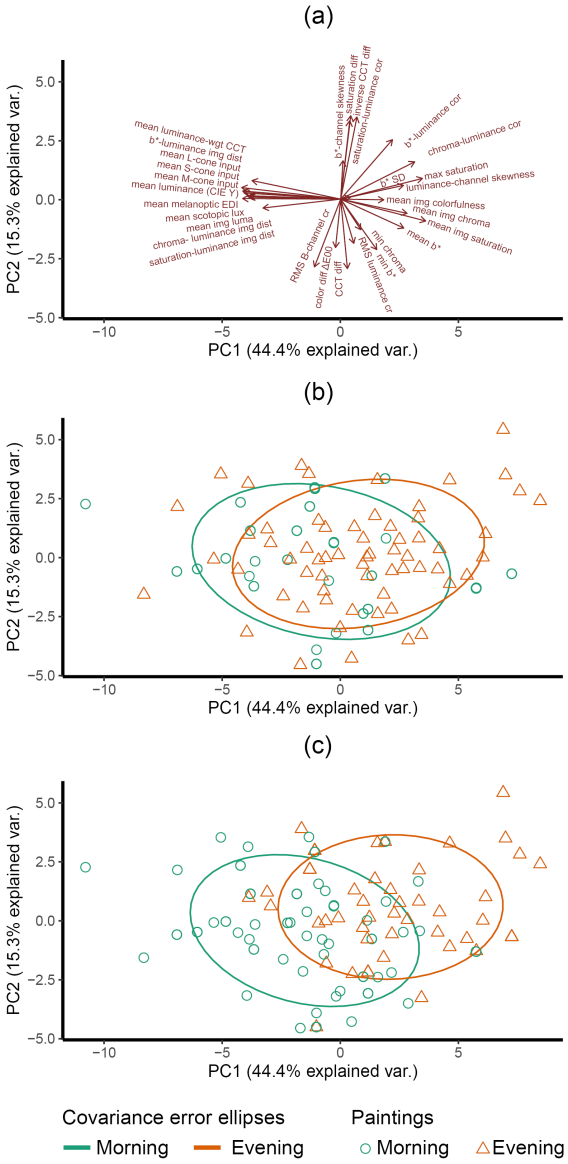

Figure 5.12: Biplot visualizations of the first two principal components. (a) Red arrows indicate the factor loadings of all image statistics. (b) Morning and evening paintings based on metadata classification, with points representing the 90 paintings and colours indicating the classification. (c) Morning and evening paintings based on observers' ratings classification, with points and colours representing the classification. Ellipses were fitted to enclose 68% of the data points within each category.

morning and evening in paintings, as well as in the human ability to differentiate between morning and evening scenes depicted in paintings.

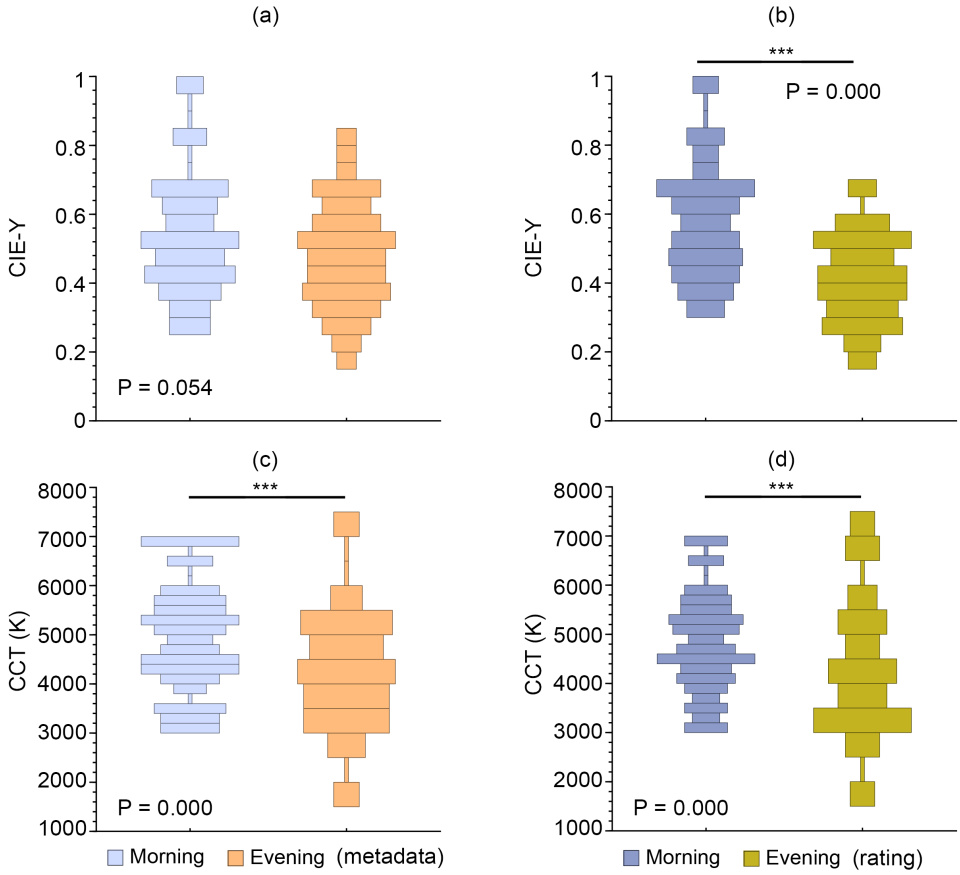

Figure 5.13: Distribution plots of mean image luminance (CIE-Y) and chromaticity (CCT). (a) and (c) Metadata classification. (b) and (d) Observers' rating classification. *** indicates statistically significant differences (Mann-Whitney test, $p < 0.0001$).

To more thoroughly understand the chromaticity factors that influenced the observers' perceptions of morning and evening in paintings, we conducted a detailed analysis of the chromaticity coordinates of the images in addition to the one-dimensional metric CCT. We concentrated on the 33% subsets of data most strongly identified by the observers as morning or evening. As shown in Figure 5.14, which displays the mean image chromaticities in the CIE xy plane based on both metadata classification (a) and observer rating classification (b), the mean image chromaticities of all paintings generally follow the daylight locus. However, when considering the metadata classification, we see that morning paintings tend to have chromaticities closer to D55, while evening paintings are clustered in the

warm white region. These chromaticity differences between morning and evening are more prominent in the observer-classified paintings. It is striking that the top 33% evening paintings have chromaticities that cover the whole daylight locus, while the morning chromaticities cluster tightly around D55. Specifically, the top 33% rated morning paintings consistently have chromaticities around D55, with a small covariance error ellipse, while the top 33% rated evening paintings have a wide range of chromaticities centered in the warm white region, with a larger covariance error ellipse.

Additionally, we analyzed the estimated airlight chromaticities of the images. Airlight colour is associated with atmospheric conditions and such scattered light contributes to the overall colour of depictions of a scene, in a depth-dependent manner. By estimating airlight chromaticities for all paintings and the top 33% morning and evening paintings, we tested whether this contributes to the observers' differentiation in perceived morning-/eveningness. Basically, we estimated the average chromaticity of the least saturated and brightest pixels, which has been shown to correlate with the chromaticity of diffuse ambient illumination [35] and with the amount of haze [34]. Dense haze can produce gray or bluish airlight colour, depending on the size of the particles.

Figure 5.14 shows the estimated airlight chromaticities of the images in the CIE xy plane based on both metadata classifications (c) and observer rating classifications (d). Overall, we see that the mean airlight chromaticities of all the paintings tend to shift towards D55. The exception to this is the observer-classified evening paintings, which cluster has a mean airlight chromaticity slightly shifted to warmer colours. One relationship we observed to be rather stable overall, that is, the chromaticities of the morning paintings on average tend to be bluer than those of the evening paintings.

5.3.4. INTERMEDIATE DISCUSSION

In Experiment 2, we set out to investigate whether there are notable differences in the way that artists depict morning and evening, and whether observers can use these differences to identify morning or evening. To this end, we selected a set of paintings with metadata indicating whether they depict a morning or evening scene, and asked observers to classify the paintings as either morning or evening. The mean image chromaticities of morning paintings were close to neutral white, while those of evening paintings varied from warm white to cool white, with a high frequency of warm white occurrences. The airlight colour chromaticities of morning paintings were on average bluer than those of evening paintings. These differences were found to be larger between observer-classified morning and evening paintings than between metadata-classified morning and evening paintings. This suggests that, overall, there may be different statistical regularities between morning and evening depictions, and that humans are able to use those to differentiate between morning and evening.

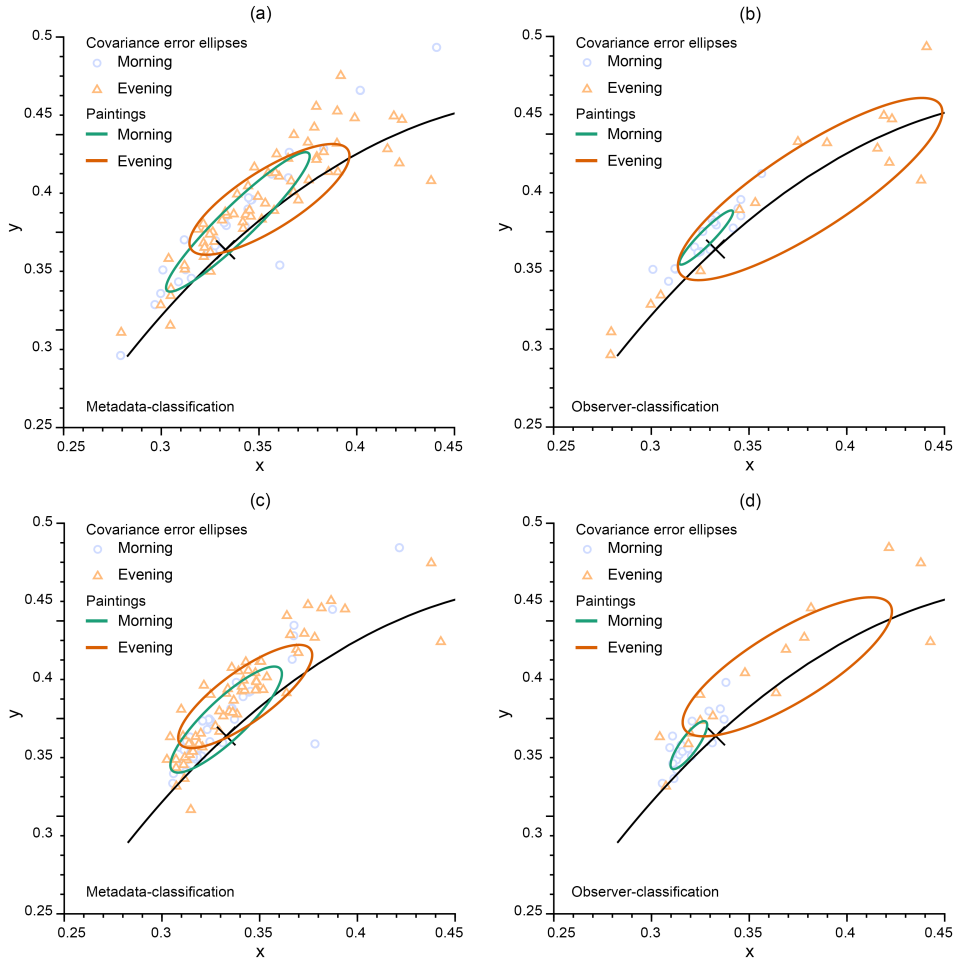

Figure 5.14: Mean image chromaticities and airlight colour chromaticities of paintings plotted in the CIE xy plane. Panels (a) and (b) show mean image chromaticities based on metadata and observer ratings respectively, with the top 33% rated morning and evening paintings included in panel (b). Panels (c) and (d) depict airlight colour chromaticities based on metadata and observer ratings respectively, with the top 33% rated morning and evening paintings included in panel (d). The black line indicates the daylight locus, and the diagonal cross indicates D55, serving as a reference for the chromaticity values.

5.4. GENERAL DISCUSSIONS

We studied the time-of-day perception using 17^{th}-20^{th}-century oil paintings. In experiment one, we collected human ratings on the time of day depicted in paintings. We collected both quantitative image statistics and qualitative perceptual data. These showed systematic correlations yielding insights into how the time of day can be perceived and predicted. Variance in the data was high, but statistical

regularities in the human data were found to be correlated with regularities in the image characteristics. We found that "morningness" was correlated with bright, high-contrast, saturated, and darker yellow/brighter blue images, and "eveningness" with darker, low-contrast, desaturated, and darker blue/brighter yellow images. This finding shows that image statistics related to light and colour in paintings reflect the characteristics of terrestrial illumination and can be used by people to perceive the depicted time of day. Specifically, luminance and chromaticity were found to be the most effective predictors of perceived time of day. The desaturation association with eveningness might also be related to the Hunt Effect; colours in darker environments are perceived as less saturated than those in brighter environments [50].

In experiment two, we examined the statistical differences between morning and evening depictions based on both human perception and metadata. We found that there are subtle differences between morning and evening depictions in terms of luminance, but more significant differences in terms of chromaticity. These differences were particularly pronounced in perception-classified paintings, as opposed to the metadata-classified paintings. People tended to associate paintings depicting morning with a CCT similar to the average daylight of D55, while they perceived paintings depicting evening as having a CCT that ranges from warm to cool white. In addition, the airlight colour of morning paintings was also bluer than that of evening paintings. One contributing factor to this differentiation might be the presence of depicted haze, which might serve as a visual cue in distinguishing between morning and evening scenes. These regularities used by observers to distinguish between morning and evening reflect recorded measurements of natural illumination. As the sun rises and solar elevation increases, the temperature transitions from low to high and the frequency of dense water vapor, haze, and fog tends to be higher in the morning than in the evening [37–40]. The presence of visible mist or haze in a scene can cause a higher level of diffuseness and lower colour differences within the light field, resulting in an overall more even distribution of white in the image. The atmospheric filtering is also far from neutral [28, 51], causing a blue-shifted airlight colour in the morning relative to the evening. On the other hand, at sunset, the temperature decreases as the sun's elevation decreases, resulting in a higher proportion of water molecules in the lower atmosphere compared to the morning. These water molecules are larger than air molecules and scatter the long-wavelength component of sunlight, along with blue scattered light from the upper levels of the atmosphere, leading to large spatial and angular colour variations in the sunset sky ranging from orangey-red to deep blue [33].

It is worth noting that the reliability of metadata is an important consideration in this study. While metadata may be a useful source of information about the time of day depicted in a painting, it is ultimately based on the interpretation and knowledge of curators, and might not necessarily reflect the original intentions of the painter. This is especially relevant for paintings created before the 19^{th} century, when metadata was not yet being systematically recorded. However, the majority of the paintings used in this study were from the 19^{th} century (Appendix Section 5.A4), allowing for a meaningful comparison between the perceptual data and metadata.

It is possible that the differences between the two could be partially attributed to the potential limitations of metadata in accurately reflecting the original intentions of the painter.

The chromaticity of a painting, calculated from the conversion of sRGB to XYZ values, may reflect the range of estimated illumination chromaticities that observers see in the painting under the assumption of a "gray world" [52]. It is worth noting that the spread of chromaticities was calculated from the RGB values of the image, which may not produce the same chromaticity on every monitor due to variations in monitor specifications. To account for this, we can calculate the spread of chromaticities for a range of different white points, or assumed chromaticities for RGB values of [1, 1, 1]. While the transformation of the spread to different regions of the chromaticity diagram may vary, the relationship between chromaticity and time of day perception remains similar (see Appendix Section 5.A5).

In addition to the confounding factors of the actual colours of the painting and the colours displayed on participants' screens, there may be a discrepancy between the artist's intended colours and the current colours due to colour degradation. One influencing factor is the yellowing of varnish, which can affect the overall colour palette of a painting and potentially influence the perceived time of day. Varnish serves as a protective layer on oil paintings, shielding them from environmental factors like dust, UV light, and moisture. While it is essential for preserving artwork and frequently employed in art restoration, the yellowing of varnish might alter perceptions of the time of day depicted, with yellow-tinted paintings possibly being seen as morning scenes. However, our experiments did not substantiate this hypothesis. Experiment 1 revealed a negative correlation between average time-of-day scores and the year of creation, with a significance level of $p = 0.0051$ (r = -0.27), indicating a weak correlation. However, a positive correlation would be expected if yellowing were occurring and influencing time-of-day judgments. In Experiment 2, the correlation was not statistically significant (r = -0.16, $p = 0.1284$). Additionally, the canvas ground used in the 19^{th} century was lighter compared to those employed in earlier periods. This led to the hypothesis that darker paintings from earlier periods might be more frequently perceived as evening scenes. However, the correlations between average scores and the year of creation were either not statistically significant or very weak in both experiments.

In addition to creating a sense of space, our study shows that light and colour in paintings are also associated with a temporal dimension: time of day in paintings. Specifically, we found that luminance and chromaticity are the most effective predictors of perceived time of day in paintings. Our findings show that image statistics might partly explain time-of-day perception in paintings.

5.5. CONCLUSIONS

In this study, we analyzed the image statistics of paintings in order to understand how people perceive the time of day depicted in these works of art. We used dimension-reduction techniques to reduce the number of image statistics and then used these statistics to predict the perceived time of day in the paintings.

In conclusion, our study showed that the image statistics of paintings varied systematically depending on the time of day depicted, reflecting the characteristics of terrestrial illumination. Two predictors - luminance-related and chromaticity-related components - were the most effective at predicting the perceived time of day in the paintings. This suggests that people are able to perceive the difference between different time-of-day depictions in paintings and use cues related to luminance and chromaticity to discern the time of day depicted. Our results also indicate that while subtle and insignificant differences exist between morning and evening depictions in terms of luminance, statistical differences are evident in chromaticity. These average chromaticity differences appeared more pronounced in people's perceptions of the two times of day in paintings, rather than in metadata classification. We found that chromaticity may be an influential factor in people's perceptions of morning and evening, and that observers can use both luminance and chromaticity to differentiate between the two times of day. Interestingly, artists portrayed morning and evening with different chromaticity but not luminance. These findings provide insight into colour statistics of paintings that contribute to their perceived time of day and could be useful for artists and researchers studying the representation of the time of day in art. The results of this study show regularity but also overlap and large variance in the data. Further research will be needed to fully understand how people perceive the time of day depicted in paintings and the role that image statistics play in this process.

ACKNOWLEDGEMENT

Cehao Yu, Sylvia C. Pont and Anya Hurlbert acknowledge support from the H2020 Marie Skłodowska-Curie Actions (H2020-MSCA-ITN-2017) 'DyViTo: Dynamics in Vision and Touch', project number 765121. Mitchell J.P. van Zuijlen, Cristina Spoiala and Maarten W.A. Wijntjes were financed by the Netherlands Organization for Scientific Research with the VIDI project 'Visual communication of material properties', project number 276.54.001.

DATA AVAILABILITY

Dataset 1 [41] contains the image stimuli and associated metadata used in this study and is publicly available for further analysis and replication of our findings.

AUTHOR CONTRIBUTIONS

Under the supervision of AH, MW, and SP, CY conducted the study. The study was jointly designed by CY, AH, and MW, while MZ and MW developed the online experiment code. CY, AH, and MW developed the data and image analysis. MZ, CS, CY, and MW collaborated on metadata collection. CY wrote the first draft of the paper. All authors were involved in editing and approving the final article.

5.A. APPENDIX

5.A1. IMAGE COLOUR CONVERSION AND STATISTICAL ESTIMATION

Colour of each pixel of a given image at position $(1 \le i \le W, 1 \le j \le H)$ is described as a triplet of colour coordinates in the sRGB colour space as [R(i, j), G(i, j), B(i, j)], where W is the width and H is the height of the image in pixel number.

To ensure robust statistical estimates for the natural images, we determined the minimum and maximum values using the 5% and 95% percentiles of the histograms, respectively. This methodology was limited to values that were designated as either minimum or maximum.

Following this preparation, we proceeded to the analysis of colour distribution in the images, which involved the computation of image statistics defined as follows:

1. sRGB → XYZ and Yxy from XYZ.

The sRGB component values, R(i, j), G(i, j), and B(i, j), range from 0 to 1. The linear values, $C_{\text{linear}}(i, j)$, are calculated as follows:

$$C_{\text{linear}}(i,j) = \begin{cases} \frac{C_{sRGB}(i,j)}{12.92}, & \text{if } C_{sRGB}(i,j) \le 0.04045, \\ \left(\frac{C_{sRGB}(i,j)+0.055}{1.055}\right)^{2.4}, & \text{if } C_{sRGB}(i,j) > 0.04045. \end{cases}$$

where C(i, j) refers to R(i, j), G(i, j), or B(i, j).

These gamma-expanded values are then multiplied by a matrix to obtain the CIE XYZ tristimulus values.

$$\begin{bmatrix} X(i,j) \\ Y(i,j) \\ Z(i,j) \end{bmatrix} = \begin{bmatrix} 0.41240 & 0.35760 & 0.18050 \\ 0.21260 & 0.71520 & 0.07220 \\ 0.01930 & 0.11920 & 0.9503 \end{bmatrix} \begin{bmatrix} R_{\text{linear}}(i,j) \\ G_{\text{linear}}(i,j) \\ B_{\text{linear}}(i,j) \end{bmatrix}$$

The CIE 1931 chromaticity coordinates (x, y) be derived from the tristimulus values (X, Y, Z) as follows:

$$x(i,j) = \frac{X(i,j)}{X(i,j) + Y(i,j) + Z(i,j)}$$
$$y(i,j) = \frac{Y(i,j)}{X(i,j) + Y(i,j) + Z(i,j)}$$

2. XYZ → LMS / rod / melanopic receptoral activations

One formula here can cover all the photoreceptor-specific irradiances/activations, by referring to a $S_I(\lambda)$ and allowing i = L, M, S, *mel*, *rod*.

Then:

The spectrum of a given pixel is estimated as:

$$\lambda_{RGB}(i,j) = \lambda_R \times R(i,j) + \lambda_G \times G(i,j) + \lambda_B \times B(i,j)$$

etc

The spectral sensitivity $S_i(\lambda)$ of the receptor can be determined as L, M, or S using the Stockman & Sharpe (2000) [44] cone fundamentals. The melanopic irradiance is calculated using the melanopsin curve specified by Lucas *et al.* (2014) [45], while the scotopic irradiance is determined using the Crawford (1949) [46] method for rods. The e receptor-specific irradiance of a pixel can be calculated as follows:

$$e(i,j) = \int \lambda_{RGB}(i,j) S_i(\lambda)\, d\lambda$$

Respectively.

3. XYZ → CIELAB

L^*, a^*, b^* quantities defined by the equations

$$L^*(i,j) = 116 f\left(\frac{Y(i,j)}{Y_n}\right) - 16$$
$$a^*(i,j) = 500\left[f\left(\frac{X(i,j)}{X_n}\right) - f\left(\frac{Y(i,j)}{Y_n}\right)\right]$$
$$b^*(i,j) = 200\left[f\left(\frac{Y(i,j)}{Y_n}\right) - f\left(\frac{Z(i,j)}{Z_n}\right)\right]$$

where

$$f\left(\frac{X(i,j)}{X_n}\right) = \left(\frac{X(i,j)}{X_n}\right)^{1/3} \quad \text{if } \frac{X(i,j)}{X_n} < \left(\frac{24}{116}\right)^3$$
$$f\left(\frac{X(i,j)}{X_n}\right) = \frac{841}{108}\left(\frac{X(i,j)}{X_n}\right) + \frac{16}{116} \quad \text{if } \frac{X(i,j)}{X_n} \geq \left(\frac{24}{116}\right)^3$$

and

$$f\left(\frac{Y(i,j)}{Y_n}\right) = \left(\frac{Y(i,j)}{Y_n}\right)^{1/3} \quad \text{if } \frac{Y(i,j)}{Y_n} < \left(\frac{24}{116}\right)^3$$
$$f\left(\frac{Y(i,j)}{Y_n}\right) = \frac{841}{108}\left(\frac{Y(i,j)}{Y_n}\right) + \frac{16}{116} \quad \text{if } \frac{Y(i,j)}{Y_n} \geq \left(\frac{24}{116}\right)^3$$

and

$$f\left(\frac{Z(i,j)}{Z_n}\right) = \left(\frac{Z(i,j)}{Z_n}\right)^{1/3} \quad \text{if } \frac{Z(i,j)}{Z_n} < \left(\frac{24}{116}\right)^3$$
$$f\left(\frac{Z(i,j)}{Z_n}\right) = \frac{841}{108}\left(\frac{Z(i,j)}{Z_n}\right) + \frac{16}{116} \quad \text{if } \frac{Z(i,j)}{Z_n} \geq \left(\frac{24}{116}\right)^3$$

X_n, Y_n, Z_n describe a specified white achromatic reference illuminant.

$$\text{CIELAB lightness: } L^* \text{ as defined above}$$
$$\text{CIELAB chroma: } C^* = \sqrt{b^{*2} + a^{*2}}$$
$$\text{CIELAB hue: } h = \arctan\left(\frac{b^*}{a^*}\right)$$

Saturation is the degree to which a colour is pure and is defined as the ratio of chroma to luminance.

$$S(i,j) = \frac{C^*(i,j)}{L^*(i,j)}$$

4. CCT (T) **- another measure of pixel chromaticity**

The CCT of a given pixel T(i,j) is derived from its chromaticity in the (u,v) plane, in turn derived from (x,y) chromaticity in the usual way [53]. We finally used a combination of triangular and parabolic calculations to estimate CCT from (u,v), reducing the error to 1K [54]. We employed the triangular solution for $|D_{\text{uv}}| < 0.002$ and the parabolic solution for other regions. By employing this method, we accurately estimated the CCT of each pixel, which is a vital measure of pixel chromaticity.

To offer a more uniform perceptual representation, we calculated the inverse CCT as 10^6/CCT in reciprocal mega-Kelvin $\left(\text{MK}^{-1}\right)$. We denoted the inverse CCT as T′(i,j), where:

$$T'(i,j) = \frac{10^6}{T(i,j)}$$

The luminance-weighted CCT, denoted as T_Y(i,j), is calculated as the product of the luminance Y(i,j) and CCT T(i,j).

The luminance-weighted CCT is given by the following:

$$T_Y(i,j) = Y(i,j) \times T(i,j)$$

5. Statistical measures for image analysis

The following formulas are used to calculate several statistical measures of an image, including the mean, minimum, maximum, variance, standard deviation, skewness, difference and RMS contrast, based on the individual pixel data points represented by $r(i,j)$:

Mean (μ):

$$\mu = \frac{1}{WH} \sum_{i=1}^{W} \sum_{j=1}^{H} r(i,j)$$

Minimum (min):

$$r_{\text{min}} = \min_{1 \le i \le W; 1 \le j \le H} r(i,j)$$

Maximum (max):

$$r_{\max} = \max_{1 \le i \le W; 1 \le j \le H} r(i,j)$$

Variance (var):

$$var = \frac{1}{WH} \sum_{i=1}^{W} \sum_{j=1}^{H} [r(i,j) - \mu]^2$$

Standard deviation (σ):

$$\sigma = \sqrt{var}$$

Skewness (g):

$$g = \frac{1}{WH} \frac{1}{[\sqrt{var}]^3} \sum_{i=1}^{W} \sum_{j=1}^{H} [r(i,j) - \mu]^3$$

Difference (Δr):

$$\Delta r = r_{\max} - r_{\min}$$

RMS contrast (C):

$$C = \sqrt{\frac{1}{WH} \sum_{i=1}^{W} \sum_{j=1}^{H} [r(i,j) - \mu]^2}$$

6. Analysis of euclidean distance and correlation coefficient between colour channels in an image

The Euclidean image distance and correlation coefficient between two colour channels of an image can be described using the following formulas, where u and v represent arbitrary colour channels.

The Euclidean image distance:

$$D_{uv} = \frac{1}{WH} \sqrt{\sum_{i=1}^{W} \sum_{j=1}^{H} [u(i,j) - v(i,j)]^2}$$

This formula calculates the root mean square of the differences between corresponding pixel values in the two colour channels over the entire image. It can be used to quantify the dissimilarity between the two colour channels.

The correlation coefficient:

$$R_{uv} = \frac{\sum_{i=1}^{W}\sum_{j=1}^{H}[u(i,j)-\bar{u})][v(i,j)-\bar{v}]}{\sqrt{\sum_{i=1}^{W}\sum_{j=1}^{H}[u(i,j)-\bar{u}]^2[v(i,j)-\bar{v}]^2}}$$

This formula calculates the correlation between the corresponding pixel values in the two channels over the entire image. It can be used to quantify the similarity between the two colour channels. This measure can be useful in a variety of image processing applications, such as colour-based segmentation and image retrieval.

7. Colour difference (ΔE_{00})

5

The colour-difference formula (CIEDE2000) is based on the LAB colour space.

$$\Delta L' = L^*_{\max} - L^*_{\min},$$

$$\bar{L} = \frac{L^*_{\max} + L^*_{\min}}{2},$$

$$\bar{C} = \frac{C^*_{\max} + C^*_{\min}}{2},$$

$$a'_{\max} = a^*_{\max} + \frac{a^*_{\max}}{2}\left(1 - \sqrt{\frac{\bar{C}^7}{\bar{C}^7 + 25^7}}\right),$$

$$a'_{\min} = a^*_{\min} + \frac{a^*_{\min}}{2}\left(1 - \sqrt{\frac{\bar{C}^7}{\bar{C}^7 + 25^7}}\right),$$

$$\bar{C}' = \frac{C'_{\max} + C'_{\min}}{2}, \quad \text{and} \quad \Delta C' = C'_{\min} - C'_{\max},$$

$$\text{where} \quad C'_{\text{max}} = \sqrt{{a'_{\text{max}}}^2 + {b^*_{\text{max}}}^2}, \quad C'_{\text{min}} = \sqrt{{a'_{\text{min}}}^2 + {b^*_{\text{min}}}^2},$$

$$h'_{\text{max}} = \text{atan2}(b^*_{\text{max}}, a'_{\text{max}}) \bmod 360^\circ, \quad h'_{\text{min}} = \text{atan2}(b'_{\text{min}}, a'_{\text{min}}) \bmod 360^\circ,$$

$$\Delta h' = \begin{cases} h'_{\text{min}} - h'_{\text{max}} & \text{if } \left|h'_{\text{max}} - h'_{\text{min}}\right| \le 180^\circ, \\ h'_{\text{min}} - h'_{\text{max}} + 360^\circ & \text{if } \left|h'_{\text{max}} - h'_{\text{min}}\right| > 180^\circ, h'_{\text{min}} \le h'_{\text{max}}, \\ h'_{\text{min}} - h'_{\text{max}} - 360^\circ & \text{if } \left|h'_{\text{max}} - h'_{\text{min}}\right| > 180^\circ, h'_{\text{min}} > h'_{\text{max}}, \end{cases}$$

$$\Delta H' = 2\sqrt{C'_{\text{max}} C'_{\text{min}}} \sin\left(\frac{\Delta h'}{2}\right),$$

$$\bar{H}' = \begin{cases} \frac{h'_{\text{min}} + h'_{\text{max}}}{2} & \text{if } \left|h'_{\text{max}} - h'_{\text{min}}\right| \le 180^\circ, \\ \frac{h'_{\text{min}} + h'_{\text{max}} + 360^\circ}{2} & \text{if } \left|h'_{\text{max}} - h'_{\text{min}}\right| > 180^\circ, h'_{\text{min}} + h'_{\text{max}} < 360^\circ, \\ \frac{h'_{\text{min}} + h'_{\text{max}} - 360^\circ}{2} & \text{if } \left|h'_{\text{max}} - h'_{\text{min}}\right| > 180^\circ, h'_{\text{min}} + h'_{\text{max}} \ge 360^\circ, \end{cases}$$

$$T = 1 - 0.17\cos\left(\bar{H}' - 30^\circ\right) + 0.24\cos\left(2\bar{H}'\right) + 0.32\cos\left(3\bar{H}' + 6^\circ\right) - 0.20\cos\left(4\bar{H}' + 63^\circ\right),$$

$$S_L = 1 + \frac{0.015(\bar{L} - 50)^2}{\sqrt{20 + (\bar{L} - 50)^2}},$$

$$S_C = 1 + 0.045\bar{C}',$$

$$S_H = 1 + 0.015\bar{C}'T,$$

$$R_T = -2\sqrt{\frac{\bar{C}'^7}{\bar{C}'^7 + 25^7}} \sin\left[60° \exp\left(-\left[\frac{\bar{H}' - 275°}{25°}\right]^2\right)\right],$$

$$K_L = K_C = K_H = 1,$$

$$\Delta E_{00}(L^*_{\max}, a^*_{\max}, b^*_{\max}; L^*_{\min}, a^*_{\min}, b^*_{\min}) = \sqrt{\left(\frac{\Delta L'}{K_L S_L}\right)^2 + \left(\frac{\Delta C'}{K_C S_C}\right)^2 + \left(\frac{\Delta H'}{K_H S_H}\right)^2 + R_T\left(\frac{\Delta C'}{K_C S_C}\right)\left(\frac{\Delta H'}{K_H S_H}\right)}$$

The colour difference between the mean of 5% brightest pixels and the mean of 5% darkest pixel is:

$$\Delta E_{00} = \Delta E_{00}\left(L^*_{\max}, a^*_{\max}\ b^*_{\max}; L^*_{\min'}, a^*_{\min}, b^*_{\min}\right)$$

8. mean image colourfulness (C)

rg is the difference between the R channel and the G channel. yb represents half of the sum of the R and G channels minus the B channel.

$$rg = R - G$$
$$yb = \frac{1}{2}(R + G) - B$$

Next, the standard deviation (σ_{rgyb}) and mean (μ_{rgyb}) are computed before calculating the final colourfulness metric, C.

$$\mu_{rg} = \frac{1}{WH}\sum_{i=1}^{W}\sum_{j=1}^{H} rg(i,j)$$
$$\mu_{yb} = \frac{1}{WH}\sum_{i=1}^{W}\sum_{j=1}^{H} yb(i,j)$$
$$\sigma_{rg} = \sqrt{\frac{1}{WH}\sum_{i=1}^{W}\sum_{j=1}^{H}[rg(i,j) - \overline{rg}]^2}$$
$$\sigma_{yb} = \sqrt{\frac{1}{WH}\sum_{i=1}^{W}\sum_{j=1}^{H}[yb(i,j) - \overline{yb}]^2}$$
$$\sigma_{rgyb} = \sqrt{{\sigma_{rg}}^2 + {\sigma_{yb}}^2}$$
$$\mu_{rgyb} = \sqrt{{\mu_{rg}}^2 + {\mu_{yb}}^2}$$

The mean image colourfulness is given by the following:

$$C = \sigma_{rgyb} + 0.3 \cdot \mu_{rgyb}$$

9. Luma

The luma Y′(i,j) of a pixel in an image is calculated as a linear combination of its RGB primary values, and is commonly used in colour video encoding in addition to luminance due to its colorimetric properties. The formula for Y'(i,j) is as follows:

$$Y'(i,j) = 0.2126R(i,j) + 0.7152G(i,j) + 0.0722B(i,j)$$

10. Airlight estimation

A practical way to estimate airlight colour comes from dehazing literature, as airlight estimation is a prerequisite for dehazing. In a commentary on the dehazing study by Kaiming He *et al.* [49], Odisio and Alessandrini [55] outline the following way of airlight estimation:

1) First apply a filter to each RGB channel that replaces each pixel value with the local minimum value, defined by some kernel width r. This step is used for local smoothing.
2) For each pixel take the minimum value of three channels, this results in a dark channel image.
3) Select the top 0.3% of the brightest pixels of the dark channel
4) Cluster these pixels and select the cluster with the highest luminance
5) Take the mean RGB colour, and this is the airlight.

5.A2. CORRELATION MATRICES OF HUMAN RATING AND IMAGE STATISTICS

In Figure 5.A1 and Figure 5.A2, we illustrate the correlations between human ratings and selected image statistics for Experiments 1 and 2, resulting from independent regressions of mean rating scores on each image statistics measure. The red time of day score corresponds to the mean score, which is the sum of all scores divided by the number of scores, representing an overall measure of the perceived time of day for each painting. The morningness score, noonness score, eveningness score, and nightness score represent the proportional score per category, indicating the proportion of scores falling into each category relative to the total count of scores.

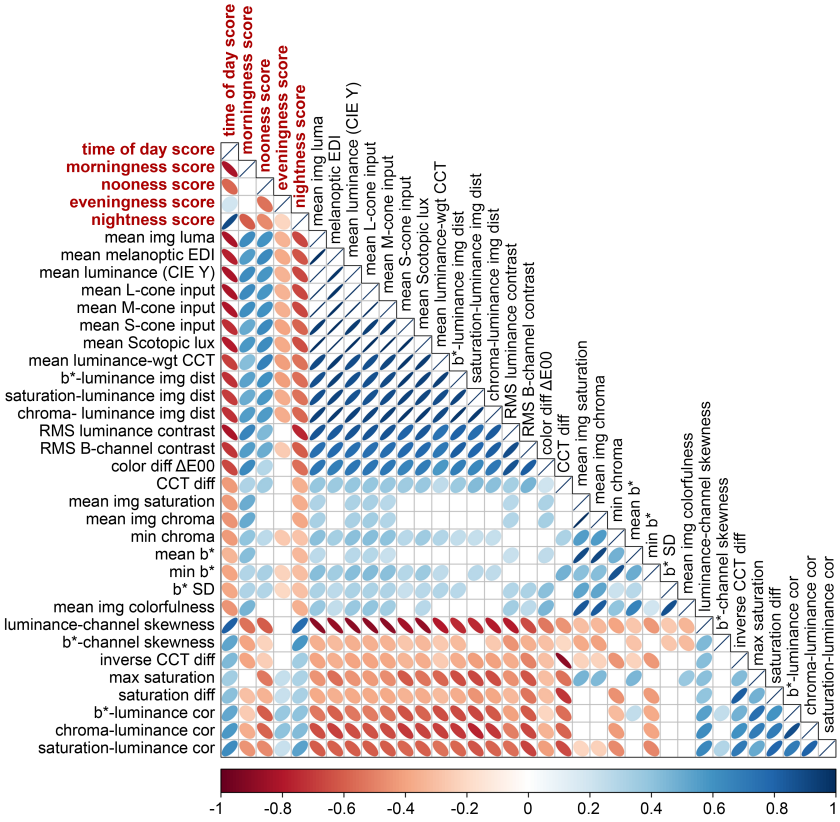

Figure 5.A1: Results of Experiment 1. Correlation matrices of human rating and image statistics are represented by ellipses that vary in thickness and colour. Thinner ellipses indicate a stronger correlation, while fatter ellipses indicate a weaker correlation. The elongation of the ellipses shows the direction of correlation, with red indicating positive correlation, blue indicating negative correlation, and white indicating zero correlation. Only correlation coefficients that have a significant effect at $p < 0.05$ are included in the matrix cells.

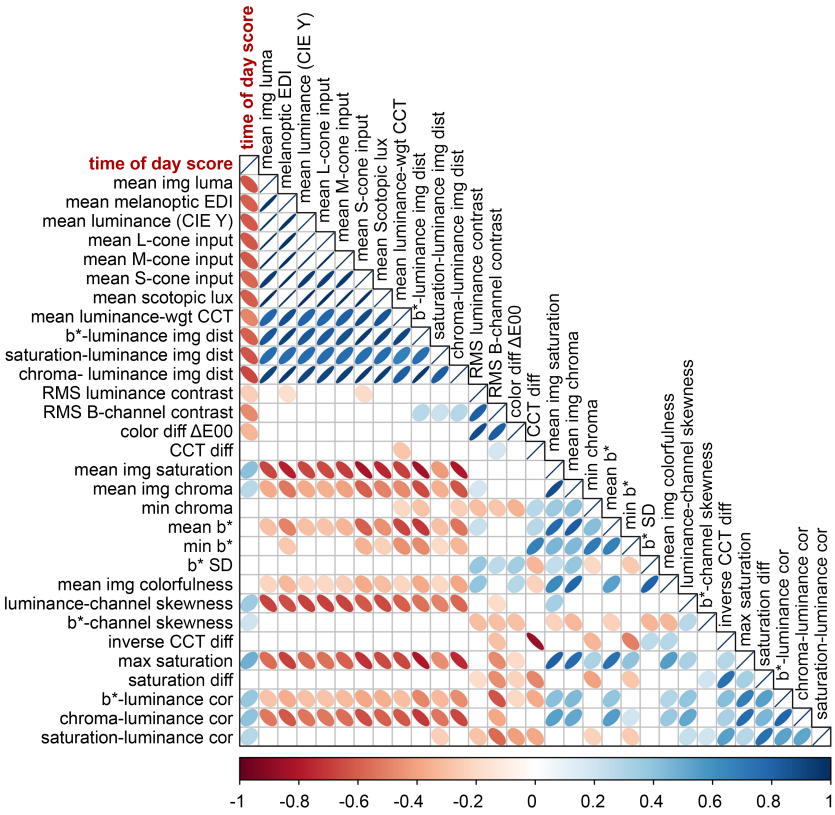

Figure 5.A2: Results of Experiment 2. Correlation matrices of human rating and image statistics are represented by ellipses that vary in thickness and colour. Thinner ellipses indicate a stronger correlation, while fatter ellipses indicate a weaker correlation. The elongation of the ellipses shows the direction of correlation, with red indicating positive correlation, blue indicating negative correlation, and white indicating zero correlation. Only correlation coefficients that have a significant effect at $p < 0.05$ are included in the matrix cells.

5.A3. PRINCIPAL COMPONENT ANALYSIS FOR EXPERIMENT 1

1. Factor loadings

Table 5.A1 displays the factor loadings for the first five principal components in Experiment 1. The table shows the loading values for each image statistic, with red indicating negative loading and green indicating positive loading.

Component Matrix[a]

	Component				
	PC1	PC2	PC3	PC4	PC5
mean image luma	-0.964	-0.100	-0.163	-0.140	-0.089
mean melanopsin input	-0.962	0.079	-0.198	-0.146	-0.03
mean luminance (CIE Y)	-0.963	-0.105	-0.162	-0.138	-0.091
mean L-cone input	-0.962	-0.121	-0.158	-0.135	-0.095
mean M-cone input	-0.966	-0.065	-0.171	-0.144	-0.079
mean S-cone input	-0.942	0.194	-0.217	-0.141	0.012
mean rod input	-0.966	0.038	-0.191	-0.147	-0.044
mean luminance-weighted CCT	-0.893	0.197	-0.241	-0.184	0.164
b^*-luminance image distance	-0.918	0.22	-0.208	0.007	0.096
saturation-luminance image distance	-0.908	0.284	-0.089	-0.058	-0.029
chroma-luminance image distance	-0.938	0.213	-0.175	-0.038	-0.082
RMS contrast (luminance)	-0.864	-0.075	-0.257	0.233	-0.223
RMS contrast (B channel)	-0.855	0.107	-0.077	0.413	0.006
colour difference (ΔE_{00})	-0.719	-0.162	-0.343	0.409	-0.158
CCT difference	-0.527	0.108	0.674	0.227	-0.19
mean image saturation	-0.244	-0.945	0.082	0.064	-0.018
mean image chroma	-0.259	-0.945	0.076	0.053	-0.036
min chroma	-0.434	-0.474	0.48	-0.45	0.201
mean b^*	-0.171	-0.888	0.163	-0.023	-0.31
min b^*	-0.43	-0.342	0.559	-0.531	-0.013
b^* SD	-0.296	-0.539	-0.341	0.251	0.621
mean image colourfulness	-0.314	-0.834	-0.204	0.188	0.305
luminance-channel skewness	0.884	0.113	0.031	0.127	0.082
b^*-channel skewness	0.385	0.286	0.043	-0.262	0.075
inverse CCT difference	0.542	0.024	-0.689	-0.287	0.148
max saturation	0.588	-0.67	-0.179	-0.172	-0.024
saturation difference	0.55	-0.015	-0.67	-0.295	-0.133
b^*-luminance correlation	0.684	-0.376	-0.343	0.001	-0.376
chroma-luminance correlation	0.779	-0.292	-0.368	0.013	-0.261
saturation-luminance correlation	0.743	-0.023	-0.49	-0.131	-0.014

Extraction Method: Principal Component Analysis.
a. 5 components extracted.

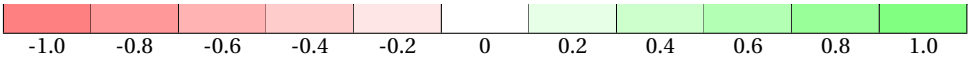

Table 5.A1: Results of Experiment 1. Factor loadings for the first five principal components.

2. Explained variance

Table 5.A2 elaborates on the results from Experiment 1, providing a detailed breakdown of the total variance explained by each of the principal components. The components are listed in descending order of the variance they account for. For each principal component, the table presents the initial eigenvalues, the percentage of total variance explained, and the cumulative percentage of variance explained up to that component. Notably, the first few components explain a substantial proportion of the total variance, indicating their significant contribution in capturing the patterns in the image data.

Total Variance Explained

	Initial Eigenvalues			Extraction Sums of Squared Loadings		
Component	Total	% of Variance	Cumulative %	Total	% of Variance	Cumulative %
1	16.292	54.307	54.307	16.292	54.307	54.307
2	5.027	16.758	71.065	5.027	16.758	71.065
3	3.205	10.682	81.747	3.205	10.682	81.747
4	1.514	5.046	86.793	1.514	5.046	86.793
5	1.069	3.563	90.355	1.069	3.563	90.355
6	0.894	2.979	93.334			
7	0.448	1.492	94.826			
8	0.347	1.156	95.982			
9	0.280	0.934	96.916			
10	0.181	0.602	97.518			
11	0.170	0.566	98.084			
12	0.132	0.439	98.523			
13	0.104	0.347	98.870			
14	0.078	0.262	99.132			
15	0.074	0.248	99.380			
16	0.049	0.164	99.544			
17	0.045	0.149	99.693			
18	0.035	0.117	99.810			
19	0.022	0.073	99.883			
20	0.016	0.054	99.937			
21	0.012	0.039	99.976			
22	0.004	0.014	99.990			
23	0.002	0.008	99.998			
24	0.000	0.001	99.999			
25	0.000	0.001	100.000			
27	0.000	0.000	100.000			
28	0.000	0.000	100.000			
29	0.000	0.000	100.000			
30	-0.000	-0.000	100.000			

Extraction Method: Principal Component Analysis.

Table 5.A2: Results of Experiment 1, showing the total variance explained by each principal component in the analysis. The components are ordered by the amount of variance they explain, from highest to lowest.

5.A4. DISTRIBUTION OF YEARS OF CREATION FOR PAINTINGS

Figure 5.A3 shows the distribution of years of creation for the paintings used in Experiments 1 and 2. The histogram demonstrates that the majority of the paintings were created around 1900, with relatively fewer paintings from earlier or later periods. This information is helpful in understanding the potential reliability of metadata.

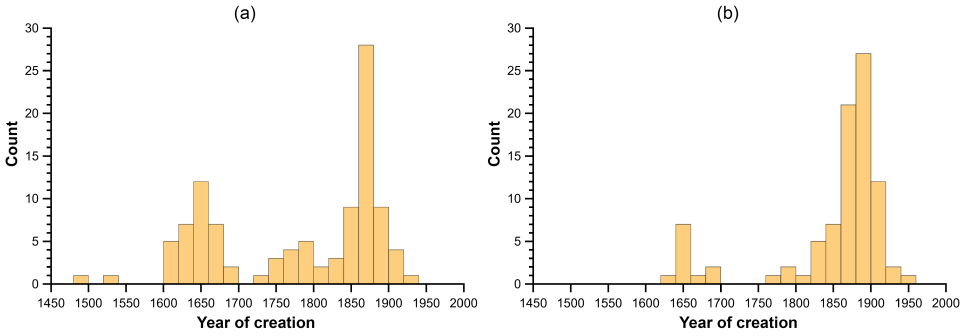

Figure 5.A3: Histogram of years of creation for paintings used in Experiment 1 (a) and Experiment 2 (b).

5.A5. DIFFERENT SCREEN WHITE POINTS ON THE MEAN CHROMATICITY OF PAINTINGS

To account for the potential impact of different white points on the calculation of chromaticities, we calculated the spread of mean image chromaticities for Experiment 1 for a range of different white points, or assumed chromaticities for RGB values of [1, 1, 1]. This allowed us to consider the effect of chromatic adaptation on the calculation of chromaticities in our study. In Figure 5.A4, we plot the mean image chromaticities in the CIE xy plane for a range of different white points, with one disk representing one image.

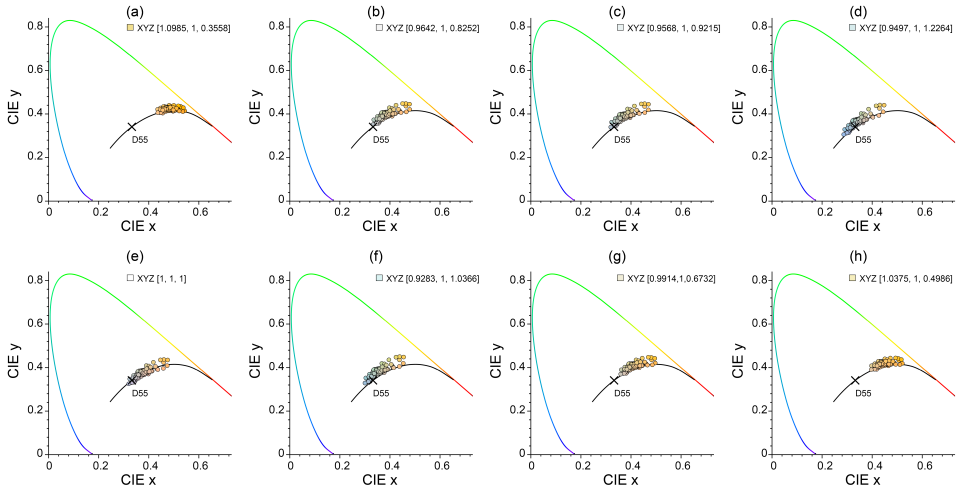

Figure 5.A4: Results of Experiment 1. Mean image chromaticities in CIE xy plane for paintings with a range of different white points, one disk per image. The disk colours represent the chromaticity of each image. The black line indicates the daylight locus and the location of D55 is marked. (a) Illuminant A. (b) D50. (c) D55. (d) D75. (e) Illuminant E. (f) Illuminant F1. (g) Illuminant F2. (h) Illuminant F3. The XYZ colour coordinates of each white point are indicated in the chromaticity diagram.

To further investigate the relationship between luminance and chromaticity across different white points, we plotted the correlation matrices of mean image luminance, CIELAB a^*, and CIELAB b^* values for nine different white points in Figure 5.A5. We found that both luminance and chromaticity are significantly and strongly correlated across different white points, while the correlation of CIELAB a^* is relatively lower. This is as expected, given that the mean image chromaticity follows a distinct pattern along the daylight locus with only minor green shift.

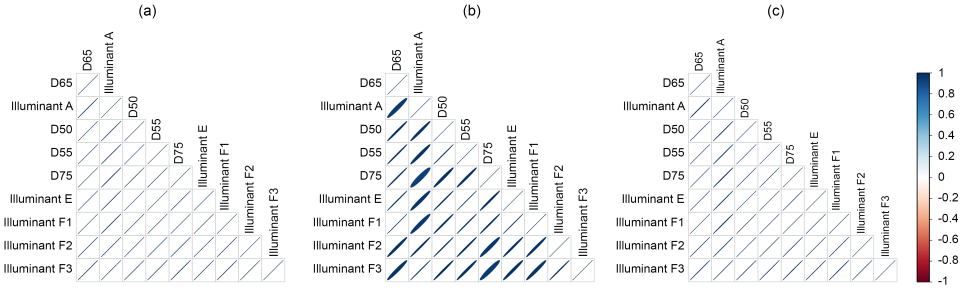

Figure 5.A5: Results of Experiment 1. Correlation matrices for mean image luminance and chromaticity values in terms of CIE-Y and CIELAB a^* and b^* for 9 different white points. Ellipses varying in thickness and colour represent the correlation strength, with thinner ellipses indicating stronger correlations and fatter ellipses indicating weaker ones. The elongation of the ellipses shows the correlation direction, with red indicating positive, blue indicating negative, and white indicating no correlation. Matrix cells only include significant correlation coefficients at $p < 0.05$. (a) Luminance. (b) a^* value. (c) b^* value.

REFERENCES

[1] P. Mamassian. “Ambiguities and conventions in the perception of visual art”. In: *Vision Research* 48.20 (2008), pp. 2143–2153.

[2] P. Cavanagh. “The artist as neuroscientist”. In: *Nature* 434.7031 (2005), pp. 301–307.

[3] J. J. Gibson. “The information available in pictures”. In: *Leonardo* 4.1 (1971), pp. 27–35.

[4] M. J. P. van Zuijlen, H. Lin, K. Bala, S. C. Pont, and M. W. A. Wijntjes. “Materials In Paintings (MIP): An interdisciplinary dataset for perception, art history, and computer vision”. In: *Plos one* 16.8 (2021), e0255109.

[5] S. Nakauchi and H. Tamura. “Regularity of colour statistics in explaining colour composition preferences in art paintings”. In: *Scientific Reports* 12.1 (2022), p. 14585.

[6] G. U. Hayn-Leichsenring, T. Lehmann, and C. Redies. “Subjective ratings of beauty and aesthetics: correlations with statistical image properties in western oil paintings”. In: *i-Perception* 8.3 (2017), pp. 1–21.

[7] B. Sayim and P. Cavanagh. “The art of transparency”. In: *i-Perception* 2.7 (2011), pp. 679–696.

[8] M. W. A. Wijntjes, C. Spoiala, and H. de Ridder. “Thurstonian scaling and the perception of painterly translucency”. In: *Art & Perception* 8.3-4 (2020), pp. 363–386.

[9] F. di Cicco, M. W. A. Wijntjes, and S. C. Pont. “Understanding gloss perception through the lens of art: Combining perception, image analysis, and painting recipes of 17th century painted grapes”. In: *Journal of vision* 19.3:7 (2019), pp. 1–15.

[10] F. di Cicco, M. J. P. van Zuijlen, M. W. A. Wijntjes, and S. C. Pont. “Soft like velvet and shiny like satin: Perceptual material signatures of fabrics depicted in 17th century paintings”. In: *Journal of vision* 21.5:10 (2021), pp. 1–22.

[11] M. G. Bloj, D. Kersten, and A. C. Hurlbert. “Perception of three-dimensional shape influences colour perception through mutual illumination”. In: *Nature* 402.6764 (1999), pp. 877–879.

[12] A. I. Ruppertsberg, M. Bloj, and A. Hurlbert. “Sensitivity to luminance and chromaticity gradients in a complex scene”. In: *Journal of Vision* 8.9:3 (2008), pp. 1–6.

[13] R. Arnheim. *Art and Visual Perception: A psychology of the creative eye*. University of California Press, 1974.

[14] T. Kartashova, H. de Ridder, S. F. te Pas, M. Schoemaker, and S. C. Pont. "The visual light field in paintings of Museum Prinsenhof: Comparing settings in empty space and on objects". In: *Human vision and electronic imaging XX*. Vol. 9394. SPIE. 2015, pp. 554–563.

[15] C.-C. Carbon and A. Pastukhov. "Reliable top-left light convention starts with Early Renaissance: An extensive approach comprising 10k artworks". In: *Frontiers in psychology* 9 (2018), p. 454.

[16] Y. Ostrovsky, P. Cavanagh, and P. Sinha. "Perceiving illumination inconsistencies in scenes". In: *Perception* 34.11 (2005), pp. 1301–1314.

[17] R. Casati. "The copycat solution to the shadow correspondence problem". In: *Perception* 37.4 (2008), pp. 495–503.

[18] M. A. Hagen. "The development of sensitivity to cast and attached shadows in pictures as information for the direction of the source of illumination". In: *Perception & Psychophysics* 20.1 (1976), pp. 25–28.

[19] J. W. Goethe. *Zur Farbenlehre*. Hofenberg, 1810.

[20] R. N. Shepard. "The perceptual organization of colors: An adaptation to regularities of the terrestrial world?" In: *The adapted mind: Evolutionary psychology and the generation of culture*. Ed. by J. H. Barkow, L. Cosmides, and J. Tooby. Oxford University Press, 1992, pp. 495–532.

[21] Y. Morgenstern, W. S. Geisler, and R. F. Murray. "Human vision is attuned to the diffuseness of natural light". In: *Journal of Vision* 14.9:15 (2014), pp. 1–18.

[22] G. S. Smith. "Human color vision and the unsaturated blue color of the daytime sky". In: *American Journal of Physics* 73.7 (2005), pp. 590–597.

[23] M. Minnaert. *Light and Color in the Outdoors*. Springer New York, NY, 1993.

[24] J. Mardaljevic. "Daylighting". In: *Encyclopedia of Color Science and Technology*. Ed. by R. Shamey. Springer Berlin Heidelberg, 2019, pp. 1–15.

[25] G. Hoeppe. *Why the sky is blue: discovering the color of life*. Princeton University Press, 2007.

[26] R. Pastilha and A. Hurlbert. "Seeing and sensing temporal variations in natural daylight". In: *Progress in Brain Research* 273.1 (2022), pp. 275–301.

[27] C. Yu and S. Pont. "Quantifying natural light for lighting and display design". In: *SID Symposium Digest of Technical Papers*. Vol. 52. S2. Society for Information Display China. 2021, pp. 99–103.

[28] C. Yu, M. Wijntjes, E. Eisemann, and S. Pont. "Quantifying the spatial, temporal, angular and spectral structure of effective daylight in perceptually meaningful ways". In: *Optics Express* 31.5 (2023), pp. 8953–8974.

[29] J. Hernández-Andrés, J. Romero, J. L. Nieves, and R. L. Lee. "Color and spectral analysis of daylight in southern Europe". In: *Journal of the Optical Society of America A* 18.6 (2001), pp. 1325–1335.

[30] D. B. Judd, D. L. MacAdam, G. Wyszecki, H. Budde, H. Condit, S. Henderson, and J. Simonds. “Spectral distribution of typical daylight as a function of correlated color temperature”. In: *Journal of the Optical Society of America A* 54.8 (1964), pp. 1031–1040.

[31] E. H. Gombrich. *The Heritage of Apelles: Studies in the Art of the Renaissance*. Cornell University Pressn, 1976.

[32] W. Beurs. *The Big World Painted Small, or Colorful Tableau of the World in Paintings*. 1692.

[33] A. Panorgias, J. J. Kulikowski, N. R. Parry, D. J. McKeefry, and I. J. Murray. “Phases of daylight and the stability of color perception in the near peripheral human retina”. In: *Journal of vision* 12.3:1 (2012), pp. 1–11.

[34] S. G. Narasimhan and S. K. Nayar. “Vision and the atmosphere”. In: *International journal of computer vision* 48.3 (2002), pp. 233–254.

[35] J. J. Koenderink. *Color for the Sciences*. MIT press, 2010.

[36] H. Koschmieder. “Theorie der horizontalen Sichtweite”. In: *Beitrage zur Physik der freien Atmosphare* (1924), pp. 33–53.

[37] P. Minnis, S. Mayor, W. L. Smith, and D. F. Young. “Asymmetry in the diurnal variation of surface albedo”. In: *IEEE Transactions on Geoscience and Remote Sensing* 35.4 (1997), pp. 879–890.

[38] O. Pechony, C. Price, and A. P. Nickolaenko. “Relative importance of the day-night asymmetry in Schumann resonance amplitude records”. In: *Radio Science* 42.02 (2007), pp. 1–12.

[39] D. H. Deutsch. “A mechanism for molecular asymmetry”. In: *Journal of molecular evolution* 33 (1991), pp. 295–296.

[40] S. Rickel and A. Genin. “Twilight transitions in coral reef fish: the input of light-induced changes in foraging behaviour”. In: *Animal behaviour* 70.1 (2005), pp. 133–144.

[41] C. Yu. “An image dataset for studying time of day perception in paintings”. In: *4TU.ResearchData. Dataset* (2023).

[42] M. J. P. van Zuijlen, S. C. Pont, and M. W. A. Wijntjes. “Painterly depiction of material properties”. In: *Journal of vision* 20.7:7 (2020), pp. 1–17.

[43] A. Stockman and L. T. Sharpe. “The spectral sensitivities of the middle-and long-wavelength-sensitive cones derived from measurements in observers of known genotype”. In: *Vision research* 40.13 (2000), pp. 1711–1737.

[44] A. Stockman, L. T. Sharpe, and C. Fach. “The spectral sensitivity of the human short-wavelength sensitive cones derived from thresholds and color matches”. In: *Vision research* 39.17 (1999), pp. 2901–2927.

[45] R. J. Lucas, S. N. Peirson, D. M. Berson, T. M. Brown, H. M. Cooper, C. A. Czeisler, M. G. Figueiro, P. D. Gamlin, S. W. Lockley, J. B. O’Hagan, *et al.* “Measuring and using light in the melanopsin age”. In: *Trends in neurosciences* 37.1 (2014), pp. 1–9.

[46] B. H. Crawford. “The scotopic visibility function”. In: *Proceedings of the Physical Society. Section B* 62.5 (1949), p. 321.

[47] I. Mallett and C. Yuksel. “Spectral Primary Decomposition for Rendering with sRGB Reflectance”. In: *Eurographics Symposium on Rendering - DL-only and Industry Track*. Ed. by T. Boubekeur and P. Sen. The Eurographics Association, 2019.

[48] M. R. Luo, G. Cui, and B. Rigg. “The development of the CIE 2000 colour-difference formula: CIEDE2000”. In: *Color Research & Application* 26.5 (2001), pp. 340–350.

[49] K. He, J. Sun, and X. Tang. “Single image haze removal using dark channel prior”. In: *IEEE transactions on pattern analysis and machine intelligence* 33.12 (2010), pp. 2341–2353.

[50] R. W. G. Hunt. “The effects of daylight and tungsten light-adaptation on color perception”. In: *Journal of the Optical Society of America A* 40.6 (1950), pp. 362–371.

[51] R. L. Lee and J. Hernández-Andrés. “Colors of the daytime overcast sky”. In: *Applied optics* 44.27 (2005), pp. 5712–5722.

[52] G. Buchsbaum. “A spatial processor model for object colour perception”. In: *Journal of the Franklin institute* 310.1 (1980), pp. 1–26.

[53] E. C. Carter, J. D. Schanda, R. Hirschler, S. Jost, M. R. Luo, M. Melgosa, Y. Ohno, M. R. Pointer, D. C. Rich, F. Viénot, L. Whitehead, and J. H. Wold. *Colorimetry, 4th Edition*. CIE Central Bureau, 2018.

[54] Y. Ohno. “Practical use and calculation of CCT and Duv”. In: *LEUKOS* 10.1 (2014), pp. 47–55.

[55] M. Odisio and G. Alessandrini. *Removing Haze from a Color Photo Image Using the Near Infrared with the Wolfram Language*. Wolfram Blog. 2014.

6

CONCLUSION

This chapter presents a summary of the key findings and contributions of this thesis, addressing the research questions outlined in **Chapter 1**. It highlights the limitations of the current study and suggests potential avenues for future research to continue advancing our understanding in this field.

6.1. MAIN FINDINGS AND CONTRIBUTIONS

THE phenomenon of a volume of space appearing to contain light [1] rather than being completely dark raises questions about the factors that determine this appearance. These factors can include the presence and type of light sources, the nature of surfaces in the space, and any obstacles that may block or reflect light [2–6]. Moreover, human perception of light and darkness can also be influenced by cognitive and psychological factors [7, 8], like prior experience, expectations, and attentional focus. To gain a deeper understanding of our experience of light in space, it is beneficial to analyse the interaction between various optical and perceptual factors.

Traditional measures of light, like lux levels on horizontal surfaces and downwelling irradiance spectra [9], do not capture the volumetric properties of environmental light and its impact on human perception and experience [10–13]. More comprehensive metrics are needed to objectively and subjectively quantify the appearance of light. This is where the concept of the light field [4, 5, 14, 15], which accounts for the distribution of light in a three-dimensional space over time and wavelength, can serve as a potential alternative metric.

To create an effective lighting design proposal, a thorough understanding of the unique characteristics of the light field and its influence on human perception is necessary. The lighting design process involves balancing various lighting concepts with the specific users and design goals of the space in question. This process requires imagining the space and its objects as they could be illuminated and a deep understanding of the unique characteristics of the light field that results. From this, the designer is able to carefully place and control luminaires and light sources to create a cohesive, functional, and aesthetically pleasing design.

The early research into characterising the light field provided a solid foundation for a light-based approach to studying and assessing the quantity and quality of light in built environments [4]. However, a lack of spectral resolution in the measurement, description, and visualisation of the light field limited the information available for understanding colour appearance. Therefore, the purpose of this thesis was to expand the light fields theory and methods in the chromatic domain through a combination of computational modelling and physical measurements. By analysing the impact of light on objects in full-room settings and combining physical measurements with behavioural psychophysics and computational modelling, this study aimed to develop and validate lighting design tools that use light field parameters instead of traditional 2D surface illuminances. This research incorporated knowledge from optics and perception science to optimise the characterisation of natural illumination and drive advancements in lighting design and technology.

Chapters 2-5 addressed the key research questions, and the results and contributions are presented in the order of the research questions.

Q1. How do the chromatic effects of indirect illumination influence the different components of physical light fields in uni-chromatic spaces, and what systematic colour variations can be expected?

This research studied the effects of indirect illumination on the structure of the physical light field in diffusely scattering scenes. The spectral properties of indirect

illumination were found to vary systematically and correspond with brightness, saturation, and hue shifts. A computational model was employed to evaluate and comprehend the spectral effects on the fundamental properties of light fields, such as the light density and light vector, by measuring and understanding these spectral effects. The model was tested via computer renderings and via measurements in real mock-up rooms under different furnishing scenarios for two types of illuminants, and found to correctly predict the spectral variations within the light field. The results suggest that indirect illumination mainly affects the light density spectrum and has less impact on the light vector spectrum, and highlight the importance of considering these differential effects for their consequences on the colour rendering of 3-dimensional objects and people.

Q2. How does indirect illumination affect the colorimetric properties of the effective light, specifically the correlated colour temperature and colour rendering, in uni-chromatic spaces?

This research aimed to investigate the colorimetric properties of the actual light, specifically the effective correlated colour temperature (CCT) and colour rendition, in spaces of one reflectance (uni-chromatic spaces). The spectra of the diffuse and directional components of the light field were measured in both physical and simulated uni-chromatic spaces illuminated by ordinary white light sources. The results showed major differences between the lamp-specified CCT and colour rendition and the actual light-based effective CCT and effective colour rendition. The study also uncovered that indirect illumination primarily impacted the CCT and colour rendition of the diffuse light element. Moreover, analysing the diffuse and directional components of the light field independently allows for a more comprehensive understanding of how the light source and scene affect each component distinctly. The findings suggest the need for a 3D version of colour checkers for lighting designers, architects and computer graphics applications, and propose simple Lambertian spheres as a solution.

Q3. How can the 7-dimensional structure of the light field be effectively quantified and translated into perceptually-relevant information using the spectral cubic irradiance method, and how do variations in the light field impact the diffuse and directed components of the actual light over time, space, colour, and direction?

This research proposed a method, called the spectral cubic illumination method, for capturing the 7-dimensional structure of light environments and translating it into perceptually-relevant information. The method allows for quantifying objective correlates of the perceptually relevant diffuse and directed light components of the actual light, including their variations over time, space, colour, and direction, and including the environmental response to sky and sunlight. We applied the method in different outdoor scenes and found that perceptually meaningful aspects of light, such as direction, colour, and diffuseness, vary over space and time in ecologically valid conditions. We also made the data collected freely available and argue that the method provides a low-cost, high-benefit solution for capturing nuanced effects of lighting on scene and object appearance, such as colour gradients over 3D shapes.

Q4. How do artists' depictions of natural illumination in paintings compare to

the statistical regularities of actual light in terms of luminance and chromaticity, and how do these comparisons relate to human viewers' perceptions of depicted time of day in terms of image statistics, specifically luminance and chromatic variations?

The study investigated whether human viewers' estimates of depicted time of day in paintings correlated with the paintings' image statistics, specifically luminance and chromatic variations. The study confirmed such relations. The results showed that higher ratings for 'morningness' were linked with higher brightness, contrast, saturation, and yellow hues, while higher ratings for 'eveningness' were correlated with lower brightness, contrast, saturation, and blue hues. These findings suggest that artists' depictions reflect the regularity of daylight in terms of chromaticity and luminance, and that observers might use these cues to estimate the time of day.

6.2. LIMITATIONS

Our research expanded the Delft light-field framework [4] into the colour domain, using the first-order spherical harmonics (SH) to describe light distribution in 3D space from a perception-based perspective. This approach, which is equivalent to describing the illumination solid [16, 17] or the first order part of Ramamoorthi's efficient represention of the radiance environment [18], forms the basis of a system of applied photometry and colorimetry. The primary focus of our studies was on quantifying the spectral effects of different light-field components that are relevant to perception [3, 4, 19–21], evaluating the spatial and directional analyses in combination with their photometric and colorimetric properties, and exploring the temporal dynamics of the light field.

We have also encountered several limitations. First, due to financial constraints, we were unable to create a grid of spectral cubic illumination meters to measure the first-order structure of the global light field as a function of various parameters. Instead, we used a single spectral irradiance meter to capture the light field through sequential measurements, limiting the spatial and especially the temporal dimensions. Furthermore, the angular resolution of the cubic approach is limited, quantifying only 94% of the matte material appearances [22]. To fully quantify the light appearance of matte materials, we would need to capture also the second-order SH light field component [23], which can be measured with a dodecahedron-shaped plenopter [24]. However, again due to financial limitations, we did not construct such a spectral plenopter.

Another limitation of our studies is that in our perception study we only measured an indirect effect of chromatic effects and not the perception of chromatic light-field components themselves. This suggests a need for future research to test which specific aspects of chromatic light-field components human observers are sensitive to.

Overall, our research highlights the importance of integrating knowledge about the perception of light with measurement of the light field, which presents unique challenges that require innovative solutions and methods.

6.3. FUTURE OUTLOOK

To design effective lighting schemes to suit human needs, it is necessary to integrate knowledge about the optical structure, how it is perceived, and how light interacts with material, shape, and space, considering both objective and subjective factors. This requires a multidisciplinary approach combining optical science and vision science. Assessing environmental light as it may reach the eye and comprehending its multidimensional characteristics offers perceptually meaningful information beyond characterizing lux levels on horizontal surfaces and downwelling irradiance spectra. Categorising environmental light into perceptually meaningful SH light field components, as we have done in this thesis, can deepen the understanding of light perception and improve the ability to create effective lighting designs and environments that enhance the human experience.

While our research in **Chapters 2** to **4** has focused on the spectral properties of the optical light field up to the 1st order, characterising higher-order components of the light field and including their spectral properties is critical for future research. This will enable a comprehensive description of the distribution of light in 3D space from a human-centred perspective and a deeper understanding of how the light field impacts object appearance. The integration of findings from both first-order and higher-order components has already provided a complete framework for describing the light distribution in 3D space [3, 4]. However, to fully account for the human visual experience of environmental light, it is important to consider the spectral-spatial-angular-temporal structure beyond the first-order light field, given the critical role that higher-order light field components plays in apparent gloss of objects [25].

Moreover, investigating human sensitivity to spectral variations within the light field is important to gain insights into its influence on our perception. A comprehensive theory of visual light fields [20, 21, 26, 27] in the spectral domain could enhance our knowledge in related areas such as lightness and colour constancy, shape from shading, and material perception. Although lighting perception has received less attention compared to other key topics in the field, it is a promising avenue for advancing our understanding of human vision, given the advancements in experimental methods and new applications.

Lastly, the polarisation state of light can yield higher-dimensional functions and is worth investigating as it affects visual perception by influencing interactions with objects and surfaces, including highlights on glossy objects [28, 29]. Although not included in our light field description, the use of polarisation filters to capture the light field could serve as an additional experimental tool to separate specular and diffuse components [28]. While humans lack true polarisation vision [30], it plays a key role in animal vision [31]. Therefore, the characterisation of environmental light beyond anthropocentric perspectives may aid in furthering the study of animal vision. Investigating polarisation variations in light fields in combination with behavioral animal studies could yield useful insights into how animals perceive their environment and navigate through it.

In conclusion, this thesis has contributed to the development of novel lighting design tools and expanded our understanding of the chromatic light field. A

perception-based approach is crucial in understanding the complex nature of environmental light by representing the endless variety of light with a few traceable canonical components, and further research is needed to fully account for the human visual experience of environmental light. The findings of this thesis have immediate implications for lighting designers, architects, and researchers dealing with 3D distributions of environmental light. It allows research into and scientifically informed design of chromatic appearance, including gradients, by leveraging the interactions between any space's colours and light source characteristics. In other words, it provides an understanding of and a means to utilize light and spectra in the wild.

REFERENCES

[1] J. A. Schirillo. “We infer light in space”. In: *Psychonomic bulletin & review* 20 (2013), pp. 905–915.

[2] B. L. Anderson. “Visual perception of materials and surfaces”. In: *Current biology* 21.24 (2011), R978–R983.

[3] S. C. Pont. “Spatial and Form-Giving Qualities of Light”. In: *Handbook of experimental phenomenology: Visual perception of shape, space and appearance* (2013), pp. 205–222.

[4] S. C. Pont. “Light: toward a transdisciplinary science of appearance and atmosphere”. In: *Annual review of vision science* 5 (2019), pp. 503–527.

[5] E. H. Adelson, J. R. Bergen, *et al.* “The plenoptic function and the elements of early vision”. In: *Computational models of visual processing* 1.2 (1991), pp. 3–20.

[6] C. Cuttle. “A new direction for general lighting practice”. In: *Lighting Research & Technology* 45.1 (2013), pp. 22–39.

[7] A. L. Gilchrist. “Perceived lightness depends on perceived spatial arrangement”. In: *Science* 195.4274 (1977), pp. 185–187.

[8] E. H. Adelson. “Perceptual organization and the judgment of brightness”. In: *Science* 262.5142 (1993), pp. 2042–2044.

[9] P. Raynham. *The SLL code for lighting.* CIBSE, 2012.

[10] C. Cuttle. “Towards the third stage of the lighting profession”. In: *Lighting Research & Technology* 42.1 (2010), pp. 73–93.

[11] C. Cuttle. *Lighting design: a perception-based approach.* Routledge, 2015.

[12] C. Cuttle. *Lighting by design.* Routledge, 2008.

[13] P. Raynham, J. Unwin, and L. Guan. “A new metric to predict perceived adequacy of illumination”. In: *Lighting Research & Technology* 51.4 (2019), pp. 642–648.

[14] A. Gershun. “The light field”. In: *Journal of Mathematics and Physics* 18.1-4 (1939), pp. 51–151.

[15] P. Moon and D. E. Spencer. *The photic field.* MIT Press, 1981.

[16] J. Lynes, W. Burt, G. Jackson, and C. Cuttle. “The flow of light into buildings”. In: *Transactions of the Illuminating Engineering Society* 31.3_IEStrans (1966), pp. 65–91.

[17] C. Cuttle. “Cubic illumination”. In: *Lighting Research & Technology* 29.1 (1997), pp. 1–14.

[18] R. Ramamoorthi and P. Hanrahan. “An efficient representation for irradiance environment maps”. In: *Proceedings of the 28th annual conference on Computer graphics and interactive techniques*. 2001, pp. 497–500.

[19] H. Boyaci, K. Doerschner, J. L. Snyder, and L. T. Maloney. “Surface color perception in three-dimensional scenes”. In: *Visual neuroscience* 23.3-4 (2006), pp. 311–321.

[20] J. J. Koenderink, S. C. Pont, A. J. van Doorn, A. M. Kappers, and J. T. Todd. “The visual light field”. In: *Perception* 36.11 (2007), pp. 1595–1610.

[21] L. Xia, S. C. Pont, and I. Heynderickx. “The visual light field in real scenes”. In: *i-Perception* 5.7 (2014), pp. 613–629.

[22] R. Basri and D. W. Jacobs. “Lambertian reflectance and linear subspaces”. In: *IEEE transactions on pattern analysis and machine intelligence* 25.2 (2003), pp. 218–233.

[23] R. Ramamoorthi. “Modeling illumination variation with spherical harmonics”. In: *Face Processing: Advanced Modeling Methods* (2006), pp. 385–424.

[24] A. A. Mury, S. C. Pont, and J. J. Koenderink. “Light field constancy within natural scenes”. In: *Applied Optics* 46.29 (2007), pp. 7308–7316.

[25] T. Morimoto, A. Akbarinia, K. R. Storrs, J. R. Cheeseman, H. E. Smithson, K. R. Gegenfurtner, and R. W. Fleming. “Color and gloss constancy under diverse lighting environments”. In: *bioRxiv* (2022), pp. 2022–12.

[26] T. Kartashova, H. de Ridder, S. F. te Pas, M. Schoemaker, and S. C. Pont. “The visual light field in paintings of Museum Prinsenhof: Comparing settings in empty space and on objects”. In: *Human vision and electronic imaging XX*. Vol. 9394. SPIE. 2015, pp. 554–563.

[27] T. Kartashova, D. Sekulovski, H. de Ridder, S. F. te Pas, and S. C. Pont. “The global structure of the visual light field and its relation to the physical light field”. In: *Journal of Vision* 16.10 (2016), pp. 9–9.

[28] S. C. Pont and J. J. Koenderink. “Bidirectional reflectance distribution function of specular surfaces with hemispherical pits”. In: *Journal of the Optical Society of America A* 19.12 (2002), pp. 2456–2466.

[29] A. C. Chadwick and R. Kentridge. “The perception of gloss: A review”. In: *Vision research* 109 (2015), pp. 221–235.

[30] J. J. Foster, S. E. Temple, M. J. How, I. M. Daly, C. R. Sharkey, D. Wilby, and N. W. Roberts. “Polarisation vision: overcoming challenges of working with a property of light we barely see”. In: *The Science of Nature* 105 (2018), pp. 1–26.

[31] J. Marshall and T. W. Cronin. “Polarisation vision”. In: *Current Biology* 21.3 (2011), R101–R105.

ACKNOWLEDGEMENTS

Completing a PhD is a monumental and challenging journey, and I am incredibly grateful to have had a supportive and encouraging network of individuals throughout this experience. I would like to extend my heartfelt appreciation to all those who contributed to my success.

First and foremost, I am deeply indebted to Prof. dr. Sylvia Pont, my primary promotor, whose technical guidance and editing support were instrumental in my research. Your expertise in dealing with research problems and life obstacles has been invaluable to me, and it has been a privilege to learn from you. I am also grateful to Prof. dr. Elmar Eisemann, my secondary promotor, for providing valuable input and guidance on my mathematical queries. Your passion for equations and problem-solving has been contagious, and I have learned a lot from you. Special thanks to Dr. Maarten Wijntjes, my daily supervisor, whose help with difficult programming questions was essential to my research. Your sense of humour has added an extra spice to my academic life, and I appreciate the lighthearted moments that you brought to our work. I am also grateful to Dr. Jan Jaap van Assen, who acted as a research advisor for half of my PhD research. I would also like to thank Baran Usta, my fellow PhD student, whose advice has been constructive, not only with mathematical problems but also with the challenges of academic life.

I would like to express my gratitude to Prof. dr. Jeroen Stumpel for his expertise in art history, and Prof. dr. Huib de Ridder for his expertise in colour science and statistics. Special thanks to Dr. Elif Ozcan Vieira for inviting me to be part of the Diversity and Inclusion team and engaging me in meaningful discussions. I would also like to thank the core lab members, including Dr. Christina Schneegass and Dr. Gijs Huisman, for their support and guidance.

My sincere thanks go to Prof. dr. Anya Hurlbert for hosting my secondment at Newcastle University and guiding me through my research on colour vision. I am also grateful to Ruben Carpinteiro Pastilha for showing me the lab facilities in Newcastle, and Prof. dr. Wendy Adams for explaining the technical details of the SYNS dataset.

I am grateful to Prof. dr. Marina Bloj and Olga Ovsepyan for coordinating the Marie Skłodowska-Curie Innovative Training Network, including reporting to funding agencies and delivering submittals. I am also grateful to the other principal investigators of this project for their support. Special thanks to the European Commission for funding my PhD studies.

I want to thank Dr. Ellen de Korte for her valuable suggestions on my research, and Dr. Müge Cavdan for her exemplary work as an early-stage researcher in the Marie Skłodowska-Curie Fellowship project. I also thank the other Marie Skłodowska-Curie fellows within this training network for their support and friendship. I am also

grateful to Dr. Fan Zhang, Yuguang Zhao, Dr. Mitchell van Zuijlen, Dr. Francesca di Cicco, Cristina Spoiala, and Karina Driller for creating a diverse atmosphere in the office.

I would like to extend my gratitude to Dr. Jess Hartcher-O'Brien for her resourcefulness and kindness in helping me relocate. I would also like to thank the Department of Human-Centered Design secretaries, including Amanda Klumpers-Nieuwpoort, Daphne van der Does, Denise Keislair, Charleyne van Zijl, Jessica Overdiep, and Joost Niermeijer, as well as Erik Schoorlemmer for their assistance with university-wide bureaucratic processes.

I would like to express my appreciation to Bert Naagen, the lab manager, for his invaluable assistance with various technical issues, including going out of his way to help me when I forgot my campus card at home. I am also thankful to my supervisor for my master's thesis, Prof. Peter Raynham, for his guidance and support, and for pointing me to open-access spectral datasets that proved to be extremely useful during my research.

In addition, I would like to extend my gratitude to the editors from Light Research and Technology, Prof. dr. Minchen Wei and Dr. Kynthia Chamilothori, for their professionalism and patience in handling my submitted articles. I am also thankful to the editor from Optics Express, Prof. dr. Javier Hernandez-Andres, for his expertise in my topic and for his editing support, which was invaluable in improving the quality of my work.

I am immensely grateful to Dr. Ling Xia for her insightful discussions on the methods of light field decompositions and for sharing her valuable advice about academic careers in China. In addition, I would like to extend my heartfelt appreciation to Dr. Haian Xue, Dr. Siyuan Huang, Xinzhi Pan, Yuexin Huang, Koos van der Linden, Keyang Wang, Vincent Kan, Dr. Yin Cheng Ng, Ting Ji, Yuhei Nakajima, Dr. Longyu Guan, Ranzhi Wei, Nitika Agrawal, Meng Li, Dr. Gubing Wang, Tingting Wang, Jun Xu, Soyeon Kim, Dr. Dajung Kim, Zhuochao Peng, Gijs Louwers, Idil Bostan, Xueqing Miao, Lyè Goto, Dr. Xueliang Li, Wendy Chan, and Dr. Yunyang Shi for your friendship and company throughout my PhD journey.

I am also grateful to Patricia Brock and Lee Baker-Field, who have been instrumental in mentoring me for my professional lighting design career. Your guidance and support have been invaluable, and I am forever grateful for your unwavering belief in my abilities.

Lastly, I would like to take this opportunity to express my deepest gratitude to my family, Dan Wang, Yumeng Zhu, Qirong Zhao and Sihui Yang, for their unwavering support and encouragement throughout my PhD journey. Your love, patience, and understanding have sustained me through the ups and downs of this challenging journey. Your unwavering support and belief in me have been my guiding light, and I could not have made it this far without you.

As I reach the end of this chapter in my life, I am reminded of the famous quote from Forrest Gump, life is like a box of chocolates, and you never know what you are going to get. This journey has been full of surprises, challenges, and growth, and I am proud to say that the time and effort invested in my PhD journey have not gone in vain.

As I look forward to the future, I am excited to see where this journey takes me next. I am filled with a sense of gratitude and appreciation for the incredible support system that helped me reach this milestone. I know that I would not be where I am today without the guidance, encouragement, and love of my family, friends, and mentors. Thank you all for your unwavering support, and I am excited to see where this next chapter takes me.

CURRICULUM VITÆ

Cehao YU

30-10-1988	Born in Chongqing, China.
2007-2012	Bachelor of Architecture Chongqing University, Chongqing, China
2012-2013	MSc Light and Lighting University College London, London, United Kingdom
2014-2018	Senior Lighting Designer AECOM, London, United Kingdom
2019-2023	PhD project in Light and Colour Science Delft University of Technology, Delft, The Netherlands

Thesis: Light and spectra in the wild
Promotors: Prof. dr. S.C. Pont, Prof. dr. E. Eisemann
Copromotor: Dr. M.W.A. Wijntjes

List of Publications

Journal Articles

4. C. Yu, M. J. P. van Zuijlen, C. Spoiala, S. Pont, M. W. A. Wijntjes, and A. Hurlbert. "Time of day perception in paintings". (in preparation)

3. C. Yu, M. Wijntjes, E. Eisemann, and S. Pont. "Quantifying the spatial, temporal, angular and spectral structure of effective daylight in perceptually meaningful ways". In: *Optics Express* 31.5 (2023), pp. 8953–8974. DOI: 10.1364/OE.479715

2. C. Yu, M. Wijntjes, E. Eisemann, and S. Pont. "Effects of inter-reflections on the correlated colour temperature and colour rendition of the light field". In: *Lighting Research & Technology* 0.0 (2022), pp. 1–22. DOI: 10.1177/14771535221126902

1. C. Yu, E. Eisemann, and S. Pont. "Effects of inter-reflections on the chromatic structure of the light field". In: *Lighting Research & Technology* 55.2 (2023), pp. 218–236. DOI: 10.1177/14771535211058202

Conference Proceedings

2. C. Yu and S. Pont. "Quantifying Natural Light for Lighting and Display Design". In: *SID Symposium Digest of Technical Papers*. Vol. 52. S2. (oral presentation). Society for Information Display China. 2021, pp. 99–103. DOI: 10.1002/sdtp.15031

1. C. Yu and S. Pont. "The influence of material colors on the effective color rendering and temperature through mutual illumination". In: *Proceeding of 28th Color and Imaging Conference*. 28. (poster presentation). Society for Imaging Science and Technology. 2020, pp. 293–298. DOI: 10.2352/issn.2169-2629.2020.28.47

Abstracts

11. C. Yu, M. J. P. van Zuijlen, C. Spoiala, S. C. Pont, M. W. A. Wijntjes, and A. Hurlbert. "Uncovering the asymmetry between morning and evening depiction and perception in paintings". In: The Visual Science of Art Conference. (poster presentation). Nicosia, Cyprus, 2023

10. C. Yu, R. Pastilha, S. Pont, and A. Hurlbert. "Daylight variability and its role in shaping visual and non-visual responses". In: Annual meeting of the Society for Light Treatment and Biological Rhythms. (poster presentation). Lausanne, Switzerland, 2023

9. C. Yu, M. Wijntjes, E. Eisemann, and S. Pont. "Effects of the directional and spectral distribution of daylight on colour gradients". In: *Perception*. European Conference on Visual Perception. Vol. 51. 1_suppl. (oral presentation). Nijmegen, Netherlands, 2022, p. 73. DOI: 10.1177/03010066221141167

8. C. Yu, M. J. P. van Zuijlen, S. C. Pont, M. W. A. Wijntjes, and A. Hurlbert. "Depicting time: the relationship between image statistics and perceived time of day in Western arts". In: The Visual Science of Art Conference. (poster presentation). Amsterdam, Netherlands, 2022

7. C. Yu, M. Wijntjes, E. Eisemann, and S. Pont. "Disentangling object color from illuminant color: The role of color shifts". In: *Journal of vision*. Optica Fall Vision Meeting. Vol. 22. 3. (oral presentation). Online, 2022, p. 37. DOI: 10.1167/jov.22.3.37

6. C. Yu, M. Wijntjes, E. Eisemann, and S. Pont. "Spatial and temporal dynamics of effective daylight in natural scenes". In: *Journal of Vision*. Annual Meeting of the Vision Sciences Society. Vol. 22. 14. (oral presentation). St Pete Beach, Florida, United States, 2022, p. 3984. DOI: 10.1167/jov.22.14.3984

5. C. Yu, M. W. A. Wijntjes, E. Eisemann, and S. C. Pont. "Spatial and temporal changes of chromatic light fields in natural scenes". In: VELUX Daylight Symposium. (oral presentation). Copenhagen, Denmark, 2021

4. C. Yu, E. Eisemann, M. W. A. Wijntjes, J. J. R. van Assen, and S. C. Pont. "Chromatic light field effects on perceived modelling and colour harmony". In: CIE Midterm Meeting. (poster presentation). Online, 2021

3. C. Yu, E. Eisemann, M. W. A. Wijntjes, J. J. R. van Assen, and S. C. Pont. "Effects of inter-reflections in box spaces on perceived object color harmony and shape". In: *Journal of Vision*. Annual Meeting of the Vision Sciences Society. Vol. 21. 9. (poster presentation). Online, 2021, pp. 1992–1992. DOI: 10.1167/jov.21.9.1992

2. C. Yu and S. C. Pont. "Spatial and angular variations of colour rendition due to interreflections". In: London Imaging Meeting. (poster presentation). Online, 2020, p. xv

1. C. Yu, E. Eisemann, and S. Pont. "Colour variations within light fields: Interreflections and colour effects". In: *Perception*. European Conference on Visual Perception. Vol. 48. (oral presentation). Leuven, Belgium, 2019, p. 59. DOI: 10.1177/0301006619863862